

*2mif*

Final Report  
Phase II Study

October, 1970 - September, 1973  
NASA Grant NGR-05-004-051

(NASA-CR-138185)	STUDY OF DYNAMICS OF	N74-21661
X-14B VTOL AIRCRAFT	Final Report, Oct.	
1970 - Sep. 1973 (California Univ.)		
253 p HC \$15.75	CSCI 01C	Unclas
		G3/02 38295

STUDY OF DYNAMICS OF X-14B VTOL AIRCRAFT

by

W. V. Loscutoff

J. L. Mitchiner

R. A. Roesener

J. A. Seevers

November, 1973

Department of Mechanical Engineering  
University of California  
Davis, California

Final Report  
Phase II Study

October, 1970 - September, 1973  
NASA Grant NGR-05-004-051

(NASA-CR-138185) STUDY OF DYNAMICS OF  
X-14B VTOL AIRCRAFT Final Report, Oct.  
1970 - Sep. 1973 (California Univ.)  
253 p HC \$15.75

N74-21661

CSCI 01C

Unclas  
G3/02 38295

STUDY OF DYNAMICS OF X-14B VTOL AIRCRAFT

by

W. V. Loscutoff

J. L. Mitchiner

R. A. Roesener

J. A. Seevers

November, 1973

Department of Mechanical Engineering  
University of California  
Davis, California

## TABLE OF CONTENTS

	<u>Page</u>
Preface . . . . .	1
I. Design and Application of Specified Closed-Loop	
Optimal Control . . . . .	3
Nomenclature . . . . .	4
1. Introduction . . . . .	6
2. Mathematical Development of Optimal Closed-Loop Specified Control . . . . .	10
3. Limitations in Application of Specified Closed-Loop Optimal Control to X-14B VTOL . . . . .	23
Appendices . . . . .	34
Bibliography . . . . .	31
II. Dynamic Estimation of an Unmeasurable State for the . . X-14B VTOL Aircraft . . . . .	63
Nomenclature . . . . .	64
1. Introduction . . . . .	66
2. The Model . . . . .	67
3. Controllability and Observability . . . . .	73
4. Discretization of Linear Differential Equations . . . . .	78
5. Limited Input Modal Control via State Variable Output . .	82
6. State Variable Output via Dynamic Observers . . . . .	88
7. The Partial Observer . . . . .	99
8. Application to Full Nonlinear System . . . . .	105
9. Conclusions . . . . .	115
Appendix . . . . .	120
Bibliography . . . . .	119

TABLE OF CONTENTS

	<u>Page</u>
III. Wind Gust Analysis of the X-14B VTOL Aircraft . . . . .	131
Nomenclature . . . . .	135
1. Introduction . . . . .	139
2. Airplane Model . . . . .	142
3. Wind Model . . . . .	160
4. Method of Analysis . . . . .	177
5. Results . . . . .	188
Appendices . . . . .	221
Bibliography . . . . .	250

CONTROL POWER REQUIREMENTS OF VTOL AIRCRAFT

## PREFACE

A vertical take-off and landing (VTOL) airplane is inherently difficult to handle since it has, among other problems, insufficient control power and imposes an extremely high task load on the pilot. Thus an automatic flight control system is desirable to improve the handling qualities of the aircraft. A number of trends in guidance and control provide the necessary tools for the task. The foremost is probably the application of modern control theory to both guidance and control problems. Of equal importance is the application of high-speed, general purpose, vehicle-borne digital computers which make the use of modern control theory possible. The research reported here was initiated to investigate certain facets of modern control theory and their integration with a digital computer to provide a tractable flight control system for a VTOL aircraft. Since the hover mode is the most demanding phase in the operation of a VTOL aircraft, the research efforts were concentrated in this mode of aircraft operation.

Subdivided into three sections, this report describes research work on three different aspects of the operation of the X-14B VTOL aircraft. In the first section, a general theory for optimal, prespecified, closed-loop control is developed. The ultimate goal was optimal decoupling of the modes of the VTOL aircraft to simplify the pilot's task of handling the aircraft. Modern control theory is used in the second section to design deterministic state estimators which provide state variables not measured directly, but which are needed for state variable feedback control. The third section examines the effect of atmospheric turbulence on the X-14B and determines a maximum magnitude gust envelope within which the aircraft could operate stably with the available control power.

Section I is part of a partially completed Doctoral thesis research; Sections II and III are Masters thesis research efforts. All sections are completely self-contained. Appropriate references and acknowledgements have been appended to the sections. Support of this research by the National Aeronautics and Space Administration, Grant NGR-05-004-051, is gratefully acknowledged.

I. DESIGN AND APPLICATION OF SPECIFIED  
CLOSED-LOOP OPTIMAL CONTROL

DESIGN AND APPLICATION OF SPECIFIED  
CLOSED-LOOP OPTIMAL CONTROL

NOMENCLATURE

MATRICES

A = system matrix

A = desired system matrix

B = system input matrix

C = system output matrix

K = feedback controller matrix

P = weighting matrix on the effort

Q = weighting matrix on the system states

R = precompensating matrix

S = Riccati matrix

VECTORS

r = reference input vectors

u = input vector

x = state vector

y = output vector

SCALARS

p = roll rate

q = pitch rate

r = yaw rate

u = forward velocity

v = side velocity



## NOMENCLATURE

## SCALARS

$w$  = vertical velocity

$L$  = roll moment

$M$  = pitch moment

$N$  = yaw moment

$\phi$  = roll angle

$\theta$  = pitch angle

$\psi$  = yaw angle

## CHAPTER 1

### INTRODUCTION

In the control design of a vertical take-off and landing (VTOL) aircraft, a large number of problems arise. Some of these are general problems associated with the complexity of multivariable systems and are related to the dimensionality of the subject systems and the interaction among their variables. The VTOL presents still additional problems to the designer. It has inherently poor stability and, due to its handling characteristics, requires the pilot to perform an unrealistically high number of tasks in order to maintain the aircraft at a desired attitude.

The additional handling difficulties associated with a VTOL arise from the supplementary control forces and moments added to the aircraft in order to maintain the aircraft in a hover or near-hover condition. For the airplane studied in the project, NASA's X-14B research aircraft, the control forces to provide lift and propulsion were obtained by vectoring the thrust of its two engines. The control moments for pitch and roll were obtained by bleeding air from the engines and ducting it to variable area nozzles in the wing tips and the tail of the airplane.

For the design of an automatic flight control system which would improve the handling qualities of the X-14B aircraft, it was felt that the state variable decoupling techniques would yield the best results. The logic behind this decision was that if the pitch, roll, heave, and yaw modes were completely decoupled from each other, the pilot's task of flying the aircraft would be enormously simpler. This was the motivation for the optimal control technique developed in this section. Although the results obtained may be used for arbitrary closed-loop system behavior specifications,

they are especially well suited for decoupling.

As background for the control technique developed in this report, a few brief comments on decoupling and optimal control theories follow.

The current literature on the subject on non-interacting, or decoupling, control is headed by Morgan [2], who arrived at sufficient conditions for decoupling and developed a procedure using a constant gain compensator with state variable feedback to obtain a decoupled controlled system. Rekasius [3] then obtained some useful results extending earlier work. A more general decoupling problem with static compensation, was solved subsequently by Falb and Wolovich [5]. Their result was the first complete solution to the decoupling problem for a significant class of linear systems. Gilbert [6] added to the results of Falb and Wolovich. The more general state feedback decoupling problem, with dynamic compensation, was formulated and solved by Wonham and Morse. Additional work on system decoupling has been done by Silverman [9], Sato and Lopresti [11], Porter [34], and Yore [35]. The last author used a model reference approach to obtain an optimally decoupled system.

The foregoing methods, while useful in many applications, were only of limited use to the X-14B and hence a different approach was sought for the aircraft. Since most physical systems cannot be decoupled exactly, a technique for approximate decoupling was sought. Thus research efforts were turned to the method of approximate decoupling with a specified index of performance.

The theory of optimal control is well defined and conceptually not very difficult to apply. However, the methods of optimal control suffer from several drawbacks. The major difficulty arises from the fact that, even in well defined problems, it is difficult to specify a meaningful performance index that is analytically tractable. Furthermore, once a

performance index is defined, it is not a simple task to interpret the meaning of the elements of the performance index or to manipulate these to create desired changes in the dynamic behavior of the controlled system or the structure of the controller.

In an effort to overcome some of the above difficulties, Solheim [15] presented a design of optimal control systems which minimized a quadratic performance index for a set of prescribed closed-loop eigenvalues. The procedure is as follows. For a performance index of the form

$$J = \int_0^{\infty} (\underline{x}' \underline{Q} \underline{x} + \underline{u}' \underline{P} \underline{u}) dt \quad (I-1)$$

The weighting matrix  $\underline{P}$  and the eigenvalues of the closed-loop system are selected by the designer. Then the  $\underline{Q}$  matrix, corresponding to the prescribed set of eigenvalues, is determined. Finally, the optimal feedback gain matrix is determined from the steady state solution of the Riccati equation.

The most exacting level of system design occurs when the engineer is given the task of designing a feedback system with specific input-output and dynamic behavior characteristics. This implies that a percompensator with a particular closed-loop system matrix must be available. Again, since precise agreement between specification and physical realization is not possible, some compromise result is usually accepted. The research reported herein considers an analytical approach based on the premise that exact system behavior cannot be dictated. The result is a design tool for finding an optimal control policy, with respect to some quadratic performance index, that yields a closed-loop system approximately equal to that desired by the designer.

The method developed herein is completely general with respect to system structure and conceptually is very easy to apply. However, there

are certain computational difficulties which are discussed in the main text of this report. Basically, it enables the control system designer to solve the following problem. A system is described by a set of input and output matrices and a system matrix  $\underline{A}$ . The specification is a desired matrix  $\bar{\underline{A}}$  and the problem is to find a feedback control matrix  $\underline{K}$  that will yield the desired closed-loop matrix and will minimize a performance index based on system error and effort. The procedure is to determine  $\underline{K}$  by direct comparison of  $\underline{A}$  and  $\bar{\underline{A}}$ , if possible, and then to determine  $\underline{P}$  and  $\underline{Q}$  from the result. This approach yields a closed-loop system behavior which is similar to the desired behavior. However, the magnitudes of state and input variables may be undesirably large. These characteristics may now be minimized, since  $\underline{P}$  and  $\underline{Q}$  are known, while the closed-loop behavior is maintained at or near the desired condition, by varying the elements of  $\underline{P}$  and  $\underline{Q}$ . The final result is a compromise between the approximate equality, between the desired and actual closed-loop system matrices and the magnitudes of the transients of the state input variables.

Since  $\bar{\underline{A}}$  may not be arbitrarily specified, the above method is somewhat restricted in application to decoupling problems. A more severe limitation to the method is that even when  $\bar{\underline{A}}$  can be calculated, there is no guarantee that corresponding weighting matrices  $\underline{P}$  and  $\underline{Q}$  can be found. Another limitation of the method is that state variable feedback must be used. Thus some form of state estimation has to be utilized.

The general theory of specified closed-loop optimal control is developed in Chapter 2. In Chapter 3, the results preapplied to controller design of the X-14B airplane and a successful design is shown. The Appendices include the derivation of the complete dynamic equations for the X-14B.

CHAPTER 2  
MATHEMATICAL DEVELOPMENT OF OPTIMAL  
CLOSED-LOOP SPECIFIED CONTROL

### 2.1 Statement of the Problem and Assumptions

In the design of a controller for a multivariable system, it is frequently necessary to impose restrictions on the behavior characteristics of the closed-loop system. These restrictions include the location of the eigenvalues of the system as well as interaction between the inputs and the outputs. The most systematic way of specifying these restrictions is to prescribe a particular closed-loop system matrix and a precompensator matrix. Ordinarily this is not possible except for certain classes of systems. What is normally obtained is a system which resembles the desired system. It is not known however, what the degree of resemblance is, and what the penalty the designer must pay for the desired operation behavior. This chapter presents an analytical procedure that will systematically design a controller such that a linear closed-loop system will behave close to a prescribed manner and is optimal for some quadratic criterion.

The assumptions made for the analysis are the following:

- the plant is represented by a set of linear, time-invariant set of state space equations,
- the plant is completely observable and completely controllable,
- all states are directly available for measurement or can be generated by estimation techniques,
- the control law is linear and constant,
- the performance index is a quadratic with constant weighting coefficients.

The class of systems considered consists of deterministic systems modeled mathematically by constant coefficient, linear differential equations in the form

$$\dot{\underline{x}} = \underline{A} \underline{x} + \underline{B} \underline{u} \quad (I-2)$$

$$\underline{y} = \underline{C} \underline{x} \quad .$$

The control policy is

$$\underline{u} = - \underline{K} \underline{x} + \underline{R} \underline{r} \quad . \quad (I-3)$$

Here,  $\underline{x}$  is an  $n$ -dimensional state vector,  $\underline{u}$  is a  $p$ -dimensional control vector,  $\underline{y}$  is an  $m$ -dimensional output vector, and  $\underline{r}$  is a  $p$ -dimensional reference input vector. The matrices  $\underline{A}$ ,  $\underline{B}$ ,  $\underline{C}$ ,  $\underline{K}$ , and  $\underline{R}$  are constant and have dimensions consistent with  $\underline{x}$ ,  $\underline{y}$ ,  $\underline{u}$ , and  $\underline{r}$ .  $\underline{R}$  is a precompensator matrix which is necessary when additional requirements on input-output relations, such as decoupling, are made.

A desired dynamic behavior may be described by the linear differential equations given by

$$\dot{\underline{x}} = \underline{\bar{A}} \underline{x} + \underline{B}_d \underline{r} \quad . \quad (I-4)$$

Substitution of Equation (I-3) into (II-2) yields

$$\dot{\underline{x}} = (\underline{A} - \underline{B} \underline{K}) \underline{x} + \underline{B} \underline{R} \underline{r} \quad . \quad (I-5)$$

Thus if a controlled system is to behave according to specifications, it must obey the Equations

$$\underline{A} - \underline{B} \underline{K} = \underline{\bar{A}} \quad (I-6)$$

$$\underline{B} \underline{R} = \underline{B}_d \quad . \quad (I-7)$$

Note that  $\underline{B}_d$  is not affected by the feedback controller  $\underline{K}$  and is affected only by the precompensator  $\underline{R}$ . In all cases  $\underline{R}$  is either

known or, for input-output decoupled systems, may be computed [4, 5] readily. Hence, the problem reduces to finding an optimal control  $\underline{u}$  which minimizes the performance index

$$J = \int_0^{\infty} (\underline{x}' \underline{Q} \underline{x} + \underline{u}' \underline{P} \underline{u}) dt \quad . \quad (I-1)$$

This is simply the optimal regulator problem except that now  $\underline{P}$  and  $\underline{Q}$  are not specified but must be determined for a given closed-loop condition. Matrix  $\underline{Q}$  is symmetric and positive and semidefinite while  $\underline{P}$  is symmetric and positive definite.

## 2.2 Development of the Specified Optimal Control Technique

The conventional approach to optimal control problems is to specify  $\underline{P}$  and  $\underline{Q}$  in the performance index and to solve for the optimal control policy. It is well known that the optimal control policy for infinite time problem is

$$\underline{u} = - \underline{P}^{-1} \underline{B}' \underline{S} \underline{x} \quad (I-8)$$

where  $\underline{S}$ , the Riccati matrix, is the steady state solution of the Riccati equation

$$\dot{\underline{S}} = - \underline{S} \underline{A} - \underline{A}' \underline{S} - \underline{Q} + \underline{S} \underline{B} \underline{P}^{-1} \underline{B}' \underline{S} \quad . \quad (I-9)$$

$\underline{S}$  is symmetric and positive definite. Comparison of Equations (I-3) and (I-8) yields

$$\underline{K} = \underline{P}^{-1} \underline{B}' \underline{S} \quad . \quad (I-10)$$

Thus, given a set of weighting matrices  $\underline{P}$  and  $\underline{Q}$ , a corresponding optimal solution is readily obtained. However, there is no guarantee that the resulting closed-loop system has the desired dynamic characteristics. Instead, one has to evaluate the closed-loop system for several sets of values of  $\underline{P}$  and  $\underline{Q}$  before arriving at a desired solution.



To develop the method of optimal specified response, consider a system matrix  $\underline{A}$  and a desired closed-loop matrix  $\bar{\underline{A}}$  defined by

$$\bar{\underline{A}} = \underline{A} - \underline{B} \underline{K} \quad (I-11)$$

If the inverse of the system input matrix  $\underline{B}$  exists, then the control matrix  $\underline{K}$  may be readily found. For the case when the rank of  $\underline{B}$  is less than the order of the system, several courses of action exist. One is to specify a set of eigenvalues and to compute  $\underline{K}$  by any technique which will provide the desired set of eigenvalues. Finally the determined value of  $\underline{K}$  is used to compute  $\bar{\underline{A}}$  from Equation (I-11). This, of course, removes some degree of arbitrariness in the specification of  $\bar{\underline{A}}$ , but still provides for a compromise between the choice of desired set of eigenvalues and the amount of effort necessary to obtain the set.

A second course of action is to specify  $\bar{\underline{A}}$ , consistent with permissible values of  $\underline{K}$ , and to determine  $\underline{P}$  and  $\underline{Q}$  for the closed-loop system. This is especially attractive when closed-loop behavior like decoupling is desired.

The mathematical equations necessary to solve the problem are obtained by first considering the optimal controller  $\underline{K}$ , given by Equation (I-10), substituting it into Equation (I-11), and solving for  $\underline{A} - \bar{\underline{A}}$ :

$$\begin{aligned} \bar{\underline{A}} &= \underline{A} - \underline{B} \underline{P}^{-1} \underline{B}' \underline{S} \\ \underline{A} - \bar{\underline{A}} &= \underline{B} \underline{P}^{-1} \underline{B}' \underline{S}. \end{aligned} \quad (I-12)$$

The last equation, when substituted into the steady state Riccati equation, yields

$$\underline{S} \underline{A} + \underline{A}' \underline{S} + \underline{Q} - \underline{S} (\underline{A} - \bar{\underline{A}}) = \underline{0}, \quad (I-13)$$

which reduces to

$$\underline{A}' \underline{S} + \underline{S} \bar{\underline{A}} + \underline{Q} = \underline{0}. \quad (I-14)$$

When the transpose of Equation (I-14) is added to it the final result, recalling that  $\underline{S}$  and  $\underline{Q}$  are symmetric, is

$$(\underline{A} + \bar{\underline{A}})' \underline{S} + \underline{S} (\underline{A} + \bar{\underline{A}}) = - 2 \underline{Q} \quad . \quad (\text{I-15})$$

Equations (I-10), (I-11) and (I-15) are fundamental to the problem of specified optimal control. The method is to determine  $\underline{K}$  from (I-11), calculate  $\underline{P}$  from (I-10), determining  $\underline{S}$  simultaneously, and determine  $\underline{Q}$  from (I-15). Once  $\underline{P}$ , which is symmetric and positive definite, and  $\underline{Q}$ , which is symmetric and positive semi-definite, are determined, they may be modified to maintain a degree of resemblance to the desired closed-loop matrix while minimizing state variable and input variables magnitudes. The nonideal systems are analyzed in the next section.

### 2.3 Analytical Development for Nonideal Systems

Consider now the case where the number of manipulated variables is less than the number of state variables ( $p < n$ ), and hence, the  $\underline{B}$  matrix is nonsquare. Assume that the  $p$  inputs are linearly independent from each other; consequently, the rank of  $\underline{B}$  is  $p$ .

Suppose a change of variables is made with

$$\underline{x} = \underline{Gz} \quad (\text{I-16})$$

where  $\underline{G}$  is an  $n \times n$  nonsingular matrix to be defined later. When this is substituted into the system equation

$$\dot{\underline{x}} = \underline{Ax} + \underline{Bu}$$

the result can be written as

$$\underline{\dot{z}} = \underline{G}^{-1} \underline{A} \underline{Gz} + \underline{G}^{-1} \underline{Bu} \quad . \quad (\text{I-17})$$

Define

$$\underline{\tilde{A}} \triangleq \underline{G}^{-1} \underline{AG} \quad (\text{I-18})$$

$$\underline{\tilde{B}} \triangleq \underline{G}^{-1} \underline{B} \quad . \quad (\text{I-19})$$

Further, define  $\underline{G}$  such that

$$\underline{\tilde{B}} = \begin{bmatrix} \underline{0} \\ \underline{\hat{B}} \end{bmatrix}$$

where  $\underline{\tilde{B}}$  is an  $n \times p$  matrix,  $\underline{0}$  represents an  $(n-p) \times p$  matrix and  $\underline{\hat{B}}$  is a nonsingular  $p \times p$  matrix. This may be obtained as follows.

If  $\underline{G} = [\underline{G}_1 \quad \underline{G}_2]$ , then

$$\underline{B} = \underline{GB} = [\underline{G}_1 \quad \underline{G}_2] \begin{bmatrix} \underline{0} \\ \underline{\hat{B}} \end{bmatrix} \quad (\text{I-20})$$

or

$$\underline{B} = \underline{G}_2 \underline{\hat{B}}$$

and

$$\underline{G}_2 = \underline{\hat{B}}(\underline{\hat{B}})^{-1} \quad . \quad (\text{I-21})$$

The matrix  $\underline{G}_1$  can be any  $n \times (n-p)$  matrix such that  $\underline{G}^{-1}$  exists. This demonstrates that a new system representation can be found of the form

$$\underline{\dot{z}} = \underline{\tilde{A}}z + \underline{\tilde{B}}u \quad (\text{I-22})$$

such that the first  $(n-p)$  rows of the matrix  $\underline{\tilde{B}}$  are identically zero with the remaining  $p$  rows forming a matrix of rank  $p$ . Therefore, for the derivations and analyses which follow, the first  $(n-p)$  rows of  $\underline{\tilde{B}}$  can be taken as zero without loss in generality. The lower  $p$  rows of  $\underline{\tilde{B}}$  are assumed to be of rank  $p$ .

For the development of the control policy for the nonideal system where  $p < n$ , consider the closed-loop representation

$$\bar{\underline{A}} = \underline{A} - \underline{BK} \quad (I-23)$$

with

$$\underline{A} = \begin{bmatrix} \underline{A}_{11} & \underline{A}_{12} \\ \underline{A}_{21} & \underline{A}_{22} \end{bmatrix} \quad \bar{\underline{A}} = \begin{bmatrix} \bar{\underline{A}}_{11} & \bar{\underline{A}}_{12} \\ \bar{\underline{A}}_{21} & \bar{\underline{A}}_{22} \end{bmatrix}$$

$$\underline{B} = \begin{bmatrix} \underline{0} \\ \underline{B}_2 \end{bmatrix}$$

The dimensions of the various matrices are as follows:

$\underline{A}(n \times n)$ ,  $\bar{\underline{A}}(n \times n)$ ,  $\underline{B}(n \times p)$ ,  $\underline{K}(p \times n)$ ,  $\underline{A}_{11}(j \times j)$ ,  
 $\underline{A}_{12}(j \times p)$ ,  $\underline{A}_{21}(p \times j)$ ,  $\underline{A}_{22}(p \times p)$ ,  $\bar{\underline{A}}_{11}(j \times j)$ ,  
 $\bar{\underline{A}}_{12}(j \times p)$ ,  $\bar{\underline{A}}_{21}(p \times j)$ ,  $\bar{\underline{A}}_{22}(p \times p)$ ,  $\underline{0}(j \times p)$  and  
 $\underline{B}_2(p \times p)$ , where  $j = n-p$ .

The Riccati equation for optimal control is given by Equation (I-13), with the control policy given by

$$\underline{K} = \underline{P}^{-1} \underline{B} \underline{S} \quad .$$

Let

$$\underline{K} = [\underline{K}_1 \quad \underline{K}_2]$$

$$\underline{S} = \begin{bmatrix} \underline{S}_{11} & \underline{S}_{12} \\ \underline{S}_{12} & \underline{S}_{22} \end{bmatrix}$$

$$\underline{Q} = \begin{bmatrix} \underline{Q}_{11} & \underline{Q}_{12} \\ \underline{Q}_{12} & \underline{Q}_{22} \end{bmatrix}$$

with  $\underline{K}_1(p \times j)$ ,  $\underline{K}_2(p \times p)$ ,  $\underline{S}_{11}(j \times j)$ ,  $\underline{S}_{12}(j \times p)$ ,  $\underline{S}_{22}(p \times p)$ ,  
 $\underline{Q}_{11}(j \times j)$ ,  $\underline{Q}_{12}(j \times p)$ ,  $\underline{Q}_{22}(p \times p)$  and  $\underline{P}(p \times p)$ .

Working with partitioned matrices, Equation (I-23) can be expressed as

$$\begin{bmatrix} \bar{\underline{A}}_{11} & \bar{\underline{A}}_{12} \\ \bar{\underline{A}}_{21} & \underline{A}_{22} \end{bmatrix} = \begin{bmatrix} \underline{A}_{11} & \underline{A}_{12} \\ \underline{A}_{21} & \underline{A}_{22} \end{bmatrix} - \begin{bmatrix} \underline{0} & \underline{0} \\ \underline{B}_2 \underline{K}_1 & \underline{B}_2 \underline{K}_2 \end{bmatrix}$$

Breaking down this matrix equation into components parts and solving for  $\underline{K}_1$  and  $\underline{K}_2$  yields

$$\begin{aligned} \underline{K}_1 &= \underline{B}_2^{-1} (\underline{A}_{21} - \bar{\underline{A}}_{21}) \\ \underline{K}_2 &= \underline{B}_2^{-1} (\underline{A}_{22} - \bar{\underline{A}}_{22}) \end{aligned} \quad (I-24)$$

Provided  $\underline{B}_2^{-1}$  exists. This was shown to be true since  $\underline{B}_2$  is of rank  $p$ . Clearly  $\underline{A}_{11} = \bar{\underline{A}}_{11}$  and  $\underline{A}_{12} = \bar{\underline{A}}_{12}$  are restrictions imposed at this time because of the limit in the number of inputs. After the transformation, the optimal weighting matrices  $\underline{P}$  and  $\underline{Q}$  can be found. Repeating Equation (I-12), we have

$$\underline{B} \underline{P}^{-1} \underline{B} \underline{S} = \underline{A} - \bar{\underline{A}}$$

In the partitioned form this becomes

$$\begin{bmatrix} \underline{0} & \underline{0} \\ \underline{B}_2 \underline{P}^{-1} \underline{B}_2 \underline{S}_{12} & \underline{B}_2 \underline{P}^{-1} \underline{B}_2 \underline{S}_{22} \end{bmatrix} = \begin{bmatrix} \underline{0} & \underline{0} \\ \underline{A}_{21} - \bar{\underline{A}}_{21} & \underline{A}_{22} - \bar{\underline{A}}_{22} \end{bmatrix} \quad (I-25)$$

or

$$\begin{aligned} \underline{B}_2 \underline{P}^{-1} \underline{B}_2 \underline{S}_{12} &= \underline{A}_{21} - \bar{\underline{A}}_{21} \\ \underline{B}_2 \underline{P}^{-1} \underline{B}_2 \underline{S}_{22} &= \underline{A}_{22} - \bar{\underline{A}}_{22} \end{aligned} \quad (I-26)$$

## 2.4 Application to an Ideal System

To illustrate the design procedure, consider an ideal second order system given by Equation (I-2) where

$$\underline{\underline{A}} = \begin{bmatrix} -3 & 2 \\ 4 & -5 \end{bmatrix} \quad \underline{\underline{B}} = \begin{bmatrix} 1 & 1 \\ 0 & 1 \end{bmatrix}, \quad \underline{\underline{C}} = \begin{bmatrix} 1 & 0 \\ 0 & 1 \end{bmatrix}$$

Let the desired closed-loop response be governed by

$$\underline{\underline{\bar{A}}} = \underline{\underline{A}} - \underline{\underline{BK}} = \begin{bmatrix} -8 & 0 \\ 0 & -8 \end{bmatrix}$$

To determine  $\underline{\underline{P}}$  and  $\underline{\underline{Q}}$  for the given  $\underline{\underline{A}}$ , the first step is to find  $\underline{\underline{K}}$  from

$$\underline{\underline{K}} = \underline{\underline{B}}^{-1} (\underline{\underline{A}} - \underline{\underline{\bar{A}}}) = \begin{bmatrix} 1 & -1 \\ 4 & 3 \end{bmatrix}.$$

The next step is to determine a symmetric, positive definite  $\underline{\underline{P}}$  from Equation (I-10) keeping in mind the condition that  $\underline{\underline{S}}$  must also be symmetric and positive definite. Thus

$$(\underline{\underline{B}}')^{-1} \underline{\underline{P}} \underline{\underline{K}} = \underline{\underline{S}},$$

where

$$\underline{\underline{P}} = \begin{bmatrix} P_{11} & P_{12} \\ P_{12} & P_{22} \end{bmatrix}, \quad \underline{\underline{S}} = \begin{bmatrix} S_{11} & S_{12} \\ S_{12} & S_{22} \end{bmatrix}.$$

Upon expansion of the last equation, the result is

$$\begin{bmatrix} P_{11} + 4 P_{12} & -P_{11} + 3 P_{12} \\ -P_{11} - 3 P_{12} + 4 P_{22} & P_{11} - 4 P_{12} + 3 P_{22} \end{bmatrix} = \begin{bmatrix} S_{11} & S_{12} \\ S_{12} & S_{22} \end{bmatrix}$$

Thus

$$S_{11} = P_{11} + 4 P_{12} \quad (i)$$

$$S_{12} = -P_{11} + 3 P_{12} = 4 P_{22} - P_{11} - 3 P_{12} \quad (ii)$$

$$S_{22} = P_{11} - 4 P_{12} + 3 P_{22} \quad (iii)$$

Because of symmetry of  $\underline{S}$ , Equation (ii) yields the relationship

$$P_{12} = \frac{2}{3} P_{22} \quad (iv)$$

Equations (i) - (ii) become

$$S_{11} = P_{11} + \frac{8}{3} P_{22} \quad (v)$$

$$S_{12} = -P_{11} + 2 P_{22} \quad (vi)$$

$$S_{22} = P_{11} + \frac{1}{3} P_{22} \quad (vii)$$

Analysis of the equations suggests that  $P_{22}$  may be chosen arbitrarily.

Since  $\underline{P}$  must be positive definite,  $P_{11} > \frac{4}{9} P_{22}$ . Thus an acceptable choice for  $\underline{P}$  is

$$\underline{P} = \begin{bmatrix} 1 & 2/3 \\ 2/3 & 1 \end{bmatrix}$$

which yields

$$\underline{S} = \begin{bmatrix} 11/3 & 1 \\ 1 & 4/3 \end{bmatrix}$$

From Equation (I-15),  $\underline{Q}$  is found directly to be

$$\underline{Q} = \frac{1}{3} \begin{bmatrix} 109 & 17 \\ 17 & 46 \end{bmatrix}$$

It may be readily verified, using Equation (I-13), that the above values of  $\underline{P}$  and  $\underline{Q}$  will yield the desired value of  $\underline{S}$  and hence the feedback matrix  $\underline{K}$ .

The time responses for the closed-loop system  $\underline{\ddot{A}} = \underline{A} - \underline{B} \underline{K}$  are shown in Table I-1 for three sets of initial conditions. While the transient behavior is as desired, let us assume that the maximum magnitude of the control variable  $u_2$  is excessive. To reduce it,  $P_{22}$ , the weighting asso-

ciated most closely with  $u_2$  is increased from  $P_{22} = 1$  to  $P_{22} = 2$  while all the other elements of  $\underline{P}$  and  $\underline{Q}$  are held constant. The resulting feedback matrix, obtained from Equations (I-10) and (I-13), is

$$\underline{K} = \begin{bmatrix} 2.90 & 0.32 \\ 1.56 & 1.39 \end{bmatrix}$$

and the closed-loop system matrix is

$$\underline{A} = \begin{bmatrix} -7.76 & -0.30 \\ 2.44 & -6.39 \end{bmatrix}$$

The time responses for this modified closed-loop system are shown in Table I-2 for the same three sets of initial conditions used in the original system. Note that the desired reduction in the magnitude of  $u_2$  has been obtained, but at a loss in the degree of decoupling between the states. A system designer would have to choose a compromise between excessive input and excessive coupling. With the foregoing information, he is in a position to make an objective choice of a control policy that most nearly meets his needs.



TABLE I-1  
 TIME RESPONSE FOR THE SECOND ORDER  
 EXAMPLE PROBLEM,  $P(2,2) = 1.0$

1.  $x_1(0) = 0, x_2(0) = 10$

TIME	$x_1$	$x_2$	$u_1$	$u_2$	$(u_1) + (u_2)$
0.0	0.00	10.00	10.00	-30.00	40.00
0.3	0.00	7.86	7.86	-23.59	31.46
0.6	0.00	6.18	6.18	-18.56	24.75
0.9	0.00	4.86	4.86	-14.60	19.47
1.2	0.00	3.82	3.82	-11.48	15.31
1.5	0.00	3.01	3.01	- 9.03	12.04
1.8	0.00	2.36	2.36	- 7.10	9.47
2.1	0.00	1.86	1.86	- 5.59	7.45
2.4	0.00	1.46	1.46	- 4.39	5.86
2.7	0.00	1.15	1.15	- 3.46	4.61
3.0	0.00	0.90	0.90	- 2.72	3.62

2.  $x_1(0) = 10, x_2(0) = 0$

TIME	$x_1$	$x_2$	$u_1$	$u_2$	$(u_1) + (u_2)$
0.0	10.00	0.00	-10.00	-40.00	50.00
0.3	7.86	0.00	- 7.86	-31.46	39.33
0.6	6.18	0.00	- 6.18	-24.75	30.93
0.9	4.86	0.00	- 4.86	-19.47	24.33
1.2	3.82	0.00	- 3.82	-15.31	19.14
1.5	3.01	0.00	- 3.01	-12.04	15.06
1.8	2.36	0.00	- 2.36	- 9.47	11.84
2.1	1.86	0.00	- 1.86	- 7.45	9.31
2.4	1.46	0.00	- 1.46	- 5.86	7.33
2.7	1.15	0.00	- 1.15	- 4.61	5.76
3.0	0.90	0.00	- 0.90	- 3.62	4.53

3.  $x_1(0) = 10, x_2(0) = 10$

TIME	$x_1$	$x_2$	$u_1$	$u_2$	$(u_1) + (u_2)$
0.0	10.00	10.00	0.00	-70.00	70.00
0.3	7.86	7.86	0.00	-55.06	55.06
0.6	6.18	6.18	0.00	-43.31	43.31
0.9	4.86	4.36	0.00	-34.07	34.07
1.2	3.82	3.82	0.00	-26.80	26.80
1.5	3.01	3.01	0.00	-21.08	21.08
1.8	2.36	2.36	0.00	-16.58	16.58
2.1	1.86	1.86	0.00	-13.04	13.04
2.4	1.46	1.46	0.00	-10.26	10.26
2.7	1.15	1.15	0.00	- 8.07	8.07
3.0	0.90	0.90	0.00	- 6.35	6.35

TABLE I-2  
 TIME RESPONSE FOR THE SECOND ORDER  
 EXAMPLE PROBLEM,  $P(2,2) = 2.0$

1.  $x_1(0) = 0, x_2(0) = 10$

TIME	$x_1$	$x_2$	$u_1$	$u_2$	$(u_1) + (u_2)$
0.0	0.00	10.00	-4.88	-13.35	18.23
0.3	0.04	8.27	-4.16	-11.11	15.28
0.6	0.06	6.84	-3.55	-9.26	12.81
0.9	0.08	5.66	-3.01	-7.71	10.72
1.2	0.09	4.68	-2.56	-6.42	8.98
1.5	0.09	3.88	-2.17	-5.34	7.51
1.8	0.09	3.21	-1.83	-4.45	6.29
2.1	0.08	2.66	-1.55	-3.70	5.26
2.4	0.07	2.20	-1.31	-3.08	4.40
2.7	0.07	1.83	-1.10	-2.57	3.68
3.0	0.06	1.51	-0.93	-2.14	3.07

2.  $x_1(0) = 10, x_2(0) = 0$

TIME	$x_1$	$x_2$	$u_1$	$u_2$	$(u_1) + (u_2)$
0.0	10.00	0.00	-29.84	-17.80	47.65
0.3	7.92	0.53	-23.91	-14.82	38.73
0.6	6.28	0.87	-19.17	-12.34	31.51
0.9	4.98	1.06	-15.38	-10.28	25.66
1.2	3.95	1.14	-12.35	-8.56	20.91
1.5	3.13	1.16	-9.92	-7.13	17.05
1.8	2.48	1.12	-7.98	-5.93	13.91
2.1	1.97	1.06	-6.42	-4.94	11.36
2.4	1.57	0.99	-5.17	-4.11	9.29
2.7	1.24	0.90	-4.16	-3.42	7.59
3.0	0.99	0.81	-3.36	-2.85	6.21

3.  $x_1(0) = 10, x_2(0) = 10$

TIME	$x_1$	$x_2$	$u_1$	$u_2$	$(u_1) + (u_2)$
0.0	10.00	10.00	-34.73	-31.15	65.89
0.3	7.96	8.81	-28.08	-25.94	54.02
0.6	6.34	7.71	-22.72	-21.60	44.32
0.9	5.06	6.72	-18.40	-17.99	36.39
1.2	4.04	5.83	-14.91	-14.98	29.89
1.5	3.22	5.04	-12.09	-12.47	24.57
1.8	2.57	4.34	-9.81	-10.39	20.20
2.1	2.06	3.73	-7.97	-8.65	16.63
2.4	1.64	3.19	-6.48	-7.20	13.69
2.7	1.32	2.73	-5.27	-6.00	11.27
3.0	1.05	2.33	-4.29	-4.99	9.29

## CHAPTER 3

LIMITATIONS IN APPLICATION OF SPECIFIED CLOSED-LOOP  
OPTIMAL CONTROL TO X-14B AIRCRAFT

## 3.1 Control Design Problems in VTOL Aircraft

The major problems in the control of VTOL aircraft, occur at the hover and near-hover conditions. Because of the low speed of the aircraft at these conditions, insufficient aerodynamic forces exist to produce an effective control system relying on aerodynamic control surfaces. Hence, supplementary controls are added to provide lift, roll moment, and pitch moment. With the added controls the pilot is required to perform a large number of tasks to maintain the aircraft at a desired attitude.

To simplify the task of controlling the airplane, a decoupling controller scheme was sought. The specified closed-loop optimal control method, developed in the previous chapter, was selected. The primary reason was that while linear decoupling techniques gave adequate results and these were used to obtain a completely decoupled system, it was necessary to minimize the magnitudes of some of the control and state variables, and it was necessary to maximize the envelope control system operation in the linear domain. The latter implied avoiding saturation of the control variables as much as possible. It is obvious that the handling characteristics of a controlled system are drastically changed when saturation is reached. To maximize the envelope of operation, it is necessary to distribute the control effort in an equitable manner.

## 3.2 Description of the X-14 VTOL Aircraft

The Bell X-14B VTOL aircraft is a fixed wing, jet-propelled, deflected-jet vehicle. It is a small (4200 pounds) two-place, side-by-side airplane

with two jet engines mounted in the fuselage. The vertical thrust is derived from cascade-type diverters on the exhausts of each engine which enables the pilot to select any desired thrust angle from vertical to horizontal. In addition to this thrust diverter, it is also assumed that a side vane is present in the exhaust enabling direct lateral movement. Angular control about the three axes is maintained through a continuous bleed from the engine compressors and discharged at the tail and wing tips of the airplane.

### 3.3 Equations of Motion for a VTOL Aircraft

The complete development of the nonlinear equations of motion for a VTOL aircraft in general and the X-14B in particular is made in Appendix A-I. A general method to linearize an  $n^{\text{th}}$  order nonlinear equation is presented in Appendix A-II. Appendix A-III is a listing of the linearized system equations for several flight conditions of the X-14B.

A common practice in analyzing aircraft is to separate, or decouple, the longitudinal mode of motion from the lateral mode. The linear equations of motion for the longitudinal mode of the X-14B in hover, after dropping the effects of the elevator, can be expressed as

$$\underline{\dot{x}} = \underline{A}x + \underline{B}u$$

where

$$\underline{A} = \begin{bmatrix} 0 & 1.0 & 0 & 0 \\ 0 & -.150 & -4.4 \times 10^{-4} & -1.5 \times 10^{-4} \\ -32.0 & 0 & -.020 & -.038 \\ 0 & 0 & 0 & -.021 \end{bmatrix}$$

$$\underline{\underline{B}} = \begin{bmatrix} 0 & 0 & 0 \\ .035 & .020 & 0 \\ 0 & .56 & 0 \\ 0 & 0 & 3.6 \end{bmatrix}$$

where

$$\underline{\underline{x}} = \begin{bmatrix} x_1 \\ x_2 \\ x_3 \\ x_4 \end{bmatrix} = \begin{bmatrix} \theta \\ q \\ w \\ u \end{bmatrix}, \quad \underline{\underline{u}} = \begin{bmatrix} \delta_y \\ \Omega \\ \sigma \end{bmatrix} = \begin{bmatrix} u_1 \\ u_2 \\ u_3 \end{bmatrix}$$

The physical variables corresponding to the state variables are  $\theta$  (radians),  $q$  (radians/second),  $u$  (feet/second), and  $w$  (feet/second), respectively, with the control vector corresponding to  $\delta_y$  (reaction nozzle about the  $y$  axis),  $\sigma$  (thrust angle measured positive from the vertical), and  $\Omega$  (engine RPM as a percent of maximum).

### 3.4 Design of a Controller for Hover Flight

In the open-loop system there is strong coupling between roll and the vertical velocity. Let the feedback control policy be given by

$$\underline{\underline{u}} = -\underline{\underline{K}}\underline{\underline{x}} = \begin{bmatrix} k_{11} & k_{12} & k_{13} & k_{14} \\ k_{21} & k_{22} & k_{23} & k_{24} \\ k_{31} & k_{32} & k_{33} & k_{34} \end{bmatrix} \underline{\underline{x}}$$

To obtain the desired decoupling a closed-loop system matrix may be specified as

$$\underline{\underline{\bar{A}}} = \begin{bmatrix} 0 & 1 & 0 & 0 \\ -4 & -3 & 0 & 0 \\ 0 & 0 & -.6 & 0 \\ 0 & 0 & 0 & -.6 \end{bmatrix} \quad (I-27)$$

It must be determined that the system is completely controllable and completely observable. Since state variable output is assumed, observability is complete. It is controllable since the rank of the controllability matrix

$$[\underline{B} \quad \underline{AB} \quad \underline{A^2B} \quad \underline{A^3B}]$$

is four.

Next, it should be determined that a feedback control matrix  $\underline{K}$ , exists that will produce the closed-loop response,  $\bar{\underline{A}}$ . The general form of this nonideal case was treated in the previous chapter. The closed-loop equation is

$$\underline{A} - \underline{BK} = \begin{bmatrix} 0 & 1 & 0 & 0 \\ 0-.035k_{11} & -.15-.035k_{12} & -1.5 \times 10^{-4}-.035k_{13} & -1.5 \times 10^{-4}-.035k_{14} \\ -.02k_{21} & -.02k_{22} & -.02k_{23} & -.02k_{24} \\ 32-.56k_{21} & 0-.56k_{22} & -.02-.56k_{23} & -.038-.56k_{24} \\ 0-3.6k_{31} & 0-3.6k_{32} & 0-3.6k_{33} & -.021-3.6k_{34} \end{bmatrix} \quad (I-28)$$

Comparing Equation (I-27) with Equation (I-28), the control matrix is found to be

$$\underline{K} = \begin{bmatrix} 146.94 & 81.43 & -0.60 & 0.03 \\ -57.14 & 0. & 1.03 & -0.06 \\ 0. & 0. & 0. & 0.16 \end{bmatrix} \quad (I-29)$$

The next step is to determine  $\underline{P}$  and  $\underline{Q}$  which, when used in conjunction with optimal control theory, would yield the same matrix  $\underline{K}$ . Following the same procedure as given in the example of Chapter 2 a set of positive semi-definite matrices  $\underline{P}$  and  $\underline{Q}$ , which yields Equation (I-10) as the optimal solution was found. This set one solution to inverse quadratic optimization problem for the X-14B airplane is

$$\underline{\underline{P}} = \begin{bmatrix} 50.000 & 28.416 & -.32301 \\ 28.416 & 17.150 & -244.47 \\ -.32301 & -244.47 & 60676. \end{bmatrix}, \quad (I-30)$$

$$\underline{\underline{Q}} = \begin{bmatrix} 649794. & 0 & -20.918 & 71.434 \\ 0 & 39392. & 116.83 & -3872.8 \\ -20.918 & 116.83 & 1.1395 & -43.576 \\ 71.434 & -3872.8 & -43.576 & 1683.6 \end{bmatrix}. \quad (I-31)$$

The corresponding solution to the steady state Riccati equation is given by

$$\underline{\underline{S}} = \begin{bmatrix} 489834. & 163518. & -133.74 & 3867.3 \\ 163518. & 116327. & -22.548 & -7.3061 \\ -133.74 & -22.548 & 1.8539 & -70.279 \\ 2867.3 & -7.3061 & -70.279 & 2715.3 \end{bmatrix}. \quad (I-32)$$

As a check, the above values of  $\underline{\underline{P}}$  and  $\underline{\underline{Q}}$  were used in the performance index (I-1) and the resultant optimal solution, obtained by conventional optimal control theory techniques, was found to be

$$\underline{\underline{\bar{A}}} = \begin{bmatrix} 0.00 & 1.00 & 0.00 & 0.00 \\ -4.00 & -3.00 & 4.77 \times 10^{-4} & -2.17 \times 10^{-9} \\ -2.35 \times 10^{-6} & -1.61 \times 10^{-6} & -0.60 & -1.11 \times 10^{-5} \\ -6.08 \times 10^{-8} & -4.17 \times 10^{-8} & 7.31 \times 10^{-9} & -0.60 \end{bmatrix}.$$

Note that the above matrix is nearly identical to the desired matrix given by (I-29) and, hence, the first part of the controller design problem is complete.

TABLE I-4 SUMMARY OF TIME RESPONSES FOR THE X-14 VERTICAL TAKEOFF AND LANDING AIRCRAFT TO INITIAL CONDITIONS

UNITS ARE -- DEGREES, DEGREES/SECOND AND FEET/SECOND FOR THE STATE VARIABLES,  
AND DEGREES AND POUNDS FOR THE MANIPULATED VARIABLES

			X1(0) = 0	X2(0) = 0	X3(0) = 0	X4(0) = 10					
P(1,1)	P(2,2)	P(3,3)	*	X1MAX	X2MAX	X3MAX	U1MAX	U2MAX	U3MAX		
50.000	17.150	60676.	*	1.842F-07	2.231E-07	6.796E-05	0.345	0.678	206.		
50.000	17.150	61282.	*	8.813F-02	0.101	32.9	49.1	86.5	161.		
50.000	17.150	60069.	*	0.197	0.747	64.5	137.	241.	333.		
50.000	17.321	60676.	*	7.600E-04	7.546E-04	0.276	6.648E-02	0.184	206.		
50.500	17.150	60676.	*	6.506E-04	6.523F-04	0.237	0.101	0.249	206.		
			X1(0) = 0	X2(0) = 0	X3(0) = 10	X4(0) = 0					
P(1,1)	P(2,2)	P(3,3)	*	X1MAX	X2MAX	X4MAX	U1MAX	U2MAX	U3MAX		
50.000	17.150	60676.	*	4.096E-09	4.907E-09	4.479E-08	6.04	10.4	2.609E-06		
50.000	17.150	61282.	*	4.436F-11	5.285E-11	5.191E-11	6.04	10.4	2.693E-09		
50.000	17.150	60069.	*	5.002E-11	6.124E-11	1.012E-10	6.04	10.4	7.551E-09		
50.000	17.321	60676.	*	1.140E-02	1.152E-02	0.109	1.76	2.81	3.89		
50.500	17.150	60676.	*	1.147E-02	1.143E-02	0.108	1.77	2.82	3.89		
			X1(0) = 0	X2(0) = 10	X3(0) = 0	X4(0) = 0					
P(1,1)	P(2,2)	P(3,3)	*	X1MAX	X3MAX	X4MAX	U1MAX	U2MAX	U3MAX		
50.000	17.150	60676.	*	2.19	8.372E-08	2.167E-09	14.2	2.19	2.586E-07		
50.000	17.150	61282.	*	2.19	5.722E-08	1.470E-09	14.2	2.19	1.679E-07		
50.000	17.150	60069.	*	2.19	1.658F-07	4.328E-09	14.2	2.19	5.847E-07		
50.000	17.321	60676.	*	2.19	0.943	2.442E-02	14.4	0.505	0.867		
50.500	17.150	60676.	*	2.19	5.13	0.133	2.28	21.0	10.8		
			X1(0) = 10	X2(0) = 0	X3(0) = 0	X4(0) = 0					
P(1,1)	P(2,2)	P(3,3)	*	X2MAX	X3MAX	X4MAX	U1MAX	U2MAX	U3MAX		
50.000	17.150	60676.	*	8.77	8.069E-08	2.088E-09	25.6	9.97	3.775E-07		
50.000	17.150	61282.	*	8.77	5.231E-08	1.341E-09	25.6	9.97	2.387E-07		
50.000	17.150	60069.	*	8.77	1.812E-07	4.734E-09	25.6	9.97	9.062E-07		
50.000	17.321	60676.	*	8.79	3.08	7.961E-02	21.0	1.87	4.18		
50.500	17.150	60676.	*	8.80	6.37	0.165	3.21	29.5	20.3		
			X1(0) = 10	X2(0) = 10	X3(0) = 10	X4(0) = 10					
P(1,1)	P(2,2)	P(3,3)	*	X1(5)	X2(5)	X3(5)	X4(5)	U1MAX	U2MAX	U3MAX	U TOTAL
50.000	17.150	60676.	*	.863E-02	-.225F-02	0.498	0.498	34.2	2.91	205.9	427.9
50.000	17.150	61282.	*	.265E-01	-.106E-01	17.2	0.937	82.9	86.1	160.9	700.0
50.000	17.150	60069.	*	.286E-02	.307F-02	-15.2	0.084	103.	242.	332.6	1004.0
50.000	17.321	60676.	*	.114E-01	-.299E-02	1.75	0.530	33.7	0.815	206.7	425.5
50.500	17.150	60676.	*	.812F-02	-.240E-02	-.208	0.480	3.82	53.1	233.4	258.2



TABLE I-3  $\mathbb{P}$ ,  $\mathbb{K}$  AND  $\mathbb{A}$  MATRICES FOR DIFFERENT CONTROL WEIGHTING MATRICES

			$\mathbb{P}$					
*****			28.416362			-0.32300667		
28.416362			*****			-244.46929		
-0.32300667			-244.46929			*****		
P(1,1) = 50.000000			P(2,2) = 17.1497930			P(3,3) = 60675.5120		
$\mathbb{K}$			$\mathbb{A}$					
146.939	41.4286	-0.604408	7.447854E-02	0	1.00000	0	0	0
-57.1429	2.875447E-06	1.03571	-6.783733E-02	-4.00000	-3.00000	4.775668E-11	-2.171268E-09	-1.109674E-05
1.689831E-08	1.157546E-08	-2.031496E-09	0.160833	-2.1350788E-06	-1.610250E-06	-0.600000	7.313349E-09	-0.600000
				-6.083391E-08	-4.167164E-08	7.313349E-09		
P(1,1) = 50.000000			P(2,2) = 17.1497930			P(3,3) = 61292.2670		
$\mathbb{K}$			$\mathbb{A}$					
146.939	41.4286	-0.604408	4.491211	0	1.00000	0	0	0
-57.1429	1.983154E-06	1.03571	-8.65069	-4.00000	-3.00000	5.118957E-13	9.395772E-04	4.80638
1.069632E-08	7.514041E-09	-2.103829E-12	0.125699	-1.500635E-06	-1.054566E-06	-0.600000	7.573783E-12	-0.473516
				-3.847075E-08	-2.705343E-08			
P(1,1) = 50.000000			P(2,2) = 17.1497930			P(3,3) = 60069.7570		
$\mathbb{K}$			$\mathbb{A}$					
146.939	41.4286	-0.604408	-13.7111	0	1.00000	0	0	0
-57.1428	6.441320E-06	1.03571	24.1193	-4.00000	-3.00000	6.134097E-13	-2.647011E-03	-13.5448
4.056542E-08	2.617900E-08	-5.899339E-12	0.259845	-5.588095E-06	-3.607139E-06	-0.600000	2.123762E-11	-0.956442
				-1.460355E-07	-9.422640E-08			
P(1,1) = 50.000000			P(2,2) = 17.3212910			P(3,3) = 60675.5120		
$\mathbb{K}$			$\mathbb{A}$					
170.557	42.4405	-0.175930	6.417091E-03	0	1.00000	0	0	0
-19.6970	1.79870	0.281049	-1.841093E-02	-4.00556	-2.99996	9.737335E-05	-6.379633E-06	-2.768988E-02
0.187003	-7.199133E-03	-3.038771E-03	0.161032	-26.0097	1.00167	-0.177365	1.093558E-02	-0.600717
				-0.673212	2.591688E-02			
P(1,1) = 50.500000			P(2,2) = 17.1497930			P(3,3) = 60675.5120		
$\mathbb{K}$			$\mathbb{A}$					
19.4146	13.0307	-0.176676	1.007950E-02	0	1.00000	0	0	0
168.949	120.348	0.282262	-2.486232E-02	-4.02349	-3.01335	9.701452E-05	-5.536012E-06	-2.407710E-02
0.010277	0.484284	-3.033709E-03	0.161006	-126.611	-67.3950	-0.178067	1.092135E-02	-0.600623
				-3.27700	-1.74436			

To determine whether the above controller was acceptable, a linear model and the controller were simulated on the digital computer. Furthermore, the diagonal elements of  $\underline{P}$  were varied by 1 percent sequentially and the corresponding control matrices were determined. These are shown in Table I-3. The resulting closed-loop systems were observed for transients due to initial conditions and the results are shown in Table I-4. The parameters recorded were the maximum values of the state and the input variables. Examination of the data for the exact decoupling controller reveals that the control effort  $u_1$  (reaction bleed control,  $\delta_y$ ) is excessive and should be reduced. The penalty on this variable,  $p_{11}$ , when increased by 1 percent causes a near 90 percent decrease in the maximum value of  $u_1$ . This was evaluated to be the most desirable of the controllers presented in Table I-3. With this choice of  $p_{11}$ , the final closed-loop configuration selected is

$$\underline{\bar{A}} = \begin{bmatrix} 0 & 1.00 & 0 & 0 \\ -4.023 & -3.013 & 9.701 \times 10^{-5} & -5.536 \times 10^{-6} \\ -126.6 & -67.40 & -.1781 & -2.408 \times 10^{-2} \\ -3.277 & -1.744 & 1.092 \times 10^{-2} & -0.6005 \end{bmatrix}$$

The disadvantage of this design is that there is some unilateral coupling. That is, pitch and pitch rate ( $\theta$  and  $q$ ) disturb the forward and vertical velocities ( $u$  and  $w$ ), but the last two affect  $\theta$  and  $q$  only minimally. Thus, the "best" controller selected is

$$\underline{K} = \begin{bmatrix} 18.416 & 13.040 & -0.176 & 0.010 \\ 168.949 & 120.348 & 0.282 & -0.025 \\ 0.911 & 0.484 & -0.003 & 0.161 \end{bmatrix} .$$

### 3.5 Conclusions

One of the goals of this study was the development of a suboptimal decoupling technique for general systems. Even though the theory of optimal control is well defined, it suffers from the fact that it is difficult to prescribe a meaningful performance index. When a degree of decoupling is desired in a controlled system, there is no means of specifying a performance index which would provide a decoupling controller. Thus the problem was investigated in a reverse order. A decoupling control policy was determined and then an attempt was made to find a performance index which, when used in a standard fashion, yielded the desired closed-loop system. The objective was to manipulate the known performance index to strike a balance between the degree of tolerable coupling and some criteria on magnitudes of states and inputs of the system.

The elements of the performance index were perturbed a finite amount, one element at a time. The resulting control policies were evaluated and the most desirable policy was finally selected. There was an increase in coupling with the new policy, but that was off set by the large decrease in the amount of control needed to maintain the airplane in the proper attitude.

The technique developed in the foregoing appears to be quite promising. Additional work, however, is necessary to define the most desirable type of control action.

## REFERENCES

1. Morse, A. S., "Status of Noninteracting Control", IEEE Trans. Automat. Contr., vol. AC-16, pp. 568-581, December, 1971.
2. Morgan, B. S. Jr., "The Synthesis of Linear Multivariable Systems by State Variable Feedback", in Proc. 1964 Joint Automat. Contr. Conf., pp. 468-472.
3. Rekasius, Z. V., "Decoupling of Multivariable Systems by Means of State Variable Feedback", Proc. Third Ann. Allerton Conf. on Circuit and System Theory, (Urbana, Ill., 1965), pp. 439-447.
4. Falb, P. L. and W. A. Wolovich, "On the Decoupling of Multivariable Systems", Preprints, 1967 JACC (Philadelphia, Pa.), pp. 791-796.
5. Falb, P. L. and W. A. Wolovich, "Decoupling in the Design and Synthesis of Multivariable Control Systems", IEEE Trans. Automat., vol. AC-12, pp. 651-659, December, 1967.
6. Gilbert, E. G., "The Decoupling of Multivariable Systems by State Feedback", SIAM J. Contr., vol. 7, pp. 50-63, February, 1969.
7. Gilbert, E. G. and J. R. Pivnichny, "A Computer Program for the Synthesis of Decoupled Multivariable Feedback Systems", IEEE Trans. Automat. Contr., vol. AC-14, pp. 651-659, December, 1969.
8. Silivinsky, C. R. and D. G. Schultz, "State Variable Feedback Decoupling and Design of Multivariable Systems", Tenth Ann. JACC (Boulder, Colo., August, 1969), pp. 869-876.
9. Silverman, L. M., "Decoupling with State Feedback and Precompensation", IEEE Trans. Automat. Contr., vol. AC-15, pp. 487-489, August, 1970.
10. Wonham, W. M. and A. S. Morse, "Decoupling and Pole Assignment in Linear Multivariable Systems: A Geometric Approach", SIAM J. Contr., vol. 8, pp. 1-18, February, 1970.
11. Sato, S. M. and P. V. Lopresti, "On The Generalization of State Feedback Decoupling Theory", IEEE Trans. Automat. Contr., vol. AC-16, pp. 133-139, April, 1971.
12. Cremer, M., "A Precompensator of Minimal Order for Decoupling a Linear Multivariable System", Int. J. Contr., vol. 14, pp. 1189-1103, 1971.
13. Marsh, K. R., J. J. Santamaria, and R. B. English, "Summary of Ling-Temco-Vought Feasibility Studies", NASA SP-116, pp. 353-387, April, 1966.
14. Miller, R. H. and R. W. Simpson, "V/STOL in the Northeast Corridor", Astronautics and Aeronautics, pp. 28-34, September, 1968.

15. Solheim, O. A., "Design of Optimal Control Systems with Prescribed Eigenvalues", *Int. J. Control*, Vol. 15, No. 1, pp. 143-160, 1972.
16. Mueller, Leo J., "Problems Unique to VTOL Automatic Flight-Control", *J. Aircraft*, 2, No. 5, pp. 357-360, September - October, 1965.
17. Marsh, K. R., "Study on the Feasibility of V/STOL Concepts for Transport Aircraft", NASA CR-670, January, 1967.
18. Lee, Y. S. et al., "Three-Axis (Self-Organizing) VTOL Flight Control System for Comparing Rate, Altitude and Velocity Commands", Tech. Rept. AFFDL-TR-69-34, June, 1969.
19. Casteal, G. R. and J. F. Hardesty, "Preliminary Analysis of XV-4B Longitudinal Interference Effects in Transition Flight", North Amer. Rockwell, L. A. Division, 10, April, 1968.
20. Henderson, D., J. Kroll, and A. Hesby, "Control Characteristics of V/STOL Aircraft in Transition", Report No. 2023-917002; AD 28308, 1, July, 1962.
21. Hirsch, D. L., W. W. Stark, and W. B. Morris, "Reaction Control System Preliminary Design Considerations for Jet-Lift Research Aircraft", AGARD Conf. Proc. No. 27, September, 1967.
22. Holladay, W. L. and J. E. Campbell, "VTOL Flight Control Design Considerations for IFR Landing", Presented at the V/STOL Technology and Planning Conference sponsored by Air Force Flight Dynamics Laboratory, pp. 23-25, September, 1969.
23. Seckel, E., Stability and Control of Airplanes and Helicopters, Academic Press, New York and London, 1964.
24. Sturcke, Erick H., "Interactive Graphics in Aircraft Landing and Take-Off Studies", Proc. of the Conf. on Applications of Continuous System Simulation Languages, June 30 - July 1, 1969, San Francisco, Calif., Sponsored by ACM/IEEE/SHARE/SC.
25. Trueblood, R. B., "Advanced Flight Control Concepts for VTOL Aircraft", AGARD, Conf. Proc., No. 7, January, 1966.
26. Kirby, R. H., and J. R. Chambers, "Flight Investigation of Dynamic Stability and Control Characteristics of 0.18- Scale Model of Fan-In-Wing VTOL Airplane", NASA TN-D-3412, August, 1966.
27. Patierno, J., and H. Asourvan, "Impact of Jet VTOL Altitude Control on Mission Performance", Northrop Norair, AFFDL, WPAFB, 1965.
28. Niessen, F. R., "Simultaneous Usage of Altitude Control for VTOL Maneuvering Determined by In-Flight Simulation," NASA TN-D-5342, July, 1969.
29. Anderson, S. B., "Considerations for Revision of V/STOL Handling Qualities Criteria", NASA SP-116, pp. 229-247, April, 1966.

30. Rahenberg, B., "Operational VTOL Control Data Technology", North Amer. pp. 68-151, 1968.
31. Grief, R. K., E. B. Fry, T. D. Gossett, R. M. Gerdes, "Simulator Investigations of Various Control Systems for VTOL Aircraft", NASA SP-116, April, 1966.
32. Garren, J. F. Jr., and J. R. Kelly, "Flight Study of On-Off Control for V/STOL Aircraft", Conf. on V/STOL and STOL Aircraft, NASA SP-116, pp. 4-5, April, 1966.
33. Mormino, M. A., "Synthesis of Optimal VTOL Handling Qualities Control Systems", North Amer. Rockwell, L. A. Division, AS-68-144, April, 1968.
34. Porter, W. A., "Decoupling of and Inverses for Time-Varying Linear Systems", IEEE Trans. Automat. Contr., vol. AC-14, pp. 378-380, August, 1969.
35. Yore, E., "Optimal Decoupling Control, Proc. 1968 Joint Automat. Contr. Conf., pp. 327-336, 1968.

## APPENDIX A

DEVELOPMENT OF THE EQUATIONS OF MOTION FOR THE X-14 AIRCRAFT

## A. General Equations of Motion for VTOL Aircraft

This development of the equations of motion for a VTOL aircraft assumes the aircraft is rigid and the origin of the coordinate system is at the mass center [1, 2, 3]. Additional assumptions used in this development of the equations of motion are:

1. The VTOL aircraft has diverters and vanes affecting the engine exhaust.
2. Any wind disturbance is irrotational.
3. Engines rotate in the same direction at the same speed.

A standard aircraft body axis system is used where the aircraft is symmetric about the x-z plane with the positive y-axis pointing out the right wing, the z-axis down, and the x-axis in the forward direction of flight (stability axes). This is a right-handed coordinate system.

For the system, the velocities, angles, angular velocities, forces and moments associated with each axis are shown in Table A-I-1 and Figure A-I-1 [4].

Table A-I-1

<u>Axis</u>	<u>Linear Velocity</u>	<u>Force</u>	<u>Angle</u>	<u>Angular Velocity</u>	<u>Moment</u>
X	u	$F_x$	$\phi$	$\dot{p}$	L
Y	v	$F_y$	$\theta$	q	M
Z	w	$F_z$	$\psi$	r	N

From Etkin [1], the time derivative of the angular quantities can be expressed as

$$\dot{\theta} = q \cos \phi - r \sin \phi$$

$$\dot{\phi} = p + q \sin \phi \tan \theta + r \cos \phi \tan \theta$$

$$\dot{\psi} = (q \sin \phi + r \cos \phi) / \cos \theta$$

Since the analysis is for a VTOL aircraft, it becomes necessary to introduce some notation not normally found in airplane equations. A listing of this additional notation is in Figure A-I-2.

### Inertial Forces

In writing the equations of motion, all inertial components are expressed as D'Alembert forces, i.e.,

$$\Sigma F_{\text{external}} + \Sigma F_{\text{inertial}} = 0$$

where

$$\Sigma F_{\text{inertial}} = -ma$$

Using this notation the inertial forces along the three axes are

$$F_{xi} = -m (\dot{u} + wq - vr)$$

$$F_{yi} = -m (\dot{v} - wp + ur)$$

$$F_{zi} = -m (\dot{w} - uq + vp)$$

Likewise, the moments are

$$M_{xi} = -\dot{p} I_x + qr (I_y - I_z) + (\dot{r} + pq) I_{xz}$$

$$M_{yi} = -\dot{q} I_y + pr (I_z - I_x) + (r^2 - p^2) I_{xz}$$

$$M_{zi} = -\dot{r} I_z + pq (I_x - I_y) + (p - qr) I_{xz}$$



Figure A-I-2

## Definitions of Non-standard Notation

1.  $w$  subscript is for wind velocity
2.  $V_j$  = jet exhaust velocity from the diverters
3.  $\sigma$  = thrust diverter angle measured in the vertical plane from the positive z-axis
4.  $\lambda$  = exhaust side vane angle measured positive about the x-axis by the right hand rule
5.  $U_0 = [(u - u_w)^2 + (w - w_w)^2]^{1/2}$
6.  $\bar{U}_0 = [(u - u_w)^2 + (w - w_w)^2 + (v - v_w)^2]^{1/2}$
7.  $\alpha$  = angle of attack;  $\sin \alpha = (w - w_w)/U_0$
8.  $\beta$  = side slip angle;  $\sin \beta = (v - v_w)/\bar{U}_0$
9.  $x_1$  = distance engine intake is in front of the center of gravity
10.  $z_1$  = distance engine intake is below the center of gravity
11.  $x_2$  = distance engine exhaust pivot point is in front of the center of gravity
12.  $z_2$  = distance engine exhaust pivot point is below the center of gravity
13.  $l_1$  is the effective length where the exhaust will impinge on the diverter vane from the end of the jet engine
14.  $I_e$  = moment of inertia of one engine about the axis of rotation
15.  $\Omega_e$  = angular velocity of an engine measured positive in the direction of the x-axis
16. N.E. = number of engines
17. T = total thrust from the diverters
18.  $L_p, M_q, N_r$  apparent aerodynamic damping near hover not directly attributable to the effects caused by  $C_{l_p}, C_{m_q}, C_{n_r}$
19.  $L_{\delta_x}, M_{\delta_y}, N_{\delta_z}$  Moment effects due to reaction control nozzles

20.  $V_{j_0}$  = jet velocity at the engine exhaust
21.  $T_0$  = total installed jet thrust
22.  $\xi_{\sigma}$  = longitudinal diverter efficiency factor
23.  $\xi_{\lambda}$  = lateral diverter vane efficiency factor

where

$$I_x \triangleq \int (y^2 + z^2) dm, \quad I_y \triangleq \int (x^2 + z^2) dm, \quad I_z \triangleq \int (x^2 + y^2) dm$$

$$I_{xz} \triangleq \int xz dm, \quad I_{xy} \triangleq \int xy dm, \quad I_{yz} \triangleq \int yz dm$$

with

$$I_{xy} = 0 \text{ and } I_{yz} = 0$$

since the aircraft is symmetric about the xz plane.

In addition to aircraft inertial terms, there is a contribution from the rotation of the engines to the moment equations. If the engine speed is almost constant, the contribution to the moment equations can be expressed as

$$M_{e_x} = 0$$

$$M_{e_y} = (N.E.) I_e \Omega_e r$$

$$M_{e_z} = -(N.E.) I_e \Omega_e q$$

### Gravitational Forces

Since the origin of the coordinate system is at the center of gravity, the gravitational forces do not enter into the moment equations. Their contribution to the force equations is

$$F_{x_g} = -W \sin \theta$$

$$F_{y_g} = W \sin \phi \cos \theta$$

$$F_{z_g} = W \cos \phi \cos \theta$$

### Mass Flow Effects

There are two contributions to mass flow effects, one at the engine intakes and a second effect at the engine exhausts. If the mass of the fuel burned is neglected, the forces due to the mass flow can be expressed as

$$F_{x_m} = -\dot{m} (u - u_w - V_j \sin \sigma \cos \lambda)$$

$$F_{y_m} = -\dot{m} (v - v_w - V_j \sin \lambda)$$

$$F_{z_m} = -\dot{m} (w - w_w + V_j \cos \sigma \cos \lambda)$$

where  $\dot{m}$  is the entering mass flow rate which is approximately equal to the mass flow rate out,  $V_j$  is the relative exhaust velocity of the jet,  $\sigma$  is the diverter angle, and  $\lambda$  is the side vane angle. Recalling that the gross thrust equals mass flow rate times relative velocity,

$$T = \dot{m} V_j$$

or

$$\dot{m} = \frac{T}{V_j}$$

Upon making this substitution, the mass flow contributions to the equations of motion can be written as

$$F_{x_{\dot{m}}} = T [\sin \sigma \cos \lambda - (u - u_w)/V_j]$$

$$F_{y_{\dot{m}}} = T [\sin \lambda - (v - v_w)/V_j]$$

$$F_{z_{\dot{m}}} = -T [\cos \sigma \cos \lambda + (w - w_w)/V_j]$$

The mass flow contributions to the moment equations enter in because the intakes and exhausts are not at the center of gravity. The moments are

$$M_{x_{\dot{m}_{in}}} = T z_1 (v - v_w)/V_j$$

$$M_{y_{\dot{m}_{in}}} = T [x_1 (w - w_w) - z_1 (u - u_w)]/V_j$$

$$M_{z_{\dot{m}_{in}}} = -T x_1 (v - v_w)/V_j$$

where  $x_1$  and  $z_1$  are the distances from the center of gravity to the center of the intakes. The moments caused by the exhaust are

$$M_{x_{\dot{m}_{out}}} = -T \sin \lambda (z_2 + \ell_1 \cos \sigma)$$

$$M_{y_{\dot{m}_{out}}} = T \cos \lambda (z_2 \sin \sigma + x_2 \cos \sigma)$$

$$M_{z_{\dot{m}_{out}}} = T \sin \lambda (x_2 - \ell_1 \sin \sigma)$$

where  $x_2$  and  $z_2$  are the distances from the center of gravity to the center of the exhausts, and  $\ell_1$  is the effective length where the exhaust will impinge on the diverter vane.

The total moments caused by engine mass flow terms can now be expressed as

$$\begin{aligned} M_{x_m} &= T [-\sin \lambda (z_2 + \ell_1 \cos \sigma) + z_1 (v - v_w)/V_j] \\ M_{y_m} &= T \{ \cos \lambda (z_2 \sin \sigma + x_2 \cos \sigma) + [x_1 (w - w_w) - z_1 (u - u_w)]/V_j \} \\ M_{z_m} &= T [\sin \lambda (x_2 - \ell_1 \sin \sigma) - x_1 (v - v_w)/V_j] \end{aligned}$$

Additional moments are caused by discharge nozzles in the tail and on the wing tips. These reaction control moments can be written as

$$\begin{aligned} M_{x_{R.C.}} &= L_{\delta_x} \delta_x \\ M_{y_{R.C.}} &= M_{\delta_y} \delta_y \\ M_{z_{R.C.}} &= N_{\delta_z} \delta_z \end{aligned}$$

where  $\delta_x$ ,  $\delta_y$  and  $\delta_z$  are the reaction nozzle openings expressed in degrees.

### Aerodynamic Expressions

The complete aerodynamic expressions for a conventional airplane can be written as

$$\begin{aligned} X_{aero} &= \frac{\rho}{2} U_o^2 S C_x \\ Y_{aero} &= \frac{\rho}{2} \bar{U}_o^2 S C_y \\ Z_{aero} &= \frac{\rho}{2} U_o^2 S C_z \\ L_{aero} &= \frac{\rho}{2} \bar{U}_o^2 S b C_\ell \\ M_{aero} &= \frac{\rho}{2} U_o^2 S c C_m \\ N_{aero} &= \frac{\rho}{2} \bar{U}_o^2 S b C_n \end{aligned}$$

where  $C_x$ ,  $C_y$ ,  $C_z$ ,  $C_\ell$ ,  $C_m$  and  $C_n$  are the non-dimensional aerodynamic coefficients,  $\rho$  is the air density,  $U_o = [(u - u_w)^2 + (w - w_w)^2]^{1/2}$ ,  $\bar{U}_o = [(u - u_w)^2 + (w - w_w)^2 + (v - v_w)^2]^{1/2}$ ,  $S$  is the wing area,  $b$  is the span and  $c$  is the wing chord.

Now use a Taylor series expansion of the non-dimensional aerodynamic forces retaining only the first terms in the series [1, 2] and let the vehicle velocities relative to the air mass be denoted by  $u_{rel} \stackrel{\Delta}{=} u - u_w$ ,  $v_{rel} \stackrel{\Delta}{=} v - v_w$  and  $w_{rel} \stackrel{\Delta}{=} w - w_w$ . Then,

$$C_x = C_{x_0} + \frac{\partial C_x}{\partial \alpha} \alpha + \frac{\partial C_x}{\partial u} u_{rel} + \frac{\partial C_x}{\partial \delta_e} \delta_e$$

$$C_y = C_{y_0} + \frac{\partial C_y}{\partial \beta} \beta + \frac{\partial C_y}{\partial p} p + \frac{\partial C_y}{\partial r} r + \frac{\partial C_y}{\partial \delta_r} \delta_r$$

$$C_z = C_{z_0} + \frac{\partial C_z}{\partial \alpha} \alpha + \frac{\partial C_z}{\partial u} u_{rel} + \frac{\partial C_z}{\partial q} q + \frac{\partial C_z}{\partial \dot{\alpha}} \dot{\alpha} + \frac{\partial C_z}{\partial \delta_e} \delta_e$$

$$C_l = C_{l_0} + \frac{\partial C_l}{\partial \beta} \beta + \frac{\partial C_l}{\partial p} p + \frac{\partial C_l}{\partial r} r + \frac{\partial C_l}{\partial \delta_a} \delta_a + \frac{\partial C_l}{\partial \delta_r} \delta_r$$

$$C_m = C_{m_0} + \frac{\partial C_m}{\partial \alpha} \alpha + \frac{\partial C_m}{\partial u} u_{rel} + \frac{\partial C_m}{\partial q} q + \frac{\partial C_m}{\partial \dot{\alpha}} \dot{\alpha} + \frac{\partial C_m}{\partial \delta_e} \delta_e$$

$$C_n = C_{n_0} + \frac{\partial C_n}{\partial \beta} \beta + \frac{\partial C_n}{\partial p} p + \frac{\partial C_n}{\partial r} r + \frac{\partial C_n}{\partial \delta_a} \delta_a + \frac{\partial C_n}{\partial \delta_r} \delta_r$$

where  $\alpha$  is the angle of attack ( $\sin \alpha = w_{rel}/U_0$ ),  $\beta$  is the side slip angle ( $\cos \beta = U_0/\bar{U}_0$ ), and  $\delta_e$ ,  $\delta_a$  and  $\delta_r$  are the elevator, aileron and rudder deflections, respectively.

Following Etkin [2], if the partial derivatives are written as non-dimensional stability derivatives, the aerodynamic portions of the equations of motion become

$$X_{aero} = \frac{\rho}{2} U_0^2 S [C_{x_0} + C_{x_\alpha} \alpha + \frac{1}{U_0} C_{x_u} u_{rel} + C_{x_{\delta_e}} \delta_e]$$

$$Y_{aero} = \frac{\rho}{2} \bar{U}_0^2 S [C_{y_0} + C_{y_\beta} \beta + \frac{b}{2\bar{U}_0} C_{y_p} p + \frac{b}{2\bar{U}_0} C_{y_r} r + C_{y_{\delta_r}} \delta_r]$$

$$Z_{aero} = \frac{\rho \bar{U}_0^2}{2} S [C_{z_0} + C_{z_\alpha} \alpha + \frac{1}{U_0} C_{z_u} u_{rel} + \frac{c}{2\bar{U}_0} C_{z_q} q + \frac{c}{2\bar{U}_0} C_{z_{\dot{\alpha}}} \dot{\alpha} + C_{z_{\delta_e}} \delta_e]$$

$$L_{\text{aero}} = \frac{\rho}{2} \bar{U}_o^2 S b [C_{l_o} + C_{l_\beta} \beta + \frac{b}{2\bar{U}_o} C_{l_p} p + \frac{b}{2\bar{U}_o} C_{l_r} r + C_{l_{\delta_a}} \delta_a + C_{l_{\delta_r}} \delta_r]$$

$$M_{\text{aero}} = \frac{\rho}{2} U_o^2 S c [C_{m_o} + C_{m_\alpha} \alpha + \frac{1}{U_o} C_{m_u} u_{\text{rel}} + \frac{c}{2U_o} C_{m_q} q + \frac{c}{2U_o} C_{m_{\dot{\alpha}}} \dot{\alpha} + C_{m_{\delta_e}} \delta_e]$$

$$N_{\text{aero}} = \frac{\rho}{2} \bar{U}_o^2 S b [C_{n_o} + C_{n_\beta} \beta + \frac{b}{2\bar{U}_o} C_{n_p} p + \frac{b}{2\bar{U}_o} C_{n_r} r + C_{n_{\delta_a}} \delta_a + C_{n_{\delta_r}} \delta_r]$$

In addition to these stability derivatives normally found in airplane equations, for VTOL aircraft it is desirable to add the rotational damping observed on a hovering airplane. This can be expressed as.

$$L_{\text{aero VTOL}} = L_p p$$

$$M_{\text{aero VTOL}} = M_q q$$

$$N_{\text{aero VTOL}} = N_r r$$

After summing the component parts, the complete non-linear equations of motion for a VTOL aircraft can be written as in Fig. A-I-3.

Figure A-I-3

## Summary of Complete Non-linear Equations of Motion for a VTOL Aircraft

$$\dot{u} = vr - wq - g \sin \theta + \frac{T}{m} \left[ \sin \sigma \cos \lambda - \frac{1}{V_j} (u - u_w) \right] \quad (\text{A-I-1})$$

$$+ \frac{1}{2m} \rho U_0^2 S \left[ C_{x_0} + C_{x_\alpha} \alpha + \frac{1}{U_0} C_{x_u} (u - u_w) + C_{x_{\delta_e}} \delta_e \right]$$

$$\dot{v} = wp - ur + g \sin \phi \cos \theta + \frac{T}{m} \left[ \sin \lambda - \frac{1}{V_j} (v - v_w) \right] + \frac{\rho \bar{U}_0^2 S}{2m} \quad (\text{A-I-2})$$

$$\left[ C_{Y_0} + C_{Y_\beta} \beta + \frac{b}{2\bar{U}_0} C_{Y_p} p + \frac{b}{2\bar{U}_0} C_{Y_r} r + C_{Y_{\delta_r}} \delta_r \right]$$

$$\dot{w} = uq - vp + g \cos \phi \cos \theta - \frac{T}{m} \left[ \cos \sigma \cos \lambda + \frac{1}{V_j} (w - w_w) \right]$$

$$+ \frac{\rho U_0^2 S}{2m} \left[ C_{z_0} + C_{z_\alpha} \alpha + \frac{1}{U_0} C_{z_u} (u - u_w) + \frac{c}{2U_0} C_{z_q} q \right] \quad (\text{A-I-3})$$

$$+ \frac{c}{2U_0} C_{z_{\dot{\alpha}}} \dot{\alpha} + C_{z_{\delta_e}} \delta_e \right]$$

$$\dot{p} = \frac{(I_y - I_z)}{I_x} qr + \frac{I_{xz}}{I_x} (\dot{r} + pq) + \frac{T}{I_x} [-\sin \lambda (z_2 + l_1 \cos \sigma)$$

$$+ \frac{z_1}{V_j} (v - v_w)] + \frac{L_p}{I_x} p + \frac{L_\delta}{I_x} \delta_x + \rho \frac{\bar{U}_0^2 S b}{2I_x} [C_{l_0} + C_{l_\beta} \beta] \quad (\text{A-I-4})$$

$$+ \frac{b}{2\bar{U}_0} C_{l_p} p + \frac{b}{2\bar{U}_0} C_{l_r} r + C_{l_{\delta_a}} \delta_a + C_{l_{\delta_r}} \delta_r]$$

$$\dot{q} = \frac{(I_z - I_x)}{I_y} pr + \frac{I_{xz}}{I_y} (r^2 - p^2) - \frac{1}{I_y} (\text{N.E.}) I_e \Omega_e r + \frac{T}{I_y}$$

$$\left\{ \cos \lambda (z_2 \sin \sigma + x_2 \cos \sigma) + \frac{1}{V_j} [x_1 (w - w_w) - z_1 (u - u_w)] \right\}$$



$$+ \frac{M_q}{I_y} q + \frac{M_{\delta y}}{I_y} \delta y + \frac{\rho U_0^2 S c}{2I_y} [C_{m_0} + C_{m_\alpha} \alpha + \frac{1}{U_0} C_{m_u} (u - u_w)]$$

(A-I-5)

$$+ \frac{C}{2U_0} C_{m_q} q + \frac{C}{2U_0} C_{m_{\dot{\alpha}}} \dot{\alpha} + C_{m_{\delta_e}} \delta_e]$$

$$\dot{r} = \frac{(I_x - I_y)}{I_z} pq + \frac{I_{xz}}{I_z} (\dot{p} - qr) + \frac{1}{I_z} (N.E.) I_e \Omega_e q$$

$$+ \frac{T}{I_z} [\sin \lambda (x_2 - \ell_1 \sin \sigma) - \frac{x_1}{V_j} (v - v_w)] + \frac{N_r}{I_z} r$$

(A-I-6)

$$+ \frac{N_{\delta_z}}{I_z} \delta_z + \frac{\rho \bar{U}_0^2 S b}{2I_z} [C_{n_0} + C_{n_\beta} \beta + \frac{b}{2\bar{U}_0} C_{n_p} p + \frac{b}{2\bar{U}_0} C_{n_r} r$$

$$+ C_{n_{\delta_a}} \delta_a + C_{n_{\delta_r}} \delta_r]$$

Figure A-I-4

Summary of the Reduced Non-Linear Equations of Motion for the X-14 Aircraft

$$\begin{aligned} \dot{u} = & vr - wq - g \sin \theta + \frac{T}{m} \left[ \sin \sigma \cos \lambda - \frac{1}{V_j} (u - u_w) \right] \\ & + \frac{1}{2m} \rho U_0^2 S \left[ (C_{L_{p. off}} + \Delta C_L) \sin \alpha - C_D \cos \alpha \right] \end{aligned} \quad (A-I-7)$$

$$\dot{v} = wp - ur + g \sin \phi \cos \theta + \frac{T}{m} \left[ \sin \lambda - \frac{1}{V_j} (v - v_w) \right] + \frac{1}{2m} \rho \bar{U}_0^2 S C_Y \quad (A-I-8)$$

$$\begin{aligned} \dot{w} = & uq - vp + g \cos \phi \cos \theta - \frac{T}{m} \left[ \cos \sigma \cos \lambda + \frac{1}{V_j} (w - w_w) \right] \\ & - \frac{1}{2m} \rho U_0^2 S \left[ (C_{L_{p. off}} + \Delta C_L) \cos \alpha + C_D \sin \alpha \right] \end{aligned} \quad (A-I-9)$$

$$\begin{aligned} \dot{p} = & \frac{(I_y - I_z)}{I_x} qr + \frac{I_{xz}}{I_x} (\dot{r} + pq) + \frac{T}{I_x} \left[ -\sin \lambda (z_2 + \ell_1 \cos \sigma) + \frac{z_1}{V_j} (v - v_w) \right] \\ & + \frac{L_p}{I_x} p + \frac{L_{\delta_x}}{I_x} \delta_x + \frac{1}{2I_x} \rho \bar{U}_0^2 S b \left( C_{\ell_0} + C_{\ell_{\delta_a}} \delta_a \right) \end{aligned} \quad (A-I-10)$$

$$\begin{aligned} \dot{q} = & \frac{(I_z - I_x)}{I_y} pr + \frac{I_{xz}}{I_y} (r^2 - p^2) - \frac{1}{I_y} 2 I_e \Omega_e r + \frac{T}{I_y} \cos \lambda \\ & (z_2 \sin \sigma + x_2 \cos \sigma) + \frac{1}{V_j} [x_1 (w - w_w) - z_1 (u - u_w)] \\ & + \frac{M_q}{I_y} q + \frac{M_{\delta_y}}{I_y} \delta_y + \frac{1}{2I_y} \rho U_0^2 S c \left[ (C_{m_0} + \Delta C_{m_0}) \right. \\ & \left. + (C_{m_{\alpha_{p. off}}} + \Delta C_{m_{\alpha}}) \alpha + \frac{c}{2U_0} C_{m_q} q + C_{m_{\delta_e}} \delta_e \right] \end{aligned} \quad (A-I-11)$$

$$\begin{aligned} \dot{r} = & \frac{(I_x - I_y)}{I_z} pq + \frac{I_{xz}}{I_z} (\dot{p} - qr) + \frac{1}{I_z} 2 I_e \Omega_e q \\ & + \frac{T}{I_z} \left[ \sin \lambda (x_2 - \ell_1 \sin \sigma) - \frac{x_1}{V_j} (v - v_w) \right] + \frac{N_r}{I_z} r + \frac{N_{\delta_z}}{I_z} \delta_z \\ & + \frac{1}{2I_z} \rho \bar{U}_0^2 S b \left( C_{n_0} + C_{n_{\delta_r}} \delta_r + C_{n_{\delta_a}} \delta_a \right) \end{aligned} \quad (A-I-12)$$

## B. Application of the Equations of Motion to the X-14 Aircraft

Several of the above aerodynamic stability derivatives have a very small effect in the representation of the dynamics of the X-14. The determination of which stability derivatives have this insignificant effect was based upon examination of wind tunnel data and a knowledge of the physical airplane. The final justification for retaining or neglecting different stability derivatives comes from the fact that an analytical model was obtained which when used in simulator studies closely approximated the physical airplane [5]. Using these findings the above aerodynamic contribution to the equations of motion can be expressed as

$$X_{\text{aero}} = \frac{\rho}{2} U_o^2 S (C_L \sin \alpha - C_D \cos \alpha)$$

$$Y_{\text{aero}} = \frac{\rho}{2} \bar{U}_o^2 S C_Y$$

$$Z_{\text{aero}} = -\frac{\rho U_o^2}{2} S (C_L \cos \alpha + C_D \sin \alpha)$$

$$L_{\text{aero}} = \frac{\rho}{2} \bar{U}_o^2 S b (C_{l_o} + C_{l_{\delta_a}} \delta_a) + I_p p$$

$$M_{\text{aero}} = \frac{\rho}{2} U_o^2 S c (C_{m_o} + C_{m_{\alpha}} \alpha + \frac{c}{2U_o} C_{m_q} q + C_{m_{\delta_e}} \delta_e) + M_q q$$

$$N_{\text{aero}} = \frac{\rho}{2} \bar{U}_o^2 S b (C_{n_o} + C_{n_{\delta_r}} \delta_r + C_{n_{\delta_a}} \delta_a) + N_r r$$

where  $C_L$  is the non-dimensional lift coefficient and  $C_D$  is the drag coefficient [2].

Continuing to follow the development in reference [5], some of the above "power on" stability derivatives are expressed as "power off" plus " $\Delta$ " terms where the " $\Delta$ " represents the difference between power on and power off effects. The aerodynamic portion of the equations of motion now becomes

$$X_{\text{aero}} = \frac{\rho}{2} U_o^2 S [(C_{L_{\text{power off}}} + \Delta C_L) \sin \alpha - C_D \cos \alpha]$$

$$Y_{\text{aero}} = \frac{\rho}{2} \bar{U}_o^2 S C_Y$$

$$Z_{\text{aero}} = -\frac{\rho}{2} U_o^2 S [(C_{L_{\text{power off}}} + \Delta C_L) \cos \alpha + C_D \sin \alpha]$$

$$L_{\text{aero}} = \frac{\rho}{2} \bar{U}_o^2 S b (C_{l_o} + C_{l_{\delta_a}} \delta_a) + L_p p$$

$$M_{\text{aero}} = \frac{\rho}{2} U_o^2 S c [(C_{m_{\text{power off}}} + \Delta C_M) + (C_{m_{\alpha_{\text{power off}}}} + \Delta C_{M_{\alpha}}) \alpha \\ + \frac{C}{2U_o} C_{m_q} q + C_{m_{\delta_e}} \delta_e] + M_q q$$

$$N_{\text{aero}} = \frac{\rho}{2} \bar{U}_o^2 S b (C_{n_o} + C_{n_{\delta_r}} \delta_r + C_{n_{\delta_a}} \delta_a) + N_r r$$

Upon incorporating these expressions for the aerodynamic forces in the complete equations of motion, the reduced non-linear equations of motion for the X-14 can be written as in Fig. A-I-4.

These equations can be put in state variable form by eliminating the derivative terms from the right hand side of equations (A-I-10) and A-1-12). Rewrite the equations as

$$\begin{aligned} I_x \dot{p} &= I_{xz} \dot{r} + L^* \\ I_z \dot{r} &= I_{xz} \dot{p} + N^* \end{aligned} \tag{A-I-13}$$

where

$$\begin{aligned}
 L^* &= (I_y - I_z) \dot{q} r + I_{xz} p \dot{q} + T [-\sin \lambda (z_2 + \ell_1 \cos \sigma) \\
 &\quad + z_1 (v - v_w) / V_j] + L_p p + L_{\delta_x} \delta_x + \\
 &\quad + 1/2 \rho \bar{U}_0^2 S_b (C_{\ell_0} + C_{\ell_\delta} \delta_a) \\
 N^* &= (I_x - I_y) p \dot{q} - I_{xz} \dot{q} r + 2 I_e \Omega_e \dot{q} \\
 &\quad + T [\sin \lambda (x_2 - \ell_1 \sin \sigma) - x_1 (v - v_w) / V_j] + N_r r \\
 &\quad + N_{\delta_z} \delta_z + 1/2 \rho \bar{U}_0^2 S_b (C_{n_0} + C_{n_{\delta_r}} \delta_r + C_{n_{\delta_a}} \delta_a)
 \end{aligned}$$

Upon solving Eqns. (A-1-13) for  $\dot{p}$  and  $\dot{r}$  it is found that

$$\begin{aligned}
 \dot{p} &= (I_z L^* + I_{xz} N^*) / (I_x I_z - I_{xz}^2) \\
 \dot{r} &= (I_{xz} L^* + I_x N^*) / (I_x I_z - I_{xz}^2)
 \end{aligned}$$

### C. Numerical Evaluation of the X-14 Equations of Motion

Numerical values for the constants in equations (A-I-7) to (A-I-12) are given in Table A-I-2. In addition, the following stability derivatives can be expressed as functional relationships [5]:

$$C_{l_{\delta a}} = 0.0030 \cos^2 \beta / \text{deg}$$

$$C_{n_{\delta a}} = -0.00014 \cos^2 \beta / \text{deg}$$

$$C_{m_{\delta r}} = 0.00118 \cos^2 \beta / \text{deg}$$

$$C_{m_{\delta e}} = -0.0178 / \text{deg}$$

Furthermore, Figures (A-I-5) through A-I-12) show graphs of  $C_{l_0}$ ,  $C_Y$ ,  $C_{n_0}$ ,  $C_{m_{\alpha \text{ power off}}}$ ,  $C_{L \text{ power off}}$ ,  $C_{M_0 \text{ power off}}$ ,  $C_D$ ,  $\Delta C_{m_0} / T_c$ ,

$\Delta C_L / T_c$  and  $T_0$  vs. RPM.  $T_c$  is the non-dimensionalized thrust with  $T_c = T / (1/2 U_0^2 S)$ .  $T_0$  is the thrust at the engine exhaust, and  $T$  is the thrust at the end of the diverters. Hence,

$$T = T_0 \xi_{\sigma} \xi_{\lambda}$$

where  $\xi_{\sigma}$  is the longitudinal diverter efficiency factor and  $\xi_{\lambda}$  is the lateral side vane efficiency factor. Also,

$$V_j = V_{j_0} \xi_{\sigma} \xi_{\lambda}$$

which demonstrate that the jet velocity is somewhat less at the exit of the diverters than at the exit of the engines. In order to reduce these graphs to a useable form, functional relationships must be obtained. It was attempted to fit all of the graphs with polynomial curves. This, however, was impractical for the more irregular functions and straight line approximations were used. The functions used are shown in Table A-I-3.

The reaction control nozzle effects were evaluated by two independent methods. The X-14's response to sinusoidal inputs was analyzed by NASA at Moffet Field. The second method is to note that

$$\text{moment} = M_{\delta_y} \delta_y = \text{Force} \cdot \text{Length}$$

or

$$M_{\delta_y} \delta_{y_{\max}} = F_{\max} \cdot \text{length}$$

where the length is the distance to the discharge nozzle.  $F_{\max}$  was

measured directly using transducers, and  $\delta_{y_{\max}}$  was also measured di-

rectly. Numerical values associated with these calculations and a comparison with the other method are shown in Table A-I-4. This agreement is quite good, especially when considering the errors and uncertainties involved in measuring quantities like the moments of inertia and the maximum force at the nozzle outlets.

Table A-I-2

## X-14 Constant Parameters

$\rho$	= $2.378 \times 10^{-3}$ slugs/ft <sup>3</sup>
weight	= 4182 lb.
$I_x$	= 2340 slug-ft <sup>2</sup>
$I_y$	= 3400 slug-ft <sup>2</sup>
$I_z$	= 5400 slug-ft <sup>2</sup>
$I_{x_z}$	= 180 slug-ft <sup>2</sup>

mass center at station 99.84 in. and 0.58 in. right of center line

$x_1$	= 6 ft.
$x_2$	= -0.0133 ft.
$z_1$	= 0.583 ft.
$z_2$	= 0.916 ft
$l_1$	= 0.167 ft.
$\Omega_e$	= 1728 rad/sec at 100% RPM
$I_e$	= 0.5 slug ft <sup>2</sup>
$S$	= 182.69 ft <sup>2</sup>
$c$	= 5.56 ft.
$m$	= 129.9 slugs
$b$	= 33.83 ft.
$M_q/I_y$	= -0.15 sec <sup>-1</sup>
$L_p/I_x$	= -0.45 sec <sup>-1</sup>
$N_r/I_z$	= -0.20 sec <sup>-1</sup>
$C_{mq}$	= -11.4



$$C_{m \delta_e} = -0.0178 \text{ deg}^{-1}$$

$$\Delta C_{m \alpha} = 0.576 \text{ rad}^{-1}$$

$$M_{\delta_y} / I_y = 0.0350 \text{ rad/sec}^2/\text{deg}$$

$$N_{\delta_z} / I_z = 0.0166 \text{ rad/sec}^2/\text{deg}$$

$$L_{\delta_x} / I_x = 0.0681 \text{ rad/sec}^2/\text{deg}$$

$$V_{j_0} = 2000 \text{ ft/sec}$$

$$\xi_{\sigma} = 0.91$$

$$\xi_{\lambda} = 1.00$$

Table A-I-3

$T = T_o(\Omega)$  with  $\Omega$  in percent of maximum RPM and  $T$  in pounds (for one engine only)

$$\begin{aligned} T_o &= 44.15011 * \Omega - 1869.205 & \Omega < 93.3 \\ &= 68.96552 * \Omega - 4184.483 & 93.3 < \Omega < 99.1 \\ &= 80 * \Omega - 5278. & 99.1 < \Omega < 100.1 \\ &= 18.18182 * \Omega + 910. & 100.1 < \Omega < 101.2 \end{aligned}$$

$\Omega = \Omega(T_o)$

$$\begin{aligned} \Omega &= 0.02265 * T_o + 42.3375 & T_o < 2250 \\ &= .0145 * T_o + 60.675 & 2250 < T_o < 2650 \\ &= .0125 * T_o + 65.975 & 2650 < T_o < 2730 \\ &= .055 * T_o - 50.05 & 2730 < T_o < 2750 \end{aligned}$$

$\Delta C_L/T_c = f(U_o)$

$$\Delta C_L/T_c = -2.248398 \times 10^{-7} U_o^3 + 2.483009 \times 10^{-5} U_o^2 - 1.332149 \times 10^{-3} U_o$$

$\Delta C_M/T_c = f(U_o)$

$$\Delta C_M/T_c = 4.900354 \times 10^{-7} U_o^3 - 3.164620 \times 10^{-5} U_o^2 + 1.529505 \times 10^{-3} U_o$$

$C_D = C_D(U_o)$

$$C_D = .11 + 1. / (2.152195 U_o + 12.5)$$

$C_{M_o}^{\text{power off}} = C_{M_o}^{\text{power off}}(U_o)$

$$\begin{aligned} C_{M_o}^{\text{power off}} &= -0.6 + 0.00237 U_o & U_o < 34 \text{ (ft/sec)} \\ &= -0.52 + 0.0148 (U_o - 34) & 34 < U_o < 51 \\ &= -0.27 + 0.001579 (U_o - 51) & 51 < U_o < 101 \\ &= -0.19 & U_o > 101 \end{aligned}$$

$$C_{M_{\alpha_{\text{power off}}}} = C_{M_{\alpha_{\text{power off}}}}(U_0)$$

$$C_{M_{\alpha_{\text{power off}}}} = -4.1 + 0.04145 U_0 \quad U_0 < 34 \text{ (ft/sec)}$$

$$= -2.7 + 0.1007 (U_0 - 34) \quad 34 < U_0 < 51$$

$$= -1.0 \quad U_0 > 101$$

$$C_Y = C_Y(\beta)$$

$$C_Y = -1.851\beta \quad 0 < \beta < 0.189 \text{ (rad)}$$

$$= -0.35 + 0.393 (\beta - 0.189) \quad 0.189 < \beta < 0.418$$

$$= -0.26 - 0.362 (\beta - 0.418) \quad 0.418 < \beta < 1.22$$

$$= -0.55 \quad \beta > 1.22$$

$$C_{n_0} = C_{n_U}(\beta)$$

$$C_{n_U} = 0.113 \beta \quad 0 < \beta < 0.1945 \text{ (rad)}$$

$$= 0.022 \quad 0.1945 < \beta < 0.594$$

$$= 0.022 + 0.1348 (\beta - 0.594) \quad 0.594 < \beta < 1.395$$

$$= 0.13 \quad \beta > 1.395$$

$$C_{\ell_0} = C_{\ell_0}(\beta)$$

$$C_{\ell_0} = -0.083 \beta \quad 0 < \beta < 0.169 \text{ (rad)}$$

$$= -0.014 + 0.0066 (\beta - 0.169) \quad 0.169 < \beta < 0.471$$

$$= -0.012 - 0.00865 (\beta - 0.471) \quad 0.471 < \beta < 1.395$$

$$= -0.02 \quad \beta > 1.395$$

$$C_{L_{\text{power off}}} = C_{L_{\text{power off}}}(U_0)$$

$$C_{L_{\text{power off}}} = 0.61 + 0.002763 U_0 \quad U_0 < 51 \text{ (ft/sec)}$$

$$= 0.75 \quad U_0 > 51$$

Table A-I-4

<u>Axis</u>	<u>Discharge Point</u>	<u>Length</u>	$\delta_{\text{max}}$	$F_{\text{max}}$	<u>Inertia</u>	<u>Calculated Sensitivity</u>	<u>NASA Sensitivity</u>
X	Wing Tip	16.9 ft.	20°	200 lbs.	2340 slug ft. <sup>2</sup>	4.13 deg/sec <sup>2</sup> /deg	3.9 deg/sec <sup>2</sup> /deg
Y	Tail	18.75 ft.	20°	130 lbs.	3400 slug ft. <sup>2</sup>	2.05 deg/sec <sup>2</sup> /deg	2.0 deg/sec <sup>2</sup> /deg
Z	Tail	18.75 ft.	20°	90 lbs.	5400 slug ft. <sup>2</sup>	.90 deg/sec <sup>2</sup> /deg	.95 deg/sec <sup>2</sup> /deg

#### D. Solution of the X-14 Equations of Motion for the Reference Control Variables

The reference values for the elements of the control vector  $\underline{u}$  are desired for any given state vector  $\underline{x}$ . Since a steady state reference condition is sought, set  $\dot{\underline{x}} = \underline{0}$ . Upon examination of the non-linear equations of motion for the X-14 (see Fig. A-I-4), it is seen that  $\dot{u}$ ,  $\dot{v}$ , and  $\dot{w}$  are only functions of  $T$ ,  $\sigma$  and  $\lambda$ . Therefore, an explicit solution for these variables should exist since there are three equations and three unknowns. To find this solution, first rewrite the equations as

$$\begin{aligned} 0 &= A + T (\sin \sigma \cos \lambda - u_{\text{rel}}/V_j + f \sin \alpha) \\ 0 &= B + T (\sin \lambda - v_{\text{rel}}/V_j) \\ 0 &= C - T (\cos \sigma \cos \lambda + w_{\text{rel}}/V_j + f \cos \alpha) \end{aligned} \quad (\text{A-I-14})$$

where

$$A = m (vr - wq - g \sin \theta) + 1/2 \rho U_0^2 S (C_{L_{\text{power off}}} \sin \alpha - C_D \cos \alpha)$$

$$B = m (wp - ur + g \sin \phi \cos \theta) + 1/2 \rho \bar{U}_0^2 S C_Y$$

$$C = m (uq - vp + g \cos \phi \cos \theta) - 1/2 \rho U_0^2 S (C_{L_{\text{power off}}} \cos \alpha + C_D \sin \alpha)$$

$$f = \Delta C_L / T C$$

After squaring, rearranging and adding equations, the result can be written as

$$DT^2 + 2ET - F = 0$$

where

$$D = 1 - \bar{U}_0^2/V_j^2 - f^2 + 2f (u_{\text{rel}} \sin \alpha - w_{\text{rel}} \cos \alpha)/V_j$$

$$E = (A u_{rel} + B v_{rel} + C w_{rel})/V_j - f (A \sin \alpha - C \cos \alpha)$$

$$F = A^2 + B^2 + C^2 \quad (A-I-15)$$

Hence,

$$T = (-E + \sqrt{E^2 + DF})/D. \quad (A-I-16)$$

Now since T is known,

$$\lambda = \sin^{-1} (v_{rel}/V_j - B/T) \quad (A-I-17)$$

and now from Eqn. (A-I-14),

$$\sigma = \sin^{-1} [(u_{rel}/V_j - f \sin \alpha - A/T)/\cos \lambda]. \quad (A-I-18)$$

Some additional information is needed to solve the moment equations since there are six unknowns and only three equations. Since both the three reaction controls and the three aerodynamic controls have approximately the same range of travel, let us assume for determining the control settings for reference flight conditions, that the aerodynamic and the reaction controls are of the same magnitude, or that

$$\delta_x = \delta_a$$

$$\delta_y = \delta_e$$

$$\delta_z = \delta_r$$

When the above numerically determined values of T,  $\lambda$  and  $\sigma$  are substituted into the summary equations for the X-14, the equations can be solved for  $\delta_z$ ,  $\delta_e$ ,  $\delta_r$ ,  $\delta_x$ ,  $\delta_y$ , and  $\delta_a$ . The results are

$$\delta_x = \delta_a = - \{ (I_y - I_z) qr + I_{xz} pq + T [-\sin \lambda (z_2 + l_1 \cos \sigma) + z_1 v_{rel}/V_j] + L_p p + 1/2 \rho \bar{U}_0^2 S_b C_{l_0} \} / (L_{\delta_x} + 1/2 \rho \bar{U}_0^2 S_b C_{l_{\delta_a}}) \quad (A-I-19)$$

$$\begin{aligned}
\delta_y = \delta_e = & - \{ (I_z - I_x) pr + I_{xz} (r^2 - p^2) - 2 I_e \Omega_e r \\
& + T [\cos \lambda (z_2 \sin \sigma + x_2 \cos \sigma) + (x_1 w_{rel} - z_1 u_{rel})/V_j] \\
& + M_q q + 1/2 \rho U_0^2 Sc [(C_{m_0} + \Delta C_{m_0}) \\
& + (C_{m_{\alpha}} + \Delta C_{m_{\alpha}}) \alpha + \frac{c}{2U_0} C_{m_q} q ] \} / (M_{\delta_y} \\
& + 1/2 \rho U_0^2 Sc C_{m_{\delta_e}})
\end{aligned} \tag{A-I-20}$$

$$\begin{aligned}
\delta_z = \delta_r = & - \{ (I_x - I_y) pq - I_{xz} qr + 2 I_e \Omega_e q + N_r r \\
& + T [\sin \lambda (x_2 - l_2 \sin \sigma) - x_1 v_{rel}/V_j] + 1/2 \rho \bar{U}_0^2 Sb (C_{n_0} \\
& + C_{n_{\delta_a}}) \} / (N_{\delta_z} + 1/2 \rho \bar{U}_0^2 Sb C_{n_{\delta_r}})
\end{aligned} \tag{A-I-21}$$

## References

1. Etkin, B., Dynamics of Flight, John Wiley & Sons, Inc., New York, 1959.
2. Seckel, E., Stability and Control of Airplanes and Helicopters, Academic Press, New York, 1964.
3. Donnasch, D., Sherby, S. and Connolly, T., Airplane Aerodynamics, Pitman Publishing Corp., New York, 1961.
4. Struke, E., "Interactive Graphics in Aircraft Landing and Take-Off Studies," Proc. of the Conf. on Applications of Continuous System Simulation Languages, San Francisco, Calif., June 30-July 1, 1969.
5. Sinacori, J., "Variable Stability System for a VTOL Aircraft," Northrop Norair Report NOR 68-21, 1968.



## APPENDIX B-I

LINEARIZATION OF NON-LINEAR EQUATIONS OF MOTIONFOR A TIME INVARIANT DYNAMIC SYSTEM

The non-linear equations of motion for a time invariant dynamic system can be expressed as:

$$\dot{\underline{x}} = \underline{f} (\underline{x}, \underline{u}) \quad (\text{B-I-1})$$

where  $\underline{x}$  is the state vector,  $\underline{u}$  is the control vector, and  $\underline{f}$  is a vector function of  $\underline{x}$  and  $\underline{u}$  [1].

Suppose that for the system represented by Eqn. (B-I-1) there is a given  $\underline{x} (t_0) = \underline{x}_0$  and  $\underline{u} (t)$  for  $t > t_0$ , then the unique solution  $\phi (t, \underline{x}_0)$  is determined and can be found. Now consider small perturbations  $\delta \underline{x} (t_0)$  in  $\underline{x}_0$  and  $\delta \underline{u} (t)$  in  $\underline{u} (t)$ . Hence, small perturbations in the solution  $\phi (t, \underline{x}_0)$  can be expected and  $\dot{\underline{x}} + \delta \dot{\underline{x}} = \underline{f} (\underline{x} + \delta \underline{x}, \underline{u} + \delta \underline{u})$ ;  $\delta \underline{x} (t_0) = \delta \underline{x}_0$

(B-I-2)

Expanding the right-hand side of Eqn. (B-I-2) in a Taylor series and retaining terms only of the first order, and after substituting equation A-2-1 for  $\dot{\underline{x}}$ , we have the variational equation

$$\delta \dot{\underline{x}} = \underline{A} \delta \underline{x} + \underline{B} \delta \underline{u}; \quad \delta \underline{x} (t_0) = \delta \underline{x}_0 \quad (\text{B-I-3})$$

where

$$A_{ij} = \frac{\partial f_i}{\partial x_j} \quad B_{ij} = \frac{\partial f_i}{\partial u_j} \quad (\text{B-I-4})$$

with the partial derivatives being evaluated along the known solution,  $\underline{x} (t) = \phi (t, \underline{x}_0)$  and control  $\underline{u} (t)$ . Hence, the motion of the dynamic system about a known path for a small perturbation is seen to be governed by the linear ordinary differential equations (B-I-3) and (B-I-4).

The numerical evaluation of the partial derivatives in equation (B-I-4) can be accomplished by using the central difference approximation. [2] A review of this method follows. The Taylor series for the function  $f_i$  expanded about  $(\underline{x}_0 + \Delta\underline{x}, \underline{u}_0)$  with

$$(\Delta\underline{x})^T = (0 \dots 0 \quad x_j \quad 0 \dots 0)$$

is

$$f_i(\underline{x}_0 + \Delta\underline{x}, \underline{u}_0) = f_i(\underline{x}_0, \underline{u}_0) + \frac{\partial f_i}{\partial x_j} \Delta x_j + 1/2 \frac{\partial^2 f_i}{\partial x_j^2} \Delta x_j^2 + \dots \quad (\text{B-I-5})$$

with  $\frac{\partial f_i}{\partial x_j}$  evaluated at  $(\underline{x}_0, \underline{u}_0)$ . Similarly, the function expanded about  $(\underline{x}_0 - \Delta\underline{x}, \underline{u}_0)$  is given by

$$f_i(\underline{x}_0 - \Delta\underline{x}, \underline{u}_0) = f_i(\underline{x}_0, \underline{u}_0) - \frac{\partial f_i}{\partial x_j} \Delta x_j + 1/2 \frac{\partial^2 f_i}{\partial x_j^2} \Delta x_j^2 + \dots \quad (\text{B-I-6})$$

Since  $\Delta x$  is small,  $(\Delta x_j)^3$  and higher order terms are neglected. If equation (B-I-6) is subtracted from (B-I-5), and the resulting equation solved for the partial derivative evaluated at the point  $(\underline{x}_0, \underline{u}_0)$  with  $\Delta x_k = 0$  for  $k \neq j$ , the result is

$$A_{ij} = \frac{\partial f_i}{\partial x_j} = \frac{f_i(\underline{x}_0 + \Delta\underline{x}, \underline{u}_0) - f_i(\underline{x}_0 - \Delta\underline{x}, \underline{u}_0)}{2\Delta x_j} \quad (\text{B-I-7})$$

In a similar manner the elements of  $\underline{B}$  are found to be

$$B_{ij} = \frac{\partial f_i}{\partial u_j} = \frac{f_i(\underline{x}_0, \underline{u}_0 + \Delta\underline{u}) - f_i(\underline{x}_0, \underline{u}_0 - \Delta\underline{u})}{2(\Delta u_j)} \quad (\text{B-I-8})$$

where  $(\Delta\underline{u})^T = (0 \quad 0 \quad 0 \quad \dots \quad \Delta u_j \quad 0 \quad \dots \quad 0)$ .

A digital computer program that performs the above operations has been developed and used in the linearization of the equations of motion of the X-14B airplane.

## References for Appendix B-I

1. Bryson, A. E., Jr., and Y. C. Ho, Applied Optimal Control, Blaisdell Publishing Co., Waltham, Mass., 1969.
2. James, M. L., G. M. Smith, and J. C. Wolford, Analog and Digital Computer Methods in Engineering Analysis, International Textbook Co., Scranton, Penn., 1964.

II. Dynamic Estimation of an Unmeasurable  
State for the X-14B VTOL Aircraft

NOMENCLATURE

MATRICES

- $\underline{A}$  = continuous time system matrix  
 $\underline{B}$  = continuous time system input matrix  
 $\underline{C}$  = continuous time system output matrix  
 $\underline{F}$  = modal continuous time output matrix  
 $\underline{G}$  = controller gain matrix  
 $\underline{G}_m$  = modal controller gain matrix  
 $\underline{H}$  = modal continuous time input matrix  
 $\underline{I}$  = identity matrix  
 $\underline{K}$  = full observer gain matrix  
 $\underline{L}$  = partial observer gain matrix  
 $\underline{I}$  = eigenvector matrix  
 $\underline{\Lambda}$  = modal continuous time system matrix  
 $\underline{\Phi}$  = discrete time system matrix  
 $\underline{\Phi}_d$  = desired discrete time modal matrix  
 $\underline{\Phi}_m$  = modal discrete time system matrix  
 $\underline{\Psi}$  = discrete time input matrix  
 $\underline{\Psi}_m$  = modal discrete time input matrix

VECTORS

- $\underline{u}$  = input vector  
 $\underline{v}$  = eigenvector  
 $\underline{x}$  = state vector  
 $\underline{y}$  = output vector  
 $\underline{z}$  = modal state vector

## NOMENCLATURE

## SCALARS

$q$	= pitch rate
$r$	= yaw rate
$t$	= time
$u$	= forward velocity
$v$	= side velocity
$w$	= vertical velocity
$\theta$	= pitch angle
$\lambda$	= continuous time eigenvalues
$\lambda_d$	= desired eigenvalues
$(\lambda)_{DIS}$	= discrete time eigenvalues
$\tau$	= time interval for difference equations
$\phi$	= roll angle

## CHAPTER 1

### INTRODUCTION

Accurate measurement of the complete state vector is an integral, and sometimes difficult, part of implementing the powerful techniques of modern control theory. This research is concerned with the development of a method to estimate the side velocity of NASA's X-14B vertical takeoff and landing vehicle during hover. When the aircraft is flying at low side velocities, particularly during hover, measurement devices are unable to give reliable readings, and thus are usually not used. Hover is defined as low speed flight where aerodynamic and inertial effects are not important. This corresponds to flight with forward velocities of less than 30 ft/sec. Determination of the side velocity is important for both completing the state vector for control and for general knowledge of flight.

The approach is to investigate the application of linear dynamic observer theory around flight operating conditions to estimate the side velocity. Both full and partial dynamic observers are developed for two linearized hover conditions.

The linear differential equations are discretized to hold computer time to a minimum. The observers are tested on the linearized systems. A linear modal control policy is also developed primarily to test the observers' ability to track the real system. Finally the developed linear observers are applied to the full nonlinear equations to determine their accuracy and range around the given operating conditions.

## CHAPTER 2

## THE MODEL

The model for the X-14B VTOL was developed in previous research by Hoffman, Loscutoff and Seevers [1] and has recently been improved by Roesener [2]. The resulting eight nonlinear differential equations are found in Figure 1. The state variables for the model are

$\theta$  = pitch angle,  
 $q$  = pitch rate,  
 $u$  = forward velocity,  
 $\phi$  = roll angle,  
 $p$  = roll rate,  
 $r$  = yaw rate,  
 $v$  = side velocity,  
 $w$  = vertical velocity.

This set of nonlinear differential equations was linearized around several operating conditions characterizing hover, transition and full flight in [1].

In this research, the system is linearized at the following operating conditions:

Case 1:  $u = .01$  ft/sec,  
 $\theta = q = w = \phi = p = r = v = 0$

Case 2:  $u = 20$  ft/sec,  
 $\theta = q = w = \phi = p = r = v = 0$  .

These conditions are used for development of linear observers and controllers. They will be referred to as Case 1 and Case 2 respectively in subsequent sections. The linearization at  $u = .01$  ft/sec was chosen because



it was believed to be the most difficult flight condition for estimating the side velocity, due to the limited coupling between the measurable states and the side velocity. The  $u = 20$  ft/sec flight condition was chosen because it is a typical hover condition. These linearized flight conditions are found in Tables 1 and 2. The output matrix,  $\underline{C}$ , in Table 1A, is the same for both Case 1 and Case 2. The output matrix shows that all states are directly measurable, except for the side velocity.

FIGURE 1

Summary of the Reduced Non-Linear Equations of Motion for the X-14 Aircraft

$$\dot{u} = vr - wq - g \sin \theta + \frac{T}{m} [\sin \sigma \cos \lambda - \frac{1}{V_j} (u - u_w)] \\ + \frac{1}{2m} \rho U_0^2 S [(C_{L_{p. \text{ off}}} + \Delta C_L) \sin \alpha - C_D \cos \alpha]$$

$$\dot{v} = wp - ur + g \sin \phi \cos \theta + \frac{T}{m} [\sin \lambda - \frac{1}{V_j} (v - v_w)] + \frac{1}{2m} \rho \bar{U}_0^2 S C_{Y_j}$$

$$\dot{w} = uq - vp + g \cos \phi \cos \theta - \frac{T}{m} [\cos \sigma \cos \lambda + \frac{1}{V_j} (w - w_w)] \\ - \frac{1}{2m} \rho U_0^2 S [(C_{L_{p. \text{ off}}} + \Delta C_L) \cos \alpha + C_D \sin \alpha]$$

$$\dot{p} = \frac{(I_y - I_z)}{I_x} qr + \frac{I_{xz}}{I_x} (\dot{r} + pq) + \frac{T}{I_x} [-\sin \lambda (z_2 + l_1 \cos \sigma) + \frac{z_1}{V_j} (v - v_w)] \\ + \frac{L_p}{I_x} p + \frac{L_{\delta_x}}{I_x} \delta_x + \frac{1}{2I_x} \rho \bar{U}_0^2 S b (C_{l_0} + C_{l_{\delta_a}} \delta_a)$$

$$\dot{q} = \frac{(I_z - I_x)}{I_y} pr + \frac{I_{xz}}{I_y} (r^2 - p^2) - \frac{1}{I_y} 2 I_e \Omega_e r + \frac{T}{I_y} \cos \lambda \\ (z_2 \sin \sigma + x_2 \cos \sigma) + \frac{1}{V_j} [x_1 (w - w_w) - z_1 (u - u_w)] \\ + \frac{M_q}{I_y} q + \frac{M_{\delta_y}}{I_y} \delta_y + \frac{1}{2I_y} \rho U_0^2 S c [(C_{M_{p. \text{ off}}} + \Delta C_{m_0}) \\ + (C_{m_{\alpha p. \text{ off}}} + \Delta C_{m_\alpha}) \alpha + \frac{c}{2U_0} C_{m_q} q + C_{m_{\delta_e}} \delta_e]$$

$$\dot{r} = \frac{(I_x - I_y)}{I_z} pq + \frac{I_{xz}}{I_z} (\dot{p} - qr) + \frac{1}{I_z} 2 I_e \Omega_e q \\ + \frac{T}{I_z} [\sin \lambda (x_2 - l_1 \sin \sigma) - \frac{x_1}{V_j} (v - v_w)] + \frac{N_r}{I_z} r + \frac{N_{\delta_z}}{I_z} \delta_z \\ + \frac{1}{2I_z} \rho \bar{U}_0^2 S b (C_{n_0} + C_{n_{\delta_r}} \delta_r + C_{n_{\delta_a}} \delta_a)$$

TABLE 1  
THE LINEARIZED SYSTEM - CASE 1

REFERENCE CONDITION

THETA = 0.0 RADIANS  
Q = 0.0 RAD/SEC  
U = 0.01 FT/SEC  
W = 0.00 FT/SEC  
PHI = 0.0 RADIANS  
P = 0.0 RAD/SEC  
V = 0.00 FT/SEC  
R = 0.0 RAD/SEC

TRIM PARAMETERS

ELEVATOR\* = 0.47 DEGREES  
REACTION NOZZLE DY = 0.47 DEGREES  
THRUST DEFLECTION ANGLE (SIGMA) = 0.00 DEGREES  
ENGINE RPM = 98.57 PERCENT OF MAXIMUM  
AILERONS\* = 0.00 DEGREES  
RUDDER\* = 0.00 DEGREES  
SIDE VANE ANGLE (LAMBDA) = 0.00 DEGREES  
REACTION NOZZLE DX = 0.00 DEGREES  
REACTION NOZZLE DZ = 0.00 DEGREES

A MATRIX

0.000000	1.000000	0.000000	0.000000	0.000000	0.000000	0.000000	0.000000
0.000000	-0.150113	-0.000436	-0.000147	0.000000	0.000000	0.000000	-0.500992
-32.035897	0.000000	-0.020130	-0.038363	0.000000	0.000000	0.000000	0.000000
0.000000	0.010000	0.000050	-0.020819	0.000000	0.000000	0.000000	0.000000
0.000000	0.000000	0.000000	0.000000	0.000000	1.000000	0.000000	0.000000
0.000000	0.024327	0.000000	0.000000	0.000000	-0.451157	0.000306	-0.015424
0.000000	0.000000	0.000000	0.000000	37.832873	0.000000	-0.022425	-0.010000
0.000000	0.316251	0.000000	0.000000	0.000000	-0.015039	-0.002452	-0.200514

B MATRIX

0.000000	0.000000	0.000000	0.000000	0.000000	0.000000	0.000000
0.034907	0.019679	0.001822	0.000000	0.000000	0.000000	0.000000
0.000000	0.562003	0.000000	0.000000	0.000000	0.000000	0.000000
0.000000	0.000004	3.600197	0.000000	0.000000	0.000000	0.000000
0.000000	0.000000	0.000000	0.000000	0.000000	0.000000	0.000000
0.000000	0.000000	0.000000	-0.033893	0.068243	0.001279	0.000000
0.000000	0.000000	0.000000	0.562003	0.000000	0.000000	0.000000
0.000000	0.000000	0.000000	-0.001310	0.002275	0.016623	0.000000

\*NEGLIGIBLE AT LOW SPEEDS, THEREFORE NOT INCLUDED AS INPUTS IN THE B MATRIX.

TABLE 1A  
THE OUTPUT MATRIX - CASE 1 AND CASE 2

C MATRIX

1.000000	0.000000	0.000000	0.000000	0.000000	0.000000	0.000000	0.000000
0.000000	1.000000	0.000000	0.000000	0.000000	0.000000	0.000000	0.000000
0.000000	0.000000	1.000000	0.000000	0.000000	0.000000	0.000000	0.000000
0.000000	0.000000	0.000000	1.000000	0.000000	0.000000	0.000000	0.000000
0.000000	0.000000	0.000000	0.000000	1.000000	0.000000	0.000000	0.000000
0.000000	0.000000	0.000000	0.000000	0.000000	1.000000	0.000000	0.000000
0.000000	0.000000	0.000000	0.000000	0.000000	0.000000	1.000000	0.000000
0.000000	0.000000	0.000000	0.000000	0.000000	0.000000	0.000000	1.000000

TABLE 2  
THE LINEARIZED SYSTEM - CASE 2

REFERENCE CONDITION

THETA = 0.0 RADIANS  
Q = 0.0 RAD/SEC  
U = 20.00 FT/SEC  
W = 0.00 FT/SEC  
PHI = 0.0 RADIANS  
P = 0.0 RAD/SEC  
V = 0.00 FT/SEC  
R = 0.0 RAD/SEC

TRIM PARAMETERS

ELEVATOR = -1.96 DEGREES  
REACTION NOZZLE DY = -1.96 DEGREES  
THRUST DEFLECTION ANGLE (SIGMA) = 0.87 DEGREES  
ENGINE RPM = 98.76 PERCENT OF MAXIMUM  
AILERONS = 0.00 DEGREES  
RUDDER = 0.00 DEGREES  
SIDE VANE ANGLE (LAMBDA) = 0.00 DEGREES  
REACTION NOZZLE DX = 0.00 DEGREES  
REACTION NOZZLE DZ = 0.00 DEGREES

A MATRIX

0.000000	1.000000	0.000000	0.000000	0.000000	0.000000	0.000000	0.000000
0.000000	-0.375150	-0.001513	-0.014664	0.000000	0.000000	0.000000	-0.501932
-32.035897	0.000000	-0.028319	-0.007426	0.000000	0.000000	0.000000	0.000000
0.000000	20.000000	-0.026590	-0.024535	0.000000	0.000000	0.000000	0.000000
0.000000	0.000000	0.000000	0.000000	0.000000	1.000000	0.000000	0.000000
0.000000	0.024373	0.000000	0.000000	0.000000	-0.451157	-0.004610	-0.015424
0.000000	0.000000	0.000000	0.000000	31.832873	0.000000	-0.082783	-20.000000

B MATRIX\*

0.000000	0.000000	0.000000	0.000000	0.000000	0.000000	0.000000
0.037416	0.019777	-0.015868	0.000000	0.000000	0.000000	0.000000
0.000000	0.564681	-0.009580	0.000000	0.000000	0.000000	0.000000
0.000000	0.008554	3.552470	0.000000	0.000000	0.000000	0.000000
0.000000	0.000000	0.000000	0.000000	0.000000	0.000000	0.000000
0.000000	0.000000	0.000000	-0.034060	0.072015	0.001329	0.000000
0.000000	0.000000	0.000000	0.564746	0.000000	0.000000	0.000000
0.000000	0.000000	0.000000	-0.001351	0.002325	0.017267	0.000000

\*(DY-ELEVATOR), (DX+AILERONS), AND (DZ+RUDDER) ARE COMBINED AS INPUTS IN THE B MATRIX.

## CHAPTER 3

## CONTROLLABILITY AND OBSERVABILITY

Controllability and observability are dual criteria that must be satisfied to allow feedback control and state estimation. Controllability is the ability to transform any state at time  $t_i$  to any other state at time  $t_j$  by applying the appropriate control input  $\underline{u}(t)$ . Observability is the ability to identify any previous state by observing the output  $\underline{y}(t)$  for a finite time interval.

Several methods for determining whether a system meets these criteria exist. The method used in this research determines controllability and observability of individual modes. This is a superior method since modal input-output signal flows can be determined and the degree of controllability and observability of modes can be determined. For example, if a system is found to be marginally controllable or observable it is important to know if the offending mode or modes are stable or unstable and to what degree.

The linearized system equations

$$\dot{\underline{x}} = \underline{A}\underline{x} + \underline{B}\underline{u} \quad (\text{II-1})$$

$$\underline{y} = \underline{C}\underline{x} \quad (\text{II-2})$$

are transformed into the modal domain through the similarity transformation

$$\underline{x} = \underline{T}\underline{z}$$

where  $\underline{T}$  is a matrix of the system eigenvectors  $\underline{v}_i$  such that

$$\underline{T} = [\underline{v}_1 \quad \underline{v}_2 \quad \underline{v}_3 \quad \dots \quad \underline{v}_n] \quad (\text{II-3})$$

The system equations become

$$\dot{\underline{z}} = \underline{\Lambda}\underline{z} + \underline{H}\underline{u} \quad (\text{II-4})$$

$$\underline{y} = \underline{F}\underline{z} \quad (\text{II-5})$$

where

$$\begin{aligned}\underline{\underline{A}} &= \underline{\underline{T}}^{-1} \underline{\underline{A}} \underline{\underline{T}} \\ \underline{\underline{H}} &= \underline{\underline{T}}^{-1} \underline{\underline{B}} \\ \underline{\underline{F}} &= \underline{\underline{C}} \underline{\underline{T}}\end{aligned}\quad (\text{II-6})$$

$\underline{\underline{A}}$  is the modal system matrix,

$$\underline{\underline{A}} = \begin{bmatrix} \lambda_1 & 0 & \dots & \dots & 0 \\ 0 & \lambda_2 & & & \vdots \\ \vdots & & \lambda_3 & & \vdots \\ \vdots & & & \lambda_4 & \vdots \\ \vdots & & & & \lambda_5 & \vdots \\ & & & & & \lambda_6 & \vdots \\ & & & & & & \lambda_7 & \vdots \\ 0 & \dots & \dots & \dots & \dots & \dots & \dots & \lambda_8 \end{bmatrix} = \text{diag} [\lambda_1, \lambda_2, \dots, \lambda_8]$$

where  $\lambda$ 's are eigenvalues.

In the event that complex roots are present, the  $\underline{\underline{T}}$  matrix takes the form

$$\underline{\underline{T}} = [\underline{\underline{v}}_{\text{IR}} \quad \underline{\underline{v}}_{\text{IC}} \quad \dots]$$

where

$\underline{\underline{v}}_{\text{IR}}$  = the real part of the eigenvector

$\underline{\underline{v}}_{\text{IC}}$  = the complex part of the eigenvector.

$\underline{\underline{v}}_{\text{IR}}$  and  $\underline{\underline{v}}_{\text{IC}}$  are complex conjugates. The resulting modal matrix,  $\underline{\underline{A}}$ , becomes

$$\underline{\underline{A}} = \begin{bmatrix} \lambda_{\text{IR}} & \lambda_{\text{IC}} & 0 & \dots & \dots \\ -\lambda_{\text{IC}} & \lambda_{\text{IR}} & 0 & \dots & \dots \\ 0 & 0 & \lambda_3 & & \\ \vdots & \vdots & & \ddots & \\ \vdots & \vdots & & & \lambda_8 \end{bmatrix}$$

where

$\lambda_{IR}$  = real part of eigenvalue

$\lambda_{IC}$  = complex part of eigenvalue.

The treatment and interpretation of systems with complex eigenvalues is the same as for any other system except for the variations noted. The case of repeated eigenvalues is neglected throughout this discussion.

$\underline{H}$  is the modal input matrix. If any complete row of  $\underline{H}$  is zero, the mode is unaffected by any control policy implemented, and is uncontrollable. Therefore, the controllability criterion is satisfied if every row of  $\underline{H}$  has at least one non-zero element.

Observability can be determined by examining the modal output matrix  $\underline{F}$ . The requirement is that every mode must appear in the output vector  $\underline{y}$ . To accomplish this, every column in  $\underline{F}$  must contain at least one non-zero element.

For Case 1, the  $\underline{A}$ ,  $\underline{H}$  and  $\underline{F}$  matrices are as shown in Table 3, while for Case 2, the  $\underline{A}$ ,  $\underline{H}$  and  $\underline{F}$  matrices are shown in Table 4. From both  $\underline{A}$  matrices, it can be seen that the linearized systems are inherently unstable. However, both linearizations are completely controllable and completely observable, and therefore can be stabilized by feedback control. The most important result is that since the side velocity is observable through the measurable state variables, dynamic observers may be used to estimate it.



TABLE 3

## THE LINEARIZED SYSTEM IN MODAL FORM - CASE 1

## A MATRIX

-0.18660	0.42555	0.00000	0.00000	0.00000	0.00000	0.00000	0.00000
-0.42555	-0.18660	0.00000	0.00000	0.00000	0.00000	0.00000	0.00000
0.00000	0.00000	-0.30996	0.02019	0.00000	0.00000	0.00000	0.00000
0.00000	0.00000	-0.02019	-0.30996	0.00000	0.00000	0.00000	0.00000
0.00000	0.00000	0.00000	0.00000	-0.12050	0.00000	0.00000	0.00000
0.00000	0.00000	0.00000	0.00000	0.00000	0.15912	0.00000	0.00000
0.00000	0.00000	0.00000	0.00000	0.00000	0.00000	0.11029	0.00000
0.00000	0.00000	0.00000	0.00000	0.00000	0.00000	0.00000	-0.02084

## H MATRIX

3.38837	1.97663	0.31828	-2.88713	5.24580	1.94411
3.31723	1.84020	0.05916	-3.45986	6.14046	-1.88379
-2.13415	-1.30327	-0.34686	-65.27828	127.52590	1.04069
-11.50003	-6.75670	-1.41944	-289.15382	569.48136	5.42458
4.30468	2.72745	1.61925	100.33871	-197.84024	-7.27932
2.01065	1.05477	0.04308	-44.71371	94.88475	-0.54612
-3.50121	-1.78538	-0.13110	-76.76226	159.69359	3.74697
0.00431	0.00251	3.86946	0.05583	-0.11182	-0.00548

## F MATRIX

0.00520	-0.01328	0.00905	-0.00063	0.00314	0.00558	-0.00407	-0.00112
0.00468	0.00469	-0.00279	0.00038	-0.00038	0.00089	-0.00045	0.00002
1.00000	0.00000	1.00000	0.00000	0.99977	-0.99772	0.99973	-0.36601
0.00002	-0.00023	-0.00008	-0.00002	-0.00046	-0.00023	0.00035	0.93061
-0.00009	-0.00078	0.00383	-0.00092	0.00006	0.00038	0.00009	0.00000
0.00035	0.00011	-0.00117	0.00036	-0.00001	0.00006	0.00001	0.00000
0.00345	-0.00364	-0.00175	0.00023	-0.00085	0.00032	-0.00064	0.00005

TABLE 4

## THE LINEARIZED SYSTEM IN MODAL FORM - CASE 2

## A MATRIX

-0.28951	0.66661	0.00000	0.00000	0.00000	0.00000	0.00000	0.00000
-0.66661	-0.28951	0.00000	0.00000	0.00000	0.00000	0.00000	0.00000
0.00000	0.00000	-0.74830	0.00000	0.00000	0.00000	0.00000	0.00000
0.00000	0.00000	0.00000	-0.17565	0.00000	0.00000	0.00000	0.00000
0.00000	0.00000	0.00000	0.00000	0.06400	0.14200	0.00000	0.00000
0.00000	0.00000	0.00000	0.00000	-0.14200	0.06400	0.00000	0.00000
0.00000	0.00000	0.00000	0.00000	0.00000	0.00000	0.10626	0.43161
0.00000	0.00000	0.00000	0.00000	0.00000	0.00000	-0.43161	0.10626

## H MATRIX

1.82635	1.03373	3.08609	18.60148	-0.03779	-0.00078
1.41645	0.67930	-2.88325	-18.16568	-0.05271	-0.00090
0.12454	0.07176	0.18701	-2.63280	-2.52081	-0.05069
0.12258	0.11941	1.09256	-40.15281	-0.02941	-0.00043
-1.94683	-0.58549	-4.16373	20.09309	-0.01219	-0.00002
-1.91553	-0.79425	22.85470	65.47933	0.08503	0.00160
-0.24056	-0.12457	-0.22805	-6.41398	-2.51054	-0.03326
-0.18510	-0.08084	0.95420	-11.89252	4.99281	0.09281

## F MATRIX

0.00811	-0.02072	0.00020	0.00436	-0.00285	-0.00444	0.00023	0.00016
0.01146	0.01140	-0.00015	-0.00077	0.00045	-0.00069	-0.00004	0.00012
1.00000	0.00000	0.00911	0.96188	1.00000	0.00000	-0.01555	0.01246
0.19109	-0.38004	0.00455	0.27063	-0.12565	0.04577	0.00397	0.00224
0.00103	-0.00059	0.02073	-0.00649	0.00000	-0.00057	0.00598	0.01345
0.00009	0.00086	-0.01551	0.00114	0.00008	-0.00004	-0.00517	0.00401
0.00459	-0.00607	-0.00027	-0.01050	0.00007	-0.00086	0.00007	-0.00018

## CHAPTER 4

## DISCRETIZATION OF LINEAR DIFFERENTIAL EQUATIONS

The linear differential equations are transformed to discrete time equations because the aircraft has an on-board digital computer for control. Thus discrete time control is more applicable. Digital computers are also more suited to adding and subtracting difference equations than to numerically integrating differential equations [3].

Difference equations are the time domain solutions to differential equations. Therefore, the set of differential equations (1) and (2)

$$\dot{\underline{x}} = \underline{A}\underline{x} + \underline{B}\underline{u} \quad (\text{II-1})$$

$$\underline{y} = \underline{C}\underline{x} \quad (\text{II-2})$$

can be transformed into the difference equations

$$\underline{x}_{k+1} = \underline{\Phi}\underline{x}_k + \underline{\Psi}\underline{u}_k, \quad (\text{II-7})$$

$$\underline{y} = \underline{C}\underline{x}_k \quad (\text{II-8})$$

Assuming  $\underline{u}(t)$  is constant over a time interval ( $0 < t < \tau$ , where  $\tau$  is the time interval), it can be shown that for linear, constant coefficient systems,

$$\underline{\Phi} = e^{\underline{A}\tau} \quad (\text{II-9})$$

$$\underline{\Psi} = [e^{\underline{A}\tau} - \underline{I}]\underline{A}^{-1}\underline{B}. \quad (\text{II-10})$$

It will now be shown that  $\underline{\Phi}$  can be simply formed from  $\underline{A}$  when in the modal domain. First, it must be shown that the similarity transformation matrix,  $\underline{I}$ , remains invariant and continues to diagonalize the system whether in difference or differential equation form.

$\underline{\Phi}$  is described by the series

$$\underline{\Phi} = e^{\underline{A}\tau} = \underline{I} + \underline{A}\tau + \frac{1}{2!}\underline{A}^2\tau^2 + \frac{1}{3!}\underline{A}^3\tau^3 + \dots \quad (\text{II-11})$$

To show that  $\underline{I}$  diagonalizes  $\underline{\Phi}$ , premultiply and postmultiply by  $\underline{I}^{-1}$  and  $\underline{I}$  respectively,

$$\underline{I}^{-1}\underline{\Phi}\underline{I} = \underline{I}^{-1}\underline{I}\underline{I} + \underline{I}^{-1}\underline{A}\underline{I}\tau + \frac{1}{2!}\underline{I}^{-1}\underline{A}^2\underline{I}\tau^2 + \dots \quad (\text{II-12})$$

Now, simplify (12) using the identity

$$\begin{aligned} \underline{\underline{A}}^2 &= \underline{\underline{A}}\underline{\underline{T}}\underline{\underline{T}}^{-1}\underline{\underline{A}} , \\ \underline{\underline{T}}^{-1}\underline{\underline{\Phi}}\underline{\underline{T}} &= \underline{\underline{I}} + \underline{\underline{A}}\underline{\underline{T}} + \frac{1}{2!}\underline{\underline{A}}^2\underline{\underline{T}}^2 + \dots \end{aligned} \quad (\text{II-13})$$

This technique can be readily extended to all higher order terms; therefore

$$\underline{\underline{T}}^{-1}\underline{\underline{\Phi}}\underline{\underline{T}} = \underline{\underline{\Phi}}_{\text{m}} = e^{\underline{\underline{A}}\underline{\underline{T}}} = \begin{bmatrix} e^{\lambda_1\underline{\underline{T}}} & 0 & \dots & 0 \\ 0 & e^{\lambda_2\underline{\underline{T}}} & \dots & 0 \\ \vdots & \vdots & \ddots & \vdots \\ 0 & \dots & \dots & e^{\lambda_n\underline{\underline{T}}} \end{bmatrix} \quad (\text{II-14})$$

The discrete time eigenvalues are defined as

$$\lambda_{\text{DIS}} = 1 + \lambda\underline{\underline{T}} + \frac{1}{2!}\lambda^2\underline{\underline{T}}^2 + \dots = e^{\lambda\underline{\underline{T}}} \quad (\text{II-15})$$

in equation(13).  $\underline{\underline{\Phi}}$  can then be obtained from  $\underline{\underline{A}}$  by the following steps.

First, transform the continuous time system into the modal domain, a step done previously to determine controllability and observability. Then create  $\underline{\underline{\Phi}}_{\text{m}}$  by transforming the individual eigenvalues of  $\underline{\underline{A}}$  into  $\lambda_{\text{DIS}}$  by using the scalar equation (15). Now, simply transform out of the modal domain,

$$\underline{\underline{\Phi}} = \underline{\underline{T}}\underline{\underline{\Phi}}_{\text{m}}\underline{\underline{T}}^{-1} . \quad (\text{II-16})$$

The input matrix,  $\underline{\underline{\Psi}}$ , can be approximated easily by noting that

$$\begin{aligned} \underline{\underline{\Psi}} &= [(\underline{\underline{I}} + \underline{\underline{A}}\underline{\underline{T}} + \frac{1}{2!}\underline{\underline{A}}^2\underline{\underline{T}}^2 + \dots) - \underline{\underline{I}}]\underline{\underline{A}}^{-1}\underline{\underline{B}} \\ \underline{\underline{\Psi}} &\approx \underline{\underline{T}}[\underline{\underline{A}} + \frac{1}{2!}\underline{\underline{A}}^2\underline{\underline{T}}]\underline{\underline{A}}^{-1}\underline{\underline{B}} \\ \underline{\underline{\Psi}} &\approx \underline{\underline{T}}[\underline{\underline{I}} + \frac{1}{2!}\underline{\underline{A}}\underline{\underline{T}}]\underline{\underline{B}} . \end{aligned} \quad (\text{II-17})$$

For this system, the time step was .05 seconds. For this second order approximation the error is on the order of 0.25 percent when the higher order terms are left out. The system equations for Case 1 are found in Table 5 and those for Case 2 are in Table 6.

TABLE 5

## THE LINEARIZED DISCRETE TIME SYSTEM - CASE 1

 $\Phi$  MATRIX

1.00000	0.04920	0.00000	0.00000	0.00000	0.00002	-0.00062	0.00000
0.00002	0.99200	-0.00002	-0.00001	0.00000	0.00000	-0.02480	0.00002
-1.50000	-0.04070	0.99990	-0.00192	0.00012	0.00202	0.00040	-0.00001
0.00000	0.00000	0.00000	0.99900	0.00000	0.00000	-0.00001	0.00000
0.00000	0.05003	0.00000	0.00000	1.00000	0.04940	-0.00002	0.00000
0.00000	0.00719	0.00000	0.00000	0.00001	0.97800	-0.00077	0.00002
0.00000	0.01570	0.00000	0.00000	-0.00010	-0.00075	0.99000	-0.00012
0.00000	0.00005	0.00000	0.00000	1.59000	0.03870	-0.00048	0.99900

 $\Psi$  MATRIX

0.00000	0.00000	0.00000	0.00000	0.00000	0.00000
0.00175	0.00098	0.00009	0.00000	0.00000	0.00000
0.00000	0.02810	0.00000	0.00000	0.00000	0.00000
0.00000	0.00000	0.18000	0.00000	0.00000	0.00000
0.00000	0.00000	0.00000	0.00000	0.00000	0.00000
0.00000	0.00000	0.00000	-0.00169	0.00341	0.00006
0.00000	0.00000	0.00000	-0.00007	0.00011	0.00083
0.00000	0.00000	0.00000	0.02810	0.00000	0.00000

TABLE 6  
THE LINEARIZED DISCRETE TIME SYSTEM - CASE 2

Φ MATRIX

1.00000	0.04950	0.00000	-0.00002	0.00000	0.00000	-0.00062	0.00000
0.00006	0.98100	-0.00007	-0.00073	0.00000	0.00001	-0.02470	0.00000
-1.60000	-0.04000	0.99900	-0.00036	0.00000	0.00000	0.00041	0.00000
0.00110	0.99000	-0.00137	0.99800	0.00000	0.00000	-0.01240	0.00000
0.00000	0.00003	0.00000	0.00000	1.00000	0.04940	-0.00002	-0.00001
0.00000	0.00119	0.00000	0.00000	-0.00018	0.97800	-0.00066	-0.00023
0.00000	0.01560	0.00000	-0.00001	0.00000	-0.00074	0.99000	0.00000
0.00000	-0.00782	0.00000	0.00000	1.59000	0.03980	-0.99300	0.99600

Ψ MATRIX

0.00000	0.00000	0.00000	0.00000	0.00000	0.00000
0.00187	0.00099	-0.00079	0.00000	0.00000	0.00000
0.00000	0.02820	-0.00048	0.00000	0.00000	0.00000
0.00094	0.00092	0.17700	0.00000	0.00000	0.00000
0.00000	0.00000	0.00000	0.00000	0.00000	0.00000
0.00000	0.00000	0.00000	-0.00170	0.00360	0.00007
0.00000	0.00000	0.00000	0.02820	0.00000	0.00000
0.00000	0.00000	0.00000	0.00003	-0.00006	-0.00043

## CHAPTER 5

## LIMITED INPUT MODAL CONTROL VIA STATE VARIABLE OUTPUT

The linearized set of difference equations, given by equations (7) and (8) and repeated here,

$$\underline{x}_{k+1} = \underline{\Phi} \underline{x}_k + \underline{\Psi} u_k \quad (\text{II-7})$$

$$\underline{y}_k = \underline{C} \underline{x}_k, \quad (\text{II-8})$$

specify a system of eighth order, with six inputs and seven outputs. For the purposes of controller design, though, state variable output will be assumed. The missing states will be provided later by dynamic observers. The control matrix  $\underline{G}$  will be designed to place six of eight eigenvalues wherever desired. The remaining two eigenvalues will be considered sufficiently stable, although a readily available extension of the following technique allows for placement of all eight poles.

To condition the first six eigenvalues, the system is transformed into the discrete time modal domain, using

$$\underline{x}_k = \underline{T} \underline{z}_k.$$

Thus

$$\underline{z}_{k+1} = \underline{\Phi}_m \underline{z}_k + \underline{\Psi}_m u_k \quad (\text{II-18})$$

$$\underline{y}_k = \underline{C} \underline{T} \underline{z}_k \quad (\text{II-19})$$

where

$$\underline{\Psi}_m = \underline{T}^{-1} \underline{\Psi}$$

$$\underline{\Phi}_m = \underline{T}^{-1} \underline{\Phi} \underline{T}.$$

Now, let us partition the system equations into two segments. The modal state vector becomes

$\underline{z}_{16}$  = the first six modes, all to be conditioned

$\underline{z}_{78}$  = the last two modes, not to be conditioned.

The  $\underline{\Phi}_m$  matrix is arranged so that

$$\underline{\Phi}_m = \begin{bmatrix} (\lambda_1)_{DIS} & 0 & \dots & \dots & 0 \\ 0 & (\lambda_2)_{DIS} & & & \vdots \\ \vdots & & (\lambda_3)_{DIS} & & \vdots \\ \vdots & & & (\lambda_4)_{DIS} & \vdots \\ \vdots & & & & (\lambda_5)_{DIS} \\ & & & & & (\lambda_6)_{DIS} \\ & & & & & & (\lambda_7)_{DIS} \\ 0 & \dots & \dots & \dots & \dots & \dots & (\lambda_8)_{DIS} \end{bmatrix}$$

$$= \begin{matrix} 6 \\ 2 \end{matrix} \begin{matrix} \overset{8}{\underline{\Phi}_{mL}} & \underline{0} \\ \underline{0} & \underline{\Phi}_{m78} \end{matrix} .$$

$\underline{\Phi}_{m78}$  consists of the last two poles, which are the most stable and therefore are ignored in the conditioning process.

Let us define a matrix of desired eigenvalues,

$$\underline{\Phi}_d = \begin{bmatrix} (\lambda_{1d})_{DIS} & 0 & \dots & \dots & 0 \\ 0 & (\lambda_{2d})_{DIS} & & & \vdots \\ \vdots & & (\lambda_{3d})_{DIS} & & \vdots \\ \vdots & & & (\lambda_{4d})_{DIS} & \vdots \\ \vdots & & & & (\lambda_{5d})_{DIS} \\ & & & & & (\lambda_{6d})_{DIS} \\ & & & & & & (\lambda_7)_{DIS} \\ 0 & \dots & \dots & \dots & \dots & \dots & (\lambda_8)_{DIS} \end{bmatrix}$$

$$= \begin{matrix} 6 \\ 2 \end{matrix} \begin{matrix} \overset{8}{\underline{\Phi}_{dL}} & \underline{0} \\ \underline{0} & \underline{\Phi}_{d78} \end{matrix} .$$



These eigenvalues will be the closed loop system poles after implementation of the control matrix  $\underline{G}$ . Partition  $\underline{\Psi}_m$  such that

$$\underline{\Psi}_m = \begin{bmatrix} 6 \\ \underline{\Psi}_{mL} \\ - - - \\ 2 \\ \underline{\Psi}_{m78} \end{bmatrix}$$

where  $\underline{\Psi}_{mL}$  is a nonsingular  $6 \times 6$  matrix. Then the control matrix in modal form is

$$\underline{G}_m = \underline{\Psi}_m^{-1} \left[ \begin{bmatrix} \underline{\Phi}_{mL} & \underline{0} \end{bmatrix} - \begin{bmatrix} \underline{\Phi}_{dL} & \underline{0} \end{bmatrix} \right] \quad (II-20)$$

to condition the first six modes. To illustrate that this will give the desired results, let us examine the system in modal form under the control policy

$$\underline{u}_k = -\underline{G}_m \underline{z}_k \quad (II-21)$$

we have

$$\underline{z}_{k+1} = \underline{\Phi}_m \underline{z}_k - \underline{\Psi}_m \underline{\Psi}_m^{-1} \left[ \begin{bmatrix} \underline{\Phi}_{mL} & \underline{0} \end{bmatrix} - \begin{bmatrix} \underline{\Phi}_{dL} & \underline{0} \end{bmatrix} \right] \underline{z}_k \quad (II-22)$$

Simplifying and rewriting in a partitioned form

$$\begin{bmatrix} \underline{z}_{16} \\ \underline{z}_{78} \end{bmatrix}_{k+1} = \begin{bmatrix} \begin{bmatrix} \underline{\Phi}_{mL} & \underline{0} \\ \underline{0} & \underline{\Phi}_{m78} \end{bmatrix} - \begin{bmatrix} \underline{I} \\ - - - \\ \underline{\Psi}_{m78} \underline{\Psi}_{mL}^{-1} \end{bmatrix} \begin{bmatrix} \underline{\Phi}_{mL} & \underline{0} \\ \underline{\Phi}_{dL} & \underline{0} \end{bmatrix} \end{bmatrix} \begin{bmatrix} \underline{z}_{16} \\ \underline{z}_{78} \end{bmatrix}_k \quad (II-23)$$

Expanding, we obtain

$$\begin{bmatrix} \underline{z}_{16} \\ \underline{z}_{78} \end{bmatrix}_{k+1} = \begin{bmatrix} \underline{\Phi}_{dL} & \underline{0} \\ \underline{\Psi}_{m78} \underline{\Psi}_{mL}^{-1} \left[ \begin{bmatrix} \underline{\Phi}_{dL} & \underline{0} \end{bmatrix} - \begin{bmatrix} \underline{\Phi}_{mL} & \underline{0} \end{bmatrix} \right] & \underline{\Phi}_{78} \end{bmatrix} \begin{bmatrix} \underline{z}_{16} \\ \underline{z}_{78} \end{bmatrix}_k \quad (II-24)$$

Note that despite the  $\underline{\Psi}_{m78} \underline{\Psi}_{mL}^{-1} \left[ \begin{bmatrix} \underline{\Phi}_{dL} & \underline{0} \end{bmatrix} - \begin{bmatrix} \underline{\Phi}_{mL} & \underline{0} \end{bmatrix} \right]$  term, the modal closed loop system matrix

$$\begin{bmatrix}
 (\lambda_{1d})_{DIS} & 0 & 0 & 0 & 0 & 0 & \cdot & 0 & 0 \\
 0 & (\lambda_{2d})_{DIS} & 0 & 0 & 0 & 0 & \cdot & 0 & 0 \\
 0 & 0 & (\lambda_{3d})_{DIS} & 0 & 0 & 0 & \cdot & 0 & 0 \\
 0 & 0 & 0 & (\lambda_{4d})_{DIS} & 0 & 0 & \cdot & 0 & 0 \\
 0 & 0 & 0 & 0 & (\lambda_{5d})_{DIS} & 0 & \cdot & 0 & 0 \\
 0 & 0 & 0 & 0 & 0 & (\lambda_{6d})_{DIS} & \cdot & 0 & 0 \\
 \hline
 & & & & & & & (\lambda_7)_{DIS} & 0 \\
 \Psi_{mL}^{-1} \Gamma_{dL}^{-1} [\Phi_{dL} - \Phi_{mL}] & & & & & & & \cdot & (\lambda_8)_{DIS} \\
 & & & & & & & & \cdot
 \end{bmatrix}$$

is in triangular form and its eigenvalues are the six elements of  $\Phi_{dL}$  and the original eigenvalues  $(\lambda_7)_{DIS}$  and  $(\lambda_8)_{DIS}$ . Thus, the first six modes have been moved to their desired values, and the last two modes have remained unchanged. To transform  $\underline{G}_{nn}$  into the control matrix, reverse the modalizing process: post multiply by  $\underline{\Gamma}^{-1}$ ,

$$\underline{G} = \Psi_{mL}^{-1} (\Phi_{mL} - \Phi_{dL}) \underline{\Gamma}^{-1} \quad (II-25)$$

The resulting closed loop equations are

$$\underline{x}_{k+1} = (\underline{\Phi} - \underline{\Psi}\underline{G})\underline{x}_k \quad (II-26)$$

Using this technique the control matrices derived for Case 1 and Case 2 are as shown in Table 7.

The modal technique allows the designer to place eigenvalues arbitrarily. The only restriction is that eigenvalues must be chosen to give the required response while remaining within control power restraints.

It should be noted here from previous development that

$$\lambda_{DIS} = e^{\lambda\tau}$$

where

$\lambda_{DIS}$  = discrete time eigenvalue

$\lambda$  = continuous time eigenvalue

$\tau$  = time interval.

For  $\lambda_{DIS}$ , the stability limit on the complex plane is the unit circle. Positive, real parts of magnitude less than one correspond to continuous time negative, real parts. Zero corresponds to infinity as the fastest response. Any eigenvalue within the real, negative half of the unit circle will oscillate with each time step, and thus, is not very useful for control. Time constants for discrete time eigenvalues can be approximated as

$$\tau.C._i = \left| \frac{\tau}{(1 - \lambda_{DIS})} \right| \quad (II-27)$$

by recalling the infinite series for an exponential function.

TABLE 7  
THE CONTROL MATRICES FOR THE LINEARIZED DISCRETE TIME SYSTEMS

## CASE 1

## G MATRIX

139.00000	72.00000	-0.70000	1.74000	-4.24000	9.70000	24.30000	0.66200
-239.00000	-83.10000	1.24000	-3.44000	25.20000	3.38000	-53.00000	-1.20000
0.27000	0.30000	0.00017	2.77000	-1.70000	-3.9300	-0.48400	0.00114
27.10000	11.70000	0.00479	-0.40100	127.00000	76.3000	12.30000	1.38000
12.80000	5.50000	0.00217	-0.18900	67.30000	48.10000	4.91000	0.68800
6.22000	12.70000	0.00877	-0.05930	13.70000	5.04000	49.30000	-0.02310

## CASE 2

## G MATRIX

-2.16000	0.00000	-0.37500	0.04670	25.40000	0.00000	-0.03490	-0.00006
25.00000	0.00000	0.70200	0.00156	-38.50000	0.00000	0.10400	0.00019
-2.02000	-0.05610	-0.00171	0.11300	-0.27000	-0.00117	0.00028	0.00000
-0.15200	0.00004	0.00000	0.00000	-0.20000	-0.00085	0.70800	0.00000
7.24000	0.00260	-0.00003	-0.00018	-19.7000	5.48000	0.34700	0.85700
-379.00000	-0.13100	0.00182	0.00968	1050.00000	3.67000	-0.61400	-46.50000

## CHAPTER 6

## STATE VARIABLE OUTPUT VIA DYNAMIC OBSERVERS

To implement the control scheme discussed previously, a full state vector is assumed for feedback. On the X-14B VTOL, seven of eight state variables are available for measurement during hover. A dynamic observer, which is a special form of filter, is used to estimate the missing state, side velocity.

The full dynamic observer is a time invariant linear model of the system to be observed. The model is driven by the same inputs as the system. Therefore, if the model is perfectly accurate, i.e., no disturbances or noise are present and the initial conditions of the system known, the system state vector is known at any time  $t$ . As can be readily seen, these are rather demanding assumptions and a method for updating the model states to the measurable system states is needed. This is the key to the usefulness of the dynamic observer.

To design a dynamic observer, assume a system is governed by equations (7) and (8). Let us define  $\hat{x}_k$  as an estimate of  $x_k$ . The model defined by  $\hat{x}$  is

$$\hat{x}_{k+1} = \underline{\Phi}\hat{x}_k + \underline{\Psi}u_k \quad (\text{II-28})$$

$$\hat{y}_k = \underline{C}\hat{x}_k \quad (\text{II-29})$$

This is the open loop model of the system. To force the model states to the system states an error feedback term,  $\underline{K}(y_k - \hat{y}_k)$ , is implemented.  $\underline{K}$  is the observer control matrix. Thus, the closed loop model becomes

$$\hat{x}_{k+1} = \underline{\Phi}\hat{x}_k + \underline{\Psi}u_k + \underline{K}(y_k - \hat{y}_k) \quad (\text{II-30})$$

$$\hat{y}_k = \underline{C}\hat{x}_k \quad (\text{II-31})$$

To illustrate that a control matrix,  $\underline{K}$ , can be chosen to drive

observer error in measurable states to zero, let us define an error state vector

$$\tilde{\underline{x}} = \hat{\underline{x}} - \underline{x} .$$

Subtracting equations (7) and (8) from (30) and (31),

$$\hat{\underline{x}}_{k+1} - \underline{x}_{k+1} = \underline{\Phi}\hat{\underline{x}}_k + \underline{\Psi}u_k + \underline{K}(y_k - \hat{y}_k) - \underline{\Phi}\underline{x}_k - \underline{\Psi}u_k$$

$$\hat{y}_k - y_k = \underline{C}\hat{\underline{x}}_k - \underline{C}\underline{x}_k$$

which becomes

$$\tilde{\underline{x}}_{k+1} = \underline{\Phi}\tilde{\underline{x}}_k + \underline{K}(y_k - \hat{y}_k)$$

$$\tilde{y}_k = \underline{C}\tilde{\underline{x}}_k$$

or the single set of equations

$$\tilde{\underline{x}}_{k+1} = (\underline{\Phi} - \underline{K}\underline{C})\tilde{\underline{x}}_k \quad . \quad (\text{II-33})$$

The eigenvalues of this homogeneous set of differential equations are determined by the arbitrarily chosen  $\underline{K}$ . By choosing  $\underline{K}$  to make this set of equations stable, it can be seen that

$$\tilde{\underline{x}}(t) \rightarrow 0 \quad \text{as } t \rightarrow \infty$$

and

$$\hat{\underline{x}}_k(t) \rightarrow \underline{x}_k(t) \quad \text{as } t \rightarrow \infty \quad .$$

The rapidity of convergence depends solely upon the error system's closed loop eigenvalues determined by  $\underline{K}$ .

The dynamic observer, then, models the system, continually forcing the measurable states' error to zero at a convergence rate determined by  $\underline{K}$ , and gives an estimate of unmeasurable states based upon the measurable states. Thus, a dynamic observer, supplying estimates of unmeasurable states, can be used in conjunction with control schemes based on state variable feedback to create control. A block diagram of the complete closed loop system can be found in Figure 2.

The matrix  $\underline{K}$  can be determined by any method desired by the designer. This system, by the simplicity of its output matrix  $\underline{C}$ , lends itself to a very simple procedure. First notice that  $\underline{C}$  is of the form  $[\underline{I} \mid \underline{0}]$ . The homogeneous error system matrix becomes

$$(\underline{\Phi} - \underline{K}\underline{C}) = (\underline{\Phi} - [\underline{K} \mid \underline{0}]) .$$

The effect of  $\underline{K}$  upon the closed loop system, in this case, is clear.

Choose

$$K_{ij} = \phi_{ij} \quad i \neq j ; \quad i = 1, 2, \dots, 8$$

$$K_{ij} = \phi_{ij} - \lambda_{d_{ij}} \quad i = j ; \quad j = 1, 2, \dots, 8$$

where  $\lambda_{d_{ij}}$  is the desired eigenvalue, and the convergence rate is determined. All but one eigenvalue can be placed using this method. To complete the arbitrary placement of all eigenvalues, determine the state which is most strongly coupled to the unaffected vector in  $\underline{\Phi}$ . Then, devise a second order system with the two states. For example, for Case 1, it is

$$\begin{bmatrix} \lambda_7 \\ x_8 \end{bmatrix}_{k+1} = \begin{bmatrix} \phi_{77} - K_{77} & \phi_{78} \\ \phi_{87} - K_{87} & \phi_{88} \end{bmatrix} \begin{bmatrix} x_7 \\ x_8 \end{bmatrix}_k \quad (11-33)$$

Obviously,  $K_{77}$  and  $K_{87}$  can be chosen to arbitrarily set the eigenvalues of this subsystem. Since all of the other states are already decoupled, the eigenvalues of the total system will be the main diagonal plus the eigenvalues determined by the second order subsystem.

This design method was used to calculate observer gain matrices for both linearized cases. For Case 1, the only coupling between the side velocity vector and the rest of the system was through yaw rate. The resulting  $\underline{K}$  matrix is shown in Table 8. For Case 2, the major coupling was between side velocity and roll rate. The resulting observer gain matrix is also shown in Table 8.

The results of applying the dynamic observers in conjunction with the control systems described earlier are illustrated in Figures 3 and 4. These simulations are done by modeling the linearized systems, setting initial conditions at  $u = 10$  ft/sec,  $v = 4$  ft/sec, and all other state variables at zero. Recall that these velocities are relative to the linearized operating conditions. The observer started with all initial conditions at zero, so that for Case 2,  $u$  is actually 30 ft/sec. Since the system itself, in the computer simulation, was a model, a comparison between the system's side velocity and the observer's estimated side velocity is possible. Time constants for both observers are around one-fifth second and by one-half second have completely converged. This is a very rapid rate of convergence. The observer converges to the other state variables, which are measurable and directly controllable as fast as or faster than the unmeasurable side velocity. It is interesting to note that side velocity is much easier to control for Case 1 (T.C.  $\approx 1.75$  sec) than for Case 2 (T.C.  $\approx 6$  sec). The inertia terms in Case 2 couple the system more strongly, but also make the control more difficult.

The full observer for Case 1 was also run with noise introduced into measurement (Figures 5 and 6). The measurement error was randomly introduced  $\pm 1.0$  ft/sec for  $u$  and  $\pm 10$  percent for all other state variables. The estimated forward velocity follows the actual forward velocity much better than the measurement of  $u$ . This is due to the filtering effect of a full observer. Since an observer converges to a measurable state at a rate determined by its eigenvalues, the fluctuations with measurement error will be slower and smaller in magnitude than the actual measured values. For instance, a measurement error of one ft/sec will result in a .4 ft/sec error for a system with a time constant of .05 sec over a .05 sec time interval. This property of observers should be considered when choosing observer eigenvalues. The faster the eigenvalues the faster the estimated



states converge on measured states, and the less filtering is accomplished; slower eigenvalues give more filtering and slower convergence. The unmeasured side velocity estimate is also shown to follow the real state; even at its worst it is off by only one ft/sec.

If filtering is of no importance, a second type of dynamic observer can be more useful. The full observer discussed here is redundant in that it recreates states which are already measured. The partial observer, discussed in the next section, eliminates this redundancy by creating estimates of only the unmeasurable states. The partial observer also uses much less computer time.

TABLE 8

THE OBSERVER CONTROL MATRICES FOR THE LINEARIZED DISCRETE TIME SYSTEMS

CASE 1

K MATRIX

0.650	0.050	0.000	0.000	0.000	0.000	-0.001
0.000	0.600	0.000	0.000	0.000	0.000	-0.025
-1.600	-0.040	0.550	-0.002	0.000	0.002	0.000
0.000	0.000	0.000	0.500	0.000	0.000	0.000
0.000	0.000	0.000	0.000	0.450	0.049	0.000
0.000	0.001	0.000	0.000	0.000	0.400	-0.001
0.000	0.016	0.000	0.000	0.000	-0.001	1.000
0.000	0.000	0.000	0.000	1.590	0.039	-2000.000

CASE 2

K MATRIX

0.650	0.050	0.000	0.000	0.000	0.000	-0.001
0.000	0.600	0.000	-0.001	0.000	0.000	-0.025
-1.600	-0.040	0.550	0.000	0.000	0.000	0.000
0.001	0.990	-0.001	0.500	0.000	0.000	-0.012
0.000	0.000	0.000	0.000	0.450	0.049	0.000
0.000	0.001	0.000	0.000	0.000	0.977	-0.001
0.000	0.016	0.000	0.000	0.000	-0.001	0.620
0.000	-0.008	0.000	0.000	1.590	-1000.000	-0.993

2

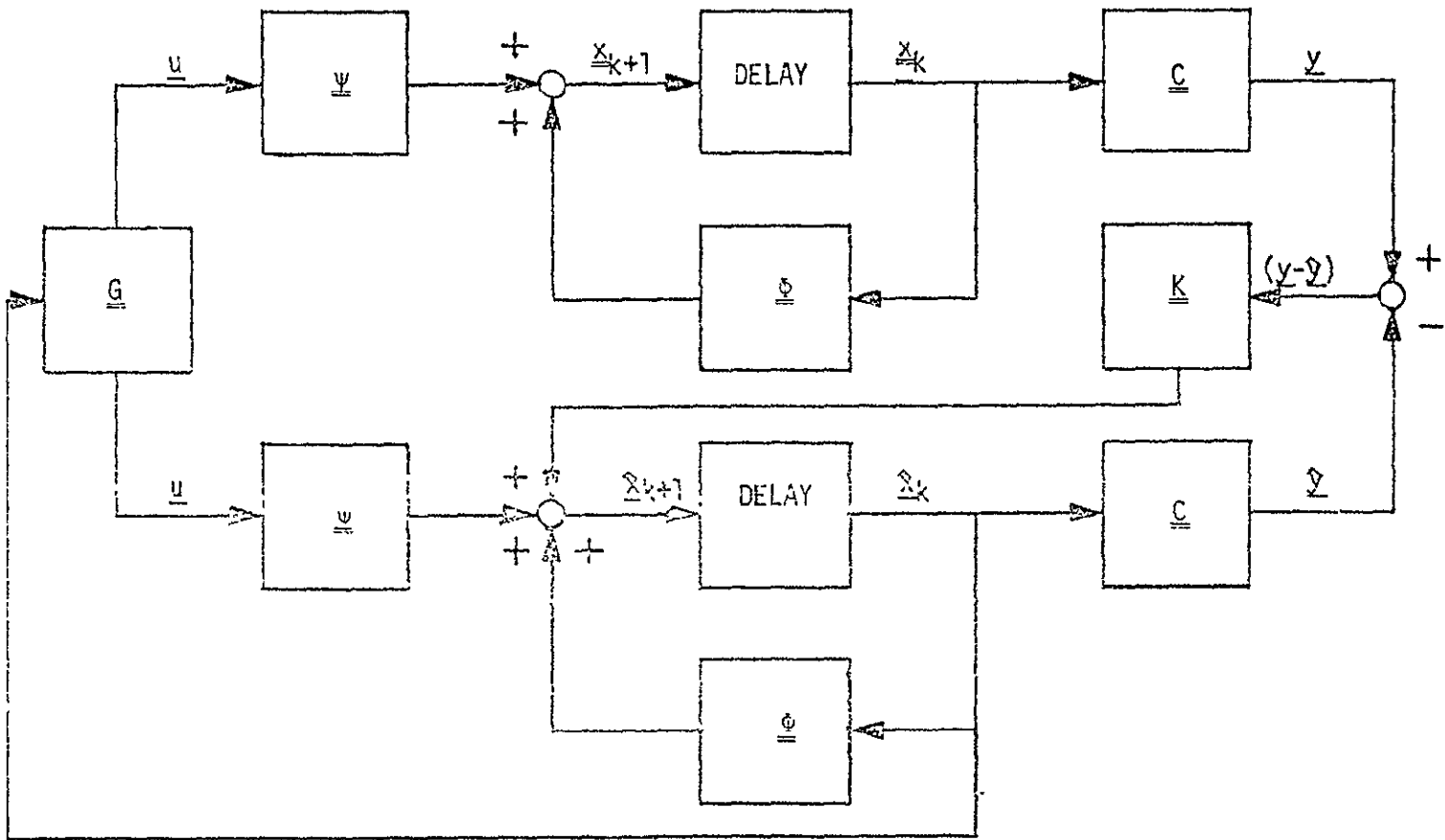


FIGURE 2. A FULL OBSERVER SYSTEM WITH FEEDBACK CONTROL

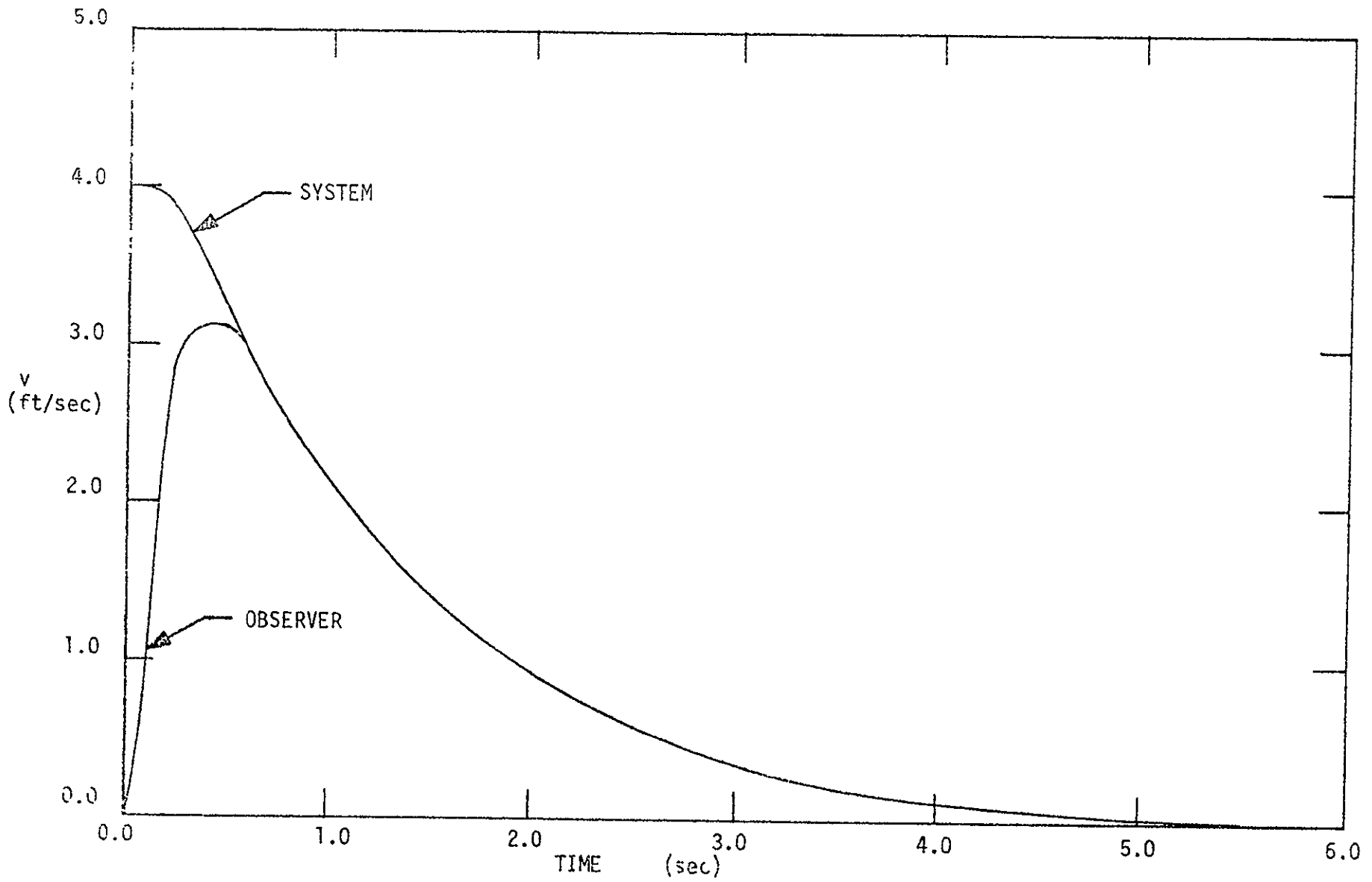


FIGURE 3. CASE 1 - A CLOSED LOOP FULL OBSERVER SIMULATION OF SIDE VELOCITY BEING OBSERVED AND CONTROLLED

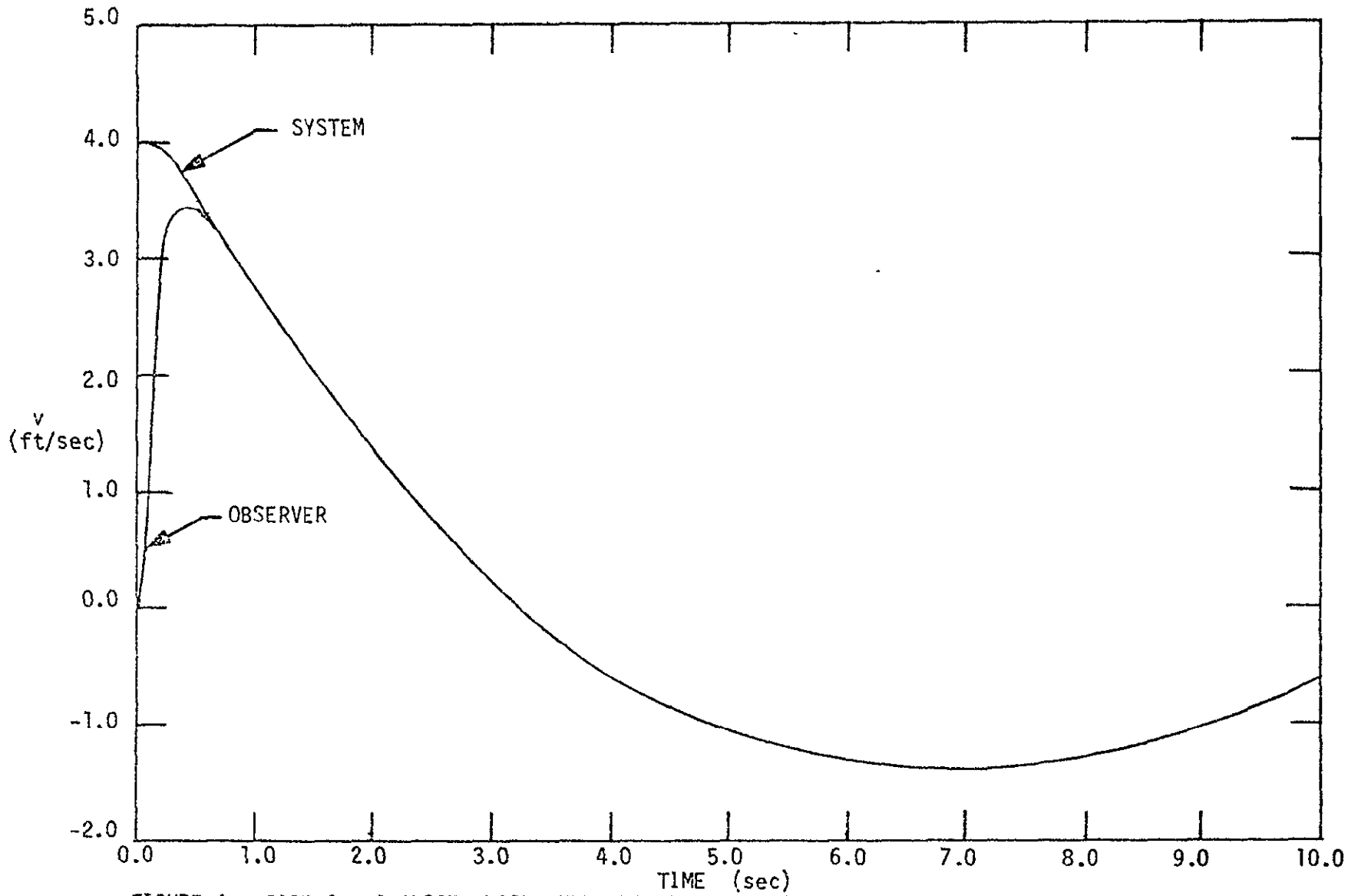


FIGURE 4. CASE 2 - A CLOSED LOOP FULL OBSERVER SIMULATION OF SIDE VELOCITY BEING OBSERVED AND CONTROLLED

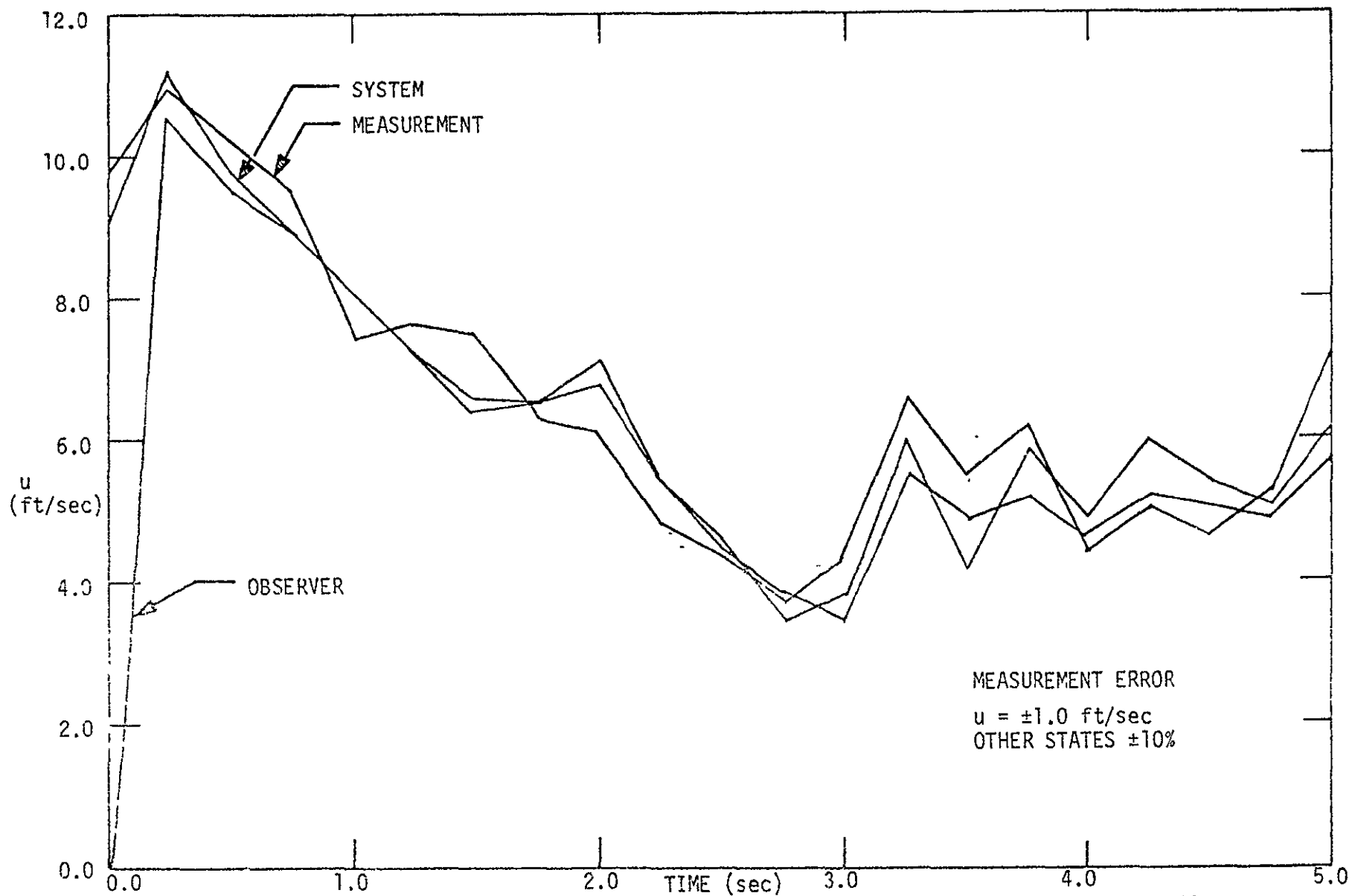


FIGURE 5. A CLOSED LOOP FULL OBSERVER SIMULATION OF FORWARD VELOCITY WITH MEASUREMENT ERROR

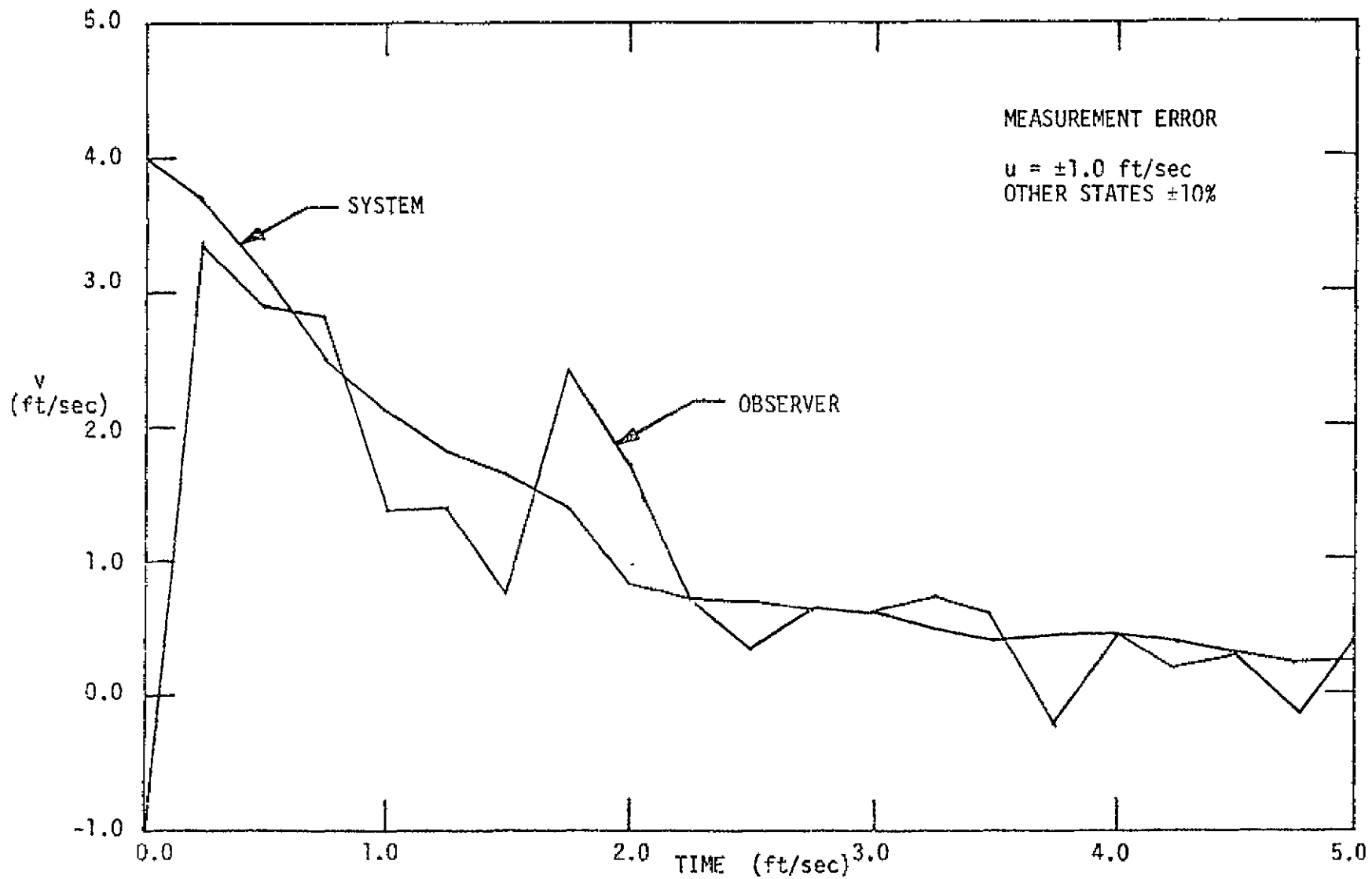


FIGURE 6. A CLOSED LOOP OBSERVER SIMULATION OF SIDE VELOCITY WITH MEASUREMENT ERROR

## CHAPTER 7

## THE PARTIAL OBSERVER

This method for the development of the partial observer is explained by Luenberger [4].

Again, assume the linear system given by equations (7) and (8) which is completely controllable and observable. The system equations, possibly by a coordinate transformation, must be transformed so that

$$\underline{C} = [\underline{I} \mid \underline{0}]$$

where  $\underline{I}$  is the identity matrix. In this case the system is especially amenable to this method because it is essentially already in this form. The transformation is done to provide a direct correspondence between the output and the transformed state variables. The new state variables are partitioned

$$\underline{x} = \begin{bmatrix} \underline{y} \\ \underline{w} \end{bmatrix},$$

where  $\underline{y}$  is the vector of measurable state variables (by the definition of  $\underline{C}$ ,  $\underline{y}$  is the same as in (8)) and  $\underline{w}$  is the vector of unmeasurable state variables.

The state equations can then be written as

$$\begin{bmatrix} \underline{y} \\ \underline{w} \end{bmatrix}_{k+1} = \begin{bmatrix} \underline{\phi}_{yy} & \underline{\phi}_{yw} \\ \underline{\phi}_{wy} & \underline{\phi}_{ww} \end{bmatrix} \begin{bmatrix} \underline{y} \\ \underline{w} \end{bmatrix}_k + \begin{bmatrix} \underline{\psi}_y \\ \underline{\psi}_w \end{bmatrix} u_k \quad (II-34)$$

The partial observer is defined from the above as

$$\hat{\underline{w}}_{k+1} = \underline{\phi}_{ww} \hat{\underline{w}}_k + \underline{\phi}_{wy} \underline{y}_k + \underline{\psi}_w u_k + \underline{1} [\underline{y}_{k+1} - \underline{\phi}_{yw} \hat{\underline{w}}_k - \underline{\phi}_{yy} \underline{y}_k - \underline{\psi}_y u_k]. \quad (II-35)$$

Notice that the term in brackets is a constant and is defined equal to zero for the correct values of  $\underline{w}$ . Rearranging the partial observer equation



$$\hat{w}_{k+1} = (\underline{\Phi}_{ww} - \underline{L}\underline{\Phi}_{yw})\hat{w}_k + \underline{\Phi}_{wy}y_k + \underline{\Psi}_w u_k + \underline{L}[y_{k+1} - \underline{\Psi}_{ww}y_k - \underline{\Psi}_y u_k] \quad (II-36)$$

it becomes apparent that the eigenvalues of the observer are the eigenvalues of

$$(\underline{\Phi}_{ww} - \underline{L}\underline{\Phi}_{yw})$$

and all other terms are inputs into the partial observer equations. To eliminate the need to calculate  $y_{k+1}$ , assume the transformation

$$z_k = \hat{w} - \underline{L}y$$

The final form of the observer is

$$z_{k+1} = (\underline{\Phi}_{ww} - \underline{L}\underline{\Phi}_{yw})z_k + (\underline{\Phi}_{ww} - \underline{L}\underline{\Phi}_{yw})\underline{L}y_k + (\underline{\Phi}_{wy} - \underline{L}\underline{\Phi}_{yy})y_k + (\underline{\Psi}_w - \underline{L}\underline{\Psi}_y)u_k.$$

(II-37)

A block diagram of the system is found in Figure 7.

The partial observer control matrix,  $\underline{L}$ , is chosen by any desirable method to place the eigenvalues. In the X-14B VTOL only the side velocity is unmeasurable and thus the partial observer is a first order system.

For Case 1,

$$\underline{L} = [0 \quad 0 \quad 0 \quad 0 \quad 0 \quad 2000 \quad -2000]$$

This placed the partial observer discrete time eigenvalue at

$$(\lambda_d)_{DIS} \approx 0.725$$

or a time constant  $\approx 0.18$  seconds.

For Case 2, the partial observer gain vector was chosen as

$$\underline{L} = [0 \quad 0 \quad 0 \quad 0 \quad 0 \quad -1000 \quad 0]$$

The partial observer eigenvalue was approximately .769. As seen through these examples the observer gains can be chosen for any desired convergence rate. Observer gains are not limited by control power constraints.

Figures 8 and 9 compare the estimated and actual side velocities, when the initial conditions of the system are  $u = 10$  ft/sec,  $v = 4$  ft/sec, and all others are set to zero. The states are again relative to the

linearized reference states. The system controllers are the same as used for the full observer simulations. Convergence is rapid and is essentially completed in both cases in less than one second.

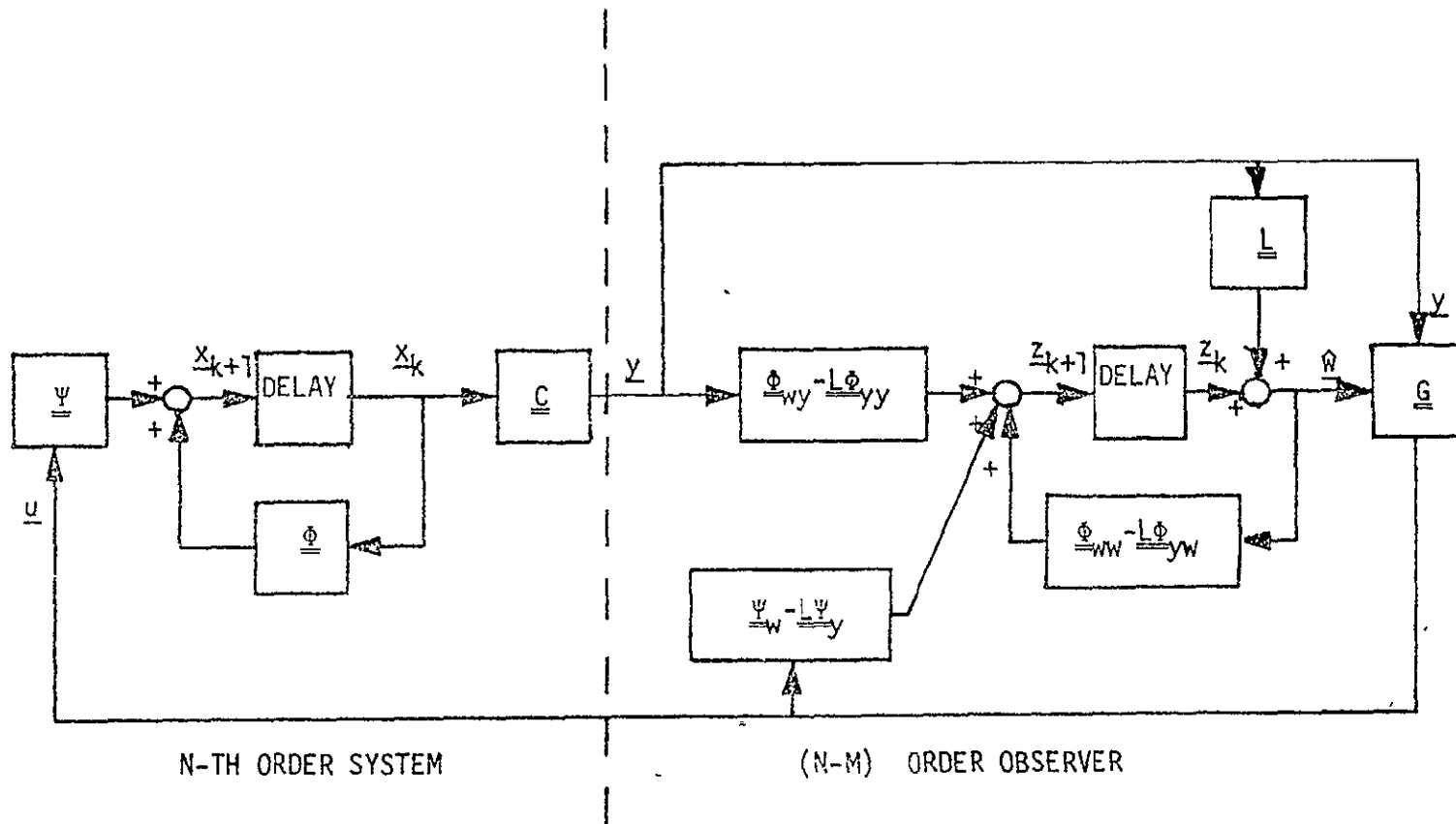


FIGURE 7. A PARTIAL OBSERVER SYSTEM WITH FEEDBACK CONTROL

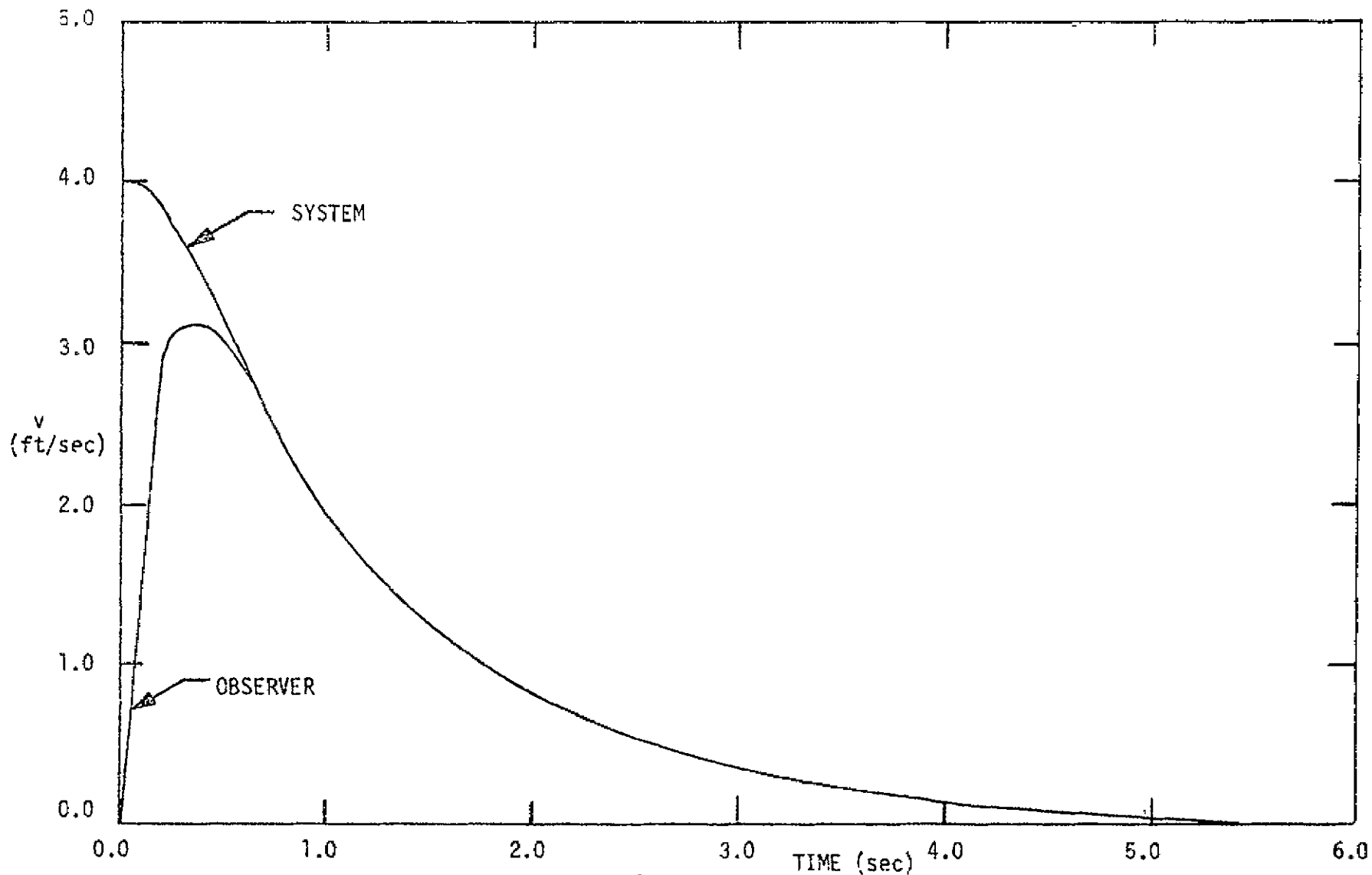


FIGURE 8. CASE 1 - A CLOSED LOOP PARTIAL OBSERVER SIMULATION OF SIDE VELOCITY BEING OBSERVED AND CONTROLLED

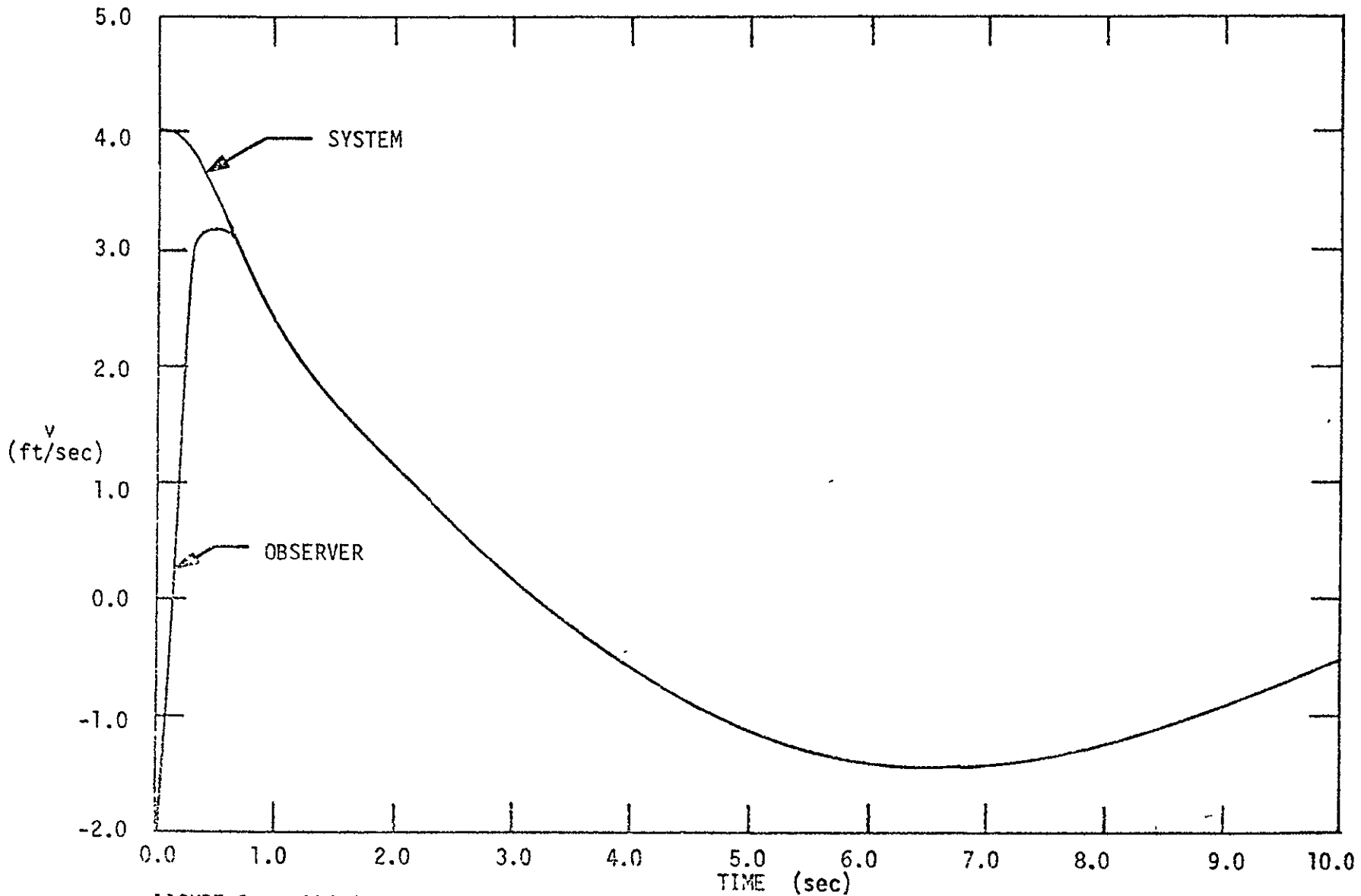


FIGURE 9. CASE 2 - A CLOSED LOOP PARTIAL OBSERVER SIMULATION OF SIDE VELOCITY BEING OBSERVED AND CONTROLLED

## CHAPTER 8

## APPLICATION TO FULL NONLINEAR SYSTEM

The linear full observer is next applied to the nonlinear model developed by Roesener [2].

The purpose is to determine the usefulness of linear observers in estimating the side velocity for the actual craft. Trim parameters for the craft were held to the nearest linearized reference values.

To test the usefulness of the linearized equations for Case 1, the nonlinear equations were initialized at  $u = 5$  ft/sec,  $v = 2$  ft/sec,  $\theta = q = w = p = \phi = r = 0$ . The essential results can be found in Figures 10 through 12. Figure 10 shows the observer estimate of forward velocity converging on the actual forward velocity within one-half second, but in Figure 11, yaw rate is shown undergoing small oscillations at approximately six cycles per second. The oscillations can be attributed to computer error as the oscillations are small ( $\approx 10^{-3}$  radians/sec) and difficulties were encountered with balancing accumulation error and truncation error. The linearized system's eigenvalues predicted no such oscillation. The observer is tracking the yaw rate very well, but the necessary .05 second time delay becomes very noticeable in an oscillation this fast. The yaw rate in the linearized versions showed no such oscillations. Remembering that yaw rate was the only significant coupling between the system and side velocity for this linearization, Figure 12 is no surprise when it shows no reasonable estimate of the actual side velocity. If computer error this small can degrade the estimate of side velocity this severely, it can safely be assumed that no accurate estimate will be developed for this operating condition on the actual craft.

For Case 2 the results were more useful. The yaw rate still oscillated as before, but for this linearization roll rate was the the major coupling between side velocity and the system. In Figure 13, for initial conditions of  $u = 20$  ft/sec and  $v = 2.0$  ft/sec, the observer gives a very good estimate of side velocity. At  $u = 25$  ft/sec,  $v = 10$  ft/sec (Figures 14 and 15) the observer forward velocity converges rapidly to the measured forward velocity. The observer side velocity rises rapidly to 6 ft/sec, and then waits until the real system side velocity slows before continuing to follow. Given the initial conditions  $u = 25$  ft/sec,  $v = 5$  ft/sec, in Figure 16, the observer estimate rapidly overshoot the system side velocity by about 20 percent and followed increasingly better as side velocity went through zero. The case of  $u = 15$  ft/sec,  $v = 5$  ft/sec is found in Figure 17. The observer again waited, this time at around 2 ft/sec, for the system side velocity to slow.

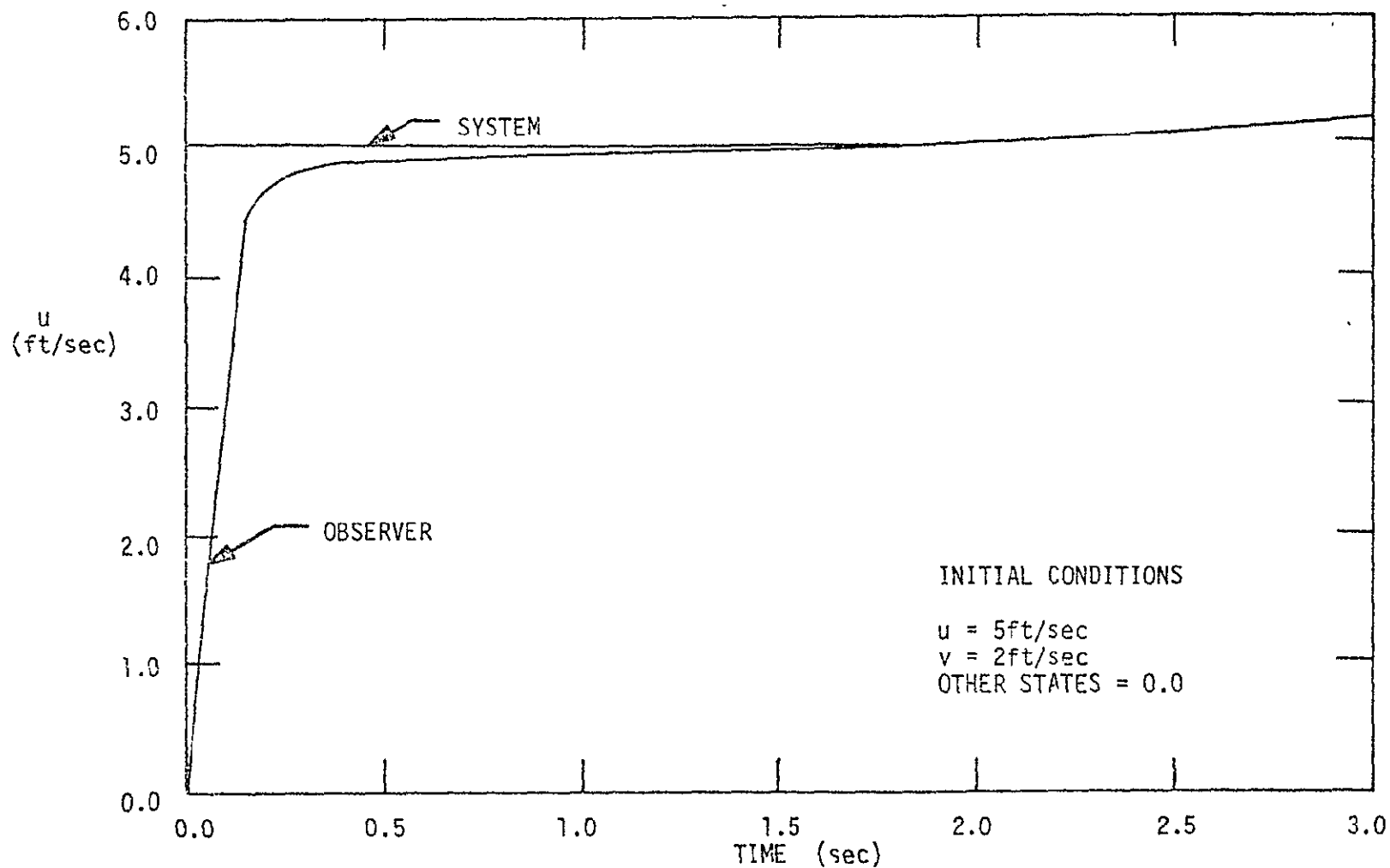


FIGURE 10. THE OPEN LOOP NONLINEAR SYSTEM WITH FULL OBSERVER ESTIMATE OF FORWARD VELOCITY FOR CASE 1,  $u=5, v=2$



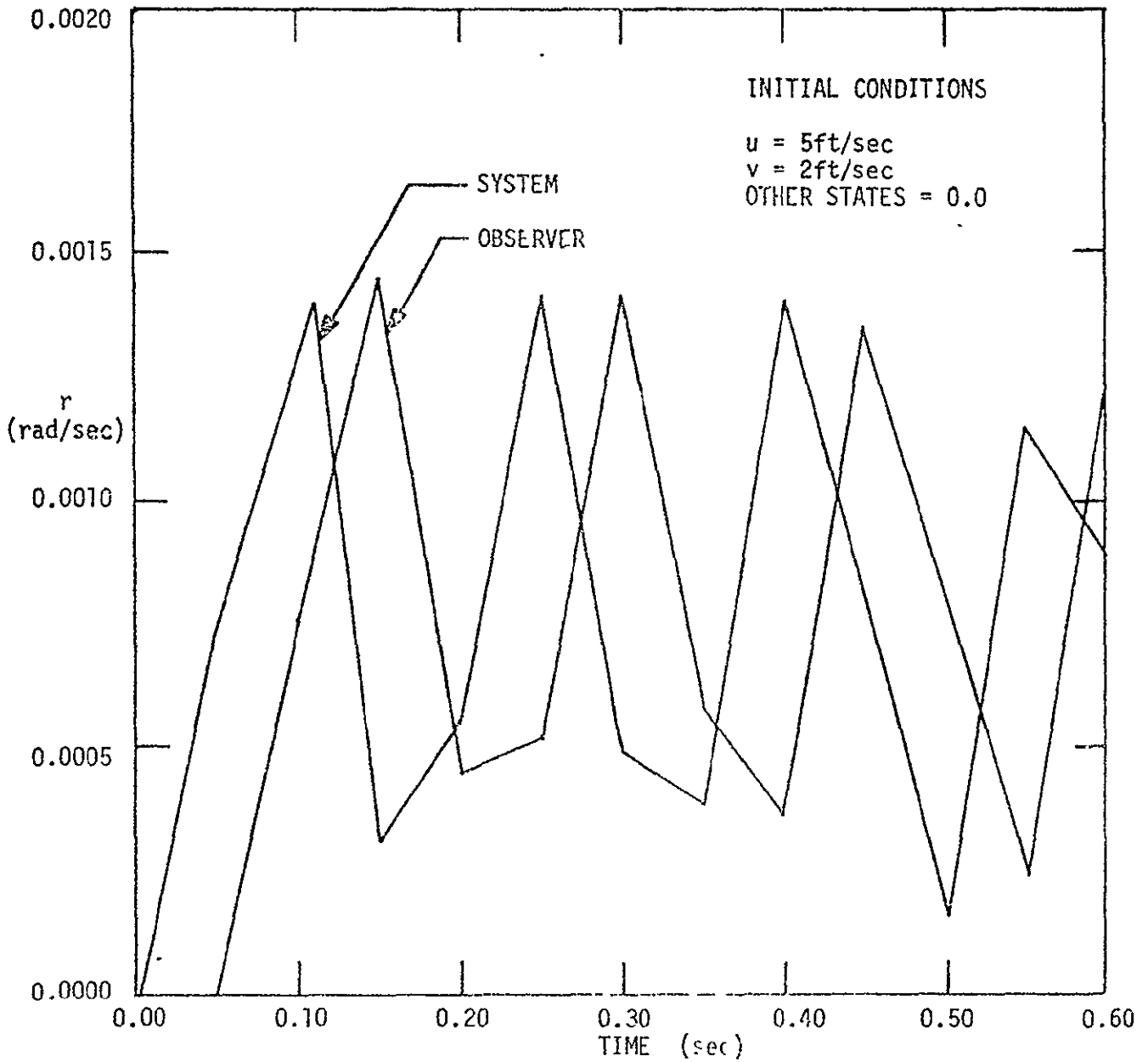


FIGURE 17. THE OPEN LOOP NONLINEAR SYSTEM WITH FULL OBSERVER  
 ESTIMATE OF ROLL RATE FOR CASE 1,  $u=5, v=2$

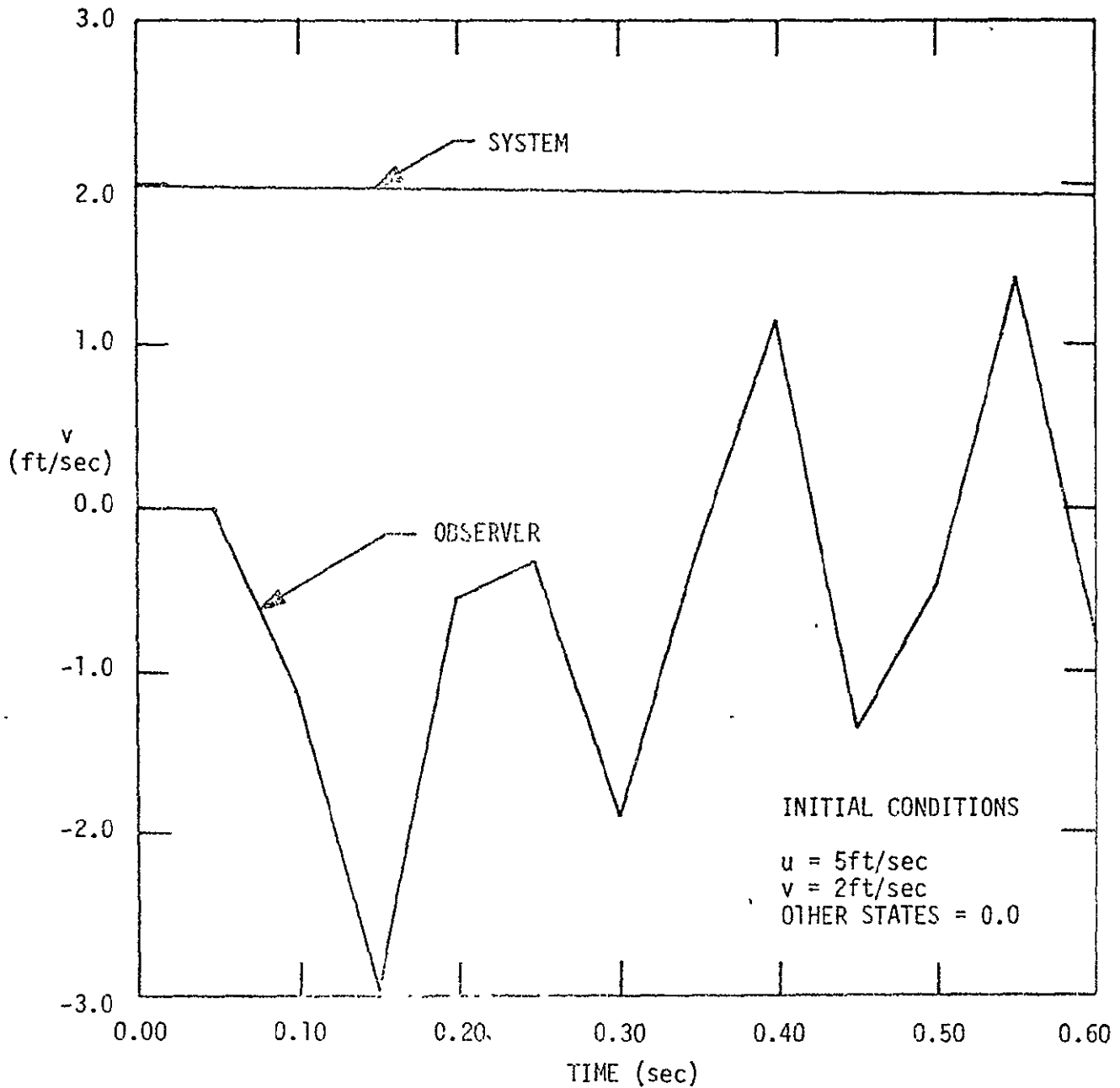


FIGURE 12. THE OPEN LOOP NONLINEAR SYSTEM WITH FULL OBSERVER ESTIMATE OF SIDE VELOCITY FOR CASE 1,  $u=5$ ,  $v=2$

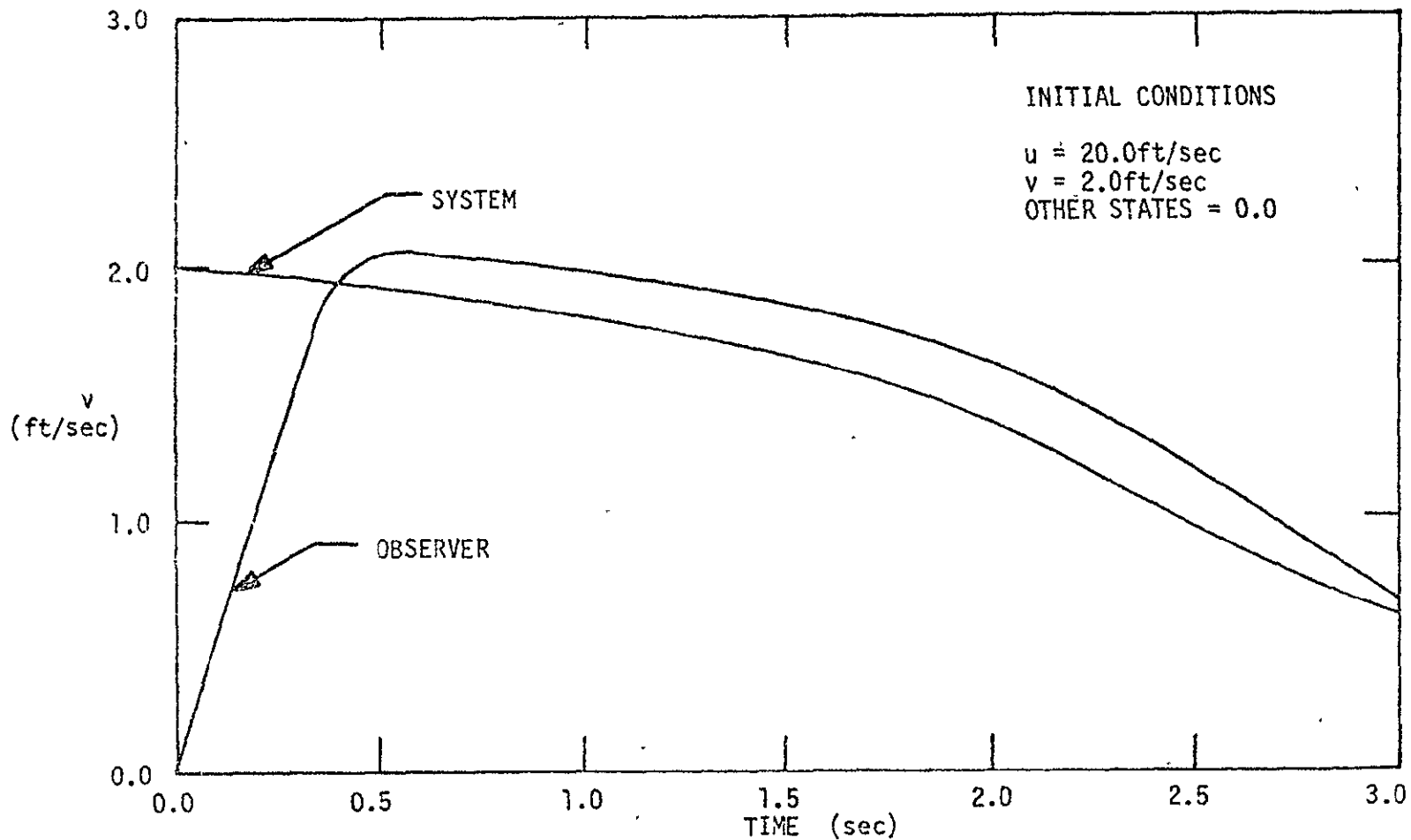


FIGURE 13. THE OPEN LOOP NONLINEAR SYSTEM WITH FULL OBSERVER ESTIMATE OF SIDE VELOCITY FOR CASE 2,  $u=20, v=2$

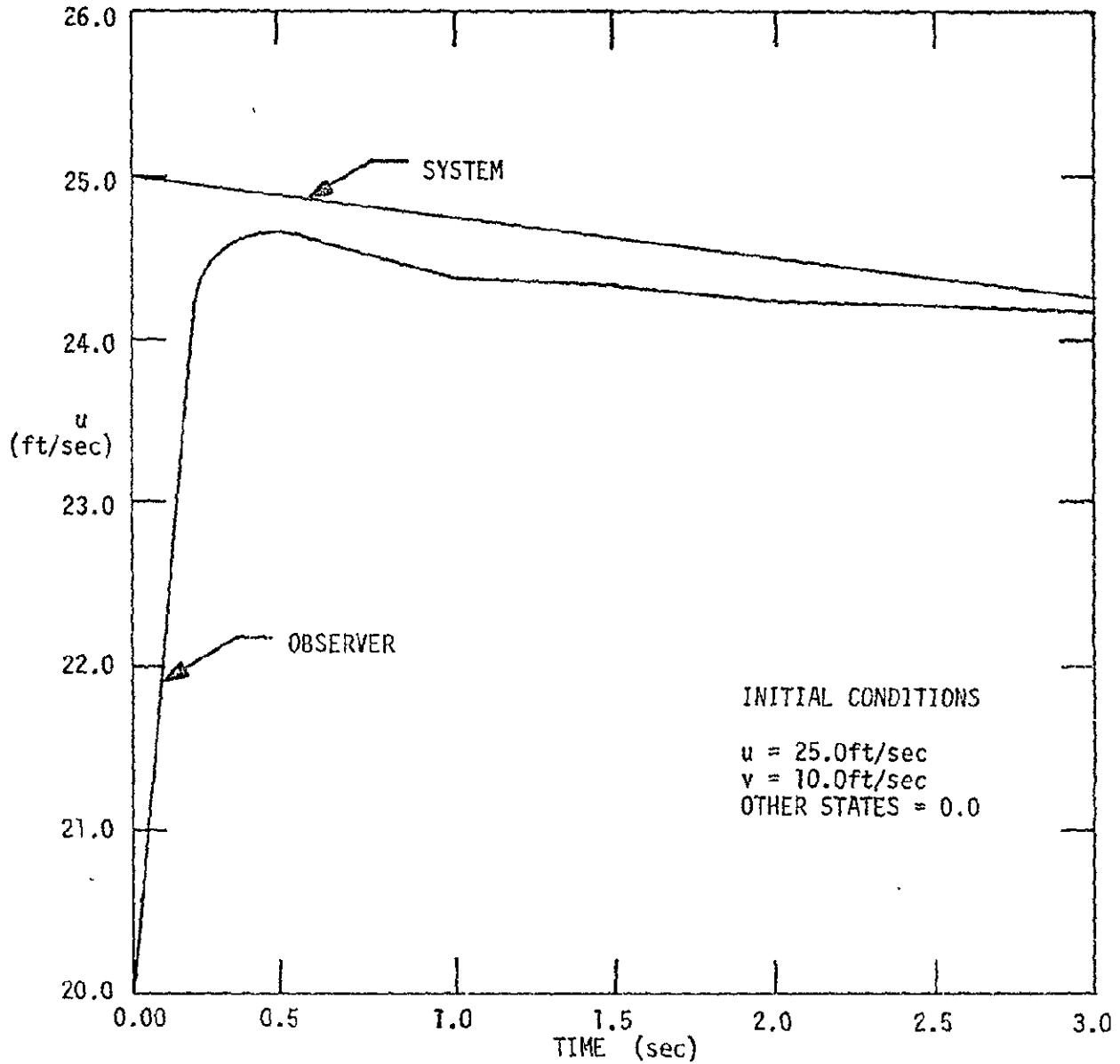


FIGURE 14. THE OPEN LOOP NONLINEAR SYSTEM WITH FULL OBSERVER ESTIMATE OF FORWARD VELOCITY FOR CASE 2,  $u=25, v=10$

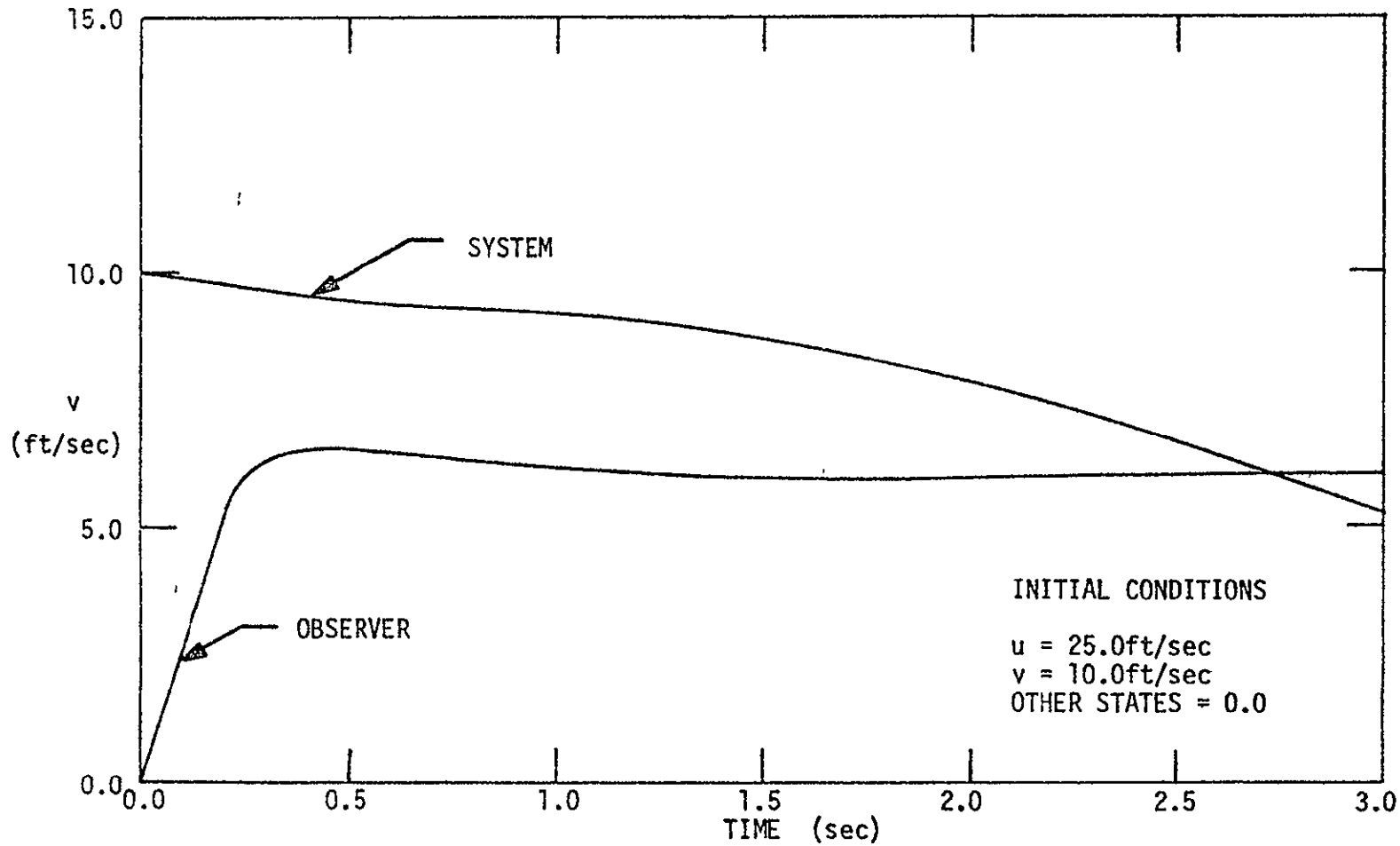


FIGURE 15. THE OPEN LOOP NONLINEAR SYSTEM WITH FULL OBSERVER ESTIMATE OF SIDE VELOCITY FOR CASE 2,  $u=25, v=10$

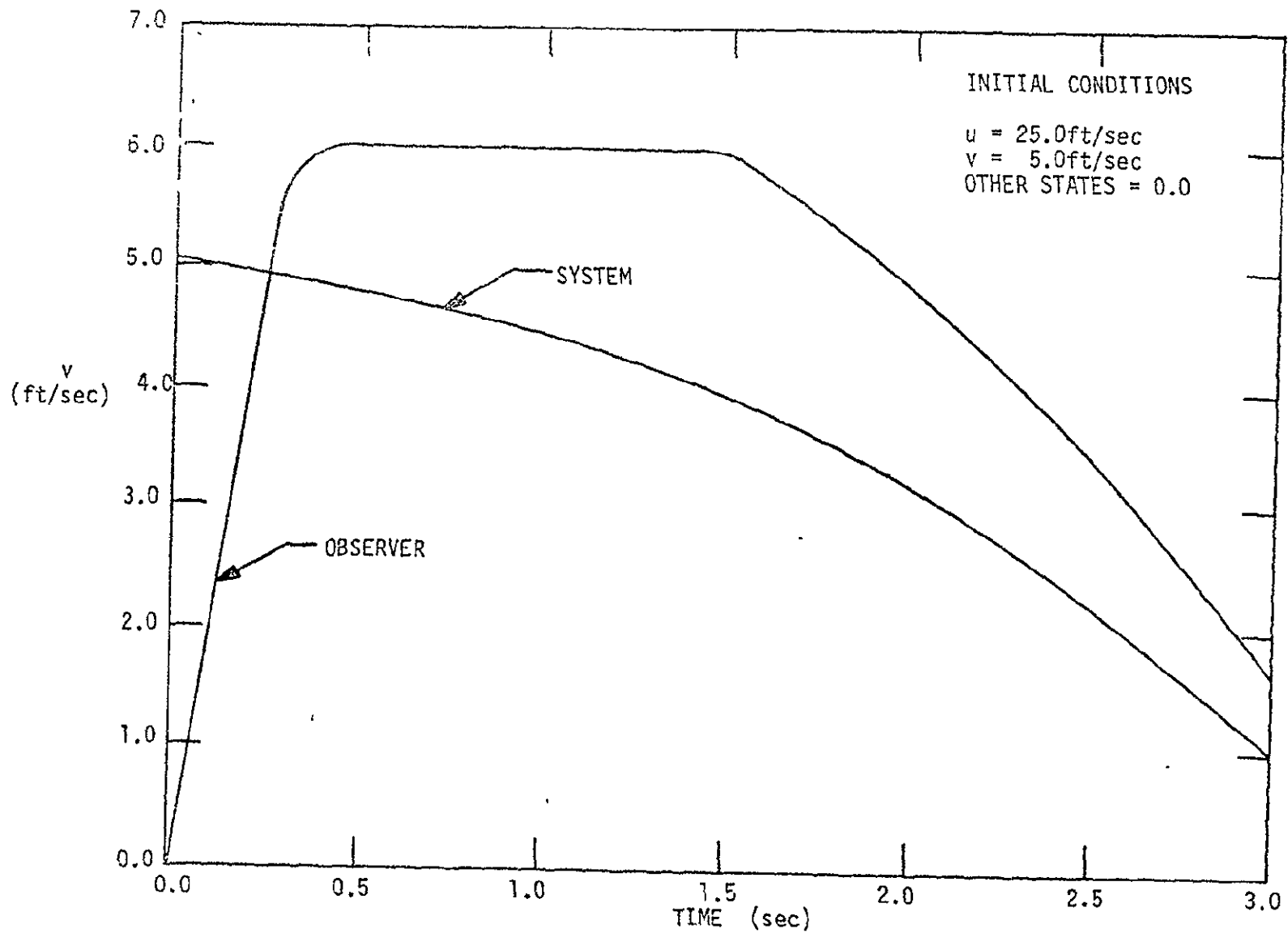


FIGURE 16. THE OPEN LOOP NONLINEAR SYSTEM WITH FULL OBSERVER ESTIMATE OF SIDE VELOCITY FOR CASE 2,  $u=25, v=5$

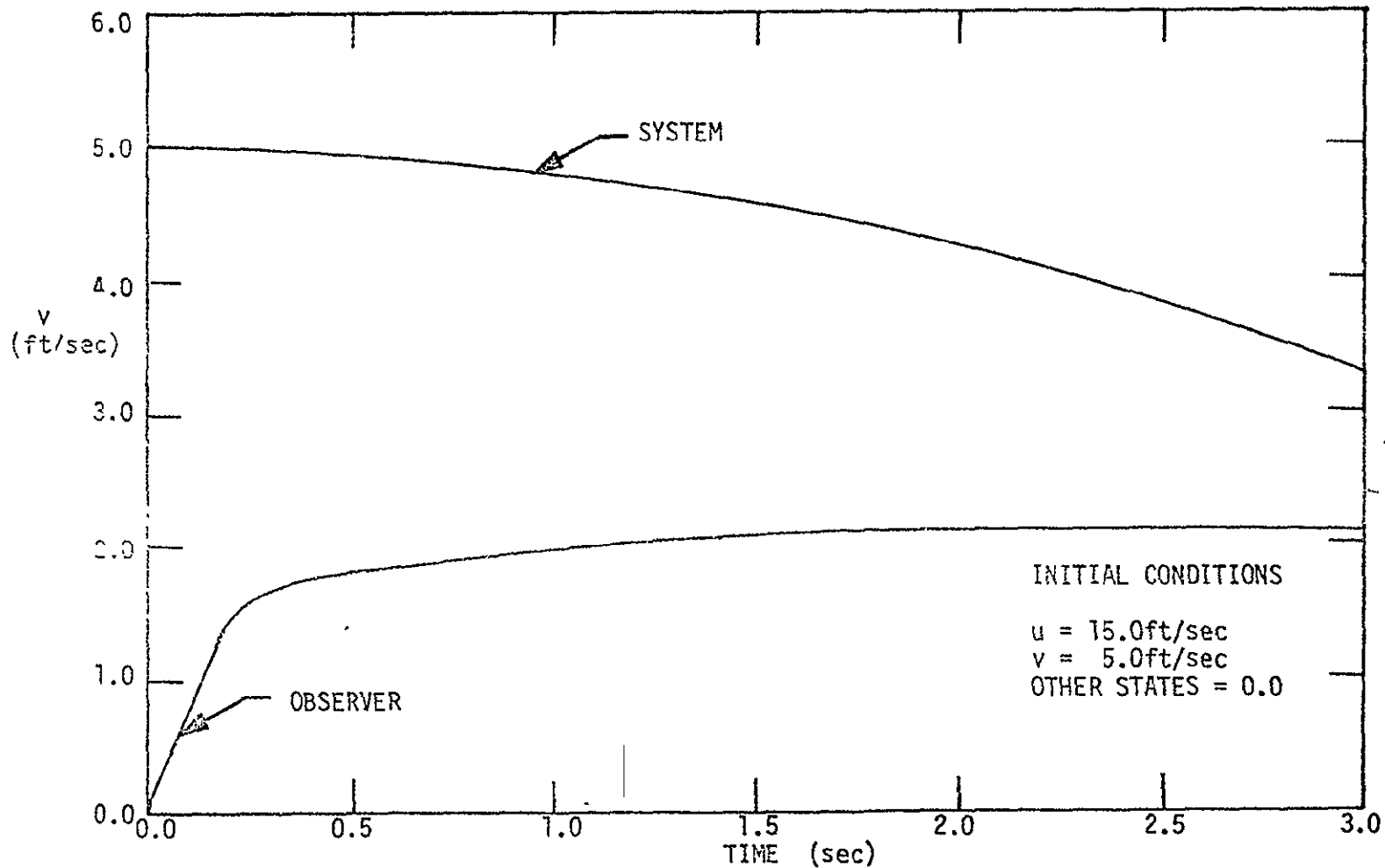


FIGURE 17. THE OPEN LOOP NONLINEAR SYSTEM WITH FULL OBSERVER ESTIMATE OF SIDE VELOCITY FOR CASE 2 , $u=15,v=5$

## CHAPTER 9

## CONCLUSIONS

Dynamic observers can be used to create an estimate of unmeasurable states needed for implementing state variable feedback control policies. Although based on linear control theory, dynamic observers can be applied to some nonlinear systems, depending upon the nature and degree of the nonlinearities.

The method applied in this research can place observer eigenvalues arbitrarily. If the output matrix is not in  $[\underline{I} \mid \underline{0}]$  form, general modal pole placement techniques could be used, as in the control section. A full dynamic observer should be used when measurement error is large and filtering of measured states desired. The only faults of a full observer are a slight time lag and an excessive use of computer time. The partial observer eliminates time lag and minimizes computer time, but offers limited filtering capabilities. The decision between full and partial observers must be made by the designer to fit the individual situation.

The results from the linearization at 20 ft/sec forward velocity indicate that the side velocity can be estimated for the full nonlinear system using linear observer theory. The effective range of each linearization must be determined for criteria such as the desired accuracy in the estimate, balanced with the computer time and memory needed to implement it. For the X-14B VTOL, these ranges seem to extend further above the operating points than below. For instance, the linearization at 20 ft/sec forward velocity did a much better job of estimating the side velocity at  $u = 25$  ft/sec and  $v = 5$  ft/sec than at  $u = 15$  ft/sec and  $v = 5$  ft/sec. The two linearized flight conditions also seem to indicate that the linearization ranges become increasingly smaller as flight becomes



slower, culminating in the condition at  $u = .01$  ft/sec which seems to have no ability to estimate the nonlinear side velocity because of a lack of coupling between the state variables.

It is recommended that a method for estimating side velocity over the entire operating range be obtained by generating a matrix of operating conditions similar to Figure 18. The aircraft, as it changed flight conditions, would switch from one set of parameters for a linear observer to another, continually using the most applicable.

Figures 13 through 17 illustrate that to make the desired estimate more accurate, more operating conditions are needed. The limiting case of mapping operating conditions would be to investigate fully adaptive observers. These would include parameter varying observer gains to control the model to the system.

Limited input modal control is a useful and relatively simple technique for designing control policies. The designer must approach pole placement in a logical and systematic manner. It is suggested that one eigenvalue be moved at a time while keeping all others stationary to determine the individual eigenvalues' effects on the gain matrix  $\underline{G}$ . Using this method for this system it was determined that some poles could be arbitrarily placed with little effect on  $\underline{G}$ , while  $\underline{G}$  was highly sensitive to others.

One effect of arbitrary pole placement of which the designer should be aware is derivative action. This is an undesirable initial overshoot during control caused by a zero dominating the initial dynamics. To eliminate this problem, the designer must place poles so that they dominate.

A most informative method for determining complete controllability and complete observability is through the modal transformation. It allows the designer to determine the degree of the system's input, output coupling

for individual modes. For the X-14B VTOL, the modal input matrix  $\underline{H}$ , for Case 1 and Case 2, was studied in detail before actual design. It can be seen readily that the magnitudes are larger for Case 1 than for Case 2, which suggests that Case 1 might be controlled more quickly. This conclusion was reinforced when control was later implemented and found to be slower for Case 2. The inertia terms in Case 2, which create a more strongly coupled system, also require more control power. Examining the output matrix,  $\underline{F}$ , the designer is also able to determine that side velocity will be much more difficult to estimate for Case 1 than for Case 2 as the maximum coupling is an order of magnitude smaller. This observation was proven true when the linear observer was applied to the nonlinear system.

All simulations of systems to be performed on a digital computer should be transformed into discrete time difference equations. The transformation is simple and easily performed through many techniques, just one of which is explained here. The method used here is again most applicable if modal control is to be used. Discrete time equations have been shown to be approximately an order of magnitude faster to execute on a digital computer than integration routines [3]. If a digital computer is to be used to implement the control at a specified time interval, it is an additional reason to use difference equations. The application of control techniques in this research proved to be no different than for continuous time control except for the interpretation of eigenvalues. Eigenvectors remain invariant.

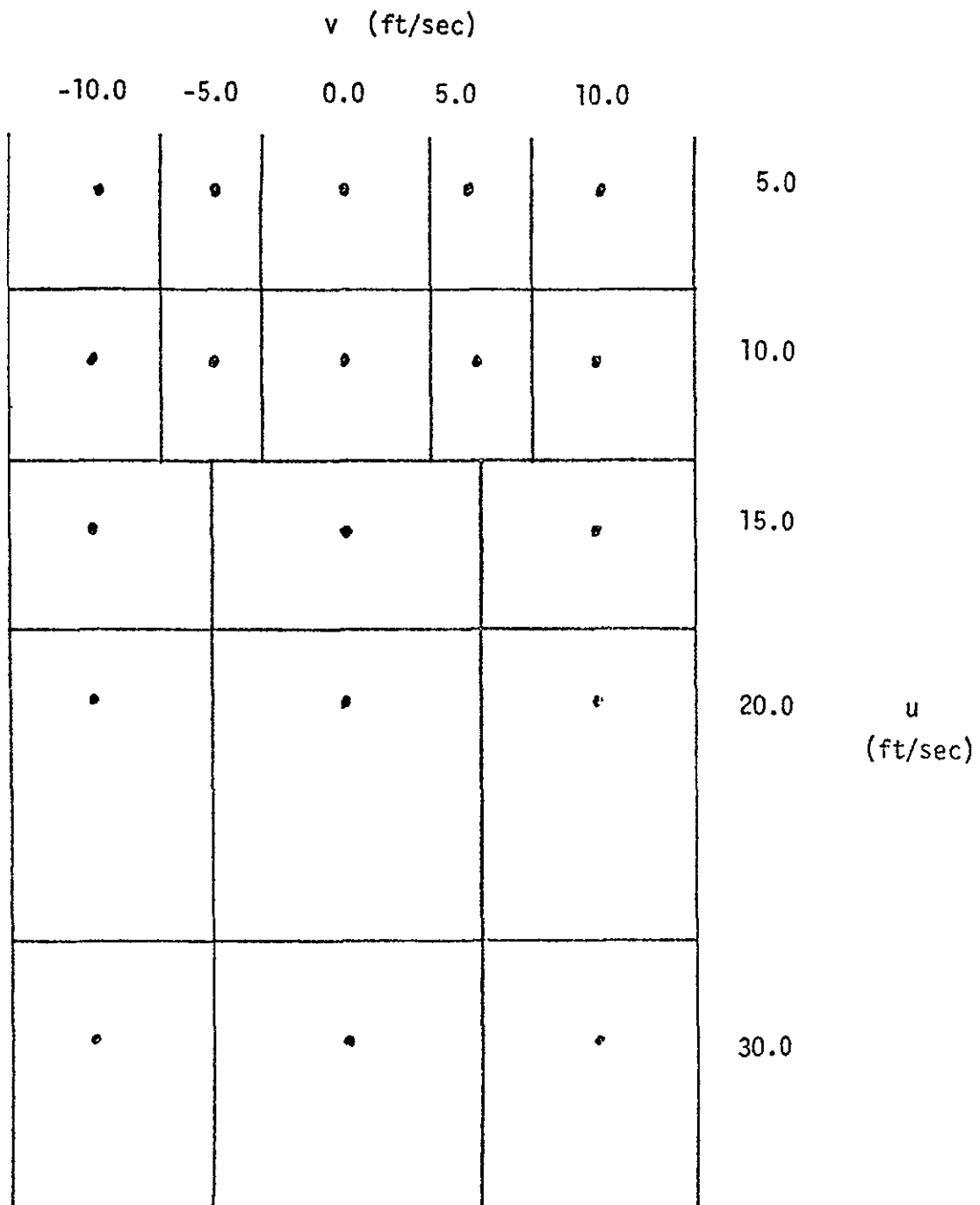


FIGURE 18. EXAMPLE SET OF LINEARIZATION POINTS AND THEIR INDICATED RANGES OF APPLICATION

## BIBLIOGRAPHY

1. Hoffman, M., Loscutoff, W. V., Seevers, J., "Equations of Motion for the X-14 Aircraft," Report NASA Grant NGR-05-004-051, 1972.
2. Roesener, R., "Wind Gust Analysis of the X14B VTOL Aircraft," M.S. Thesis, Department of Mechanical Engineering, University of California, Davis, 1973.
3. Davison, E., "A High Order Crank-Nicholson Technique for Solving Differential Equations," Computer Journal 10(2), August 1967.
4. Luenberger, D., "An Introduction to Observers," IEEE Trans. on Automatic Control, AC-16(6), December 1971.
5. Takahashi, Y., Rabins, M., Auslander, D., Control, Reading, Mass.: Addison-Wesley Publishing Co., 1970.
6. Ogata, K., Modern Control Engineering, Englewood Cliffs, New Jersey: Prentice-Hall, Inc., 1970.

# CONTROLLABILITY AND OBSERVABILITY

```


DIMENSION ROR(8),ROF(8),VECR(8,8),VECI(8,8),INDIC(8)
DOUBLE PRECISION R(R,6),THAT(8,8),TMAT(8,8),L(8),M(8),TIA(8,8)
1 TIA(8,8),TIB(8,6),F(7,8),CPHAT(7,8),A(8,8)
2 OFN(8,8)=0
3 FI(8,8)
C THIS PROGRAM IS USED TO DETERMINE IF THE SYSTEM IS COMPLETELY
C CONTROLLABLE AND COMPLETELY OBSERVABLE READ THE SYSTEM MATRICES
C AND THE SIMILARITY TRANSFORMATION MATRIX THAT
READ(5,1) A

HEAD(5,1) R
HEAD(5,2) CPHAT
DO 21 I=1,8
DO 21 J=1,8
21 AI(I,J)=A(I,J)
CALL EIGENP(8,8,AI,39,ROR,ROC,VECR,VECI,INDIC)
DO 22 I=1,8
DO 22 J=1,8
22 THAT(J,J)=VECR(I,J)
DO 23 J=1,8
THAT(J,2)=VECI(J,1)
23 THAT(J,4)=VECI(J,3)
WRITE(5,24) ROR,ROF,((VECR(I,J),J=1,8),I=1,8),((VECI(I,J),J=1,8),
I=1,8),INDIC
24 FORMAT('THE REAL ROOTS',/,'0E14.6',/,'THE COMPLEX ROOTS',/,'0E14.6',
1//,'THE REAL EIGENVECTORS',/,'0(3E14.6)',/,'
3 'THE COMPLEX EIGENVECTORS',/,'0(2E14.6)',/,'THE INDICATOR',/,'0E14
A,6)
WRITE(7,25)((THAT(I,J),I=1,8),J=1,8)

25 FORMAT(4E15,7)
1 FORMAT(4F15,6)
2 FORMAT(7F10,0)
WRITE(6,11)((A(I,J),J=1,8),I=1,8)
WRITE(6,12)((R(I,J),J=1,6),I=1,8)
WRITE(6,11)((CPHAT(I,J),J=1,8),I=1,7)
WRITE(5,17)((TMAT(I,J),J=1,8),I=1,8)
11 FORMAT(6F15,5)
12 FORMAT(6F15,5)

```

Reproduced from  
 best available copy.



```

DO 3 I=1,8
DO 3 J=1,8
TMAT(I,J)=TMAT(J,I)
3 CONTINUE
CALL MINV(TMAT,8,8,L,M)
WRITE(6,1) 0
WRITE(6,1)((TMAT(I,J),J=1,8),I=1,8)
CALL HPRC(TMAT,THAT,8,8,0,0,8)
WRITE(6,1)((DEY(I,J),J=1,8),I=1,8)
CALL HPRC(TMAT,A,7,8,8,8,0,0,8)
CALL HPRC(TA,THAT,7,8,8,8,0,0,8)
WRITE(6,1)((TIAT(I,J),J=1,8),I=1,8)
CALL HPRC(TMAT,B,7,8,8,8,0,0,8)
CALL HPRC(PMAT,THAT,7,8,8,8,0,0,8)
WRITE(6,4)((TIAT(I,J),J=1,8),I=1,8),((TIB(I,J),J=1,8),I=1,8),
1 ((F(I,J),J=1,8),I=1,8)
4 FORMAT(//,'THE CONTINUOUS TIME MODAL MATRIX',/,'B(BF10.5/)',//,
1 'THE MODAL INPUT MATRIX ALL ROWS MUST HAVE VALUE',/,'B(BF10.5/)',
2 '//','THE MODAL OUTPUT MATRIX ALL COLUMNS MUST HAVE VALUE',/
3 '(BF10.5/)',
STOP
END

```

# DETERMINATION OF MODAL CONTROL GAIN MATRIX AND RESULTING SIMULATION

```

DIMENSION MMAT(4,5), PHIM(8,8), TMA(8,8), PHM(1,6)
1,4, T(6,5), OMAT(1,8), APMAT(6,8), HPMAT(6,8), CMAT(6,8), PHM(8,8)
ICON(8,8), L(8), Y(8), TMAT(8,8), FOP(8), FCC(8), INDIC(8), VECE(8,8)
IVECI(8,8), PHIML(6,8), PHIDL(6,9), CPMAT(7,8), BMAT(8,6), PHII(8,8)
DOUBLE PRECISION TMA, BMAT, MMAT, PHM, PHII, TMA, PHIM, PHIML, PHIDL,
IAR, MAT, OMAT, COM, HLM, BKMAT, D, TMA(8,8)
COMMON OMAT, MMAT, PHM
WRITE(5,22)

22 FORMAT(1H1,5X,'SIMULATED CONTROLLED T=0.05')
READ(5,11)((B=IT(I,J),J=1,6),I=1,2)

11 FCPMAT(2E14,7)
WRITE(6,31)
51 FCPMAT(1H0,5X,'THE ORIGINAL INPUT MATRIX BMAT')
WRITE(6,25)((BMAT(I,J),J=1,6),I=1,8)
25 FCPMAT(6F14,5)
READ(9,10) PHID
10 FCPMAT(8E10,8)
WRITE(6,23)
23 FCPMAT(1J,5X,'THE DESIRED CLOSED LOOP SYSTEM MATRIX PHM')
WRITE(6,27)((PHM(I,J),J=1,8),I=1,8)
27 FCPMAT(8F14,5)
READ(9,9)((PHI(I,J),J=1,8),I=1,8)
9 FCPMAT(4E14,7)
WRITE(6,30)
30 FCPMAT(1H0,5X,'THE DISCRETIZED SYSTEM MATRIX PHM')
WRITE(6,27)((PHI(I,J),J=1,8),I=1,8)
PE=1(5,9)((TMA(I,J),J=1,8),I=1,8)
DO P I=1,8
TMA(1,1)=TMA(I,5)
TMA(1,2)=TMA(I,1)
TMA(1,3)=TMA(I,2)
TMA(1,4)=TMA(I,4)
TMA(1,5)=TMA(I,6)
TMA(1,6)=TMA(I,8)
TMA(1,7)=TMA(I,7)
TMA(1,8)=TMA(I,3)
P
CONTINUE
WRITE(6,32)
32 FCPMAT(1H0,5X,'THE MODAL SIMILARITY TRANSFORM MATRIX TMA')
WRITE(6,27)((TMA(I,J),J=1,8),I=1,8)
DO P I=1,8
DO Q J=1,8
TMA(I,J)=TMA(I,J)
P
CONTINUE
CALL MINV(TMA,8,D,L,M)
WRITE(6,33)
33 FCPMAT(1H0,5X,'THE INVERSE OF THE TRANSFORMATION MATRIX TMA')
WRITE(6,31)((TMA(I,J),J=1,8),I=1,8)
31 FCPMAT(6F14,5)

```

```

CALL MPRD ( IMAT, BMAT, HMAT, 8,8,0,0,6)
WRITE(5,24)
24  FORMAT(1H0,5X,' INPUT MAT,IX      HMAT')
     WRITE (5,25)((HMAT (I,J),J=1,6),I=1,8)
CALL MPPD(IMAT, PHI,PHI1,8,6,0,0,6)
CALL MPRD(PHI1, IMAT, PHIM,8,8,0,0,8)
WRITE(5,26)

26  FORMAT(1H0,5X,'SYSTEM MATRIX IN DISCRETIZED MOEAL FORM  PHIM')
     WRITE (5,27)((PHIM (I,J),J=1,6),I=1,8)
     DO 90 I=1,6
     DO 90 J=1,6
     PHIM(I,J)=PHIM(I,J)
     PHIL(I,J)=PHID(I,J)
     IF (J-7) 5,90,90
5     HL(I,J)=HMAT(I,J)
     HLM(I,J)=HLM(I,J)
90    CONTINUE
     WRITE(5,31)
34  FORMAT(1H0,5X,'THE PARTIONED OUTPUT MATRIX  HLM')
     WRITE (5,29)((HLM (I,J),J=1,6),I=1,6)
29  FORMAT(6F14.5)
     CALL MIMV(HLM, 5,6,1,1)
     WRITE(5,38)
38  FORMAT(1H0,5X,'THE INVERSE OF THE PARTIONED INPUT MATRIX  HLM')
     WRITE (5,29)((HLM (I,J),J=1,6),I=1,6)
     CALL MIVS(RM1,PHID1,AKMAT,6,8,0,0)
     WRITE(5,40)
40  FORMAT(1H0,5X,'THE CONTROL MATRIX IN MOEAL FORM  AKMAT')
     WRITE (5,27)((AKMAT(I,J),J=1,8),I=1,6)
     CALL MPPD(HLM1, AKMAT, GAMAT,5,6,0,0,8)
     WRITE(5,41)
41  FORMAT(1H0,5X,'GAMAT  HLM1 TIMES AKMAT  ')
     WRITE(5,27)((GAMAT(I,J),J=1,8),I=1,6)
     CALL MPPD(GAMAT, HMAT, CMAT,6,8,0,0,8)
132  FCMAT(1F10.0)
     READ(5,132) CMAT(1,1)
     READ(5,132) CMAT(1,2)
     READ(5,132) CMAT(1,3)
     READ(5,132) CMAT(1,4)
     READ(5,132) CMAT(1,5)
     READ(5,132) CMAT(1,6)
     READ(5,132) CMAT(1,7)
     READ(5,132) CMAT(1,8)
     READ(5,132) CMAT(5,5)
     READ(5,132) CMAT(5,6)
     READ(5,132) CMAT(5,7)
     WRITE(5,42)
42  FORMAT(1H0,5X,'THE CONTROL MATRIX IN ORIGINAL FORM  CMAT')
     WRITE (5,27)((CMAT (I,J),J=1,6),I=1,6)
     CALL MPRD(BMAT, CMAT, OMAT, 8,6,0,0,8)
     CALL MIVS(H1,OMAT,CON,8,6,0,0)
     WRITE(5,41)
44  FCMPAT(1H0,5X,'THE CLOSED LOOP SYSTEM MATRIX  CON')
     WRITE (5,27)((CON (I,J),J=1,6),I=1,6)
     CALL EIGENP(0,8,CON, 39, KOR,KOC,VECR,VECI,INDIC)

```



```

WRITE(6,111)
111 FORMAT(11),5('THE PEAL ROOTS OF THE CLOSED LOOP SYSTEM')
WRITE(6,221) P05
221 FORMAT(8F14.6)
WRITE(6,121)
121 FORMAT(14J,5X,'THE COMPLEX ROOTS OF THE CLOSED LOOP SYSTEM')
WRITE(6,221) ROC
WRITE(6,101)
101 FORMAT(14J,5X,'THE INDICATOR')
WRITE(6,221) INDIC
110 CONTINUE
CALL SEX

STOP
END

SUBROUTINE SEX
DIMENSION XK(8),XK1(8),KMAT(8,6),CPMAT(6,8),PHI(8,8)
1,FMAT(8,8),YKO(8),PCMAT(8,6),RO(8),ROC(8)
2,GMAT(8,6),GCMAT(6,8),VECK(8,8),VECI(8,8)
3,INDIC(8)
COMMON CMT,BMAT,PHI
DOUBLE PRECISION YK,XK1,KMAT,CPMAT,FMAT,XKO,KCMAT,GMAT,BMAT,PHI
WRITE(6,1) X
10 FORMAT(8F16.0)
I=0
L=9
XC=.05
CALL MPRD(BMAT,GMAT,KCMAT,8,6,0,0,8)
CALL MSUB(PHI,KCMAT,FMAT,8,8,0,0)
DO 20 I=1,500
L=L-1
CALL MPFD(FMAT,XK,XK1,8,8,0,0,1)
IF(L.LE.10)GO TO 25
WRITE(6,26) I
26 FORMAT(8I9.5)
WRITE(6,27) XK
L=L-1
27 FORMAT(8E9.3)
26 DO 19 J=1,8
19 XK(J)=XK1(J)
I=I+1
20 CONTINUE
STOP
END

```

0000

# FULL OBSERVER SIMULATION

```

DIMENSION XK(8),KHAT(8,7),PHI(8,8),CPMAT(7,8),PSIG(8,6),XKQ(8)
1,GHAT(6,8),KCHAT(8,8),AXK(8),PSIQ(8,8),IN(8),XKI(8),CON(8,8)
2,XKIP(8),XKE(8),XKEC(8),XKI0(8),PHI0(8,8),PSI0(8,6),XKI1(8)
3,XR(8)
REAL KHAT,KCHAT,IN
READ(5,9) XK

9 FORMAT(6F10.0)
READ(5,10)((PHI(I,J),J=1,8),I=1,8)
10 FORMAT(4E14,7)
DO 997 IJK=1,8
DO 998 JK=1,7
998 KHAT(IJK,JK)=PHI(IJK,JK)
997 CONTINUE
KHAT(1,1)=.65
KHAT(2,2)=.6
KHAT(3,3)=.55
KHAT(4,4)=.50
KHAT(5,5)=.45
KHAT(6,6)=.40
KHAT(7,7)=1.0
KHAT(8,7)=2000.
READ(5,13) CPMAT
13 FORMAT(7F10.0)
READ(5,11)((PSI(I,J),J=1,6),I=1,8)
11 FORMAT(3E14,7)
READ(5,10) GHAT
T=0.0
TC=.05
CALL MPRD(KHAT,CPMAT,KCHAT,3,7,0,0,8)
CALL MPRD(PSI,GHAT,PSIQ,8,8,0,0,8)
X=1
XKI(3)=10.
DO 25 I=1,200
DO 91 K=1,7
91 XK(K)=XK(K)+RANDOM(X)*.2+XK(K)*-.1+XK(K)
XK(3)=XKI(3)+RANDOM(X)*2.-1.0
CALL MPRD(PHI,XK,AXK,8,8,0,0,1)
CALL MPRD(PSIG,XKQ,IN,8,8,0,0,1)
CALL MSUB(AXK,IN,XKI,8,1,0,0)
CALL MPRD(PHI,XKQ,XKI,8,8,0,0,1)
CALL MSUB(XKI,IN,XKIP,8,1,0,0)
CALL MSUB(XKQ,XK,XKE,8,1,0,0)
CALL MPRD(KCHAT,XKE,XKEC,8,8,0,0,1)
CALL MSUB(XKIP,XKEC,XKI0,8,1,0,0)
WRITE(6,31) T

```

```
31  FORMAT(F10.5)
    WRITE(6,33) XR
    WRITE(6,33) XK
    WRITE(6,33) XK0
33  FORMAT(8F9.3)
    WRITE(6,33) XKE
    T=T+10
    DO 25 J=1,8
    XR(J)=XK1(J)
    XK(J)=XK1(J)
    XK0(J)=XK10(J)
25  CONTINUE
    STOP
    END
```

# PARTIAL OBSERVER SIMULATION

```

DIMENSION PSI(8,8),U(6,1),XK(8),XK(8),PHI(8,8),GHAT(7,8),
1 YR(7),ALA(1,7),BLB(1,6),GHAT(6,8),LMAT(1,7),AXK(8),INR(8)
2 OUT(8),AHY(1,7),AYY(7,7),AYYL(1,7),BM(1,6),BY(7,6),BYL(1,6),
3 AYW(7),AYWL(1),YQL(1),YALA(1),IN(1)
REAL GHAT,LMAT,OUT,INR,IN,INI
READ(5,8) XK
-----
9  FORMAT(7F10.0)
   READ(5,12) GHAT
-----
8  FORMAT(8F10.0)
   READ(5,9) CCHAT
-----
   READ(5,10)((PSI(I,J),J=1,8),I=1,8)
-----
10  FORMAT(3E14,7)
   READ(5,12)((PHI(I,J),J=1,8),I=1,8)
-----
12  FORMAT(4E14,7)
   READ(5,9) LMAT
-----
   DO 62 J=1,7
     AHY(1,J)=PHI(8,J)
-----
   DO 62 I=1,7
     62  AYY(I,J)=PHI(I,J)
     CALL MPRD(LMAT,AYY,AYYL,1,7,0,0,7)
     CALL MSUR(AHY,AYYL,ALA,1,7,0,0)
     DO 63 J=1,6
       63  BM(1,J)=PSI(8,J)
-----
     DO 63 I=1,7
       63  BY(1,J)=PSI(I,J)
       CALL MPRD(LMAT,BY,BYL,1,7,0,0,6)
       CALL MSUR(BM,BYL,BLB,1,6,0,0)
-----
     DO 64 I=1,7
       64  AYW(I)=PHI(I,8)
       AXW=PHI(8,8)
       CALL MPRD(LMAT,AYW,AYWL,1,7,0,0,1)
       AYWL=AYWL(1)
       ILC=AXW-AYWL
       T=0.00
       TC=.05
       L=0
-----
29  FORMAT(7F14.5)
-----
27  FORMAT(8F14.5)
-----
28  FORMAT(6F14.5)
   X=1
-----
   DO 25 I=1,300
-----
   DO 91 K=1,7
     91  YR(K)=YR(K)+RANDOM(X)*.2+YR(K)*.1+YR(K)
     L=L+1
     CALL MPRD(CCHAT,XK,YR,7,8,0,0,1)
     CALL MPRD(PHI,XK,AXK,8,8,0,0,1)
     CALL MPRD(PSI,U,INR,8,6,0,0,1)
     CALL MSUR(AXK,INR,XK,8,1,0,0)
-----

```

```

YRL1=0.0
YALA1=0.0
DO 20 J=1,7
YALA1=YALA1+ALA(1,J)*YR(J)
YRL1=YRL1+LMAT(1,J)*YR(J)
20 CONTINUE
ZYRL=Z+YPL1
ZCLOSE=ALC*ZYRL
Z1=YALA1-IN1+ZCLOSE

DO 61 J=1,7
61 OUT(J)=YR(J)
OUT(8)=ZYRL
CALL MPRD(GHAT,CUT,U,6,0,0,0,1)
IN1=0.0
DO 101 J=1,6
IN1=IN1+BLB(1,J)*UC(J,1)
101 CONTINUE
ERROR=XX(8)-ZYRL
IF(L.NE.1) GO TO 60
WRITE(6,31)Z

31 FORMAT(F10.5)
WRITE(6,33)XK
WRITE(6,33)ZYRL,ERROR
33 FORMAT(2E9,3)
L=0
80 CONTINUE
T=T+TC
Z=Z1
DO 25 J=1,6
XK(J)=XK1(J)
25 CONTINUE
STOP
END

```

# SIMULATION OF NONLINEAR SYSTEM WITH FULL OBSERVER

```

REAL MASS,IX,IY,IZ,IXZ,LDNE,IENG,LDXIX,LPIX,MDYIY,
1MOIY,NDZIZ,NRIZ,NDNOIM,LANRDA
REAL KMAT(8,7),KMAT(8,7),PHI(8,8),PHI(8,8),CPMAT(7,8)
1PKIS(4,4),PSIF(8,6),KND(8),GMATS(6,8),GMATF(6,8),KCMATS(8,8),
2KCMAT(8,8),PSIS(8,8),PSIG(8,8),IN(8),XKIP(8),XKE(8),XKID(8),
3XKI(8),XKEC(8)
4YSHORT(8),IHO(8),XREF(8)
COMMON/ESQD4/N,KI,YI(99),X,Y(??),TR,H,KSTP,DY(99)
COMMON/FUNCI/G,THRUST,MASS,SIGMA,LAMBDA,
1UO,AREA,CLPO,DFLCL,ALPHA,CD,VREL,UORAR,CY,IX,IZ,IXZ,IY,
2ZIN,LDNE,ZONE,LPIX,LDXIX,DELX,SPAN,HREL,CLD,CLDELA,
3DEL,CLDETA,IENG,OMEGA,XTHO,XONE,NRIZ,NDZIZ,DELZ,CNO,
4CNDEL,DEL,CNDELA,MDYIY,DELY,KAIY,CHORD,CHORD,
5DEL,CD,CMALPO,DELCHA,CMQ,CMQELE,DELE,BETA,J,VREL,VJET,RHO
COMMON/CONT/IN
DATA G,MASS,VJET,RHO,AREA,SPAN,CHORD,IX,IY,IZ,IXZ,ZONE,IENG,XONE,
1LDXIX,MDYIY,KAIY,DELCHA,CMDELE,NDZIZ,NRIZ,CMQ/32.179,130.3537,
21613.,0.,002378,182.69,33.63,5.56,2340.,3400.,5400.,180.,0.563,0.5,
36.0,0.0661,0.0350,0.15,0.576,0.0178,0.0166,0.020,11.8/
DATA LPIX,ANGVEL/=9.45,1728./
DATA XTHO,ZTHO,LDNE/=0.0133,0.215,0.167/
UI=10.0
10 EORMAT(5E10.0,15)
11 FORMAT(5F12.1)
HR,01
READ(5,2001)((PHI(I,K),K=1,8),I=1,8)

2001 FORMAT(4E14,7)
READ(5,2003)CPMAT
2003 FORMAT(7F10.0)

N=8
XI=0.0
KSTP=0
KOFF=1
DO 15 IFLY=1,3
FFAD(5,102) YI(3)
READ(5,102) YI(8)
Y(3)=YI(3)
102 FORMAT(F10.0)
Y(8)=YI(8)
DO 15 J=1,2000
URFL=Y(3)
VREL=Y(8)
WRFL=-Y(4)
UORAR=SQRT(UREL**2+VREL**2+WRFL**2)
UO=SQRT(HREL**2+WRFL**2)
ALPHA=ARCSIN(WRFL/UO)
BETA=ARCSIN(VREL/UORAR)
IS(LD,LT,51) CLPO=0.61+0.002743*UO
IF(UO.GE.51) CLPO=0.75
DELCL=2.3+3.007E-03*UO**2-2.2A*3.94E-07*UO**3=1.332149E-03*UO
CO=0.11+1./(2.152915*UO+12.5)
IF(ABS(CO)A).LT.0.189) CY=1.051*BETA
IF(ABS(CO)A).GE.0.189) AND,ABS(BETA).LT.0.418)CY=(-0.35+0.393*

```

```
1(CAPS(BETA)=0.1893)+(ABS(BETA)/BETA)
IF (ABS(BETA).GT.0.018) AND (ABS(BETA).LT.1.22) C10=(0.26*0.36*
(CABS(BETA)+0.018)/(ABS(BETA)/BETA)
IF (ABS(BETA).GT.1.22) C10=0.55*(ABS(BETA)/BETA)
IF (CAPS(BETA).LT.0.187) CLD=0.083*BETA
IF (ABS(BETA).GE.0.169) AND (ABS(BETA).LT.0.071) CLD=(0.014*0.0066*
(ABS(BETA)+0.147)/(ABS(BETA)/BETA)
IF (ABS(BETA).GT.0.071) AND (ABS(BETA).LT.1.395) CLD=(0.012*0.00005*
(CABS(BETA)+0.071)/(ABS(BETA)/BETA)
IF (ABS(BETA).GT.1.395) CLD=0.02*(ABS(BETA)/BETA)
CLCE1=0.003*(COS(BETA)+1)
CLFETA=0.0045*(CLD+0.012)
IF (CLD.LT.34.1) CNOPD=0.6+0.00271*UD
IF (UD.GT.34.0) AND (UD.LT.51.1) CNOPD=0.52+0.0148*(UD-34.1)
IF (UD.GT.51.0) AND (UD.LT.101.1) CNOPD=0.22+0.001379*
1(UD-51.1)
IF (UD.GT.101.1) CNOPD=0.19
DE1=CNOPD*.9035E+07*(0.43+3.1647E-05*UD+2+1.52950E-03*UD)
IF (UD.LT.34.1) CHALPD=4.1+0.00145*UD
IF (UD.GT.34.0) AND (UD.LT.51.1) CHALPD=2.7+0.1007*(UD-34.1)
IF (UD.GT.51.1) CHALPD=1.0
IF (ABS(GF)) .I. 1.0-1905) CNOPD=113*BETA
IF (ABS(BETA).GT.0.1305) AND (ABS(BETA).LT.0.504) CNOPD=22*(ABS(BETA)
1/BETA)
IF (ABS(BETA).GE.0.594) AND (ABS(BETA).LT.1.395) CNOPD=0.027*0.1344*
1(ABS(BETA)+0.594)/(ABS(BETA)/BETA)
IF (ABS(BETA).GE.1.395) CNOPD=13*(ABS(BETA)/BETA)
CNOP1=0.00114*(COS(BETA)+1)
CNDE1=0.00012*(COS(BETA)+1)
41 CALL CSUB1(KNOE+1)
KNOE+1)
PHI(0:3)=Y(7)/20.
PHI(4:2)=Y(3)/20.
PHI(4:5)=Y(8)/20.
PHI(3:7)=Y(18)/20.
PHI(4:7)=Y(3)/20.
PHI(8:3)=Y(7)/20.
PHI(4:2)=Y(4E)/(20.*VJET)
PHI(3:5)=Y(2)/20.
PHI(4:8)=Y(7)/(20.*VJET)
PHI(8:4)=Y(THRUST)/(20.*MASS*VJET)
PHI(7:9)=Y(XONE)/(20.*VJET)
ICOU=1+ICOUIT+1
DO 10 K=1,8
10 YSMO=1E7*Y(K)
DO 105 L=1,8
DO 105 M=1,7
105 KMAT(L,4)=PHI(L,4)
KMAT(1,1)=.05
YMAT(2,2)=.5
KMAT(3,3)=.55
KMAT(4,4)=1.50
YMAT(5,5)=.45
KMAT(6,6)=.977
KMAT(5,6)=11.00
KMAT(7,7)=.02
CALL NORD(KMAT,CPMAT,KCMAT,3,7,0,0,8)
CALL NPRO(PHI,XND,CKIP,S,8,0,0,0,1)
CALL NSUB(XND,YSDPT,XRE,0,1,0,0)
```

```

CALL MPRC(KCMAT,XFE,XKEC,8,8,0,0,1)
CALL MSHF(XK1P,XKFC,XK1D,8,1,0,0)
IF(XK1C(3)).LE.10,GO TO 100
101 DELE=1.96
DELY=1.96
SIGMA=.87/57.3
OMEGA=98.76*1728.
DELA=0.0
THRUST=2.*(68.96552*98.76-4184.033)*.804
IF(ICOUNT.LT.5)GO TO 15
GO TO 4001
100 DELE=.47
DELY=.37
SIGMA=0.0
OMEGA=98.57*1728.
THRUST=2.*(68.96552*98.57-4184.083)*.804
IF(ICOUNT.LT.5)GO TO 15
4001 WRITE(6,2005)X,(Y(I),I=1,4),YR,XKO,XKE
2005 FORMAT('TIME IS',F10.5,' SYSTEM = ',9E11.3,/,
1, 'ORSERVCH=',9E11.3,/, 'ICRDR = ',9E11.3,/)
ICOUNT=0
DO 3003 K=1,8
XKO(K)=XK1D(K)
3003 CONTINUE
15 CONTINUE
8000 STOP
END

```

```

FUNCTION FC1(X,Y)
COMMON/ESQ/NO80
REAL Y(99),IN(8),MASS,LAMBDA,IX,IZ,IXZ,IY,LDNE,LP1X,LDY1X
1, IENG,NRIZ,NDZIZ,MDY1Y,MD1Y
COMMON/CONT/IN
COMMON/FUNCT/R,THRUST,MASS,SIGMA,LAMBDA,
1ND,YAREA,CLPO,DELCL,ALPHA,CD,VREL,VQBAR,CY,IX,IZ,IXZ,IY,
2ZT,C,LOE,ZONE,LP1X,LDX1X,DELX,SPAN,HREL,CLO,CLOELA,
3CELA,CLEETA,IENG,OMEGA,XTMC,YDNE,NRIZ,NDZIZ,DELZ,CND,
4CNDE1P,DELR,CNDELA,MDY1Y,DFLY,MD1Y,CMRD,CMRPO,
5DELCD,CALPO,DELCA,CND,CMDEL,DELBETA,1,VREL,VJET,RND
MASS=130.3537
IF(I.EQ.3) F=Y(8)*Y(7)-Y(4)*Y(2)+G*SIN(Y(1))*(THRUST/MASS)
1*(SIN(SIGMA)*COS(LAMBDA)-VREL/VJET+DELCL*SIN(ALPHA))+0.5/
2MASS*RND*UD*2*AREA*(CLPO+SIN(CALPA)-CD+COS(ALPHA))
I=IN(3)
IF(I.EQ.3) RETURN
IF(I.EQ.9) F=Y(4)*Y(6)+Y(3)+Y(7)+G*SIN(Y(5))+COS(Y(1))
1*THRUST/MASS*2*SIN(LAMBDA)-VREL/VJET+0.5/MASS*RRND*UQBAR
2*2*YAREA*CY=IN(8)

```



```

IF(I.EQ.3), RETURN
IF(I.EQ.4) F=Y(3)+Y(2)+Y(8)+Y(6)+G+COS(Y(5))+COS(Y(1))
1=THRUST/MASS*(COS(SIGMA)+COS(LAMBDA))+VREL/VJET+DELZ+
2COS(ALPHA)+0.5/MASS*(RH7*UD**2+WAREA*(CLPO+COS(ALPHA))+C0*SIN
3(ALPHA))-IN(4)
IF(I.F7.4) RETURN
IF(I.EQ.6) F=(IX+IZ/(IX+IZ-IXZ**2))*((IY-IZ)+Y(2)+Y(7))/IX
1+IY2+Y(6)+Y(2)/IX+THRUST/IY*(ZONE+VREL/VJET*SIN(LAMBDA)+
2(ZTND+LONF+COS(SIGMA)))+LPIX*Y(6)+LDXIX*DELX+0.5/IX
3*RHO*(URAR**2+WAREA*SPAN*(CLO+CLDELA+DFLA+CLRETA*BETA)
4+IY2/IX*((IX-IY)*Y(6)+Y(2))/IZ-IXZ*Y(2)+Y(7)/IZ+2.*IENG
5+OMEGA*Y(2)/IZ+THRUST/IZ*(SIN(LAMBDA)+(XTND-LONE)*SIN
6(SIGMA))-XONE*VREL/VJET+NRIZ*Y(7)+NDZIZ*DELZ+0.5/IZ*RHO
7*UBAR**2+WARFA*SPAN*(CNO+CNDEL+DEL+CNDELA+DELA))
8=I(6)
IF(I.EQ.6) RETURN
IF(I.EQ.2) F=(IZ-IX)+Y(6)+Y(7)/IY+IXZ*(Y(7)**2+Y(6)**2)
1/IY**2+IENG*OMEGA*Y(7)/IY+THRUST/IY*(VREL+XONE+VREL
2+ZONE)/VJET+COS(LAMBDA)*(ZTND*SIN(SIGMA)+XTND*COS
3(SIGMA))+CHORD*(CNDP0+CNDALP0+DELCA)*ALPHA+0.5/IX*RHO*UD**2
4+WAREA*CHORD*(CNDP0+CNDALP0+DELCA)*ALPHA+0.5*CHORD*CH0*Y(2)/UD
5+CNDGLE*DFLE)-IN(2)
IF(I.EQ.2) RETURN
IF(I.EQ.7) F=(IX+IZ)/(IX+IZ-IXZ**2)*(IXZ/IZ*((IY-IZ)+Y(2)
1+Y(7)/IZ+IX*Y(6)+Y(2))/IX+THRUST/IX*(ZONE+VREL/VJET*SIN(LAMBDA
2)+(ZTND+LONF+COS(SIGMA)))+LPIX*Y(6)+LDXIX*DELX+0.5/IX+
3RHO*UBAR**2+WAREA*SPAN*(CLO+CLDELA+DELA+CLRETA*BETA))+((IX-IY)*
4Y(7)+Y(2))/IZ-IY*Y(2)+Y(7)/IZ+2.*IENG*OMEGA*Y(2)/IZ+THRUST/IZ*
5(SIN(LAMBDA)+(XTND-LONE)*SIN(SIGMA))-XONE*VREL/VJET+NRIZ*
6Y(7)+NDZIZ*DELZ+0.5/IZ*RHO*UBAR**2+WARFA*SPAN*(CNO+CNDEL+
7DEL+CNDELA+DELA))-IN(7)
IF(I.F7.7) RETURN
IF(I.EQ.1) F=Y(2)*COS(Y(5))+Y(7)*SIN(Y(5))
1=IN(1)
IF(I.EQ.1) RETURN
IF(I.EQ.5) F=Y(6)+Y(2)*SIN(Y(5))+TAN(Y(1))+Y(7)+COS(Y(5))
1=TAN(Y(1))+IN(5)
RETURN
END

```

### III. Wind Gust Analysis of the X-14B VTOL Aircraft

Wind Gust Analysis of the  
X-14B VTOL Aircraft

NOMENCLATURE

<u>Variable or Constant</u>	<u>Description</u>	<u>Value-units</u>
$u$	forward velocity of the X-14	fps
$v$	side velocity of the X-14	fps
$w$	vertical velocity of the X-14	fps
$p$	roll rate of the X-14	rad/sec
$q$	pitch rate of the X-14	rad/sec
$r$	yaw rate of the X-14	rad/sec
$x$	longitudinal displacement of the X-14	feet
$y$	lateral displacement of the X-14	feet
$z$	vertical displacement of the X-14	feet
$\theta$	pitch attitude of the X-14	rad
$\phi$	roll attitude of the X-14	rad
$\psi$	yaw attitude of the X-14	rad
$T_{\text{net}}$	net thrust	pounds
$\bar{\sigma}$	diverter vane angle	rad
$\lambda$	side vane angle	rad
$\delta_x$	roll reaction control nozzle angle	degrees
$\delta_y$	pitch reaction control nozzle angle	degrees
$\delta_z$	yaw reaction control nozzle angle	degrees
$\delta_a$	aileron control angle	degrees
$\delta_e$	elevator control angle	degrees
$\delta_r$	rudder control angle	degrees

<u>Variable or Constant</u>	<u>Description</u>	<u>Value-units</u>
$\Omega$	engine angular velocity	rad/sec
UW	steady-state longitudinal wind	fps
VW	steady-state lateral wind	fps
WW	steady-state vertical wind	fps
UG	longitudinal gust component	fps
VG	lateral gust component	fps
WG	vertical gust component	fps
g	acceleration due to gravity	32.174 fps <sup>2</sup>
m	mass of the aircraft	130.35 slugs
$I_x$	moment of inertia of the aircraft with respect to the x-axis	2340 slug-ft <sup>2</sup>
$I_y$	moment of inertia of the aircraft with respect to the y-axis	3400 slug-ft <sup>2</sup>
$I_z$	moment of inertia of the aircraft with respect to the z-axis	5400 slug-ft <sup>2</sup>
$I_{xz}$	product of inertia of the aircraft with respect to the x and z axes	180 slug-ft <sup>2</sup>
$I_e$	moment of inertia of one engine with respect to the axis of rotation	0.5 slug-ft <sup>2</sup>
S	wing area	182.69 ft <sup>2</sup>
b	wing span	33.83 ft
c	mean aerodynamic chord	5.56 ft
$\rho$	density of the atmosphere at sea level	0.002378 slug/ft <sup>3</sup>
$x_1$	distance the center of the engine intake is forward of the center of gravity	6.0 ft
$x_2$	distance the center of the engine exhaust is behind the center of gravity	-0.0133 ft
$z_1$	distance the center of the engine intake is below the center of gravity	0.583 ft
$z_2$	distance the center of the engine exhaust is below the center of gravity	0.916 ft

<u>Variable or Constant</u>	<u>Description</u>	<u>Value-units</u>
$l_1$	effective length between engine exhausts and diverter vanes	0.167 ft
$V_{jet}$	net exhaust velocity of the engines	1613 fps
$C_{Lpo}$	lift coefficient, power off	
$\Delta C_L$	difference in lift coefficient between power off and power on	
$C_D$	drag coefficient	
$C_y$	coefficient of side force due to side velocity	
$C_{l\dot{\alpha}}$	rolling moment coefficient	
$C_{l\delta_a}$	rolling moment coefficient due to aileron deflection	deg <sup>-1</sup>
$C_{Mopo}$	pitching moment coefficient, power off	
$\Delta C_{Mo}$	difference in pitching moment coefficient between power off and power on	
$C_{M\dot{\alpha}}$	pitching moment coefficient due to angle of attack	
$C_{L\alpha}$	lift coefficient due to angle of attack	
$C_{D\alpha}$	drag coefficient due to angle of attack	
$\Delta C_M$	difference in pitching moment coefficient due to angle of attack between power off and power on	0.576 rad <sup>-1</sup>
$C_{Mq}$	pitching moment coefficient due to pitch rate	-11.4
$C_{M\delta_e}$	pitching moment coefficient due to elevator deflection	-0.0178 deg <sup>-1</sup>
$C_{n\dot{\alpha}}$	yawing moment coefficient	
$C_{n\delta_r}$	yawing moment coefficient due to rudder deflection	deg <sup>-1</sup>
$C_{n\delta_a}$	yawing moment coefficient due to aileron deflection	deg <sup>-1</sup>
$C_{l\beta}$	rolling moment coefficient due to side velocity	

<u>Variable or Constant</u>	<u>Description</u>	<u>Value-units</u>
$L_p/I_x$	rotational damping in roll	$-0.45 \text{ sec}^{-1}$
$M_q/I_y$	rotational damping in pitch	$-0.15 \text{ sec}^{-1}$
$N_r/I_z$	rotational damping in yaw	$-0.20 \text{ sec}^{-1}$
$L_{\delta_x}/I_x$	reaction control rolling moment	$0.0681 \text{ rad/sec}^2/\text{deg}$
$M_{\delta_y}/I_y$	reaction control pitching moment	$0.0350 \text{ rad/sec}^2/\text{deg}$
$N_{\delta_z}/I_z$	reaction control yawing moment	$0.0166 \text{ rad/sec}^2/\text{deg}$
$\xi_{\tilde{\sigma}_\Omega}$	longitudinal diverter efficiency factor based on engine speed	0.9139
$\xi_{\tilde{\sigma}_T}$	longitudinal diverter efficiency factor based on engine thrust	0.807
$\alpha$	angle of attack	rad
$\beta$	sideslip angle	rad

## CHAPTER 1

### INTRODUCTION

#### 1.1 Air Turbulence.

Nature confronts man with certain obstacles in his use of the air as a medium of transportation. One of those obstacles, turbulent motion of the atmosphere, was the subject of this research. An airplane is subject to random external forces which result in random variations of attitude and trajectory. The time scale and intensity of these responses are governed by the scale and intensity of the turbulence, as well as the characteristics of the aircraft. Their effect is to produce fatigue in both the pilot and the vehicle, to produce an uncomfortable ride, and to impair precise control along the flight path.

#### 1.2 Vertical Take-off and Landing Aircraft.

A vertical take-off and landing (VTOL) aircraft is affected to a greater extent by the turbulence of the atmosphere whenever the aircraft is in the hover or transition modes of flight than when in normal aerodynamic flight. The aerodynamic forces used for control have negligible effect in hover. The only control available to a hovering VTOL is the stability augmentation system built into the aircraft. There exist different control systems for different VTOL configurations. A particular control system for a specific aircraft is the subject of this research.

The airplane studied in this project was NASA's X-14 research VTOL aircraft. The control of this particular aircraft is accomplished by vectoring the thrust of its two engines (to provide thrust for hover and propulsion) and by bleeding air from the engines and ducting it to control nozzles in the wing tips and the tail (to provide thrust for attitude

control). The control effort available is limited since too much air bled from the engines lowers the thrust capabilities. A trade-off between thrust capabilities and control effort available is a major factor in designing VTOL control systems. Therefore, the knowledge of control effort needed is vital in designing the VTOL.

Control effort is defined as the angular acceleration produced by a control input. If an angular acceleration produced by an input disturbance, such as a wind gust, exceeds the control power available, then the aircraft is considered unstable. The line between stability and instability depends not only on the criteria used to define stability, but also upon the characteristics of the aircraft. For the X-14 the stability is based on the angular accelerations and the attitude of the aircraft. These criteria were applied to the hover mode where they are far more important than for regular aerodynamic flight.

It is important then to be able to calculate accurately the angular accelerations produced by the turbulence of the atmosphere. A model of atmospheric disturbances is necessary to perform this task. Modeling the atmosphere is difficult using explicit functions of time. Studies of VTOLs and other aircraft involving the wind most frequently use a statistical, probabilistic model for the wind model.

### 1.3 Research Objectives.

The objective of this research was to find the maximum allowable gusts which the X-14 could encounter while in hover and still maintain a stable flying condition. The general procedure for solving the problem was to generate a simulated velocity field from a standard wind model. This field was then imposed on the simulated aircraft as a disturbance. Due to the



nonlinearities of the aircraft, there were changes in its aerodynamic characteristics. These changes resulted in a modified aircraft motion and were duly considered. The aircraft control system sought to drive the aircraft to its reference flight condition, hover.

The basic solution was found by arbitrarily selecting a wind model, observing the output variables of consequence, and changing the amplitude of the wind model until the aircraft failed to return to its nominal state.

The models for the aircraft and wind are presented in Chapters 2 and 3 respectively. The solution procedure, in more detail, is presented in Chapter 4. The results of this study and a discussion and interpretation of these results are presented in Chapter 5.

## CHAPTER 2

### AIRPLANE MODEL

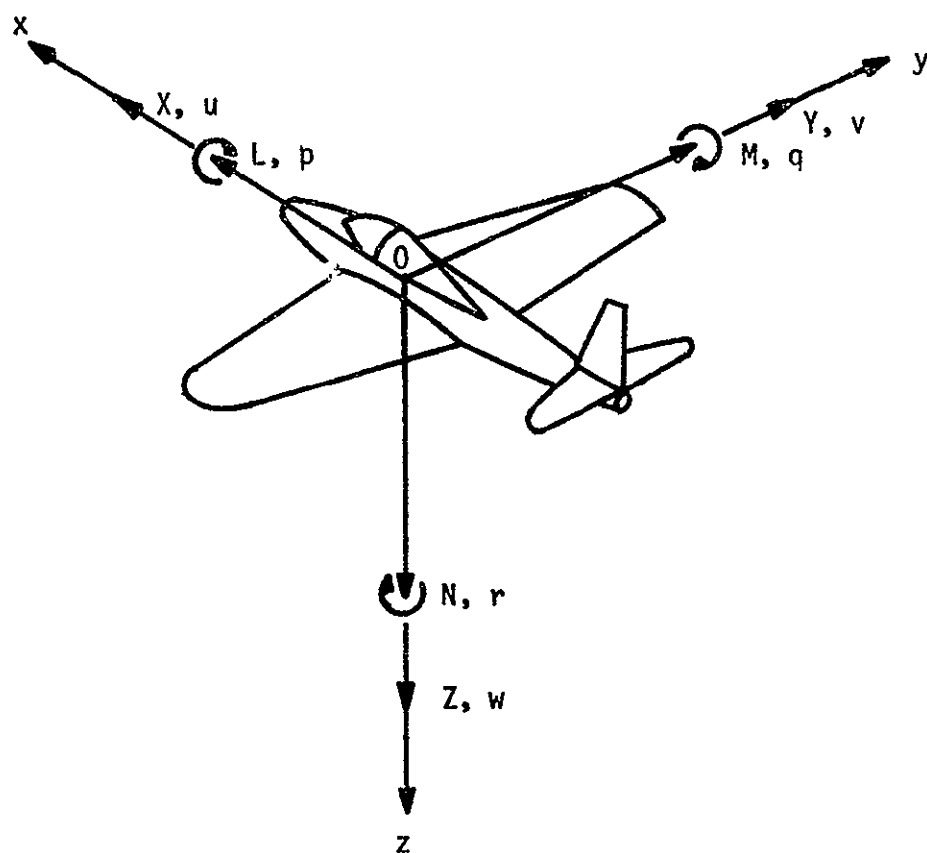
#### 2.1 X-14 VTOL Airplane.

The aircraft used for this project is the NASA X-14 VTOL research aircraft stationed at the NASA Ames Research Center, Moffett Field, California. The airplane was built by the Bell Aircraft Corporation as a research vehicle for the study of VTOL flight.

The X-14 is a thrust-vectoring VTOL airplane. Two General Electric J85-19 jet engines are fixed on the aircraft. The thrust of the engines is vectored by diverter vanes at the jet exits. The thrust is diverted down for hover, whereas, for the transition of the aircraft from hover to normal aerodynamic flight, the thrust is rotated rearward.

The X-14 is equipped with a stability augmentation system for control in the hover and transition modes of flight. The control effort is obtained by bleeding air from the compressor stages of the engines. The air is ducted to reaction control nozzles located in each wing tip and in the tail. The aircraft attitudes, rates, and accelerations are monitored by gyros and accelerometers. Various types of controllers had been tested and used, but they were not of importance to this study. Some type of control system was needed to do the simulations of this project and an acceleration command (manual) mode was used.

The airplane was assumed to be a rigid body and therefore had a body-fixed reference frame with the origin located at the mass center (Figure 1). The aircraft was symmetrical about the x-z plane with the positive y-axis pointing out the right wing, the positive z-axis pointing down, and the positive x-axis pointing in the direction of forward flight. The



$L$  = rolling moment  
 $M$  = pitching moment  
 $N$  = yawing moment  
 $p$  = roll rate  
 $q$  = pitch rate  
 $r$  = yaw rate

$[X, Y, Z]$  = components of resultant aerodynamic force  
 $[u, v, w]$  = components of velocity of  $O$  relative to the atmosphere

Figure 1. Body-fixed Reference Frame.

translational displacements, velocities, accelerations, and the components of the resultant aerodynamic forces were considered positive in the same sense as the coordinate axes (body axes).

The airplane also had another reference frame attached to it. The vehicle-carried vertical frame (see Chapter 4) had its origin located at the vehicle mass center. The angular orientation of the vehicle was then the relation of the body axes to this vehicle-carried frame. The relative orientation was expressed by the Euler angles  $\theta$ ,  $\phi$ , and  $\psi$ .

The position angles were considered positive if an observer, located at the origin of the reference frame (the vehicle-carried frame in this case), looked along the axes and saw a clockwise rotation of the airplane axes (body axes). The yaw angle,  $\psi$ , was positive for a clockwise rotation about the z-axis (i.e., the right wing goes back). The pitch angle,  $\theta$ , was positive for a clockwise rotation about the y-axis (i.e., the nose of the airplane goes up). The bank, or roll, angle,  $\phi$ , was positive for a clockwise rotation about the x-axis (i.e., the right wing goes down). The angular velocities and accelerations and the aerodynamic moments were considered positive in the same manner as the angular displacements.

The stability augmentation system reacted to disturbances by creating reaction control moments opposite to the induced disturbance moments. The reaction control moments were dependent upon the angular displacements of the sleeves located in the ends of the air ducts (see Figure 2). For zero displacements, the sleeves were oriented so that the air was expelled through the top and bottom control nozzles to provide equal amounts of thrust. Zero displacement was the reference flight condition.

The reaction control nozzles in the wing tips corrected any induced rolling or yawing moments. Rolling moments were generated by changing the difference between the left nozzle exit area and the right nozzle exit

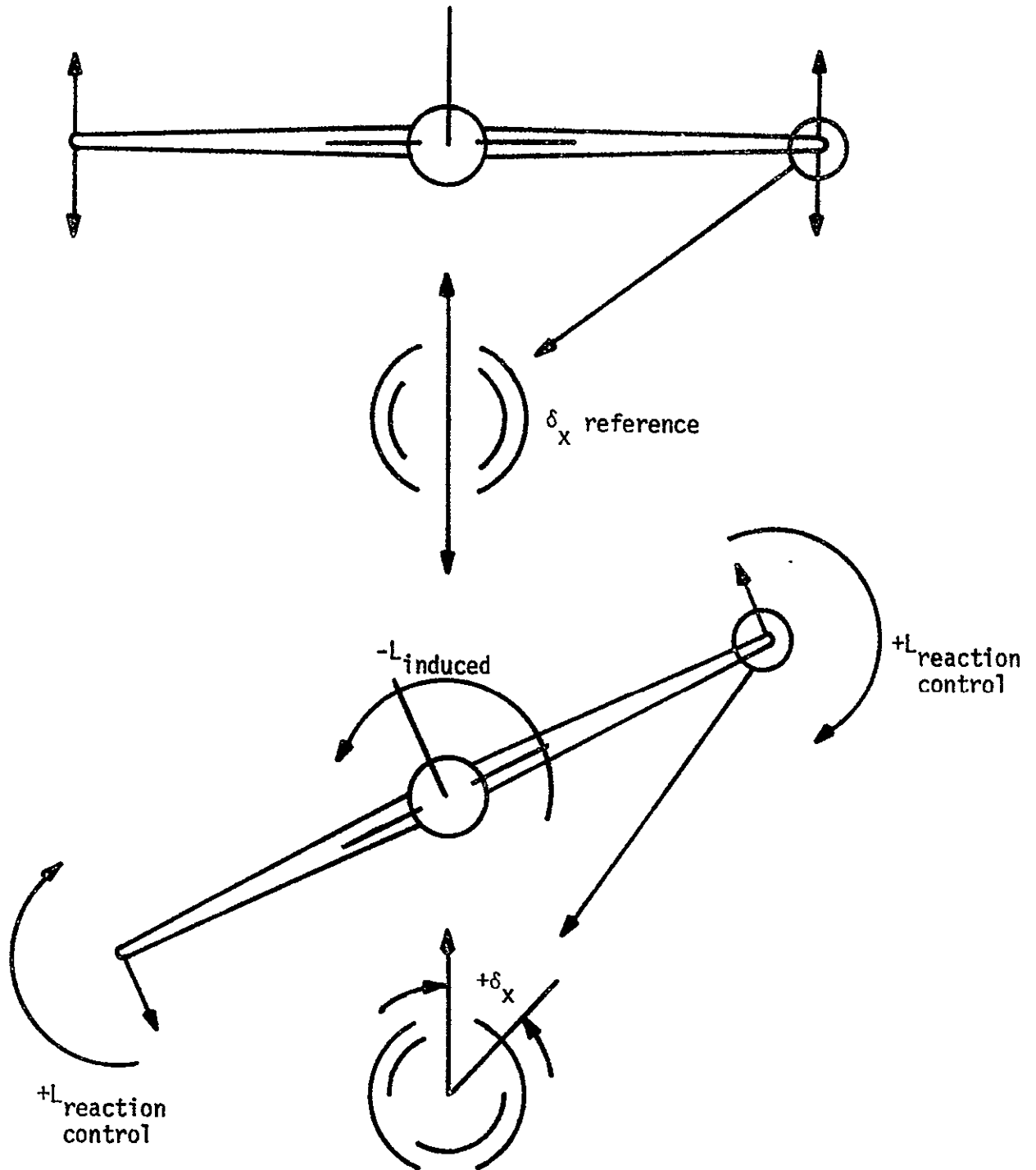


Figure 2. Definition of  $+\delta_x$ .

area. The angular displacement,  $\delta_x$ , of the sleeve in the control nozzle was considered positive if it created a positive rolling moment (Figure 2). Yawing control moments were created by rotating the thrust vectors from the left and right nozzles in opposite directions about the lateral axis (y-axis) of the aircraft. Pitching control moments were created by a reaction control nozzle located in the tail. Changing the differential area between the top and bottom exit areas produced the pitching control moment. The reaction control angles for pitch,  $\delta_y$ , and yaw,  $\delta_z$ , were considered positive if they produced positive pitching and yawing moments respectively.

The aerodynamic controls were directly coupled to the reaction controls through the pilot controls (the stick and the pedals) as follows:

$$\text{aileron control angle, } \delta_a = \delta_x, \quad (\text{III-1a})$$

$$\text{elevator control angle, } \delta_e = \delta_y, \text{ and} \quad (\text{III-1b})$$

$$\text{rudder control angle, } \delta_r = \delta_z. \quad (\text{III-1c})$$

Two angles were associated with the thrust vectoring. The diverter angle,  $\delta$ , had a range from zero degrees displacement (thrust vectored straight down for hover) to 70 degrees displacement for full aerodynamic flight. This angle was measured in the vertical plane counterclockwise from the positive z-axis (body axis). The exhaust side vane angle,  $\lambda$ , was measured about the x-axis (body axis) by the right hand rule and had a range of  $\pm 25$  degrees.

## 2.2 Basic Model.

The equations of motion for the X-14 were taken from [1]. The model in [1] was a ninth-order system with the state variables being  $u$ ,  $v$ ,  $w$ ,  $p$ ,  $q$ ,  $r$ ,  $\theta$ ,  $\phi$ , and  $\psi$ . These variables are defined in Appendix 4. For this project three other state variables were added which allowed the

displacements to be calculated. The model was of the basic form

$$\dot{\underline{x}} = f(t; \underline{x}, \underline{u}, \underline{w}) \quad (\text{III-2})$$

where  $\underline{x}$  was a twelve-dimensional vector of state variables,  $\underline{u}$  was a nine-dimensional vector of control parameters, and  $\underline{w}$  was a six-dimensional vector of input disturbances.

The problem was to solve for the transient response of the aircraft subject to a disturbance(s). The hover mode,  $\underline{x} = \underline{0}$ , represented the initial conditions. The disturbance vector,  $\underline{w}$ , was known for each instant of time. The control vector was calculated by setting  $\dot{\underline{x}} = \underline{0}$ , the reference flight condition, and solving equation (2) for  $\underline{u}$  at a specific instant of time. Equation (2) was then solved for  $\underline{x}$  at the next instant of time. This was continued until the nature of the transient, whether a recovery or a crash, was determined.

### 2.3 Changes in the Original Model.

The equations of motion of the basic model were reviewed by the author, more for a better understanding of the model than to see if they were correct. The equations were found to be nearly correct. Only a few discrepancies were found in certain terms of the equations.

The term accounting for the rolling moment due to side velocity was omitted from the original model. This term, the stability derivative,  $C_{l\beta}$ , was derived following methods of [2]. The derivation of this term is presented in Appendix 1.

In the interim period between the time the basic equations were first written and this project started, the engines of the airplane were replaced with newer, more powerful engines. The newer engines, the GE J85-19 engines, had greater thrust capabilities. With the new engine data incorpo-

rated into the model, a simulation for the hover mode was conducted and a discrepancy between simulation results and actual flying results was discovered.

In hover the actual airplane was flying with the engines running at 98 to 99 percent of maximum engine speed. The model calculated the engine speed to be only 90 percent. The conclusion drawn from this was the efficiency of the diverter vane had been neglected in the model. An efficiency factor was added to the model to adjust the engine speed to that of the actual aircraft. This factor also had a direct effect on the thrust and the exit velocity of the jet exhausts.

Reference [1] also calculated this factor and reported it to be 0.91. This was based on a direct correlation between the engine speeds of the model and the actual aircraft. For this project, the engine speed,  $\Omega$ , could not be calculated by any means other than from the thrust,  $\Omega = \Omega(\text{thrust})$ . The thrust was an integral part of the model and was included in the control vector  $\underline{u}$ . Therefore, the efficiency factor was re-calculated based on the ratio of the gross thrust for hover as calculated by the model and the gross thrust for hover of the actual aircraft. The factor was calculated to be 0.807. This factor was assumed to be constant over the range of operating conditions of the aircraft. The calculation of this factor,  $\xi_{\Omega}$ , is presented in Appendix 2.

The nature of the solution procedure (see Chapter 4) required the modification of two aerodynamic coefficients,  $\Delta C_L$ , lift interference, and  $\Delta C_{M_0}$ , pitching moment interference. The corresponding lift interference force appeared in the equations for forward and vertical velocity. The pitching interference moment appeared in the equation for the pitch rate. These terms required that the value of the net thrust be known before it had been calculated. Both coefficients were defined as functions of two



parameters, the relative velocity between the aircraft and the atmosphere,  $U_0$ , and a non-dimensionalized thrust coefficient,  $T_c$ . The equations for  $\Delta C_L$  and  $\Delta C_{M_0}$  were

$$\frac{\Delta C_L}{T_c} = f(U_0) = -2.248398 \times 10^{-7} \cdot U_0^3 + 2.483009 \times 10^{-5} \cdot U_0^2 - 1.332149 \times 10^{-3} \cdot U_0 \quad (\text{III-3a})$$

$$\frac{C_{M_0}}{T_c} = f^1(U_0) = 4.900354 \times 10^{-7} \cdot U_0^3 - 3.164620 \times 10^{-5} \cdot U_0^2 + 1.529505 \times 10^{-3} \cdot U_0 \quad (\text{III-3b})$$

where  $T_c = T_{\text{net}} / (1/2 \cdot \rho \cdot U_0^2 \cdot S)$ .

These aerodynamic terms were incorporated into the thrust terms of their respective equations by algebraic manipulation (see Appendix 3). This "rearrangement" eliminated the necessity of having to arbitrarily select an initial value for the thrust.

The last change involved the aerodynamic coefficients  $C_{n_0}$ ,  $C_{\ell_0}$ , and  $C_y$ . These coefficients were "extended" to be defined for the full range of the sideslip angle,  $\beta$ , +90 degrees to -90 degrees (see Figure 3). The extended portion of the curves were based on the known curves.

#### 2.4 Final Study Model.

The model finally used for the study was a twelfth-order system. The state variables were the three translational velocities ( $u, v, w$ ), the three angular displacements ( $\theta, \phi, \psi$ ) and associated angular velocities ( $p, q, r$ ), and the displacements ( $x, y, z$ ). The full set of equations of the system are presented in Appendix 4.

These equations of the model that define the dynamics of the X-14 were nonlinear differential equations. More correctly, equation (2) was written as

$$\dot{\underline{x}} = f\{t; \underline{x}(t), \underline{u}(t), \underline{w}(t)\} . \quad (\text{III-4})$$

With the control vector assumed to be a known function of state variables,

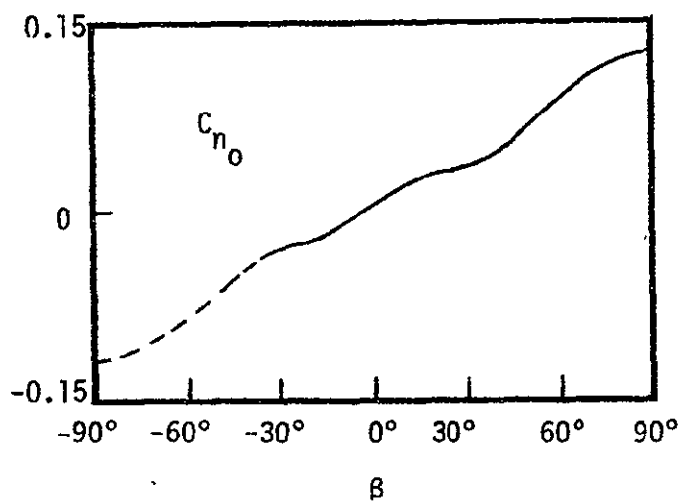
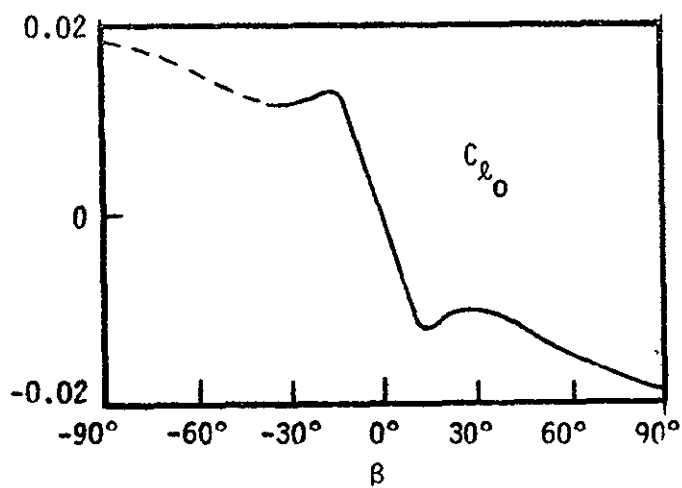
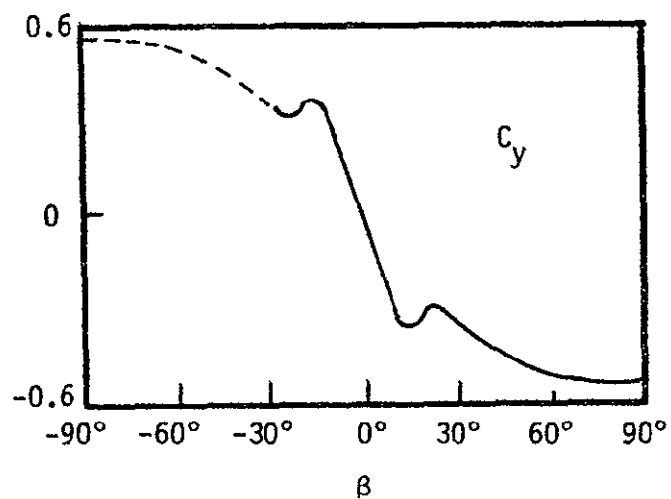


Figure 3.  $C_y$ ,  $C_{\xi_0}$ ,  $C_{n_0}$  "extended" to  $\beta = -90^\circ$ .

equation (4) then became

$$\dot{\underline{x}} = f\{t; (t), \underline{u}(\underline{x}(t)), \underline{w}(t)\} . \quad (\text{III-5})$$

and was the equation of a closed-loop system.

The nonlinearities of the system were due in part to the inertia terms of the fundamental dynamical equations. The kinematic variables (angular positions and velocities) were nonlinear also. The external forces, especially the aerodynamic forces contained inherent nonlinearities. Nonlinearities were also introduced into the system by the aerodynamic coefficients. However, in this project, the biggest nonlinear contribution was made by the control system of the feedback loop, the pilot [6].

To model the pilot control system is very difficult. A pilot model must be able to perceive rates, predict attitudes, and then provide the proper lead time in control inputs so that it can maintain some degree of precision. The control policy should be one that is capable of driving all the state variables to some reference condition, which, for hover, is the zero vector. For a nonlinear system, as was the X-14, the derivation of such a controller was a difficult task without first producing a linear model. For large disturbances as those considered in this study, many linear models would be required with each one linearized about a different operating condition. The analysis would then switch models as the conditions warranted. This approach would optimize the use of the control effort available, but it would be extremely difficult to construct. Therefore, the control policy of [1] was used because of its simplicity.

Reference [1] calculated the control vector by setting  $\dot{\underline{x}} = 0$  and solving for  $\underline{u}$  (see Appendix 5 for the equations). This control would not return the aircraft to its original position, but would control the aircraft to some steady-state reference. For example, if a disturbance caused the aircraft to roll, the present control would seek to drive the roll

acceleration,  $\dot{p}$ , to zero. This meant that the roll rate would be a constant and that the roll angle,  $\phi$ , would continue to increase at a constant rate until the critical roll angle was exceeded. Using this type of control would tend to give results on the conservative side for the calculation of maximum permissible gusts.

The pilot introduces a time delay into the system due to his time response, which includes his reaction time and the time required for the pilot's response to be transmitted to the physical control system through servos [6]. Reference [7] gave a nominal reaction time delay of 0.15 seconds. A neuromuscular lag of 0.10 seconds was also given.

The pilot represented the majority of the time delay. The response of the control to a command input was taken to be 0.05 seconds. Equation (5) was then written as

$$\dot{\underline{x}} = f\{t; \underline{x}(t), \underline{u}(\underline{x}(t-\tau), w(t))\} . \quad (\text{III-6})$$

where  $\tau$  was the time delay.

The control system just mentioned was affected by the time delay of the pilot. The control vector  $\underline{u}$  was calculated every 0.30 seconds. During this response time interval, the aircraft was assumed to be in a state of flight in free conditions with locked controls.

A second control was used in which the pilot was assumed to apply full control when a disturbance was sensed. Full control in this sense meant that full control effort was available to him through the stability augmentation system. The throttle for the thrust was assumed to be controlled just enough to keep the airplane flying. The thrust and the vane angle(s) were calculated for  $\dot{\underline{x}} = \underline{0}$ .

This type of control,  $\underline{u}_{\max}$ , was more representative of a pilot's reaction to disturbances. The design was very basic in nature and could not be regarded as sophisticated enough to be useful in other applications.

Figure 4 shows a schematic of the control policy using pitch as an example. A disturbance (in the form of a step) was introduced to the system and the pilot reacted (after the time delay) by applying full control effort to counteract the disturbance. This should have resulted in an immediate change in sign of the pitch acceleration. Full control effort was applied until the pitch rate passed through zero. Then the control was returned to the "other" control. The pitch angle was then watched to see if it exceeded its critical value.

The preceding  $\underline{u}_{\max}$  control sequence was only applied to step disturbances. A simpler sequence of applying  $\underline{u}_{\max}$  was used for disturbances other than steps. Whenever the aircraft exceeded a certain attitude, usually one half the critical value, the control was changed from  $\underline{u}_{\dot{x}=0}$  to  $\underline{u}_{\max}$ . When the attitude dropped below one half its critical value, then  $\underline{u}_{\max}$  was returned to  $\underline{u}_{\dot{x}=0}$ .

For the remainder of this study, the two control "schemes" will be designated as

<u>reference</u>	<u>control</u>	
$\dot{x} = 0$	$\underline{u}_{\dot{x}=0}$	( III-7a)

maximum control effort	$\underline{u}_{\max}$	( III-7b)
------------------------	------------------------	-----------

The nine parameters of the control vector were the net engine thrust ( $T_{\text{net}}$ ), the two diverter angles ( $\bar{\sigma}, \lambda$ ), the three reaction control angles ( $\delta_x, \delta_y, \delta_z$ ), and the three aerodynamic control angles ( $\delta_a, \delta_e, \delta_r$ ). For hover and low speed flight the aerodynamic controls have negligible effect on controlling the aircraft.

The exhaust side vane angle,  $\lambda$ , was set to zero because the present aircraft does not use it. Since the primary function of the side vane was to produce lateral forces for lateral translation, some simulations were conducted with it present. These simulations were restricted to the case of lateral disturbances only. Also, only the hover condition was considered.

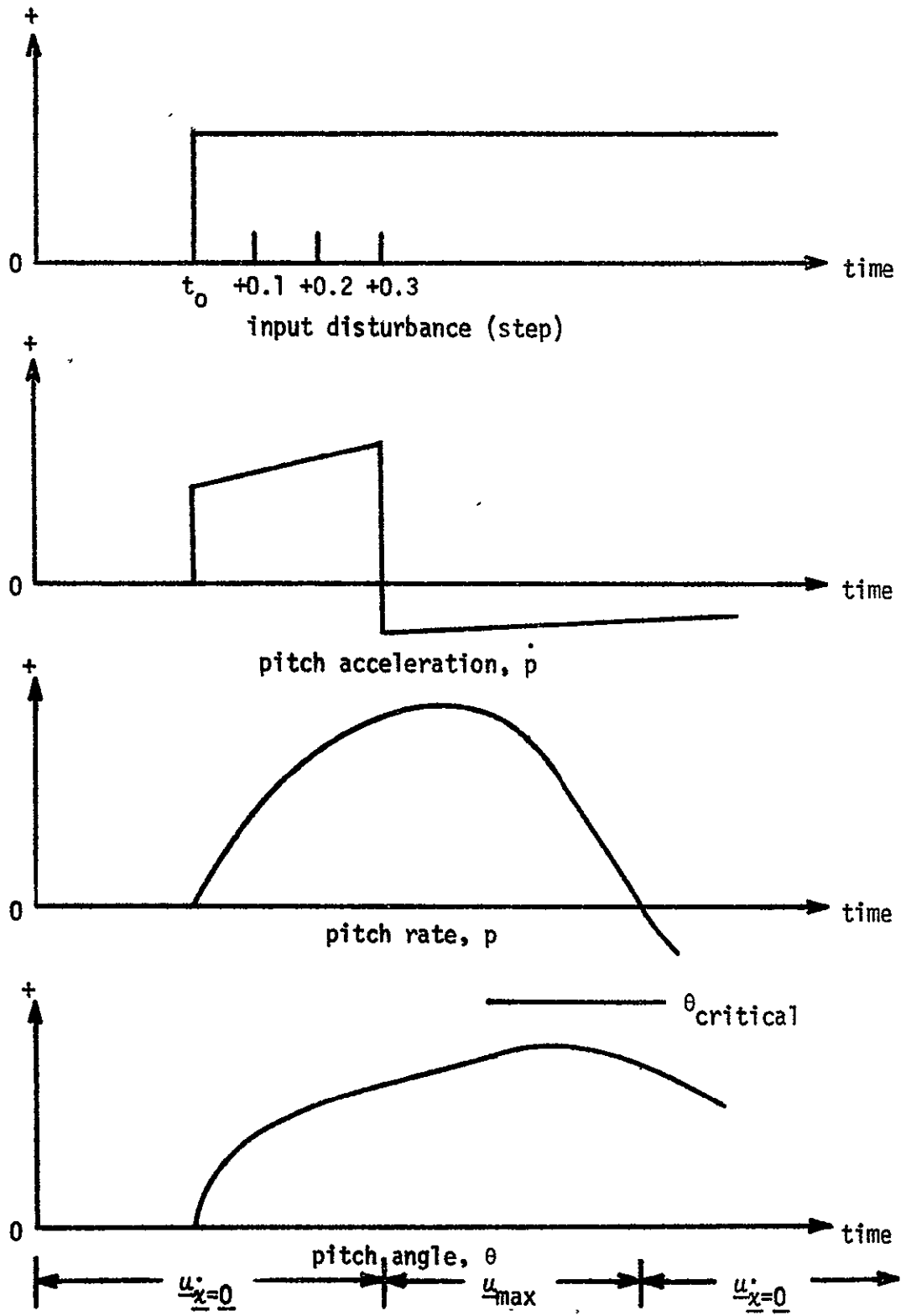


Figure 4. Schematic of  $\underline{\underline{u}} = \underline{\underline{u}}_{max}$ .

Therefore, for the major part of this study, the nine-dimensional control vector was actually a vector of only five dimensions.

The disturbance inputs represented the three orthogonal components of the wind and the three orthogonal components of the gusts. As discussed in more detail in the next chapter, the airplane was assumed to be facing into a headwind with no crosswinds or vertical winds. Therefore, the disturbance vector was reduced by two dimensions to a four-dimensional vector.

The valid range of the model was dependent on four variables [16].

The variables with their limits were

forward velocity ( $u$ )	-	+101 fps (+60 knots),
		-17 fps (-10 knots),
side velocity ( $v$ )	-	$\pm 51$ fps ( $\pm 30$ knots),
angle of attack ( $\alpha$ )	-	$\pm 20$ degrees, and
sideslip angle ( $\beta$ )	-	$\pm 90$ degrees .

The conditions for hover were defined as

forward velocity ( $u$ )	-	+30 fps,
		-10 fps,
side velocity ( $v$ )	-	$\pm 30$ fps, and
vertical velocity ( $w$ )	-	$\pm 10$ fps .

## 2.5 Stability Criteria.

The objective of this project was to find an envelope of wind gusts in which the aircraft could operate safely. Therefore, certain criteria for instability were established. In hover, close to the ground, the attitude of the aircraft is always very critical. It was assumed that the aircraft would be considered unstable, or unable to recover to its reference flying condition, if either the roll or pitch angle exceeded 25 degrees.

Since the control effort available was limited, the aircraft was also considered unstable whenever it exceeded its maximum control effort. The maximum available control efforts were

$$\begin{array}{lll} \ddot{\phi} \text{ (roll)} & - & 1.361 \text{ rad-sec}^{-2}, \\ \ddot{\theta} \text{ (pitch)} & - & 0.698 \text{ rad-sec}^{-2}, \text{ and} \\ \ddot{\psi} \text{ (yaw)} & - & 0.332 \text{ rad-sec}^{-2} . \end{array}$$

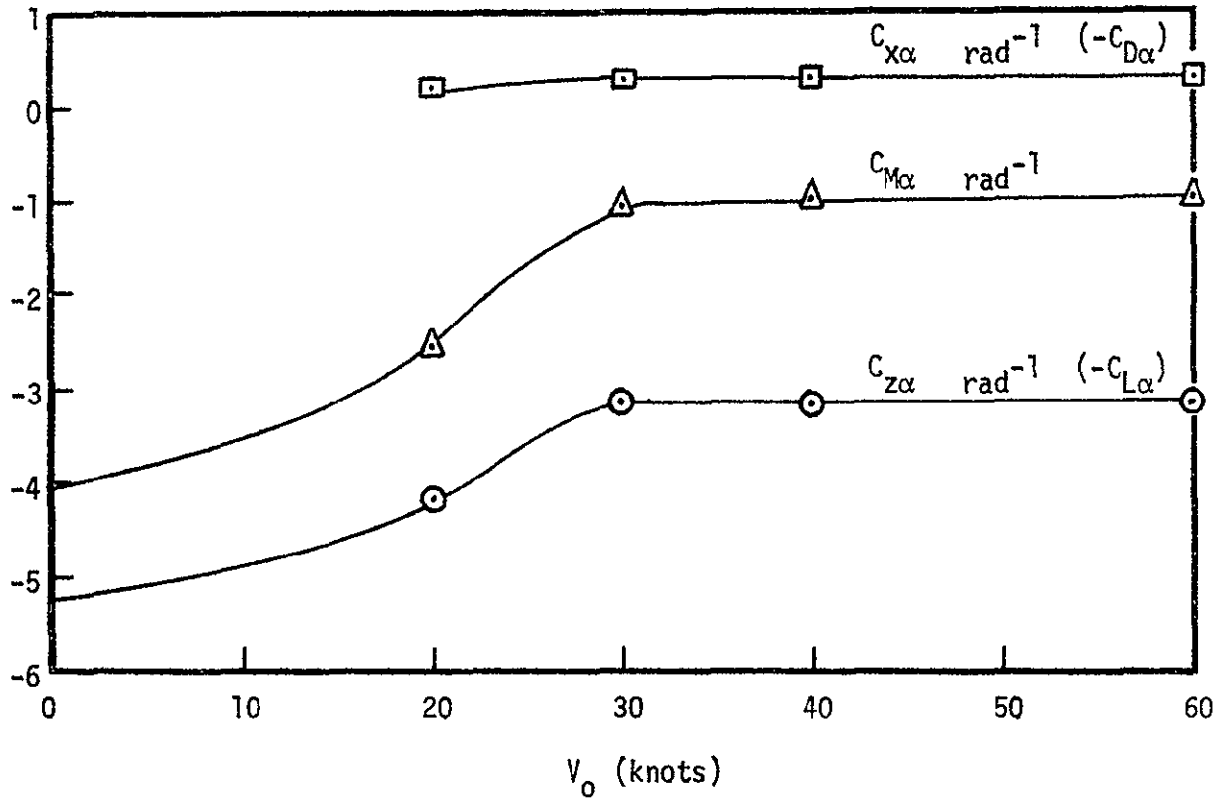
The altitude for the aircraft was initially set at 100 feet. This gave the aircraft reasonable room to operate vertically and eliminated the altitude as a critical criterion in determining unsafe flying conditions. A change in altitude would be an important factor to watch since this would be critical at lower altitudes on the order of a few feet. Also, this altitude was assumed to be great enough to eliminate any effect the ground might have on a hovering VTOL (e.g., re-ingestion of engine exhausts).

## 2.6 Comment on the Aircraft Model.

As stated in Section 2.2, the aircraft model was based on the work of [1] which in turn was based on the work of [16]. One aspect of the latter work raised certain questions regarding the aerodynamic forces and moments that appeared in some of the equations. In particular, the points in question concerned the angle of attack,  $\alpha$ . Reference [16] included the pitching moment due to  $\alpha$  in its model, but it neglected the lift and drag due to  $\alpha$ . Figure 5 was reproduced from [16] and shows the moment, lift, and drag coefficients with respect to  $\alpha$ . Three things were immediately obvious. First, unlike most aerodynamic procedures, these coefficients were given as functions of relative velocities and not as functions of  $\alpha$ . Secondly, the drag coefficient had a negative value which indicated that the drag force acts as a propulsive force (i.e., a contribution to the thrust) and not as a resistive force. Thirdly, there existed some ambi-



X-14A\* Longitudinal Aerodynamics  
 Static Data 40'x80' Wind Tunnel Body Axes  
 "Power Off"  $\alpha=0$  Controls Neutral

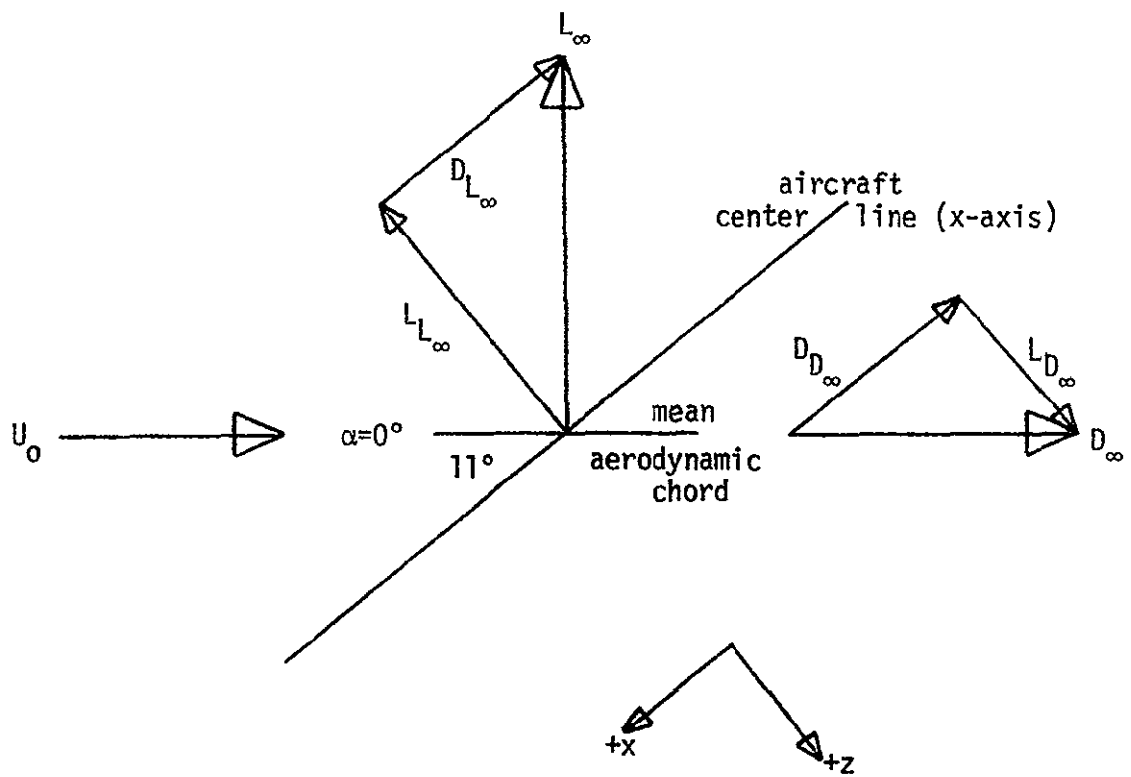


\* A notation refers to the aircraft before the new engines were installed.

Figure 5. Copy of  $C_{L\alpha}$ ,  $C_{D\alpha}$ ,  $C_{M\alpha}$  from [16].

guity in the heading of the graph. The statements " $\alpha=0$ " and "body axes" were left to be defined by the user. Digressing slightly in order to interpret this, [15] showed that the wings were at an incidence of 11 degrees at the root and 6 degrees at the tip with respect to the aircraft center line (body axes). This then meant the statement " $\alpha=0$ " implied that the aircraft was "pitched down" at an angle of 6 to 11 degrees (11 degrees will be used for the illustration). To the author, the statement "body axes" implied that the forces and moments represented by the coefficients were defined to be parallel to the body axes. However, the forces of lift and drag,  $L_\infty$  and  $D_\infty$ , were generated perpendicular and parallel to the relative velocity vector (Figure 6). For  $\alpha=0$ , this then meant that lift and drag were defined with respect to the mean aerodynamic chord. Therefore, lift and drag had to be rotated into the body axes system through an angle equal to the incidence of the wing with respect to the body axes (i.e., 11 degrees). Rotation of these forces,  $L_\infty$  and  $D_\infty$ , showed that drag with respect to the body axes was a positive quantity (Figure 6). This contradicted the information presented in Figure 5. At the present time, only a partial copy of [16] is available. The previous discrepancies may be resolved when a complete copy is referred to.

For this study, the original equations as defined in [1] were used in which  $C_{M\alpha}$  was included and  $C_{L\alpha}$  and  $C_{D\alpha}$  were neglected. However, a set of simulations, with  $C_{L\alpha}$  and  $C_{D\alpha}$  included in the aircraft model, was conducted. Also, since the atmosphere and aircraft reference frames were parallel (see Chapter 4), the angle of attack had an initial value of 11 degrees. Therefore, another set of simulations was conducted where 11 degrees was added to the angle of attack. The results of both sets of simulations are presented in Section 5.3.c.



positive lift  $\rightarrow$   $-z$  direction  
 positive drag  $\rightarrow$   $-x$  direction

$$L_{\text{body axes}} = L_{L_\infty} - L_{D_\infty}$$

$$D_{\text{body axes}} = D_{L_\infty} + D_{D_\infty}$$

Figure 6. Interpretation of " $\alpha=0$ " and "body axes".

## CHAPTER 3

### WIND MODEL

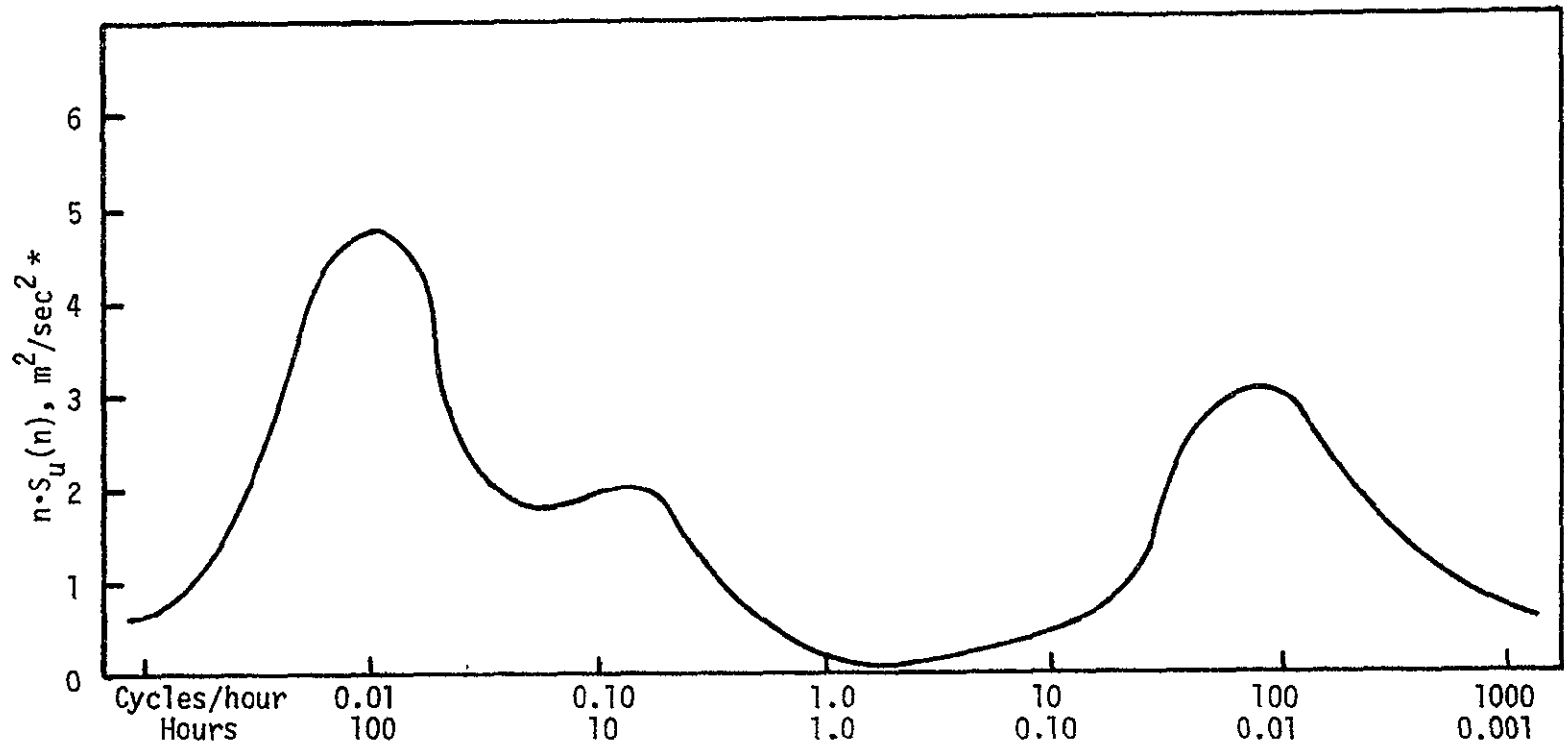
#### 3.1 Background.

A hovering aircraft, either a VTOL or a helicopter, is limited to hovering within the so-called Earth boundary layer. This boundary layer extends from the surface of the Earth through the lowest few hundred feet of the atmosphere. Due to the nature of many factors present in the planetary boundary layer, turbulence is nearly always present [9].

Turbulence is defined by [8] to be rotational, dissipative, three-dimensional, nonlinear, stochastic, diffusive, and a continuum phenomenon. Turbulence can then be defined as a random process that cannot be described by explicit functions of time; only a statistical, probabilistic approach can be taken [5]. Therein lies the problem of modeling the wind.

Reference [5] stated that much of the extensive information available on wind-induced turbulence near the ground is inconclusive and even contradictory. This made a low altitude turbulence model seemingly impossible to derive. However, with certain assumptions, a reasonable representation of presently available information was constructed.

The first assumption was that turbulence can be broken down into a slowly-time-varying component and a rapidly-time-varying component. This was seen by observing a typical spectrum of wind speed near the ground (Figure 7). The spectrum showed that measured winds contain high-frequency and low-frequency modes with a wide gap of frequency where the wind contains little energy. Because of the long periods associated with the low-frequency mode (on the order of hours), this low-frequency mode was assumed to be constant over the relative short period of time (10 seconds) of the



\* n=frequency  
 $S_u(n)$ =power spectral density

Figure 7. Schematic Spectrum of Horizontal Wind Speed Taken as a Function of Time at a Fixed Point.

computer simulation. This then defines a constant velocity mean wind. The high-frequency mode was assumed to represent the irregularly fluctuating wind gusts.

Another assumption was that there was no dependence of the statistical properties of turbulence on time. Turbulence was therefore assumed to be a stationary process. Turbulence was also assumed to be homogeneous (i.e., the statistical properties were the same at each point in the gust field). The last assumption was that the gust velocity components were Gaussian. This was necessary in the development of the gust part of the model in Section 3.3.

### 3.2 Wind.

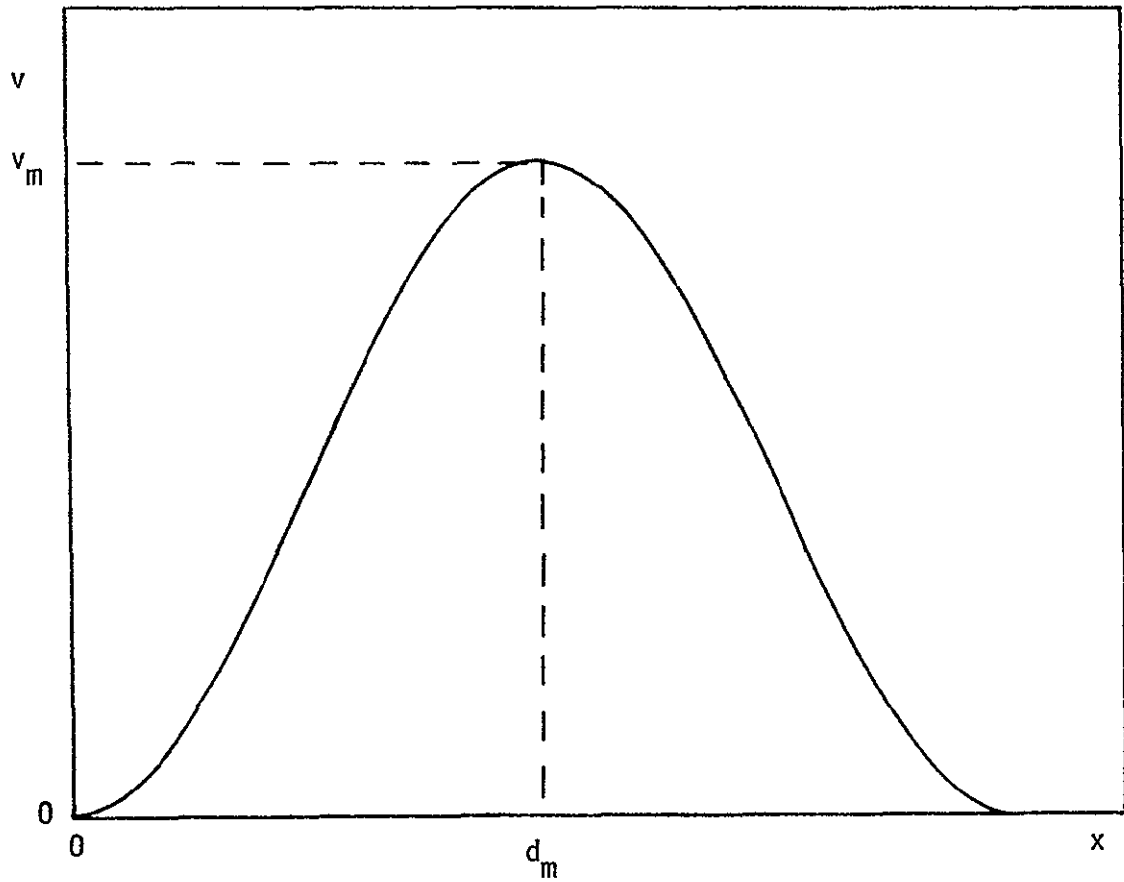
It was stated in Section 3.1 that the low-frequency wind was assumed to be a constant because of the short time period of the simulation. This was also carried over and used to assume that the direction of the wind would be constant over the time period of the simulation.

The reference frame of the wind was an atmosphere-fixed reference frame (see Chapter 4), the axes of which point north, east, and vertically down. The wind model assumed the mean wind to be blowing from north to south (a negative direction) parallel to the north-south axis of the reference frame. Therefore, the crosswind and vertical wind were zero.

The mean wind was assumed to be constant over the entire width and height of operation of the aircraft (see Figure 15).

### 3.3 Gusts.

A discrete model of gust velocity is described in [13]. The discrete model has the "1 - cosine" shape and is shown in Figure 8. The equation of the discrete gust model is



$$\begin{aligned}
 v(x) &= 0 & x < 0 \\
 v(x) &= v_m/2 \cdot (1 - \cos(\pi \cdot x/d_m)) & 0 \leq x \leq 2d_m \\
 v(x) &= 0 & x > 2d_m
 \end{aligned}$$

Figure 8. Discrete Gust Velocity Profile.

$$v(x) = \frac{v_m}{2} \cdot \left\{ 1 - \cos\left(\pi \cdot \frac{x}{d_m}\right) \right\} \quad (8)$$

This model is an arbitrary model that relates the gust magnitude in a rational manner to the expected intensity of continuous random turbulence. The model has a gust velocity  $v(x)$  defined spatially in terms of a magnitude  $v_m$ , which occurs at a distance  $x=d_m$ , where  $d_m$  is a physical dimension of the gust velocity field. This model can be applied to any of the three gust components [13]. This model describes an average of all conditions for clear air turbulence. The model neglects the effects on turbulence of terrain roughness, atmospheric stability (lapse rate), mean wind magnitude, and all other meteorological factors, except altitude. Too few data are available to incorporate these factors into the model.

The validity of a discrete model for gust magnitudes was discussed in [2] and [13]. Reference [13] stated that a discrete gust provides spike-type inputs that may not be apparent in the simulated Gaussian random turbulence. These gusts affected a vehicle in a specific way, but one which was likely to be encountered.

The discrete gust model jointly considers gust magnitude and gust gradient, both of which are important parameters. A study of these parameters was the objective of this research.

The discrete model was a function of three parameters,  $d_m$ , already mentioned,  $L$ , the scale length of turbulence, and  $\sigma$ , the root-mean-square intensity of continuous random turbulence. The last two parameters were functions of altitude. A conditional probability density function of the random turbulence was the key to the discrete model. The derivation of the model is presented in [13]. However, a basic description and some of the assumptions used will be repeated here.

The discrete model was developed by arbitrarily choosing reasonable values of the scales and then determining values for the intensities so



that the mathematical spectral form matched the measured spectra data. The root-mean-square intensity of vertical velocity,  $\sigma_w$ , was the basis for the model. The statistical properties of  $\sigma_w$  were developed in [13].

First, the discrete probability ( $P_1$ ) of encountering turbulence was obtained from Figure 9 (Figure 3, page 443 of [13]). As can be seen, it is a function of altitude. The value of  $\sigma_w$  at a particular altitude was taken to be that rms turbulence which was exceeded with a probability of exactly 0.01 (i.e., 99 percent of all time spent in flight at a given altitude will be spent in either turbulence with less than the specified  $\sigma_w$  or in turbulent free air). If  $P(\sigma_w)$  is the probability that  $\sigma_w$  equals or exceeds a given value, then by definition of  $\sigma_w$ ,

$$P(\sigma_w) = P_1 \cdot \hat{P}(\sigma_w) = 0.01 \quad (\text{III-9})$$

where  $P(\sigma_w)$  and  $P_1$  are defined as above and  $\hat{P}(\sigma_w)$  is the conditional probability of equalling or exceeding a given  $\sigma_w$  once turbulence has been encountered. The function  $\hat{P}(\sigma_w)$  was obtained from Figure 10 (Figure 2, page 442 of [13]), which was based on fitting a Rayleigh distribution to known gust data. From the graph, the value of  $\hat{P}(\sigma_w)$  necessary to make  $P(\sigma_w) = 0.01$  was found and the corresponding  $\sigma_w$ , as a function of altitude, was found.

The vertical scale of turbulence,  $L_w$ , had been established to a reasonably good approximation as a function of altitude. Reference [13] cites two different scales for clear air turbulence, the preferred von Karman scales and the Dryden scales. The vertical scale of turbulence was found from one of the following equations,

$$L = 2500 \text{ feet} \quad \text{altitude (h) > 2500 feet,} \quad (\text{III-10a})$$

$$\text{or} \quad L = h \text{ feet} \quad \text{altitude (h) < 2500 feet.} \quad (\text{III-10b})$$

The scales of turbulence for longitudinal,  $L_u$ , and lateral,  $L_v$ , turbulence were calculated from one of the following equations,

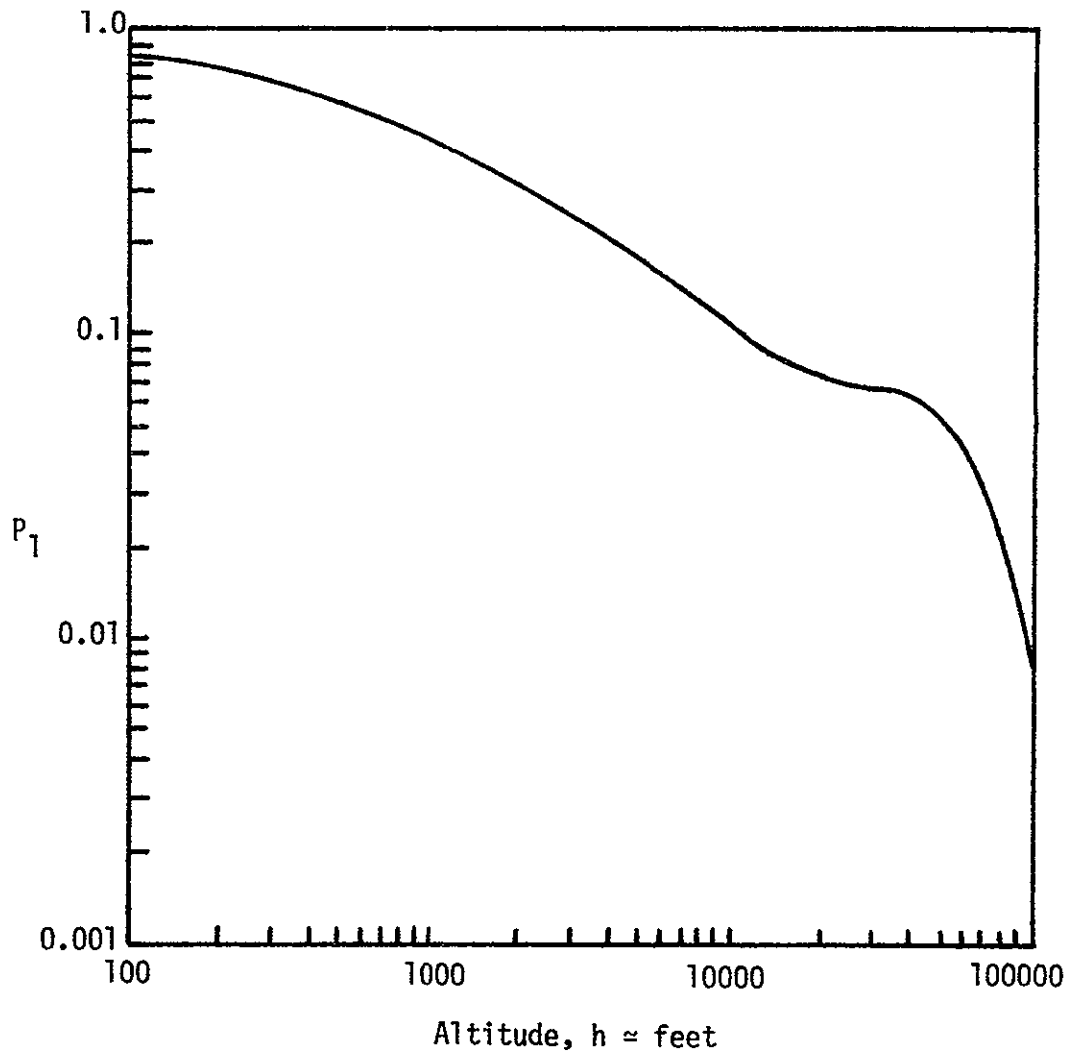


Figure 9. Probability of Encountering Turbulence.

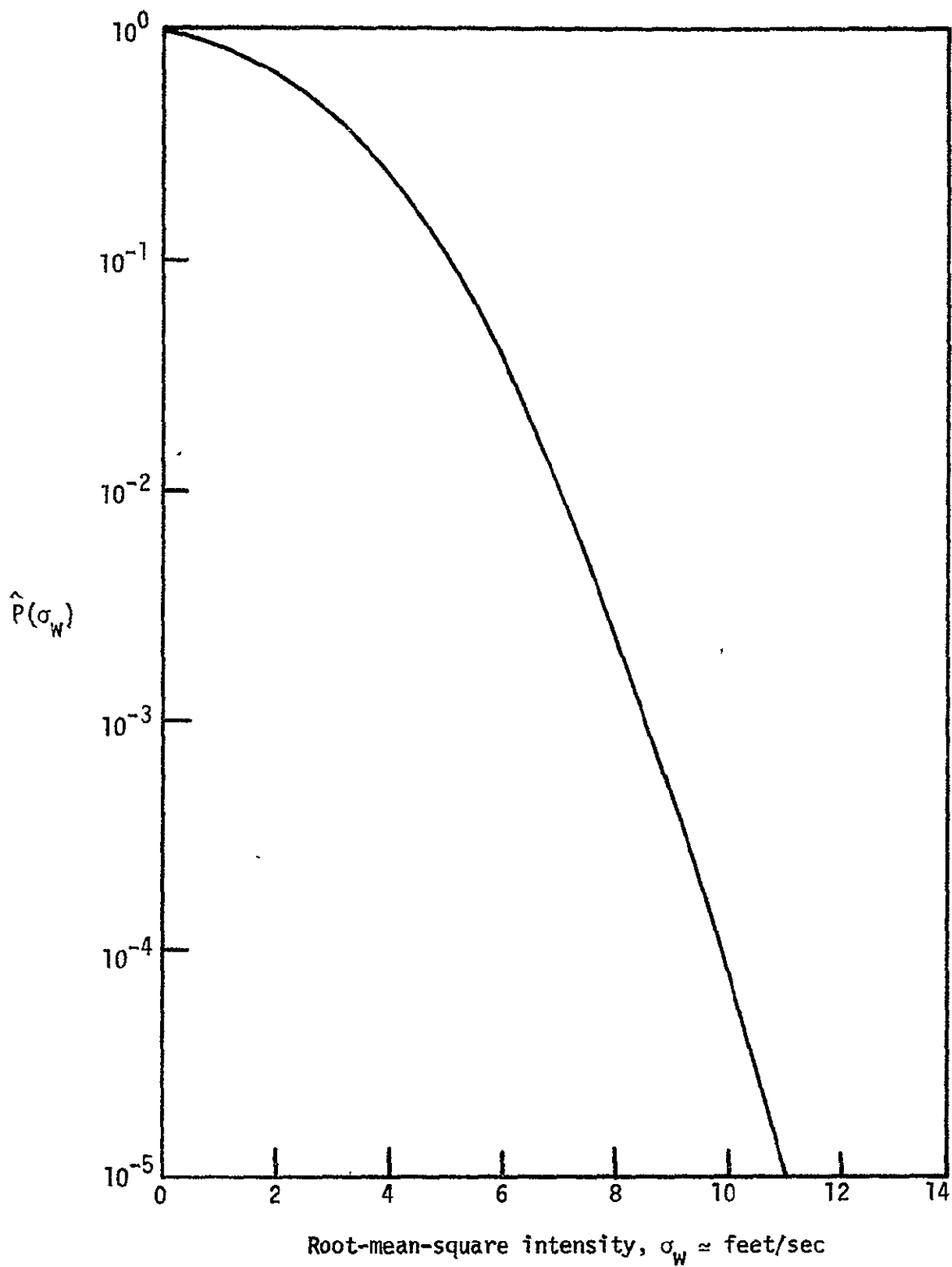


Figure 10. Probability of Equalling or Exceeding a Given  $\sigma_w$  Once Turbulence Has Been Encountered.

$$L_u = L_v = 2500 \text{ feet} \quad \text{altitude (h) > 2500 feet,} \quad (\text{III-10c})$$

$$\text{or } L_u = L_v = 184 \cdot h^{1/3} \text{ feet} \quad \text{altitude (h) < 2500 feet.} \quad (\text{III-10d})$$

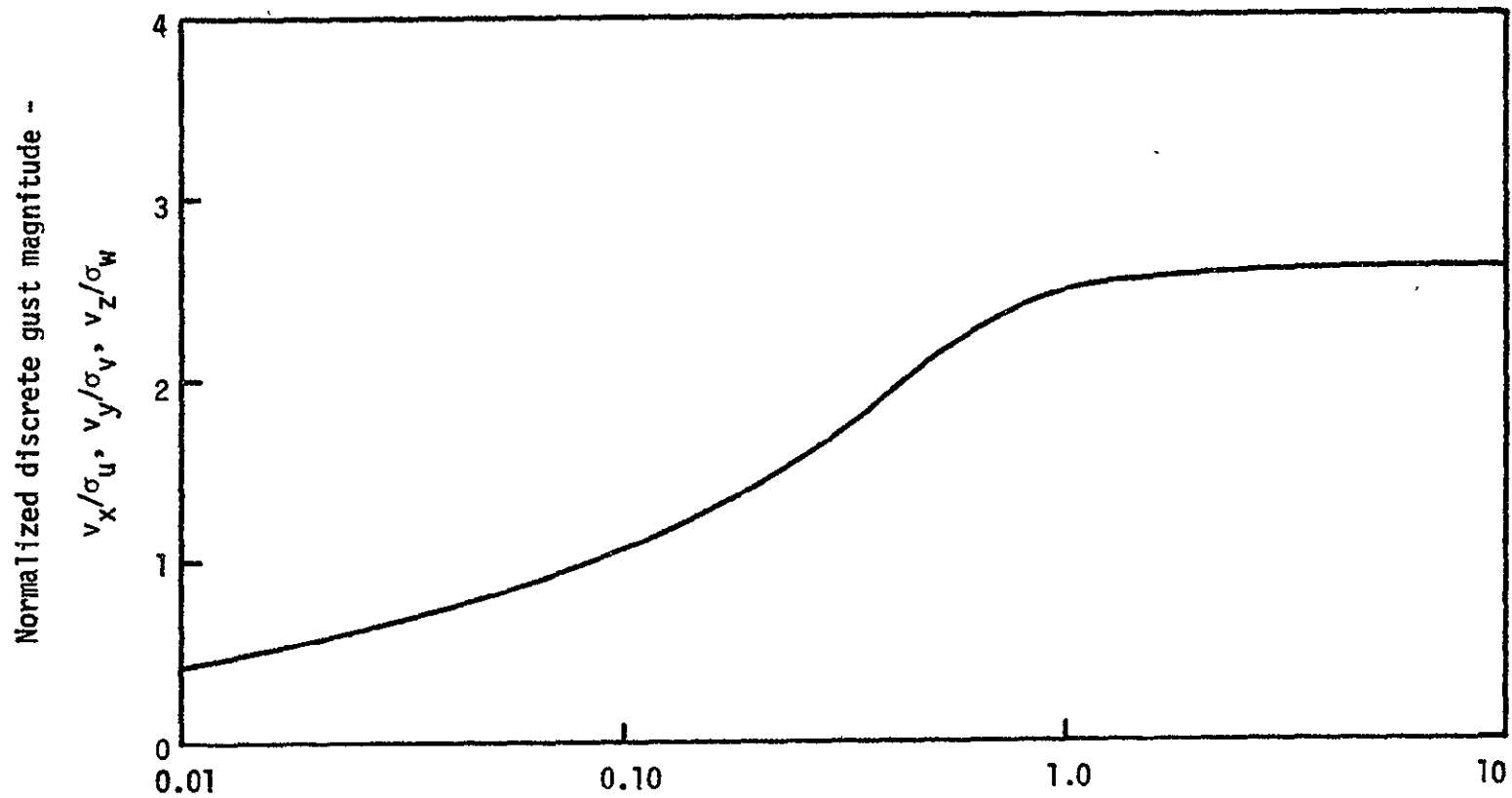
The root-mean-square intensities for the longitudinal and lateral clear air turbulence were derived from the von Karman relationship

$$\frac{\sigma_u^2}{L_u^{2/3}} = \frac{\sigma_v^2}{L_v^{2/3}} = \frac{\sigma_w^2}{L_w^{2/3}} \quad (\text{II-11})$$

For any component of clear air turbulence, the scale of turbulence and the rms intensities were known. By arbitrarily selecting several values of  $d_m$ , corresponding values of  $v_m$  were obtained from Figure 11 (Figure 7, page 429 of [13]). Figure 11 was derived by cross-plotting the values of  $v_m/\sigma$  and  $d_m/L$  from Figure 12 that corresponded to a probability of occurrence of 0.01. Figure 12 is a Gaussian cumulative distribution,  $P(v_m/\sigma)$ , in a normalized form. The variable  $d_m/L$  was a parameter used in calculating  $P(v_m/\sigma)$ . Therefore, for a given altitude and a given probability of being in a specific turbulent field, a discrete model was found.

This was a partial solution to the problem of determining the maximum gust fields in which the aircraft can safely fly. The approach taken in this research was to find the envelope of maximum  $v_m$ 's and, then, knowing the lengths,  $d_m$ , from basic relationships regarding each  $v_m$ , working back to find the probabilities of encountering such turbulence.

A change was made in the discrete equation (8) in order to apply it to the problem. The procedure used in [13] was for an aircraft flying through the velocity field. The total time the aircraft was subjected to the turbulence was the length of the gust field,  $2d_m$ , divided by the airspeed of the aircraft. For this project, the length of time the X-14 was subjected to the turbulence was the distance traveled by the gust divided by the speed at which the gust field was traveling. The length of time was specified based on previous knowledge about gusts [10]. The pro-



Normalized discrete gust length -  $d_x/L_u, d_y/L_v, d_z/L_w$ .

$[u,v,w]$  and  $[x,y,z]$  refer to longitudinal, lateral, and vertical gusts respectively.

Figure 11. Obtaining  $v_m$  Knowing  $L$  and  $\sigma$  and Selecting  $d_m$ .

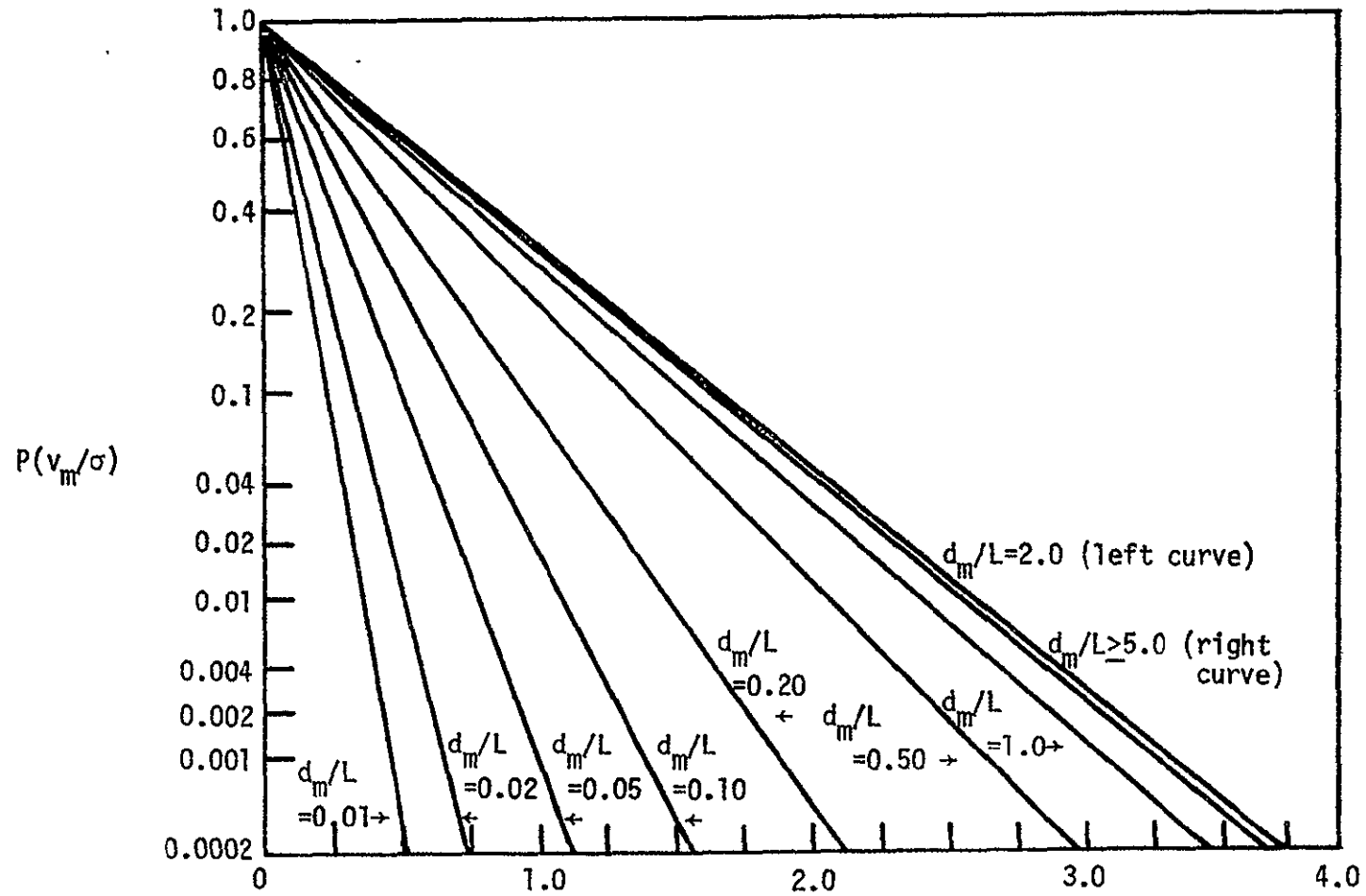


Figure 12. Probability of Equalling or Exceeding a Given Gust Magnitude  $v_m$  for Various Values of  $d_m/L$ .

duct of the time and the speed of the gust field then gave an approximation to the length  $2d_m$  (see Figure 30).

Examination of Figure 7 shows that the period associated with the peak of the high-frequency component occurs around 0.05 hours (3 minutes). However, [10] stated that analysis suggests at least two-thirds of turbulent energy is associated with fluctuations lasting less than five seconds. This latter information was used as a basis for establishing testing frequencies of the gusts. Another conclusion was that, at moderate heights, the eddying energy was equally divided along all three axes. This then was the basis for modifying the discrete equation to be a function of time rather than length, and for it to be equally representative of any one of the three gust components. Therefore, equation (8) became

$$v(t) = \frac{v_m}{2} \cdot \left\{ 1 - \cos\left(\pi \cdot \frac{t}{t_m}\right) \right\}, \quad (\text{III-12})$$

where the distances were replaced by times. The time  $t$  was any instant of time during the simulation between  $t=0$  and  $t=10$  seconds. The time  $t_m$  was the "half-life" of the gust frequency and was when  $v_m$  occurred.

Three "base" times,  $t_m$ , were selected for the model. Times were limited to the length of the simulation or less. The "base" times were ten, five, and three seconds. These times corresponded to frequencies of 0.10, 0.20, and 0.33 cycles-sec<sup>-1</sup> (cps) respectively. The fourth representation of a gust, the step, was also used since a step represents the most severe type of turbulence an aircraft may encounter [2], [14].

### 3.4 Equations of the Wind Model.

The final model of the wind consisted of a mean wind with gusts in the three component directions. The gust opposite in direction to the

mean wind was omitted for the reason that this condition would violate the validity of the model in that it would force  $\beta$  to be greater than 90 degrees. The mean wind was considered to blow from the north at a constant velocity of UWI fps. The gusts were considered positive if they blew in the direction of the positive body axes. The mean wind was transformed from the atmosphere-fixed reference frame into the body-fixed reference frame by the Euler angles. The equations were

$$UW_{bf} = UWI_{af} \cdot \cos(\psi) \cdot \cos(\theta) \quad , \quad (\text{III-13a})$$

$$VW_{bf} = UWI_{af} \cdot \{\cos(\psi) \cdot \sin(\theta) \cdot \sin(\phi) - \cos(\phi) \cdot \sin(\psi)\} \quad , \quad (\text{III-13b})$$

$$WW_{bf} = UWI_{af} \cdot \{\cos(\phi) \cdot \cos(\psi) \cdot \sin(\theta) + \sin(\psi) \cdot \sin(\phi)\} \quad , \quad (\text{III-13c})$$

where the subscripts bf and af referred to body reference and atmospheric reference frames respectively.

The gust components were also transformed into the body reference frame of the aircraft by the Euler angles. The equations were

$$UG_{bf} = UG_{af} \cdot \cos(\psi) \cdot \cos(\theta) + VG_{af} \cdot \cos(\theta) \cdot \sin(\psi) - WG_{af} \cdot \sin(\theta) \quad , \quad (\text{III-14a})$$

$$VG_{bf} = VG_{af} \cdot \{\cos(\psi) \cdot \cos(\phi) + \sin(\phi) \cdot \sin(\psi) \cdot \sin(\theta)\} - UG_{af} \cdot \{\cos(\phi) \cdot \sin(\psi) - \cos(\psi) \cdot \sin(\phi) \cdot \sin(\theta)\} + WG_{af} \cdot \cos(\theta) \cdot \sin(\phi) \quad , \quad (\text{III-14b})$$

$$WG_{bf} = UG_{af} \cdot \{\cos(\psi) \cdot \cos(\phi) \cdot \sin(\theta) + \sin(\psi) \cdot \sin(\phi)\} - VG_{af} \cdot \{\cos(\psi) \cdot \sin(\phi) - \cos(\phi) \cdot \sin(\psi) \cdot \sin(\theta)\} + WG_{af} \cdot \cos(\phi) \cdot \cos(\theta) \quad , \quad (\text{III-14c})$$

where  $UG_{af} = 1/2 \cdot v_{mu} \cdot \{1 - \cos(\pi \cdot t / t_{mu})\} \quad , \quad (\text{III-15a})$

$$VG_{af} = 1/2 \cdot v_{mv} \cdot \{1 - \cos(\pi \cdot t / t_{mv})\} \quad , \quad (\text{III-15b})$$

$$WG_{af} = 1/2 \cdot v_{mw} \cdot \{1 - \cos(\pi \cdot t / t_{mw})\} \quad . \quad (\text{III-15c})$$

### 3.5 Input to the Aircraft Model.

The approach to this study is illustrated in Figure 13. The wind



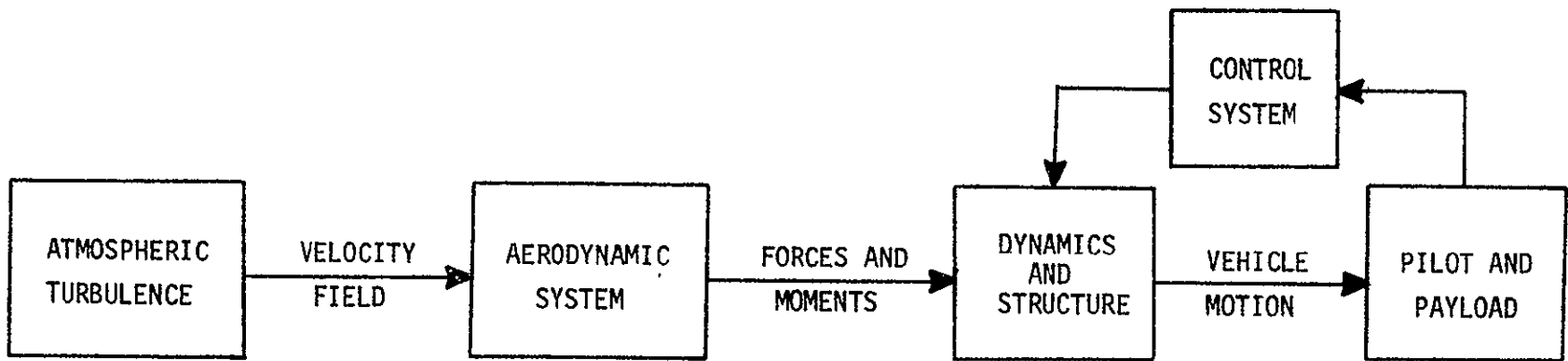


Figure 13. Problem Approach.

model described the atmospheric turbulence, the output of which was a velocity field. This velocity field acted as a disturbance on the aircraft in the form of changes in aerodynamic forces and moments. These forces and moments were then fed into the aircraft model. The stability of the output, or the vehicle motion, of the aircraft model was used in determining the maximum gust field the aircraft could withstand.

The velocity field of the atmosphere may be regarded, over the time and space intervals of interest, as composed of a steady mean value with turbulent fluctuations superposed. This leads to the assumption that the structure of turbulence takes the form of individual patches, in each of which the turbulence is approximately random, homogeneous, and isotropic. This is based on the fact that the statistical properties of the disturbance input to an airplane flying through a turbulent field are not appreciably affected by the variation of that field with time. Essentially, turbulence may be treated as a frozen pattern in space.

Another assumption must be made in order to deal with a hovering VTOL aircraft like the X-14. Reference [5] stated that an assumption of a frozen turbulence model was invalid for a stationary point. However, [8] and [12] stated that the hypothesis of a gust field frozen in time moving downwind with the mean wind speed (known as Taylor's hypothesis) was acceptable at low airspeeds. The lower limit of airspeed at which this assumption was valid was put at one-third the mean wind speed. Therefore, the model of the aircraft was assumed to have a forward airspeed equal to one-third the mean wind speed. This does not violate the definition of the hover conditions as a 30 fps forward velocity was defined as the limiting forward velocity for the hover mode.

It was assumed that there was no variation of the gusts over the physical dimensions of the aircraft. The longitudinal gust was assumed

constant along the wing span, the lateral gust was assumed constant along the fuselage, and the vertical gust was assumed constant along the wing span and fuselage. The aircraft was in effect treated as a point [5].

Treating the airplane as a point simplified the model as far as defining the input to the aircraft. However, it restricted the usefulness in calculating certain responses. The point approximation was valid provided the wavelengths of the gusts were much greater than the physical dimensions of the aircraft. This was valid for lower frequencies only. Reference [5] limited the upper frequency for validity to  $2/(\text{wing span})$  which, for the X-14, was 0.059 cps. This was the upper limit for considering the plane vanishingly small compared to the gust wavelength. The smallest frequency used in the model was 0.100 cps, or almost twice the limiting value. This would indicate that the point approximation assumed in this study would yield somewhat limited results.

To consider the higher frequencies would then require treating the airplane as a finite plane in space where the gusts vary along the dimensions of the aircraft. Variations in longitudinal gusts along the wing span would result in induced rolling moments and pitching moments. Variations in vertical gusts along the wing span and fuselage would result in pitching and rolling moments also. Variations in lateral gusts along the fuselage would result in yawing moments.

The gust model would need to be modified in order to produce these variations. The modifications would entail splitting the gust velocity field into smaller parts, each of which possessed different magnitudes and, each of which acted on a separate section of the aircraft. The aircraft model would then also need modification in order to calculate the response of the aircraft to each gust input. These modifications would increase the complexity of each model, which, at this time, is beyond the scope of

this project.

Treating the aircraft as a point also neglects the effect of gust penetration (i.e., wing-to-tail delays). Gust penetration is important for high gust magnitude to airspeed ratios, which was the case for this project. However, this would require that the response of the tail to gusts be known. At the present time these responses are not available.

For the altitude considered in this project, 100 feet, this model derived in the foregoing was assumed to be a reasonable representation of clear air random turbulence.

## CHAPTER 4

### METHOD OF ANALYSIS

#### 4.1 Reference Frames.

Four frames of reference were needed for the definition of this problem. An inertial reference frame was needed in which Newton's Second Law is valid for motion of a particle or a rigid body. The inertial frame chosen was as Earth-fixed reference,  $F_e$ , with Earth surface axes  $0_e x_e y_e z_e$  (Figure 14). The origin of this frame was placed near the vehicle with the  $0_e z_e$  axis pointing vertically down, the  $0_e x_e$  axis pointing north, and the  $0_e y_e$  axis pointing east. The rotation of the Earth and its curvature were neglected, thus being called a Flat-Earth approximation (i.e., treating the Earth as a stationary plane in inertial space).

A reference frame defining the aircraft was also needed. In this case, two were defined. First, a vehicle-carried vertical frame,  $F_v$ , with axes  $0_v x_v y_v z_v$  was attached to the aircraft at the mass center. The  $0_v z_v$  axis was directed vertically down and the remaining axes,  $0_v x_v$  and  $0_v y_v$ , were chosen to point north and east respectively. For hover, the movement of the aircraft from its original position was small enough to consider the origin of  $F_v$  near enough to the origin of  $F_e$  so that the axes of each could be considered parallel.

The second reference frame associated with the airplane was a body-fixed reference frame,  $F_b$ , with body axes  $Oxyz$ . The origin of this frame was located at the aircraft mass center (see Figure 1). The axes were the same as those defined in Chapter 2. As mentioned previously, the Euler angles gave the orientation of the body axes relative to  $F_v$ . However, by considering the origins of  $F_e$  and  $F_v$  to be coincidental, or nearly so, because of hover, the Euler angles also gave the orientation of the aircraft

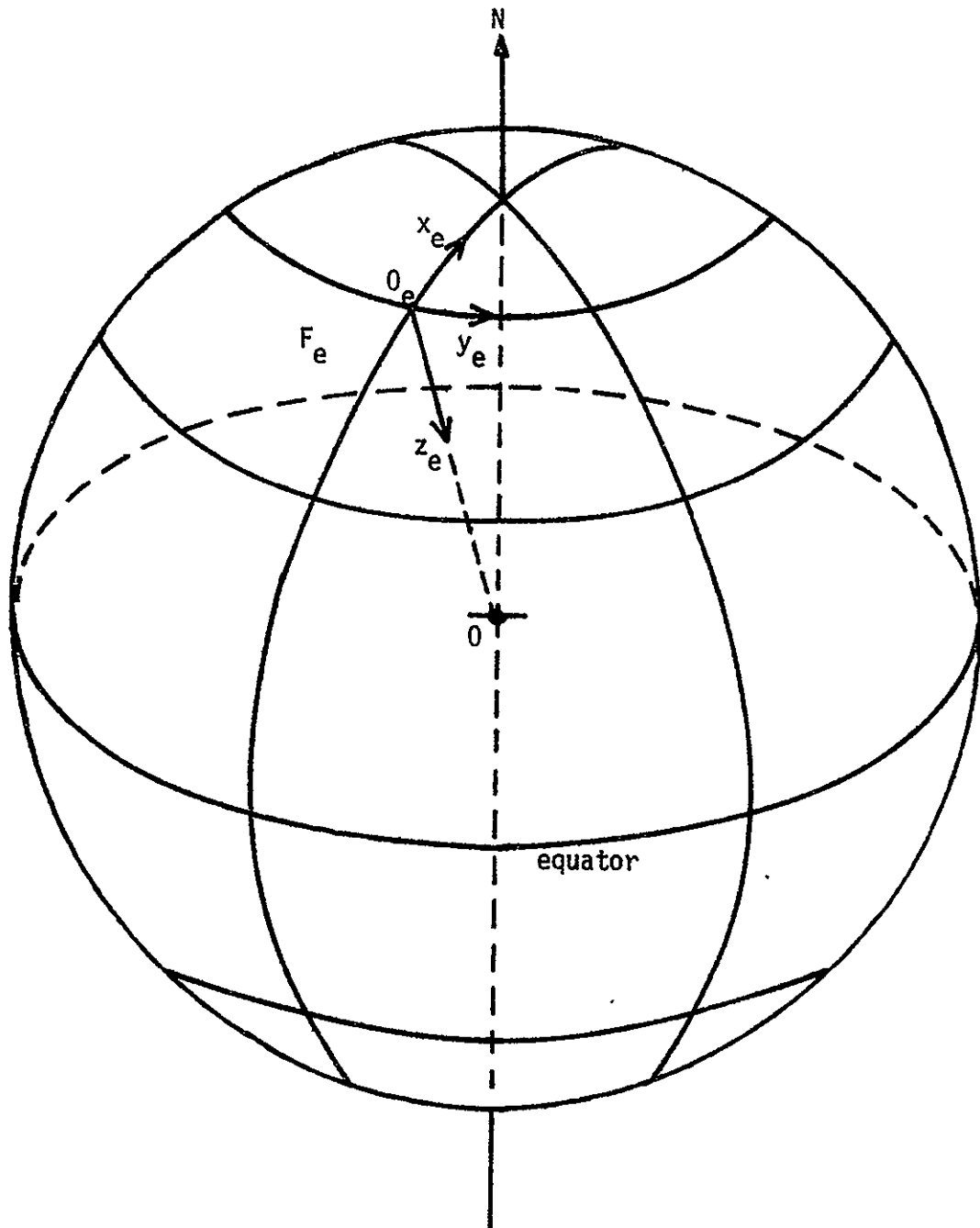


Figure 14. Earth Surface Reference Frame,  $F_e$ .

relative to the inertial reference frame,  $F_b$  relative to  $F_e$ .

The fourth reference needed to define the problem was one to be used with the motion of the atmosphere. The atmosphere-fixed reference frame,  $F_a$ , with axes  $O_a x_a y_a z_a$ , was necessary to define the relative velocity between the aircraft and the atmosphere for the calculation of aerodynamic forces and moments. When the atmosphere was at rest relative to the Earth,  $F_a$  and  $F_e$  were the same. When the atmosphere was in non-uniform motion relative to the Earth,  $F_a$  was chosen so that the average motion of the atmosphere relative to  $F_a$  was zero [5]. Therefore, non-uniform and uniform motion of the atmosphere relative to the Earth resulted in motion of  $F_a$  relative to  $F_e$ . By selecting  $F_a$  parallel to  $F_e$  initially,  $F_a$  then moved parallel to  $F_e$  at constant velocity.

All reference frames were assumed to have the same origin at the start of the simulation, or at time zero, as shown in Figure 15. The changes in the references for an incremental time  $\Delta t$  are shown in Figure 16. Reference  $F_a$  has moved a distance of  $UWI \cdot \Delta t$  feet in the negative x-direction. The aircraft has flown along a trajectory path P and has undergone angular displacements in roll, pitch, and yaw. For purposes of derivations to follow, these displacements were assumed to be positive. The aircraft was no longer orthogonal to the other three reference frames. Disturbances parallel to  $F_a$  were transformed into  $F_b$  by the Euler angles. The aircraft now "saw" orthogonal components of the wind and the gusts.

The transformations were carried out in a particular sequence as shown in Figure 17 [5]. The sequence was 1) a rotation  $\psi$  about  $O_v z_v$  carrying the axes to a temporary position  $O_v x_2 y_2 z_2$ , 2) a rotation  $\phi$  about  $O_v y_2$  carrying the axes to another temporary position  $O_v x_3 y_3 z_3$ , and 3) a rotation  $\theta$  about  $O_v x_3$  carrying the axes to their final position  $Oxyz$ .

#### 4.2 Method of Solution.

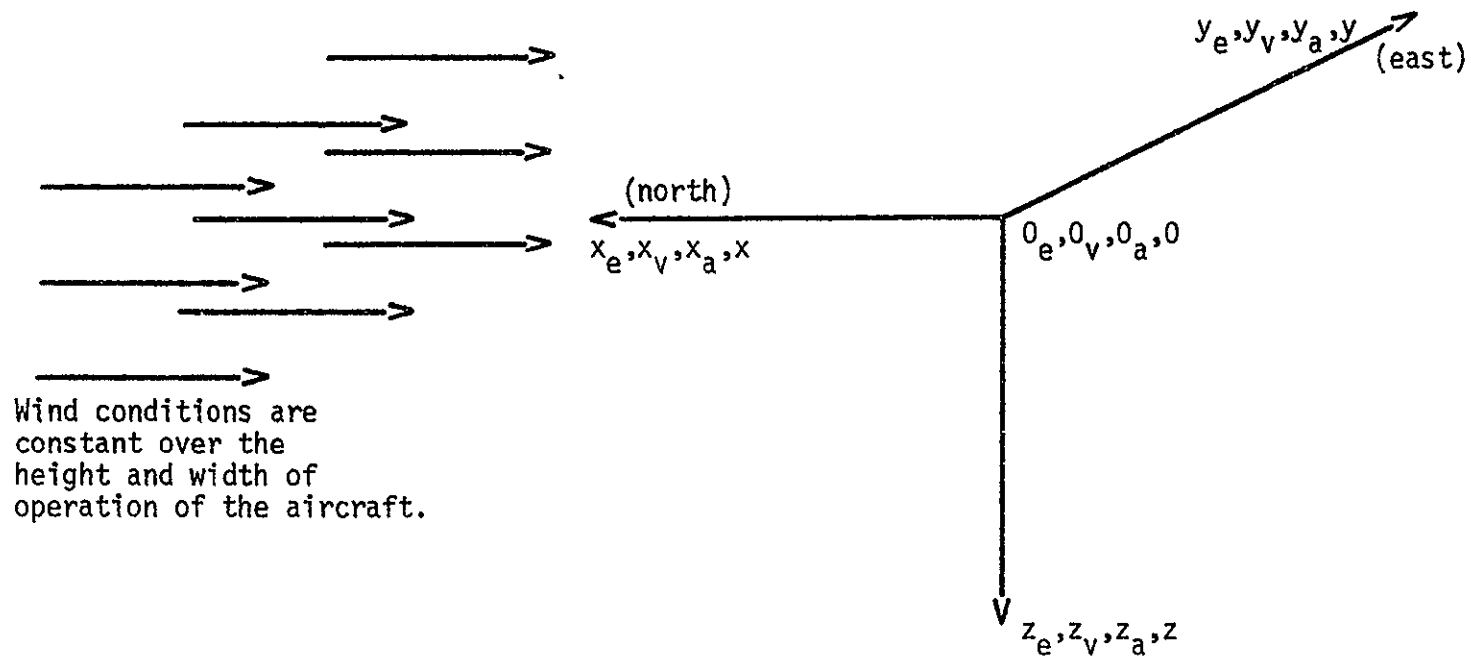


Figure 15. Relative Positions of the Reference Frames for Initial Conditions.



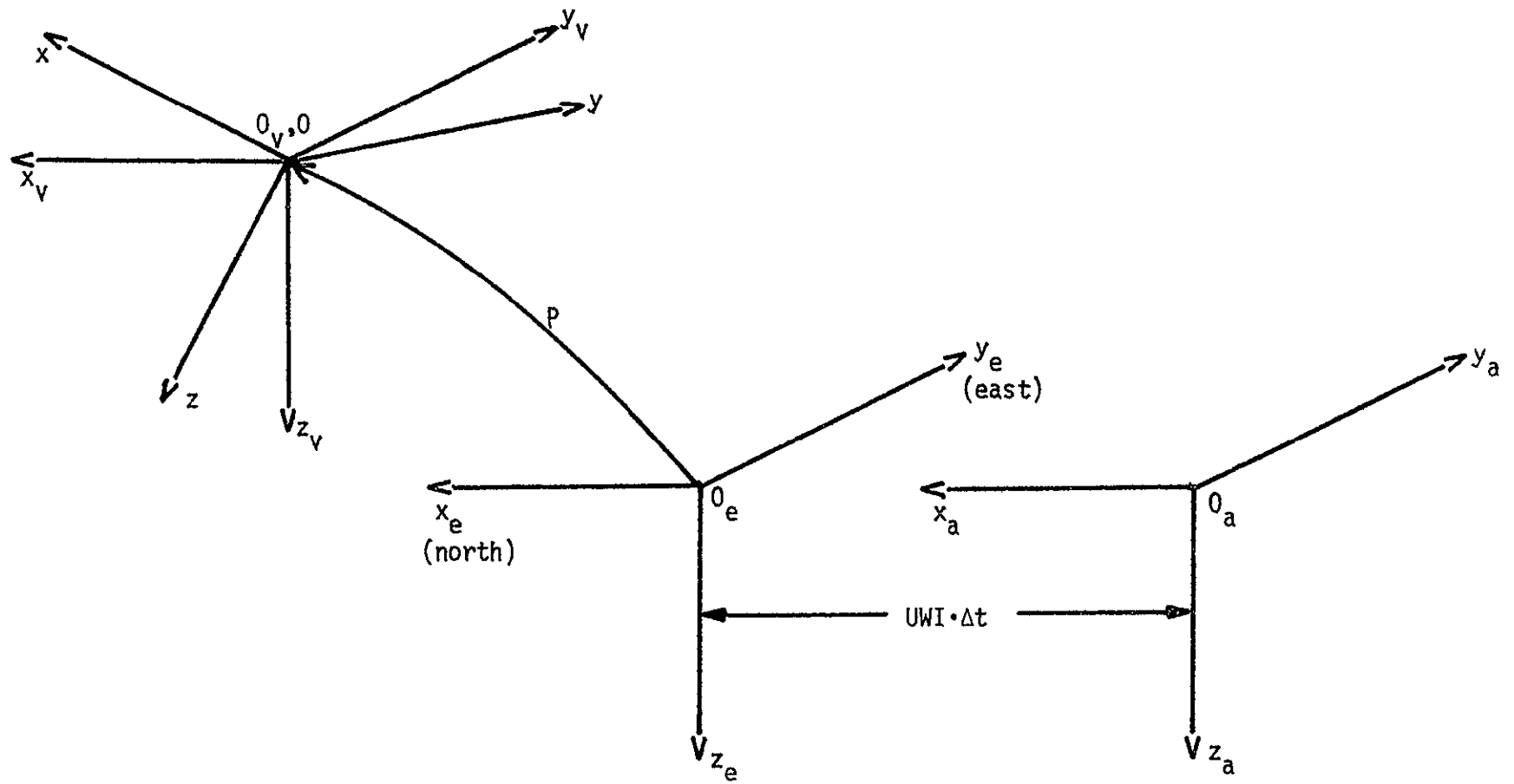


Figure 16. Relative Positions of Reference Frames  $\Delta t$  Seconds After Gust Input.

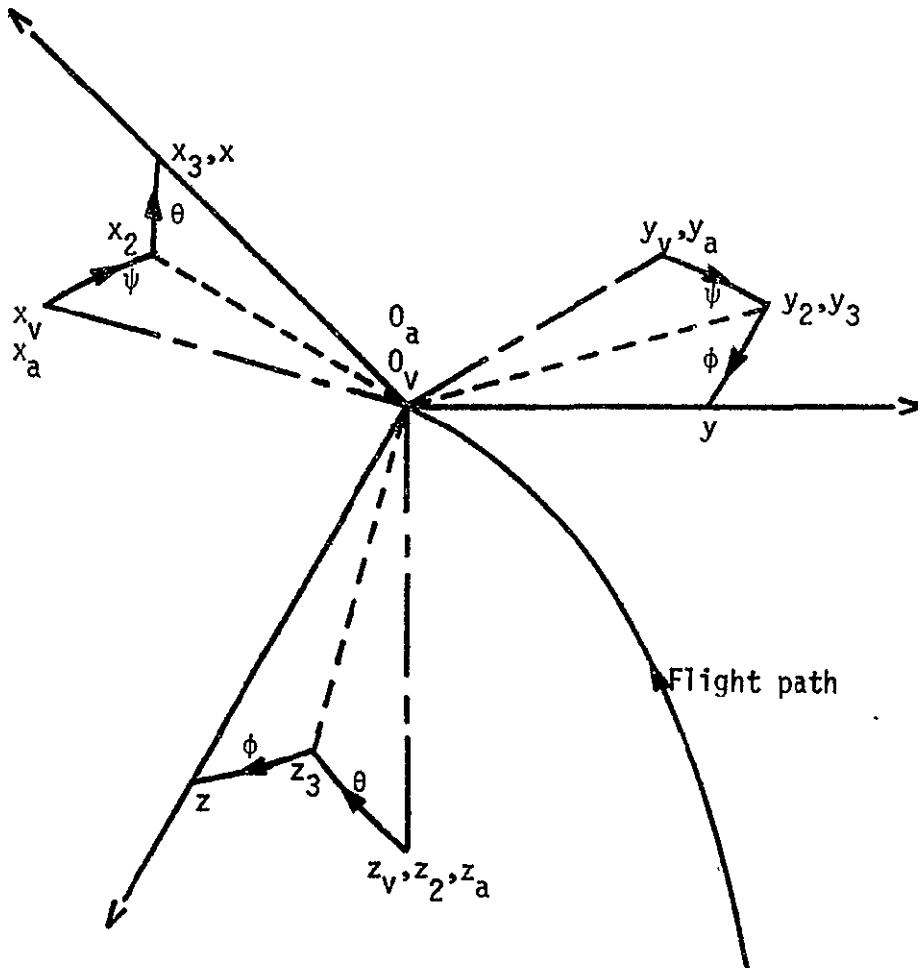


Figure 17.  $F_v$  and  $F_a$  Transformed into  $F_b$  Through the Euler angles  $\theta$ ,  $\phi$ , and  $\psi$ .

The objective of this research was to find the largest gust field the aircraft could encounter and still maintain a stable flying condition. The stability of the aircraft was defined by certain constraints or limits on some of the state variables and control parameters.

The procedure was to solve equation (6)

$$\dot{\underline{x}} = f\{t; \underline{x}(t), \underline{u}(\underline{x}(t-\tau)), \underline{w}(t)\} ,$$

for maximum  $\underline{w}$  with constraints and limits imposed on  $\underline{x}$  and  $\underline{u}$ . Due to the nonlinearity and time variance of the equations,  $\underline{w}$  could not be solved for directly.

A simple iteration technique to solve for  $\underline{w}$  indirectly was used. An arbitrary wind model was selected and introduced into the aircraft model. If the airplane flew in a stable manner for ten seconds, the wind model was increased in magnitude. If the airplane could not recover, the magnitude was decreased. The iteration was carried out until the largest values of wind and gusts the aircraft could withstand were found.

The problem was then an initial value problem with a known set of initial conditions and a set of 12 first-order differential equations that could be integrated by numerical methods.

The initial conditions of the aircraft represented the hover mode. The forward velocity,  $u$ , was set equal to one-third the mean wind speed, a necessary condition for Taylor's hypothesis. The remaining state variables, except for the altitude, were set to zero.

The length of time for the observation of the aircraft was arbitrarily set at ten seconds. The solution of the differential equations was obtained by integrating over the time interval in steps of 0.10 seconds. The integration routine used a fourth-order Runge-Kutta iteration to calculate the initial values of the integration and a four-point Adams-Bashforth-Moulton predictor-corrector method to continue the integration.

The first part of the solution to the problem was to determine the maximum steady-state headwind the airplane could withstand. No other components of the wind were calculated because of the assumption that the aircraft was always facing initially into the steady-state headwind. The second part of the solution consisted of finding operational envelopes of maximum gust magnitude for various gust frequencies, headwinds, and control policies.

#### 4.3 Computer Program.

The flow chart for the program WINDY, used to calculate the operational envelopes, is shown in Figure 18. The program was given the initial conditions for hover and the velocity of the headwind. For these conditions, the aerodynamic coefficients used in calculating the aerodynamic forces were calculated. These aerodynamic coefficients changed instantaneously for each change in relative velocity of the atmosphere with respect to the aircraft.

At some time  $t_0$  the gust disturbances were introduced. These gusts were parallel to the atmosphere-fixed reference frame. The program transformed the gusts and the wind into the aircraft reference frame.

The initial values of the control vector were then calculated by WINDY. These values were stored by the program. They represented the state of the aircraft before any disturbance was encountered.

The solutions of the system of differential equations describing the aircraft motion were obtained and stored for a particular instant of time. Next, the angular accelerations were calculated and stored. These values were obtained by treating the equations involving angular motion (i.e., the  $\dot{p}$ ,  $\dot{q}$  and  $\dot{r}$  equations) as algebraic equations. For the particular time (of the simulation) in question, these equations take the form

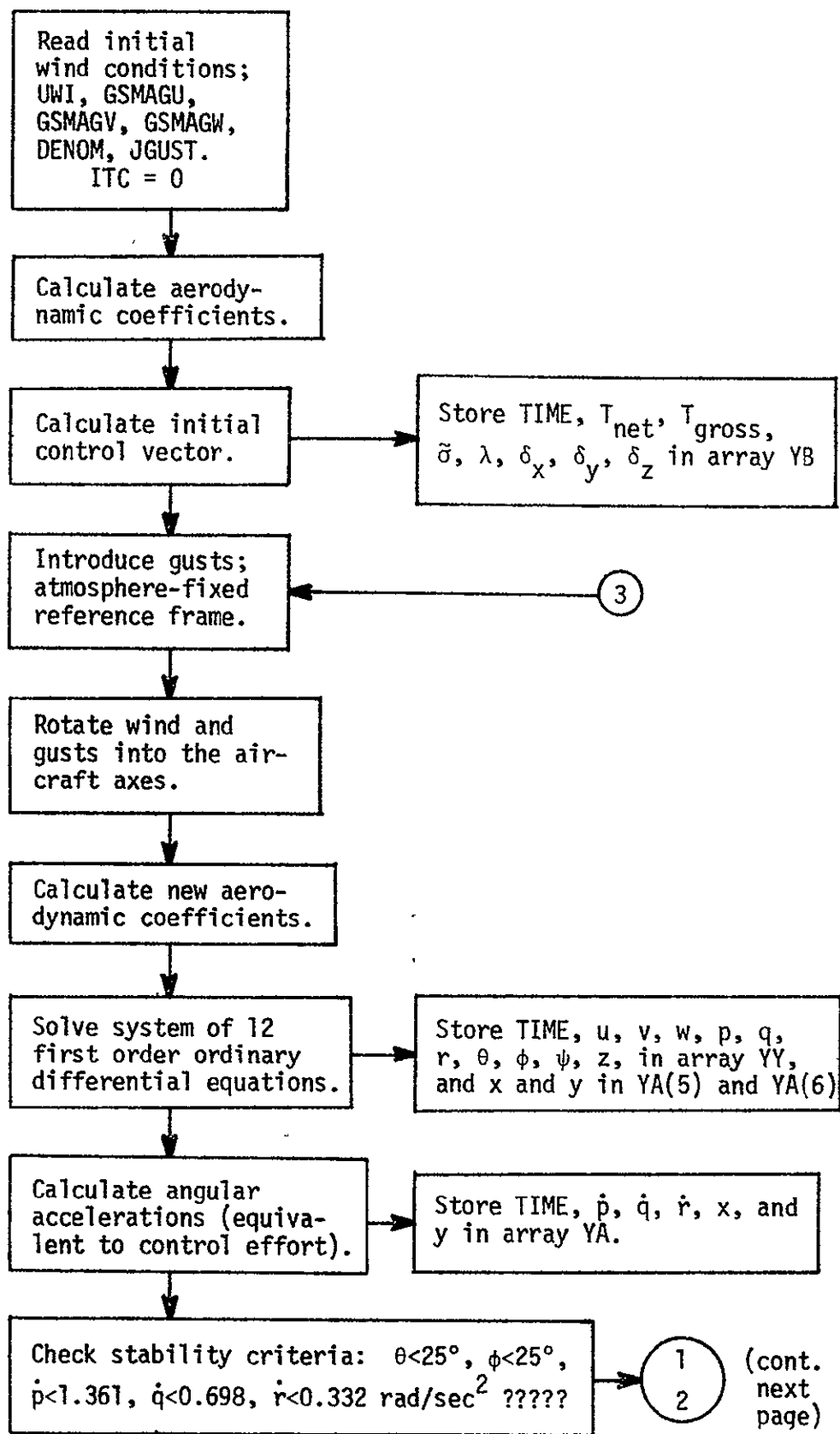


Figure 18. Flow Chart for Windy.

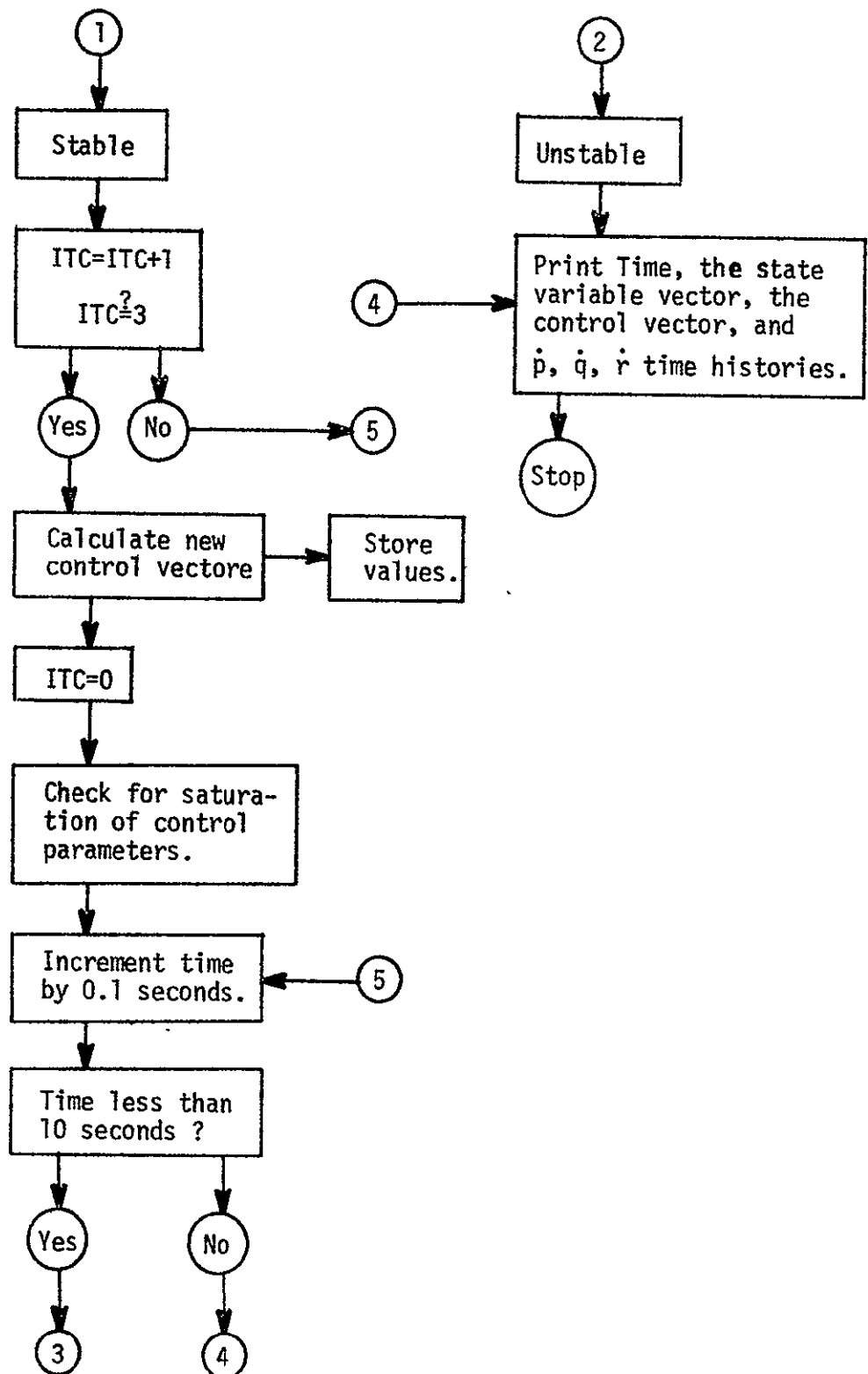


Figure 18. (continued)

$$\dot{p}_j = f(x_j, u_j, w_j) \quad , \quad (\text{III-16a})$$

$$\dot{q}_j = f(x_j, u_j, w_j) \quad , \quad \text{and} \quad (\text{III-16b})$$

$$\dot{r}_j = f(x_j, u_j, w_j) \quad . \quad (\text{III-16c})$$

The current values of the state variables,  $x_j$ , the control parameters,  $u_j$ , and the disturbances,  $w_j$ , were substituted directly into the above equations. These equations also gave the control effort requirements since these requirements and the angular accelerations were equivalent.

The stability criteria were checked as the program proceeded to the next part. If the aircraft was found to be unstable, the program printed the time history of the motion up to that point and then stopped. The time, the state variables, the control parameters, and the angular accelerations were printed for every 0.10 seconds. If the aircraft was stable, the time was checked to see if it was time to calculate new values for the control parameters. The control parameters were calculated every third step after the introduction of the disturbances. This simulated the time lag due to the pilot.

Upon every calculation of a new control vector, the program checked the saturation limits of the various parameters. Any control parameter exceeding its saturation point was set equal to that saturation point.

The time was then incremented by 0.10 seconds. If the time was less than ten seconds, the program introduced the gusts with their new velocities and then went through the same procedure as just outlined. If the simulation was complete (ten seconds) the program printed the complete time history.

A copy of WINDY is presented in Appendix 6.

## CHAPTER 5

### RESULTS, DISCUSSIONS, AND CONCLUSIONS

#### 5.1 Steady-state Wind (Headwind).

The first part of the project was to find the maximum headwind (with no gusts) in which the aircraft could maintain a hovering flight condition. The computer simulations found the maximum headwind to be 61 fps (36 knots). The aircraft was found to remain virtually motionless with only the thrust and the pitch control nozzle angle,  $\delta_y$ , differing from hover conditions. The net thrust was lower by 449 pounds (obviously due to the lift created by the wind) and  $\delta_y$  was nearly saturated at -19.2 degrees.

The next higher value of headwind, 62 fps, resulted in the aircraft being unable to counteract the pitching moment created by the lift due to the wind. The pitch control angle was saturated (-20 degrees) for the entire simulation. The aircraft exceeded +25 degrees in pitch attitude after 5.6 seconds.

#### 5.2 Maximum Gust Envelope.

Table 1 presents the maximum gust envelope for the X-14. The values in this table represent the variable  $v_m$  of equation (12) in Chapter 3.

##### 5.2.a Analysis of Longitudinal Gusts.

Table 1 shows the longitudinal gust magnitude (UG) to be independent of frequency. All three frequencies have nearly the same magnitude, 52 fps. The computer simulations showed that  $\delta_y$  became saturated whenever the gust magnitudes approached their maximum values (52 fps).

An analysis of the next higher magnitude for each frequency showed



HEADWIND	LONGITUDINAL GUST	LATERAL GUST		VERTICAL GUST		FREQUENCY
UWI	-UG	+VG	-VG	+WG	-WG	
-10	-52	+65	-67	+23	-19	0.10 cps
-10	-52	+65	-66	+23	-17	0.20 cps
-10	-53	+72	-74	+23	-21	0.33 cps
-10	---	+27	-27	+16	-15	step
-61	maximum headwind					

All magnitudes are fps.

Table 1. Maximum Permissible Gust Envelope.

the aircraft to exceed +25 degrees in pitch for the two lower frequencies (0.10 and 0.20 cps). The pitch control effort, equivalent to  $\dot{q}$ , was exceeded in the third case.

#### 5.2.b Analysis of Lateral Gusts.

Examination of Table 1 shows that the permissible magnitudes for the lateral gusts to be the largest of the three component magnitudes. The limiting factors were the aircraft side velocity and the pitch angle, depending on the frequency content of the gust. At 0.10 and 0.20 cps, the side velocity exceeded the definition of hover for all gust magnitudes in excess of 65 fps. At 0.33 cps the pitch angle exceeded +25 degrees for gusts in excess of 72 fps. It should be noted that if the side velocity was ignored, the maximum permissible gusts were 88 and 73 fps for 0.10 and 0.20 cps respectively.

Detailed analysis showed that a large yaw angle,  $\psi$ , was indirectly responsible for the large pitch angle (0.33 cps case and for the two cases where side velocity was ignored). For a large  $\psi$ , typically 50 to 60 degrees, the lateral gust provides a component which resembles longitudinal velocity,  $U_0$ . Figure 19 shows the relationship between  $U_0$  and  $\theta$  for a longitudinal gust of 53 fps and 0.10 cps (minimum case of instability). Also shown are  $U_0$  and  $\theta$  for a lateral gust of 89 fps and 0.10 cps (minimum case of instability also--one fps above the limiting case). The figure shows a close resemblance between the two sets of curves as  $\psi$  increases. This substantiates  $\psi$  as being indirectly responsible for  $\theta$  exceeding its critical value.

The lateral gusts in the form of a step function resulted in more limited responses because of excessive yaw control effort ( $\ddot{\psi}$  or  $\dot{r}$ ) demanded by the aircraft. The permissible magnitude was 27 fps. Ignoring aircraft

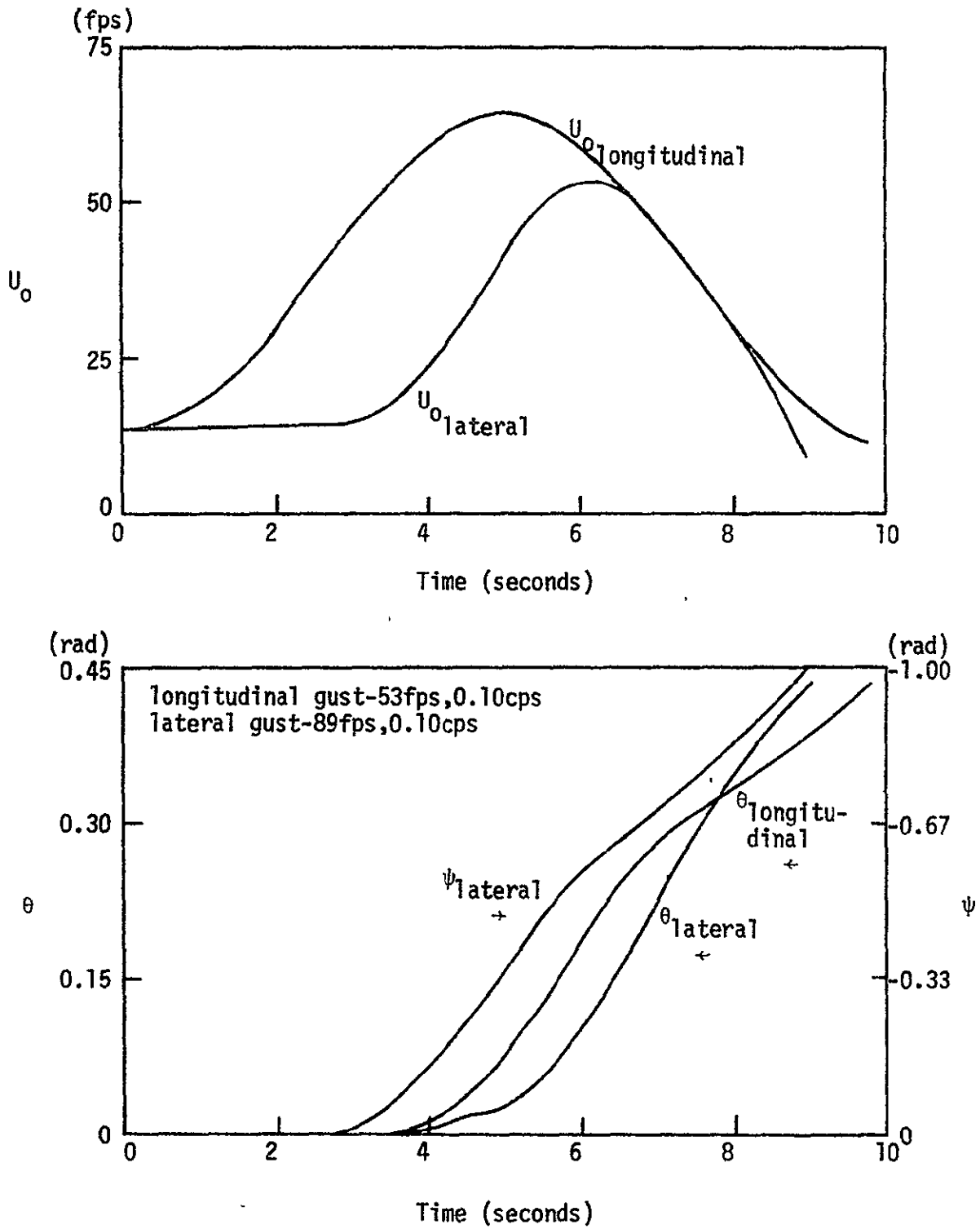


Figure 19.  $U_0$  and  $\theta$  for Minimum Unstable Longitudinal and Lateral Gusts.

side velocity, the permissible magnitude was 53 fps.

### 5.2.c Analysis of Vertical Gusts.

Table 1 shows the aircraft to be the most sensitive to the vertical gusts. In all cases the critical parameter in determining instability was  $\theta$ . For both positive (down) and negative (up) vertical gusts, the pitch angle exceeded +25 degrees before any of the other hover criteria were violated. The maximum gust magnitudes were +23 and -19 fps for 0.10 cps, +23 and -17 fps for 0.20 cps, +23 and -21 fps for 0.33 cps, and +16 and -15 fps for the steps.

Figure 20 shows the time history for  $\theta$  for +23 and -19 fps (0.10 cps), the limiting hover case. The responses were normal for the first half of the simulation. Normal responses meant positive pitch from a down gust (gust striking a larger surface area behind the center of gravity of the aircraft and thus forcing the nose up) and negative pitch from an up gust (same reasoning, nose down). The initial  $-\theta$  created by the up gust resulted in an increase in  $u$ , forward velocity. This increase results in a larger positive pitching moment which should tend to return the aircraft to an "even keel". Figure 20 shows this to be the case over the first six seconds of the simulation. However, at that time, the aircraft acquired a large positive pitch rate which rapidly drove the aircraft unstable. The pitch control effort did not respond as would be expected for this situation. Figure 21 shows  $\delta_y$  for both cases. As can be seen,  $\delta_y$  never approached saturation at any time for the up gust case. The reason for this can be found by examining the equation for  $\delta_y$  (equation (A5-5), Appendix 5). In detailed analysis it was found that the angle of attack exceeded its valid range for the model,  $\pm 20$  degrees. Typically  $\alpha$  approached 50 to 60 degrees. This was the cause for the unusual results.

13

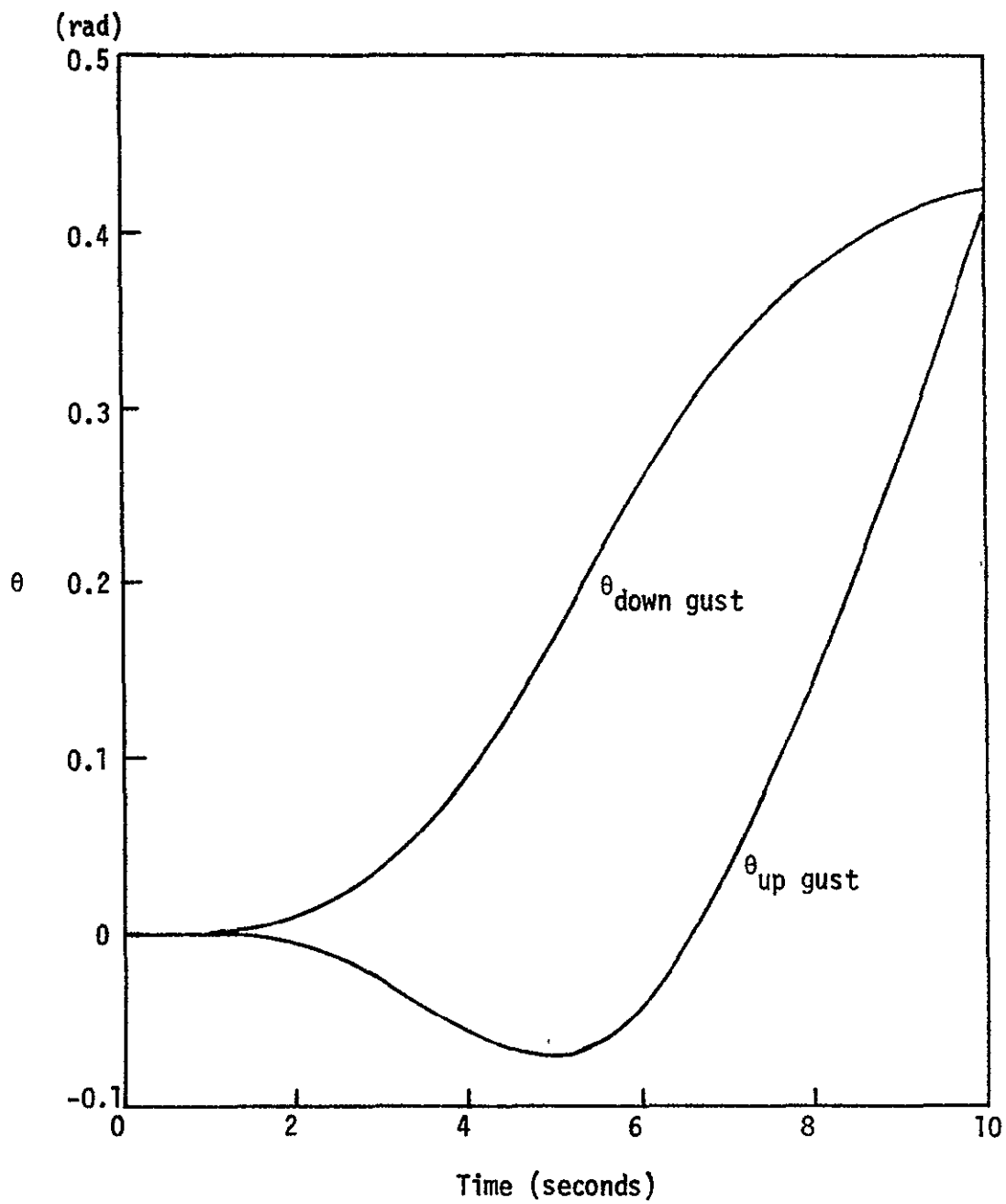


Figure 20.  $\theta$  for Positive and Negative Vertical Gusts.

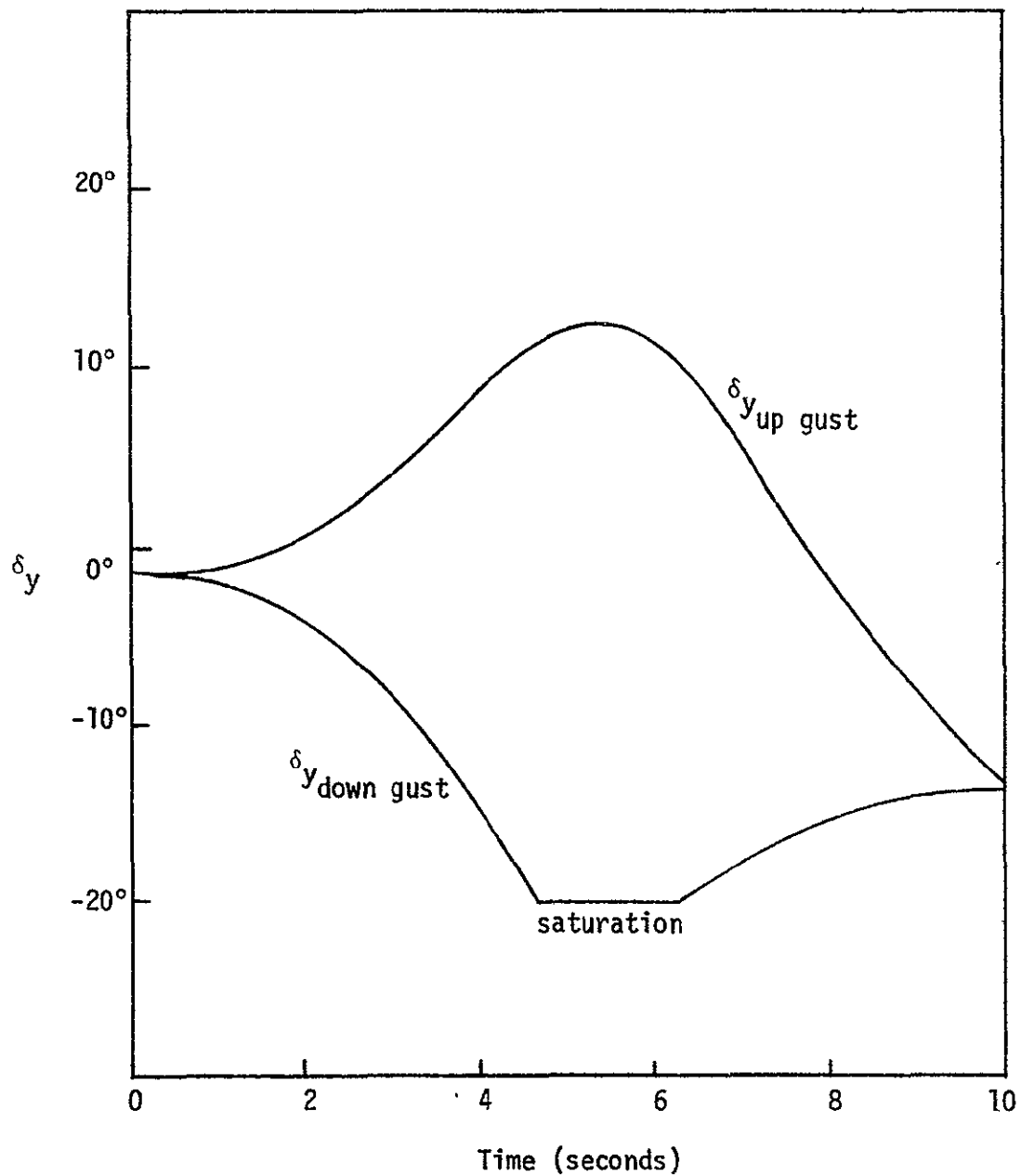
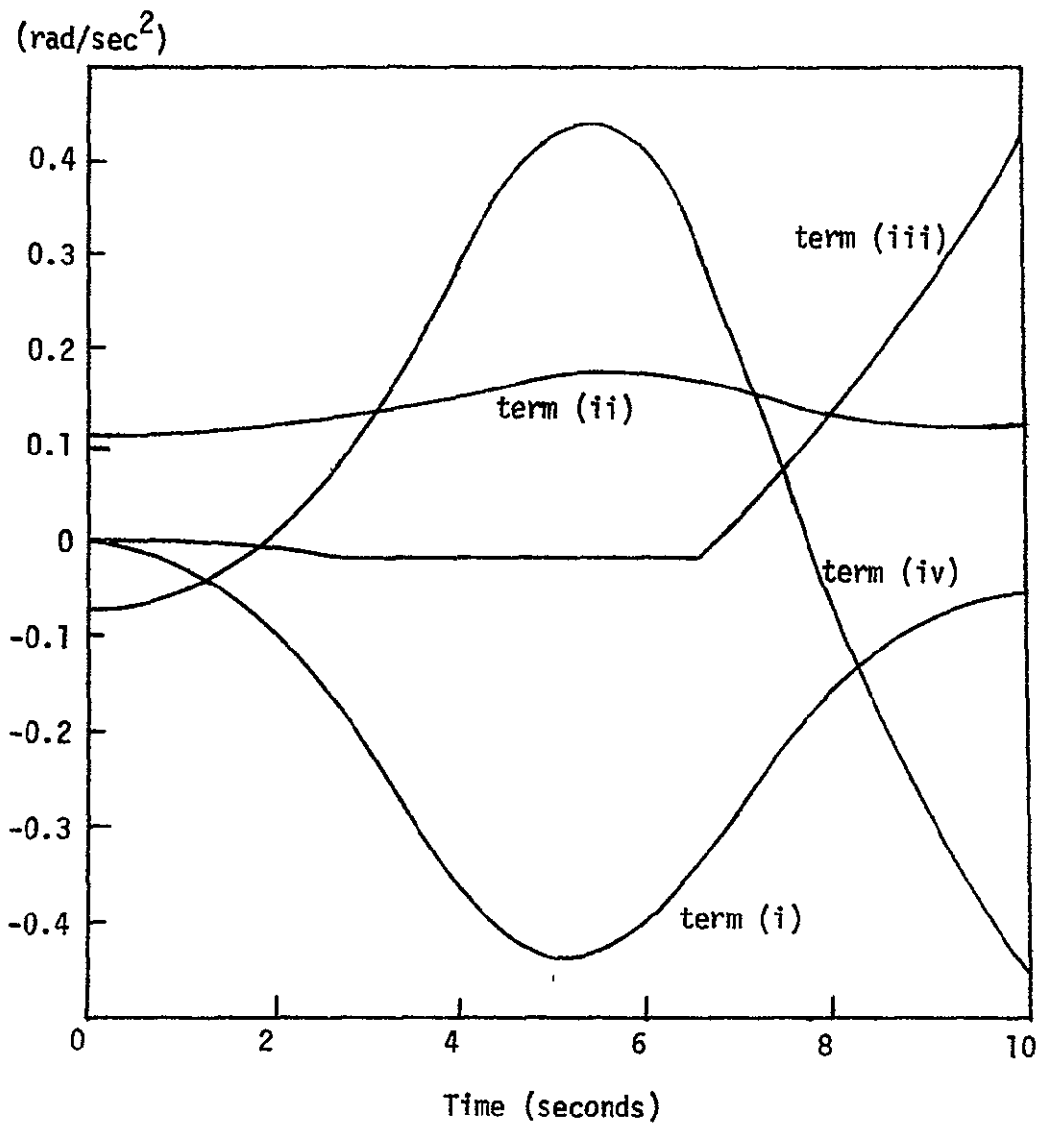


Figure 21.  $\delta_y$  for Positive and Negative Vertical Gusts.

PRECEDING PAGE BLANK NOT FILMED



$$\text{term (i)} \quad (1/2) \cdot (1/I_y) \cdot \rho \cdot U_0^2 \cdot S \cdot c \cdot (C_{M\alpha} + \Delta C_{M\alpha}) \cdot \alpha$$

$$\text{term (iii)} \quad T_{\text{net}}(j) \cdot (z_2 \cdot \sin(\bar{\sigma}(j)) + x_2 \cdot \cos(\bar{\sigma}(j))) / I_y$$

$$\text{term (ii)} \quad T_{\text{net}}(j) \cdot \Delta C_{M0} \cdot c / I_y \quad \text{and} \quad \text{term (iv)} \quad M_{\delta_y} \cdot \delta_y / I_y$$

Figure 22. Analysis of Selected Terms of  $\dot{q}$  (up gust case).

$\dot{q}$  increased through term (iii) which resulted in an increasingly larger  $\theta$ . As  $\theta$  increased (positively),  $\tilde{\sigma}$  increased again and the cycle started again. This phenomenon can be seen by examining the equation for  $\tilde{\sigma}$ ,

$$\tilde{\sigma} = \sin^{-1}(U_{rel}/V_{jet} - A/T_{net}(j) - AA \cdot \sin(\alpha)) . \quad (III-17a)$$

The second term,  $A/T_{net}(j)$ , was the dominating term of the equation.

Examining it more closely revealed that  $\theta$  and  $\tilde{\sigma}$  were closely related.

The term, with the proper substitution for A, was

$$\dots - \{m \cdot (v \cdot r - w \cdot q - g \cdot \sin(\theta)) + 1/2 \cdot \rho \cdot U_0^2 \cdot S \cdot (C_{L0} \cdot \sin(\alpha) - C_D \cdot \cos(\alpha))\} / T_{net}(j) \dots$$

The dominant part of this expression was  $m \cdot g \cdot \sin(\theta) / T_{net}(j)$ . This term reduced essentially to  $\sin(\theta)$  since  $m \cdot g / T_{net}(j)$  was nearly unity because  $m \cdot g$ , the weight, was canceled by the thrust, which, for hover, was slightly less than the weight. Therefore, the expression for  $\tilde{\sigma}$  was approximately

$$\tilde{\sigma} \approx \sin^{-1}(\dots \sin(\theta) \dots) \quad (III-17b)$$

which reduced to

$$\tilde{\sigma} \approx \theta \quad (III-17c)$$

for large positive  $\theta$ .

This showed the model to be inherently unstable for any condition that resulted in a positive pitch angle. It must be remembered that this occurred because of the way the control vector, of which  $\tilde{\sigma}$  was a part, was defined. The next two subsections attempted to alleviate this problem with  $\alpha$  by restricting  $\alpha$  through gust combinations and by utilizing more of the control effort available.

#### 5.2.c.1 Analysis of Longitudinal and Vertical Gust Combinations.

The large angles of attack were responsible for the initial positive pitching motion. These large angles resulted when the vertical relative velocity component,  $W_{rel}$ , was large compared to the relative longitudinal velocity,  $U_0$ . The equation for  $\alpha$ ,



$$\alpha = \sin^{-1}(W_{rel}/U_0) \quad , \quad (III-18)$$

then forced the ratio  $W_{rel}/U_0$  to be restricted to a value less than  $\pm 0.342$  in order for  $\alpha$  to be within  $\pm 20$  degrees. Placing a restriction on  $W_{rel}/U_0$  complicated the iterative procedure used to find the vertical gusts of the gust envelope. This was abandoned in favor of observing the response of the aircraft to "typical" gust fields. In these gust fields the longitudinal gust was also considered since it was an integral part of  $U_0$  (i.e.,  $U_0 = (U_{rel}^2 + W_{rel}^2)^{1/2}$ ).

Reference [8] stated that the only successful non-zero cross-correlation between different velocity components recorded at the same points involved the longitudinal and vertical gust components. The procedure of Section 3.3 was used to find "typical" gusts for both components. These combinations were used to give an estimate of the maximum magnitude of  $\alpha$ . Only the combinations that kept  $\alpha$  close to  $\pm 20$  degrees or less were used. Table 2 gives the 10 combinations that were used. The gust combinations were calculated on probabilities of occurrence of 0.10, 0.01, and 0.001. Two different headwinds, 10 and 25 fps, were used in determining the gust combinations. The total effects of the two headwinds will be discussed in more detail in a later subsection.

The aircraft was unable to withstand the gust field for the last three cases of Table 2. In all three situations, the pitch angle exceeded  $+25$  degrees. Table 3 gives the maximum values of the pitch angle for the 10 cases. The data showed the aircraft to be more stable for the combinations with positive vertical gusts than those with negative vertical gusts. This was true only for the lower value of headwind (cases a to d, Table 2). The behavior of the aircraft "switches" for the higher headwind as the aircraft was more stable for those combinations with negative vertical gusts than for those with the positive vertical gusts. The degrees of stability

	HEADWIND	LONGITUDINAL GUST	VERTICAL GUST	PROBABILITY OF OCCURRENCE	APPROXIMATION OF ALPHA	ACTUAL ALPHA
a.	-10	-8.4	-7.2	0.10	21°	16°
b.	-10	-8.4	+7.2	0.10	-21°	-16.5°
c.	-10	-19.1	-16.3	0.01	28°	21°
d.	-10	-19.1	+16.3	0.01	-28°	-22.5°
e.	-10	-29.8	-25.4	0.001	30°	*
f.	-10	-29.8	+25.4	0.001	-30°	*
g.	-25	-11.5	-7.2	0.10	11°	7.5°
h.	-25	-11.5	+7.2	0.10	-11°	-7°
i.	-25	-25.7	-16.3	0.01	18°	16.5°
j.	-25	-25.7	+16.3	0.01	-18°	-11.5°
k.	-25	-40.0	-25.4	0.001	21°	37.5°
l.	-25	-40.0	+25.4	0.001	-21°	-13°

\* these two were not used.

all gust frequencies were 0.10 cps; all magnitudes were fps.

Table 2. "Typical" gusts, longitudinal and vertical combinations.

CASE	MAXIMUM PITCH ANGLE	CHANGE IN ALTITUDE	MAXIMUM $\delta_y$
a.	-.041 to .117 rad	+0.51 ft	+3° to -4°
b.	.083 rad	+1.26 ft	-6.7°
c.	-.084 to .379 rad	+4.22 ft	+13° to -12°
d.	.202 rad	+3.10 ft	-15.2°
g.	-.040 rad	-0.64 ft	+2° to -1°
h.	.098 rad	+4.81 ft	-9.1°
i.	-.016 to .060 rad	+4.53 ft	+1.5° to -9°
j.	>25° at 6.4 secs	+5.45 ft	-20° 3.9-6.4*
k.	>25° at 6.2 secs	+6.20 ft	-20° 3.9-6.2*
l.	>25° at 4.6 secs	+3.41 ft	-20° 3.0-4.6*

\*time during which  $\delta_y$  was saturated.

Table 3.  $\theta$ ,  $\Delta z$ , and  $\delta_y$  for "Typical" Gust Combinations.

here were based upon the relative absolute magnitudes of  $\theta$ , which was the critical parameter. The three conditions at which the aircraft became unstable were characterized by a rapid increase in  $\dot{\alpha}$  over the last few seconds of the simulations, Table 4. Again the aircraft model was shown to be inherently unstable due to the interdependence between  $\dot{\alpha}$  and  $\theta$ . For these cases, the larger magnitude for the headwind created the positive pitch which led to the instability of the aircraft.

#### 5.2.c.2 Use of All Available Control Effort, $u_{\max}$

Since the unstable cases for vertical gusts (limiting cases) involved  $\theta$ ,  $u_{\max}$  was applied only to  $\delta_y$ . Whenever  $\theta$  exceeded 12.5 degrees (1/2 of its critical value), the control switched from  $\underline{u_{\dot{x}=0}}$  to  $u_{\max}$  (i.e.,  $\delta_y = \pm 20$  degrees depending on the sign of  $\theta$ ). Table 5b compares the results of using  $u_{\max}$  against not using it for the gusts of Table 5a. The effect of  $u_{\max}$  was to reduce the maximum pitch rate and thus, allow the operational envelope to be expanded. The control was more effective for up gusts than down gusts. Figure 23 shows that  $u_{\max}$  did a better job in controlling  $\theta$  by using more of the control effort available. The other control,  $\underline{u_{\dot{x}=0}}$ , never reached a saturated state and therefore, did a poorer job in controlling  $\theta$ . At this point it must be stated again that these limiting conditions of vertical gusts were beyond the valid range of the model in that  $\alpha$  exceeded  $\pm 20$  degrees.

The results of using  $u_{\max}$  in determining maximum vertical gust magnitudes are presented in Table 6, which shows relative values between the vertical gusts of Table 1 and those using  $u_{\max}$ . The results were affected by the fact  $\alpha$  exceeded 20 degrees for a good portion of the time. However, Table 6 does demonstrate the effectiveness of using all the control effort available.

CASE	TIME	$\ddot{\theta}$
j.	3.3 secs	.111 rad
	6.4 secs	.474 rad
k.	4.8 secs	.121 rad
	6.2 secs	.411 rad
l.	2.7 secs	.117 rad
	4.6 secs	.501 rad

Table 4. Rapid Increase of  $\ddot{\theta}$  for Unstable Cases j, k, and l.

CASE	HEADWIND	VERTICAL GUST	FREQUENCY
a'.	-10 fps	+23 fps	0.10 cps
b'.	-10 fps	-19 fps	0.10 cps
c'.	-10 fps	+23 fps	0.20 cps
d'.	-10 fps	-17 fps	0.20 cps
e'.	-10 fps	+23 fps	0.33 cps
f'.	-10 fps	-21 fps	0.33 cps
g'.	-10 fps	+16 fps	step
h'.	-10 fps	-15 fps	step

Table 5a. Vertical Gust Magnitudes (repeated from Table 1).

CASE	MAXIMUM $\theta$ AND TIME, $\underline{u_{x=0}}$	MAXIMUM $\theta$ AND TIME, $\underline{u_{max}}$
a'.	.425 rad at 10 secs	.335 rad at 7.3 secs
b'.	.413 rad at 10 secs	.266 rad at 9.1 secs
c'.	.365 rad at 10 secs	.328 rad at 8.9 secs
d'.	.401 rad at 10 secs	.223 rad at 7.3 secs
e'.	.324 rad at 10 secs	.290 rad at 8.5 secs
f'.	.411 rad at 10 secs	.236 rad at 7.3 secs*
g'.	.432 rad at 10 secs	.240 rad at 4.9 secs
h'.	.402 rad at 10 secs	.238 rad at 7.5 secs

\* $\dot{q}$  exceeded  $-0.698 \text{ rad/sec}^2$  at 7.3 secs.

Table 5b. Comparison of  $\theta_{max}$  between  $\underline{u_{x=0}}$  and  $\underline{u_{max}}$ .

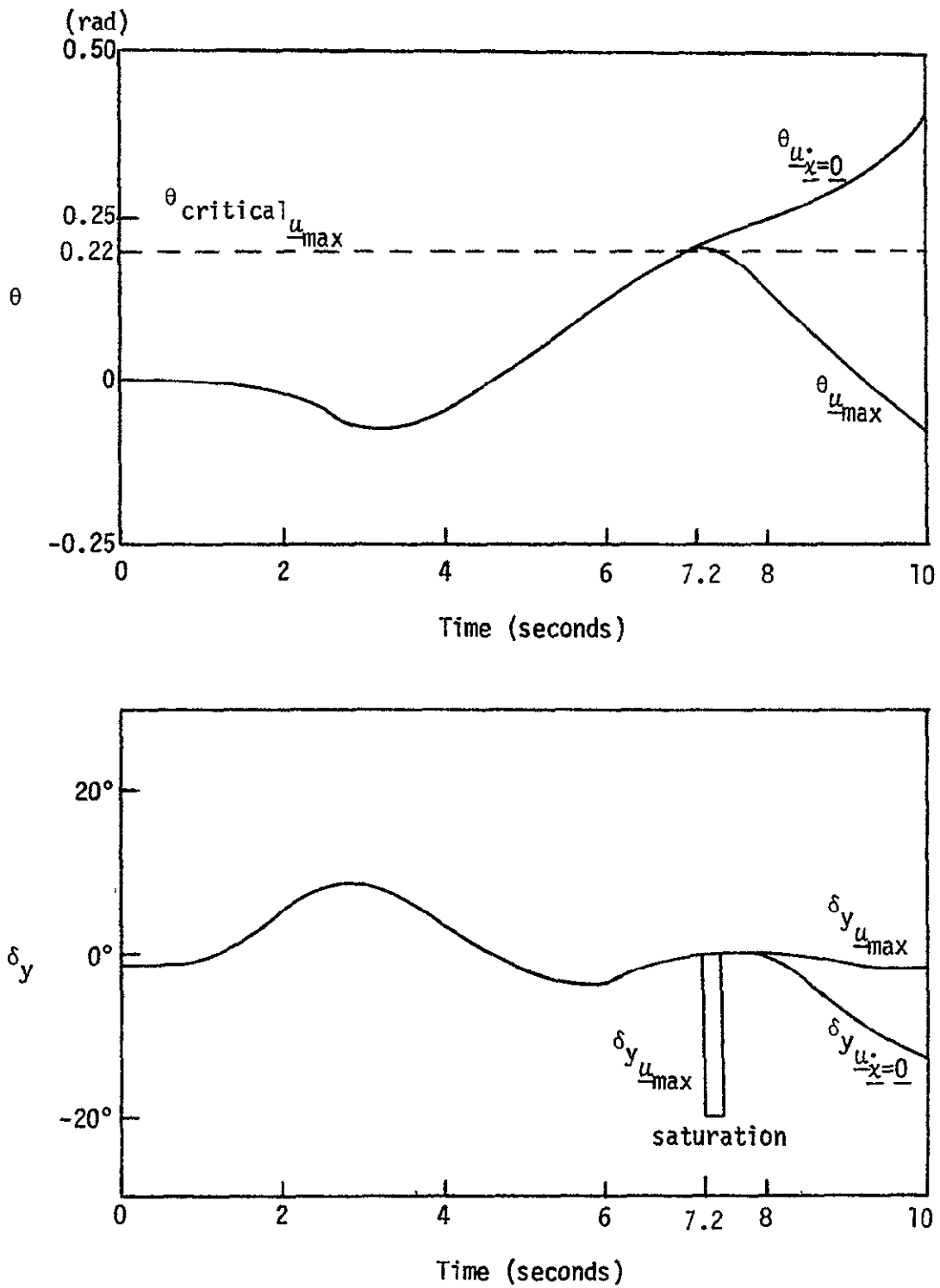


Figure 23.  $\theta$  and  $\delta_y$  for  $u_{\text{max}}$  and  $u_{\dot{x}=0}$ ,  
Vertical Gust (+23 fps, 0.10 cps).

The analysis of Table 6 showed that, with the use of  $\underline{u}_{\max}$ , the aircraft became less sensitive to positive gusts and more sensitive to negative gusts (step functions excluded) as the gust frequency increased. The results for the negative gusts showed the aircraft to call for more thrust than it was capable of producing (thrust saturation), to acquire a high forward velocity, and to call for radical changes in  $\underline{u}_{\max}$ , Figure 24. As the figure shows, the forward velocity and the pitch angle diverge while the net thrust and the reaction control angle change radically.

Step functions for vertical gusts were also investigated. The control policy for  $\underline{u}_{\max}$  described in Section 2.4 was applied to this type of disturbance. Table 7 compares the maximum vertical gusts for  $\underline{u}_{\max}$  (different than the  $\underline{u}_{\max}$  used with the step functions of Table 6) and  $\underline{u}_{\dot{x}}=0$ . Tables 6 and 7 show that some form of control by a  $\underline{u}_{\max}$  type of policy was definitely beneficial.

### 5.3.a Model Variation, the Effect of the Side Vane Angle, $\lambda$ .

The present configuration for the X-14 does not include the side vane angle. The side vane angle was introduced in the study to see its effect in combatting the high side velocities induced by lateral gusts. The lateral gusts were limited to positive-valued step functions and the control was  $\underline{u}_{\dot{x}}=0$ .

The resulting analysis is presented in Table 8. The maximum gust magnitude dropped slightly from 53 to 45 fps. The side vane angle reduced the side velocity of the aircraft considerably at a consequence of increased rolling and yawing moments. A slight loss of lift was noted since the aircraft required higher thrusts with  $\lambda$ .

### 5.3.b Model Variation, the Effect of Increasing the Magnitude of the Headwind.

FREQUENCY	MAXIMUM VERTICAL GUST	MAXIMUM VERTICAL GUST
	$\underline{u}_{\underline{x}=0}$	$\underline{u}_{\text{max}}$
0.10 cps	+23 fps	+23 fps
0.10 cps	-19 fps	-35 fps
0.20 cps	+23 fps	+28 fps
0.20 cps	-17 fps	-26 fps
0.33 cps	+23 fps	+30 fps
0.33 cps	-21 fps	-26 fps
step	+16 fps	+16 fps
step	-15 fps	-15 fps

Table 6. Maximum Vertical Gusts for  $\underline{u}_{\underline{x}=0}$  and  $\underline{u}_{\text{max}}$ .

#### MAXIMUM VERTICAL GUSTS (STEP FUNCTION)

$\underline{u}_{\underline{x}=0}$	+16 fps	-15 fps
$\underline{u}_{\text{max}}$	+22 fps	-19 fps

Table 7. Maximum Vertical Gusts (Step Function) for  $\underline{u}_{\underline{x}=0}$  and  $\underline{u}_{\text{max}}$ .

	$\lambda$ INCLUDED	WITHOUT $\lambda$
Maximum lateral gust velocity (step)	+45 fps	+53 fps
Maximum aircraft side velocity, v	+3.23 fps	+58.34 fps
Maximum roll angle, $\phi$	.402 rad	.201 rad
Maximum yaw angle, $\psi$	-.453 rad	-.250 rad
Change in lateral displacement, $\Delta y$	12.5 ft	265 ft
Change in altitude, $\Delta z$	3.2 ft	24.2 ft
Maximum yaw control effort, $\ddot{\psi}$	-.195 rad/sec <sup>2</sup>	-.322 rad/sec <sup>2</sup>
and time of occurrence	0.2 secs	0.2 secs
Minimum net thrust	4194 lbs	4122 lbs

Table 8. Comparison of Lateral Mode Parameters for Control With and Without the Side Vane Angle.

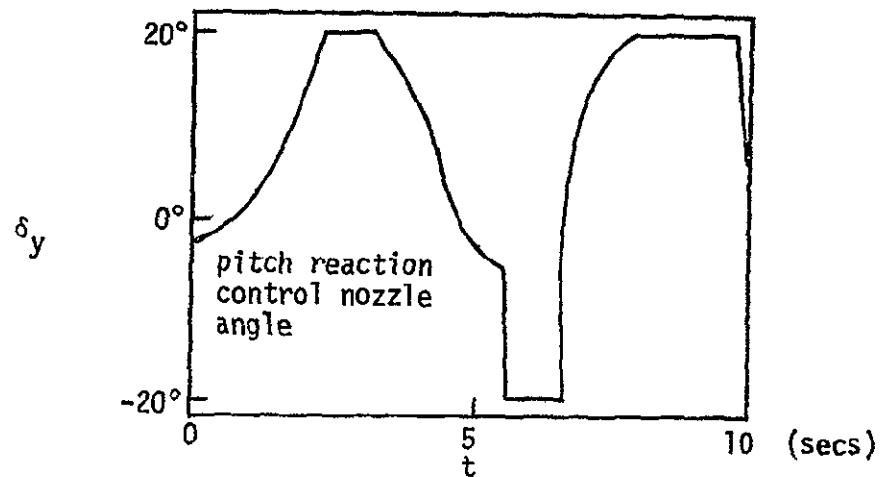
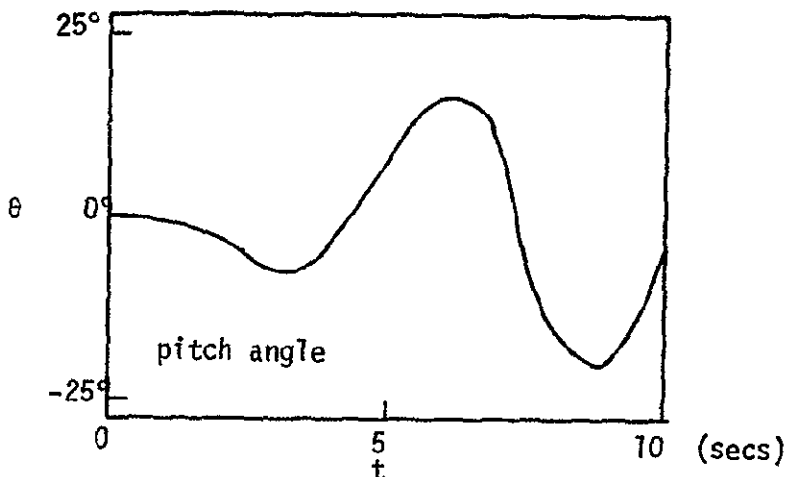
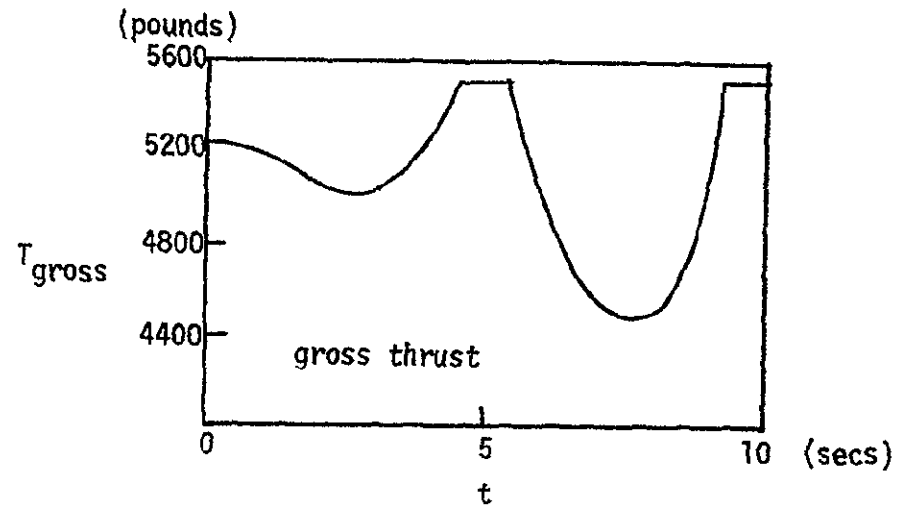
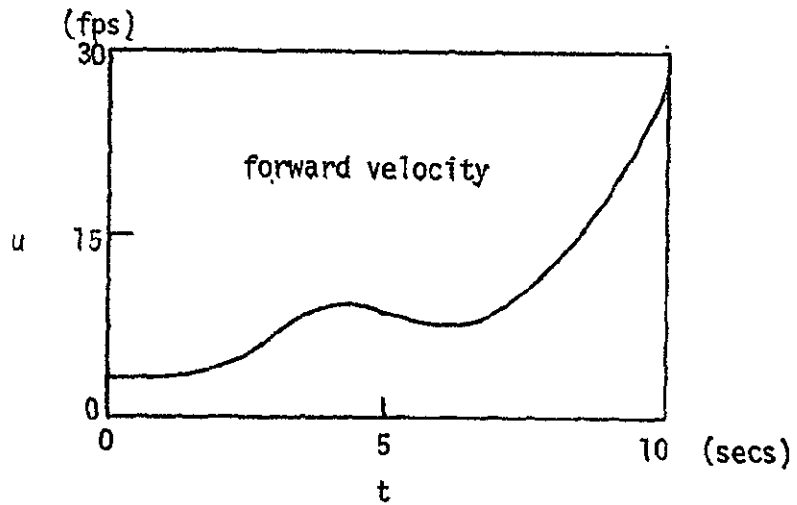


Figure 24.  $u$ ,  $\theta$ ,  $T_{gross}$ ,  $\delta_y$  for  $u_{max}$  and a Negative Vertical Gust (-19 fps and 0.10 cps).



Table 9 compares the maximum allowable lateral gusts (ignoring the limitations on aircraft side velocity) and vertical gusts for two headwinds, 10 and 25 fps. Increasing the headwind had little effect on the vertical gusts, except for the step functions which showed slight decreases in magnitude. The pitch angle was the limiting factor in determining stability. Again, as with the other simulations involving vertical gusts, it must be remembered that  $\alpha$  plays an important role when interpreting results.

The larger-valued headwind increased slightly the operational envelope of the aircraft when it was subjected to lateral gusts. The exception was the step functions where an increase in headwind resulted in a big decrease in gust magnitude. For the step functions, the limiting factor for stability was the yaw control effort. Large requirements for it occurred during the time delay before the control was initiated.

The 25 fps headwind was felt to be a practical maximum which would be encountered in actual conditions. Hence, it was felt that there was no need for analyzing aircraft responses at still higher magnitudes.

### 5.3.c Considerations of $C_{L\alpha}$ , $C_{D\alpha}$ , and $(\alpha+11^\circ)$ .

Section 2.6 pointed out the ambiguities and uncertainties of  $C_{L\alpha}$ ,  $C_{D\alpha}$ ,  $C_{M\alpha}$ , and  $\alpha$  as used by [16]. The major concern was centered on the fact that [16] used  $C_{M\alpha}$  in its model, but neglected  $C_{L\alpha}$  and  $C_{D\alpha}$ . The following simulations were run to test the effects of adding these two coefficients to the model. These coefficients appeared in the equations for forward and vertical velocities and were present in calculating the thrust requirements (see Appendix 7).

The first simulation was concerned with the effect of  $C_{L\alpha}$  and  $C_{D\alpha}$  on the response of the aircraft to longitudinal gusts. The effect was

GUST	HEADWIND (-10fps) (Table 1)	HEADWIND (-25 fps)
+VG (step)	+53 fps	+10 fps
+WG (step)	+16 fps	+11 fps
-WG (step)	-15 fps	-13 fps
+VG (0.10 cps)*	+88 fps	+95 fps
+VG (0.20 cps)*	+73 fps	+78 fps
+VG (0.33 cps)	+72 fps	+76 fps
+WG (0.10 cps)	+23 fps	+22 fps
+WG (0.20 cps)	+23 fps	+23 fps
-WG (0.10 cps)	-19 fps	-19 fps

\*ignores aircraft side velocity.

Table 9. Comparison of the Limiting Lateral and Vertical Gusts for Two Different Headwinds.

negligible. The same result occurred when  $C_{L\alpha}$  and  $C_{D\alpha}$  were added to the simulations involving gust combinations. Results of these two series of simulations are presented in Table 10.

Section 2.6 mentioned that the aircraft possessed an initial angle of attack of 11 degrees when the aircraft and atmosphere reference frames were parallel. The last series of simulations were conducted with  $C_{L\alpha}$  and  $C_{D\alpha}$  included in the model and with the angle of attack increased by a constant of 11 degrees [5]. The simulation with the longitudinal gusts showed that the addition of 11 degrees to  $\alpha$  resulted in slightly higher forward and vertical velocities and significantly lower thrust requirements (Table 11). The lower thrusts were a result of higher lift generated by the wing due to the higher angle of attack. As a consequence, the simulation also resulted in a slightly larger pitch angle which in turn required more pitch control effort (see Figure 25).

The gust combinations that were considered were combinations (i) and (j) of Table 2, longitudinal gust of 25.7 fps and 0.10 cps and vertical gusts of  $\pm 16.3$  fps and 0.10 cps. The effect of  $(\alpha+11^\circ)$  was to reverse the responses from the original responses (without  $\alpha+11^\circ$ ). The aircraft remained stable when subjected to the down gust and it became unstable when subjected to the up gust. Table 12 compares the simulations without the additions of  $C_{L\alpha}$ ,  $C_{D\alpha}$ , and  $(\alpha+11^\circ)$ , the simulations with  $C_{L\alpha}$  and  $C_{D\alpha}$  only, and the simulations with  $C_{L\alpha}$ ,  $C_{D\alpha}$ , and  $(\alpha+11^\circ)$ . Figures 26a and 26b show  $\theta$  for the positive and negative vertical gusts. The figures show the reversed responses due to  $(\alpha+11^\circ)$ . Figures 27a and 27b show the effects of  $(\alpha+11^\circ)$  on the net thrusts for each case.

#### 5.4 Interpretation of Wind Gusts.

The data presented in the first three subsections of this chapter

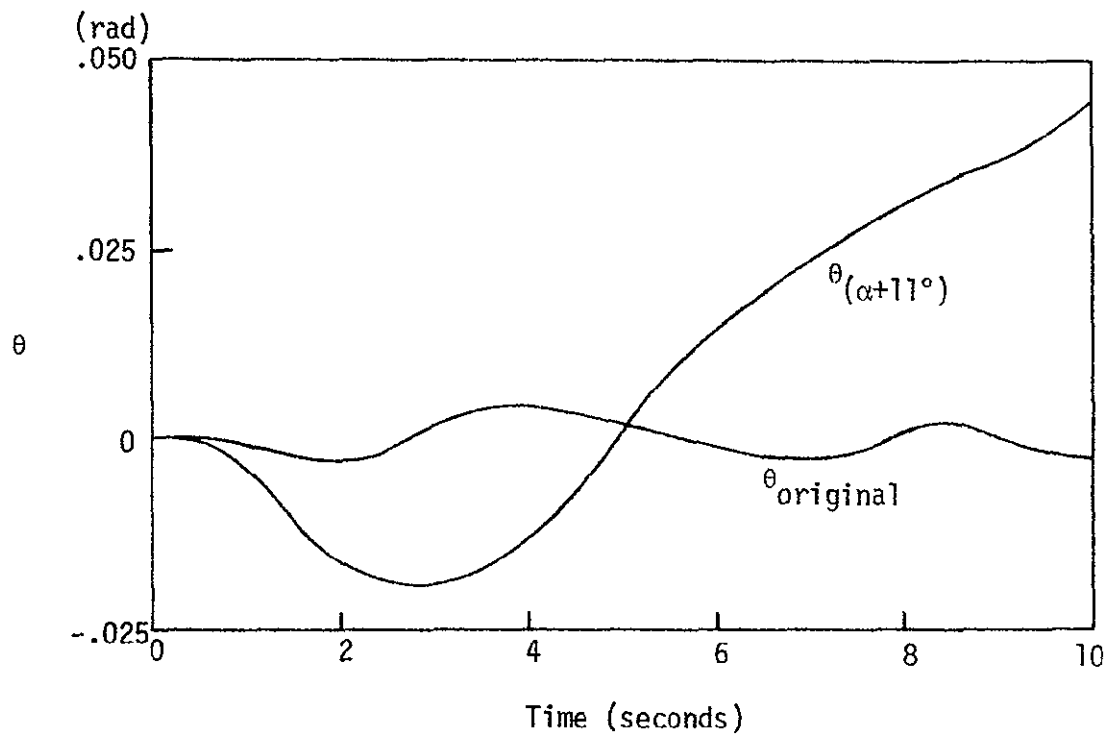
LONGITUDINAL GUST ONLY	GUST COMBINATIONS				
MAGNITUDE, 19 fps	LONGITUDINAL MAGNITUDE, 25.7 fps				
FREQUENCY, 0.20 cps	VERTICAL MAGNITUDE, $\pm 16.3$ fps				
HEADWIND, 20 fps	FREQUENCY, 0.10 cps				
	HEADWIND, 25 fps				
No significant differences in any parameters between using or not using $C_{L\alpha}$ and $C_{D\alpha}$ .	The most significant differences occurred in $T_{net}$ .				
	25.7, +16.3	25.7, -16.3			
	time (sec)	without (lb <sub>f</sub> )	with (lb <sub>f</sub> )	without (lb <sub>f</sub> )	with (lb <sub>f</sub> )
		(lb <sub>f</sub> )	(lb <sub>f</sub> )	(lb <sub>f</sub> )	(lb <sub>f</sub> )
	0.0	4130	4130	4130	4130
	4.2	3942←	→4402		
	5.1			3720←	
	5.4				→3022
	6.1		→3861		
	6.4	4095←			
	10			4119←	→3985

Table 10. Effects of  $C_{L\alpha}$  and  $C_{D\alpha}$  on Longitudinal Gusts and Combination Gusts.

LONGITUDINAL GUST ONLY: MAGNITUDE, 19 fps; FREQUENCY, 0.20 cps  
HEADWIND, 20 fps

	without $C_{L\alpha}$ , $C_{D\alpha}$ , ( $\alpha+11^\circ$ )	with $C_{L\alpha}$ , $C_{D\alpha}$ , ( $\alpha+11^\circ$ )	
$u_{max}$ :	6.67 fps	7.38 fps	
w:	-0.285 fps at 2.8 secs	-0.496 fps at 2.7 secs	(minimums)
	.000 fps at 5.2 secs	.008 fps at 5.2 secs	(maximums)
	-0.286 fps at 7.6 secs	-0.577 fps at 7.6 secs	(minimums)
	-0.002 fps at 10 secs	-0.041 fps at 10 secs	(maximums)
$T_{net}$ :	4182 lbf at 0.0 secs	4046 lbf at 0.0 secs	(initially)
	3994 lbf at 2.7 secs	3716 lbf at 2.7 secs	(minimums)
	4182 lbf at 5.1 secs	4056 lbf at 5.1 secs	(maximums)
	3993 lbf at 7.5 secs	3664 lbf at 7.5 secs	(minimums)
	4180 lbf at 10 secs	4032 lbf at 10 secs	(maximums)

Table 11. Comparison of Relative Maximums and Minimums of  $u$ ,  $w$ , and  $T_{net}$  With Regard to ( $\alpha+11^\circ$ ).



note. Longitudinal gusts only.

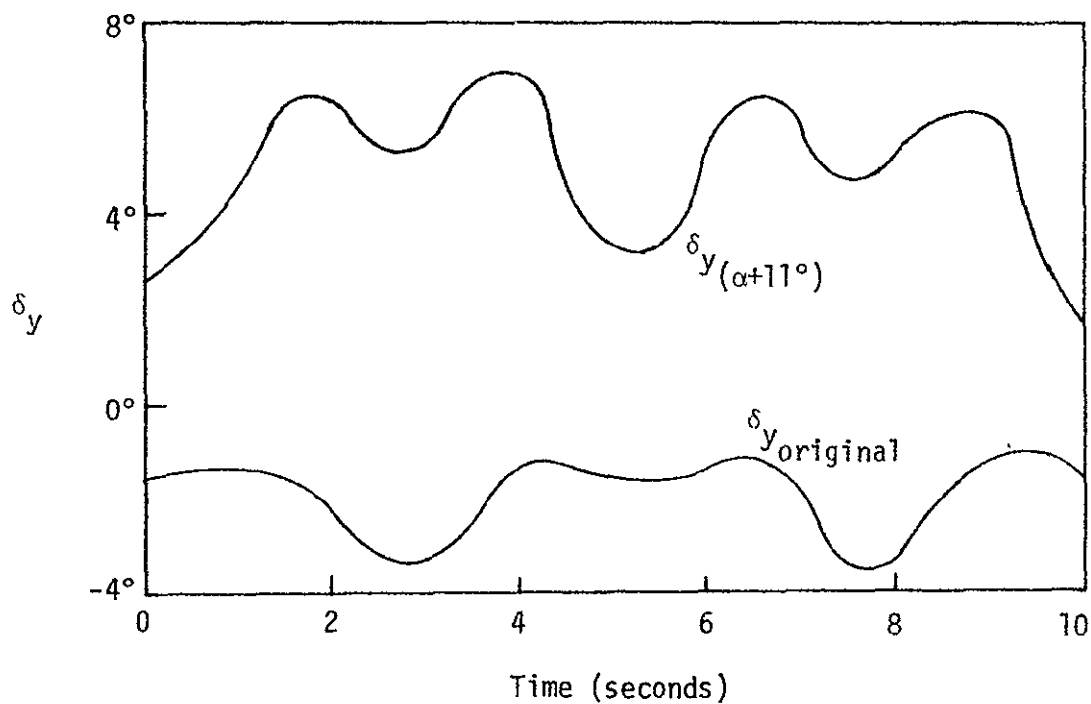


Figure 25. Effect of  $(\alpha+11^\circ)$  on  $\theta$  and  $\delta_y$ .

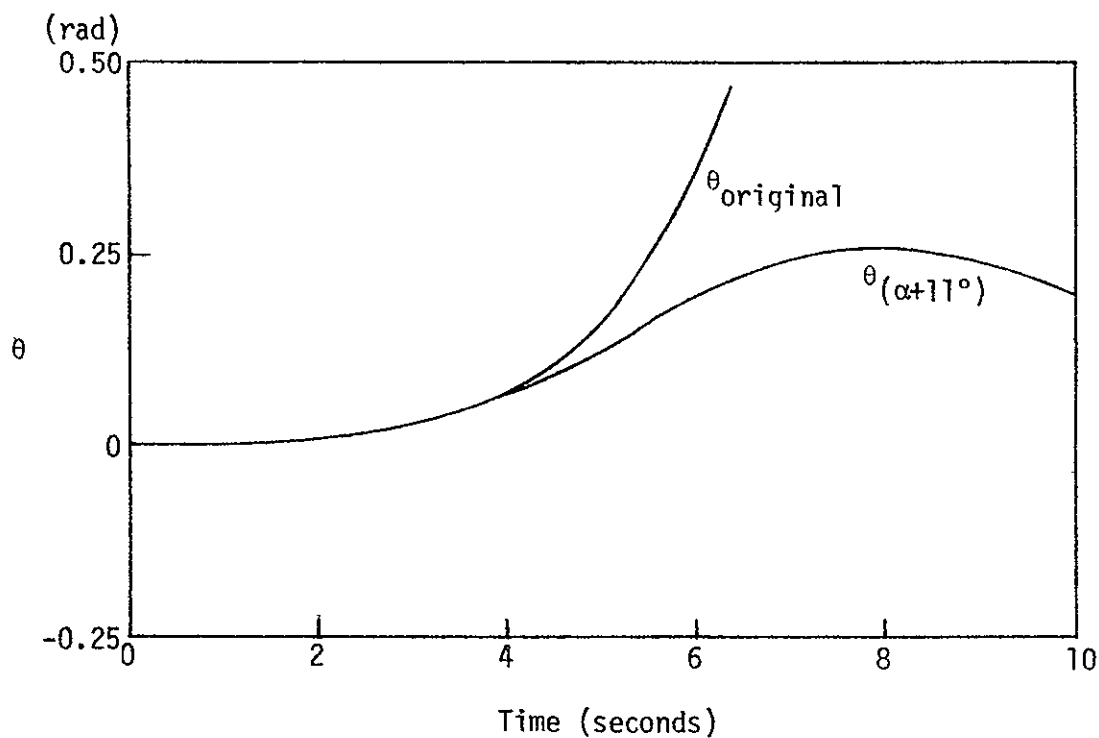
A: LONGITUDINAL GUST: 25.7 fps and 0.10 cps  
 VERTICAL GUST: -16.3 fps and 0.10 cps

B: LONGITUDINAL GUST: 25.7 fps and 0.10 cps  
 VERTICAL GUST: +16.3 fps and 0.10 cps

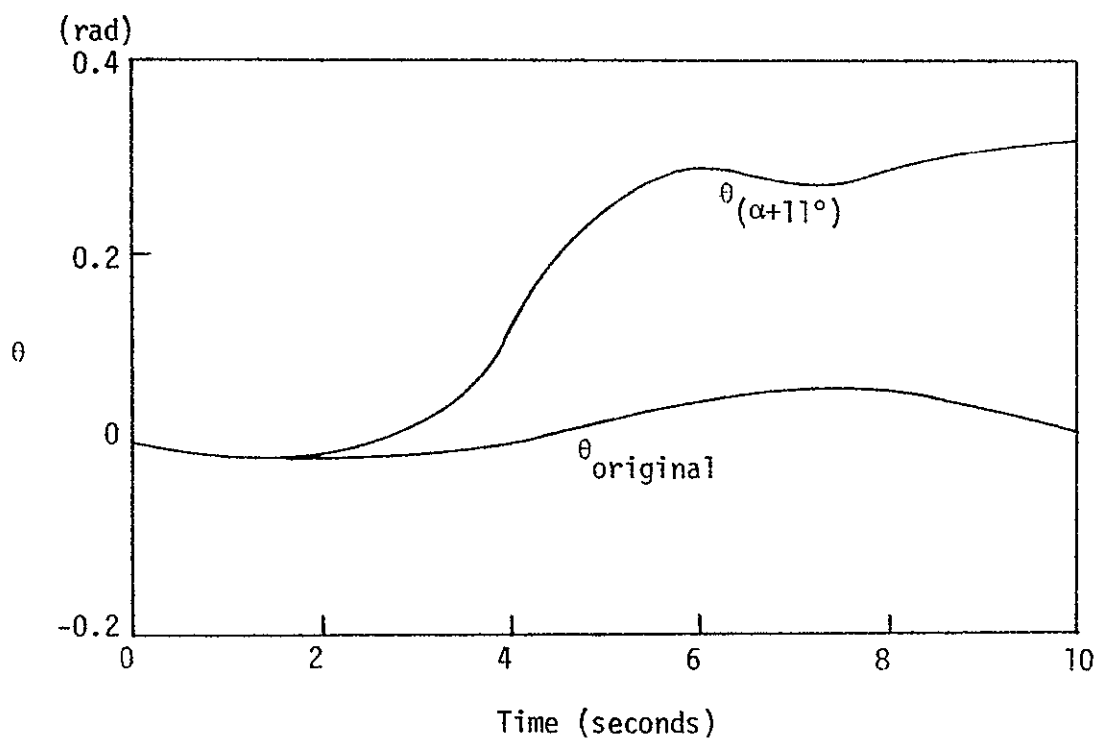
without  $C_{L\alpha}$ ,  $C_{D\alpha}$ , ( $\alpha+11^\circ$ ); with  $C_{L\alpha}$ ,  $C_{D\alpha}$  only; with  $C_{L\alpha}$ ,  $C_{D\alpha}$ , ( $\alpha+11^\circ$ )

A.	ok	ok	$\theta > 25^\circ$ at 8.3 secs
B.	$\theta > 25^\circ$ at 6.4 secs	$\theta > 25^\circ$ at 6.1 secs	ok
A.	( $u_{max}$ ) 8.33 fps	10.2 fps	17.8 fps
B.	( $u_{max}$ ) 8.33 fps	8.33 fps	8.33 fps
A.	( $w_{max}$ ) -.62 fps	-1.67 fps	-3.00 fps
B.	( $w_{max}$ ) -.74 fps	-1.07 fps	-.595 fps
A.	( $T_{net}$ ) 4130 at 0.0 secs 3720 at 5.1 secs 4119 at 10 secs	4130 at 0.0 secs 3022 at 5.4 secs 3985 at 10 secs	3927 at 0.0 secs 2246 at 6.0 secs 3190 at 8.3 secs
B.	( $T_{net}$ ) 4130 at 0.0 secs 3942 at 4.2 secs 4095 at 6.4 secs	4130 at 0.0 secs 4402 at 4.2 secs 3861 at 6.0 secs	3927 at 0.0 secs 3650 at 6.6 secs 3788 at 10 secs
A.	( $\delta_{y_{max}}$ ) -8.9° at 5.7 secs	9.2° at 5.1 secs	+20°, 3.6 to 6.5
B.	( $\delta_{y_{max}}$ ) -20°, 3.9 to 6.4	-20°, 3.9 to 6.1	-20°, 4.8 to 5.6

Table 12. Effects of  $C_{L\alpha}$ ,  $C_{D\alpha}$ , and ( $\alpha+11^\circ$ ) on Combination Gusts.

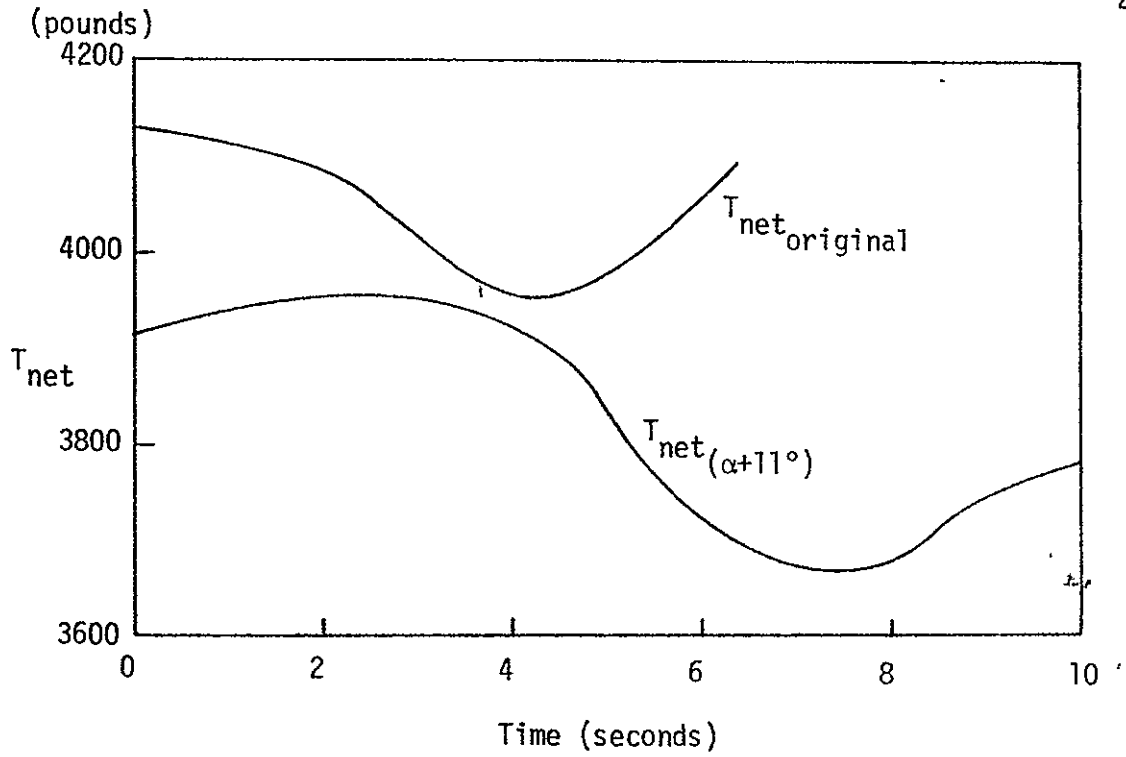


(a) Longitudinal gust: -25.7 fps, 0.10 cps  
Vertical gust: +16.3 fps, 0.10 cps

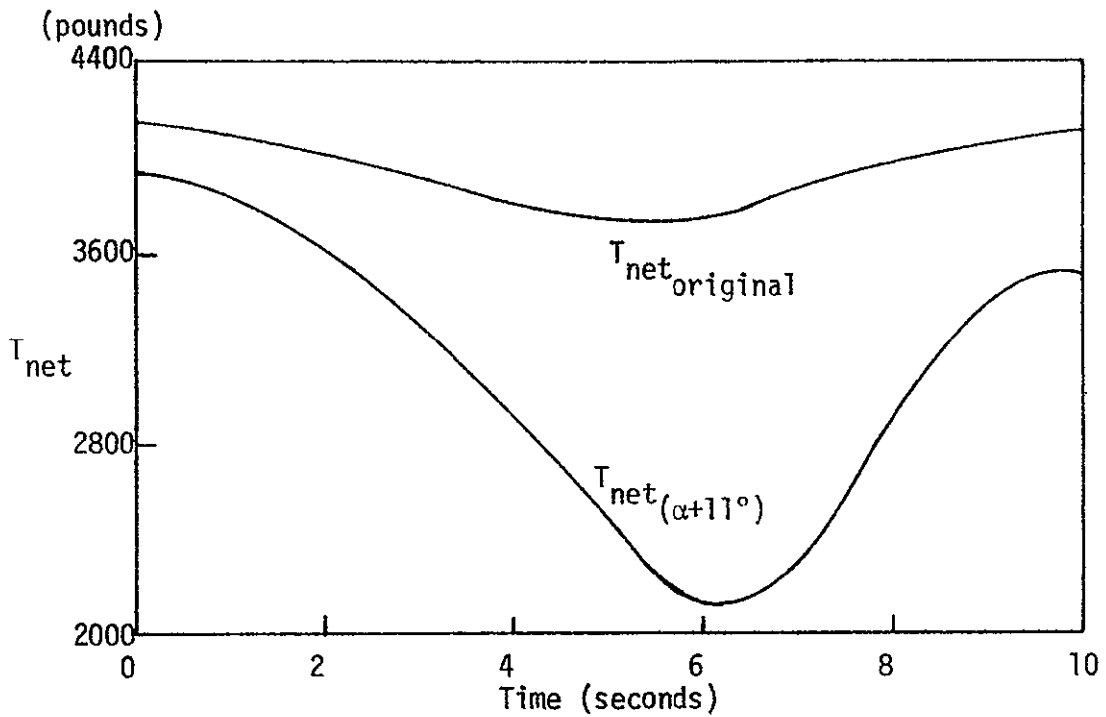


(b) Longitudinal gust: same as (a)  
vertical gust: -16.3 fps, 0.10 cps

Figure 26. Effect of  $(\alpha+11^\circ)$  on  $\theta$  for Combination Gusts ( $\pm$ vertical gusts).



(a) Gusts same as Figure 26(a).



(b) Gusts the same as Figure 26(b).

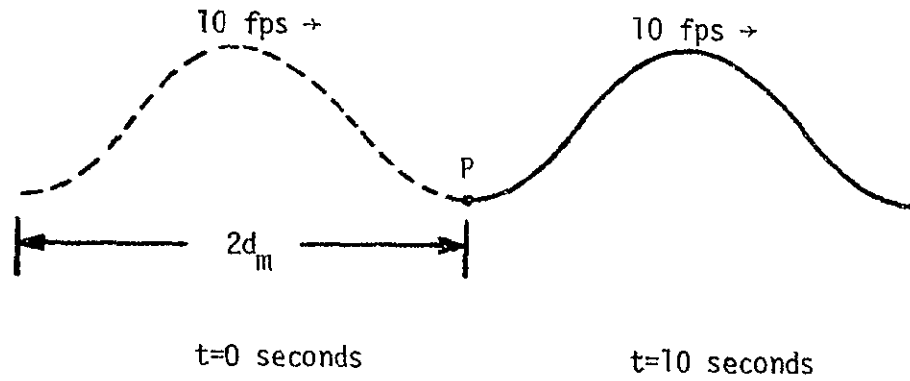
Figure 27. Effect of  $(\alpha+11^\circ)$  on Net Thrust for Combination Gusts (vertical gusts).



PRECEDING PAGE BLANK NOT FILMED

represented the maximum magnitudes of gusts for the discrete model. Real world wind gusts do not appear in such a well-behaved manner. Section 3.3 defined a method for determining root-mean-square intensities from the discrete model. The only detail lacking was some measure of the variable  $2d_m$ . This variable was interpreted as the distance between the points where the gust velocities were zero (see Figure 8). The measure of this length was affected to a great extent by the speed at which the frozen gust field was moving. By considering the airplane as a point, only the movement of the gust field past that point was needed. A first approximation to  $2d_m$  would be the velocity of the gust field times the time duration of that field (Figure 28a). However, the point moves also and its displacement must be taken into account (Figure 28b). The last figure shows that if the displacement was in the same direction as the gust field was moving, the displacement was subtracted from the first approximation. For the opposite case, the displacement (of the point) was added.

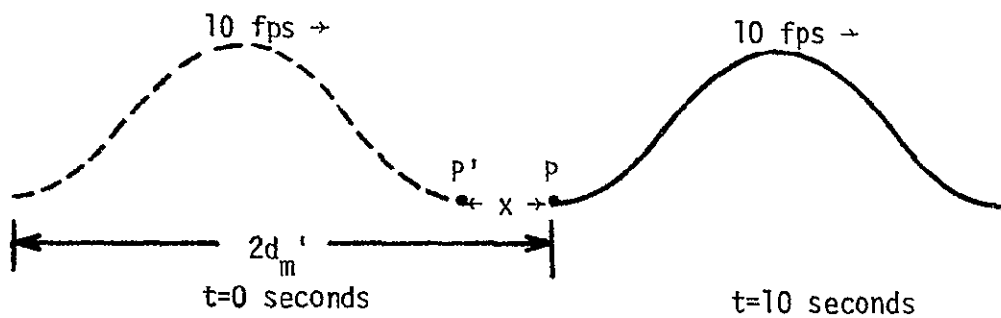
Now, at this point the speed at which the gust field is moving takes importance. For longitudinal gusts, this speed was assumed to be the mean wind speed. The longitudinal displacement of the aircraft was then needed to completely determine  $2d_m$ . Once  $2d_m$  was obtained, the rms intensities for longitudinal gusts could be determined. Table 13 presents the rms intensities for the longitudinal gusts of Table 1. The rms intensities were calculated for probabilities of occurrence (for 100 feet in altitude) of 0.10, 0.01, and 0.001. This meant, for example, that for a rms intensity of 41.6 fps (24.7 knots), which was the lowest rms intensity for longitudinal gusts, a gust with a magnitude of 52 fps ( $v_m$  from Table 1) would occur only 0.10 percent of the time. The conclusion drawn was that the aircraft could withstand a severe longitudinal gust environment. A sample calculation for rms intensity is presented in Appendix 8.



$$2d_m = 10 \text{ fps} \cdot 10 \text{ seconds}$$

$$= 100 \text{ feet}$$

(a) P stationary.



To pass P, in 10 seconds,  $2d_m' = 100$  feet.

If  $2d_m = 100$  feet, point P will not be completely passed in 10 seconds.

Therefore,  $2d_m$  must be altered in order to completely pass P in 10 seconds.

The displacement of P must be subtracted from  $2d_m'$  (i.e.,  $2d_m = 2d_m' - x$ ).

(b) P mobile.

Figure 28. Interpretation of  $2d_m$ .

$v_m$ (of Table 1)	rms Intensity		
	.10 (10%)	.01 (1%)	.001(0.1%)
52 fps 0.1 cps	84.0	54.7	41.6
52 fps 0.2 cps	115.5	74.3	57.7
53 fps 0.33 cps	151.5	88.4	75.7

Table 13. rms Intensities for Longitudinal Gusts.

PROBABILITY OF OCCURRENCE								
0.10 (10%)			0.01 (1%)			0.001 (0.1%)		
$\sigma_u$	$\sigma_v$	$\sigma_w$	$\sigma_u$	$\sigma_v$	$\sigma_w$	$\sigma_u$	$\sigma_v$	$\sigma_w$
84.0	60.0	39.0	54.7	39.2	25.4	41.6	29.8	19.3
115.5	82.5	53.6	74.3	53.0	34.5	57.7	41.2	26.8
151.5	108.1	70.4	88.4	63.1	41.0	75.7	54.1	35.2

Table 14. Lateral and Vertical rms Intensities, Based on Longitudinal Intensities, Using  $\sigma_u/\sigma_v/\sigma_w=2.8/2.0/1.3$ .

The length  $2d_m$  did not exist for the lateral and vertical gusts because of the assumption that there did not exist any mean winds in these directions to transport the gust fields. Therefore, the rms intensities cannot be calculated for these gusts. Reference [12] stated that nominal values for component gust intensity ratios differ among the various literature. However, [12] picked nominal values for the longitudinal/lateral/vertical ( $\sigma_u/\sigma_v/\sigma_w$ ) gust ratio of 2.8/2.0/1.3 to agree with available data. Table 14 presents the lateral and vertical gust intensities based on this ratio and on the  $\sigma_u$ 's of Table 13. The smallest intensity for a vertical gust was 19.3 fps rms. From Figure 10 it was determined that the probability of  $\sigma_w$  equalling 19.3 fps rms was much smaller than  $10^{-5}$ . Therefore it was concluded that the likelihood of the aircraft encountering a velocity field possessing enough energy to upset it was very remote.

### 5.5 Closing.

The results presented above must be compared against some standard in order to assess them. The pilots of the X-14 have arbitrarily set limits on wind conditions. They will not fly in winds over 12 knots (20.3 fps--longitudinal direction) and they would prefer not to fly in winds over eight knots (13.5 fps). On research flights, data measurements will not be taken if the winds exceed five to eight knots [17].

Based on the assumptions made for this project (listed in Table 15), the following conclusion was made. The arbitrary limits set on the wind conditions by the pilots were within the limits determined by this study. The limits were

52 fps, 0.10 cps

52 fps, 0.20 cps

53 fps, 0.33 cps for longitudinal gusts;

+65 and -67 fps, 0.10 cps

+65 and -66 fps, 0.20 cps

+72 and -74 fps, 0.33 cps

±27 fps, step for lateral gusts; and

+23 and -19 fps, 0.10 cps

+23 and -17 fps, 0.20 cps

+23 and -21 fps, 0.33 cps

+16 and -15 fps, step for vertical gusts.

Assumptions, Aircraft Model

1. Rigid body.
2. Forward velocity equals one-third the mean wind velocity (initially).
3. No variations in the gusts over the physical dimensions of the aircraft.
4. No gust penetration effects.
5.  $\xi_{\tilde{\sigma}}$  constant over the entire range of operating speeds of the engines.
6. Considering the angular accelerations equivalent to the reaction control efforts required.
7. Excluding  $C_{L\alpha}$  and  $C_{D\alpha}$  in the model (as does [1] and [16]) has negligible effect.
8. A 0.30 second delay exists between the introduction of a disturbance and the application of control.

Assumptions, Wind Model

1. Turbulence is stationary, homogeneous, and isotropic.
2. Turbulence is a frozen pattern in space.
3. Gust velocity components are Gaussian.
4. The direction and velocity of the headwind are constant.
5. Effects of terrain roughness, lapse rate, mean wind magnitude, etc. on turbulence are neglected.
6. Periods of less than ten seconds represent most of the turbulent energy.
7. Gust fields move at a speed equal to the mean wind speed .
8. No crosswinds or vertical winds (steady-state winds) exist.
9. Estimation of  $2d_m$  is reasonable.

Table 15. Assumptions Concerning Aircraft and Wind Models.

APPENDICES

APPENDIX 1

Modification of the Rolling Moment Equation.

The rolling moment,  $L$ , due to side velocity,  $v$ , was omitted from the set of original equations for the X-14. This characteristic of the airplane, known as the dihedral effect, is represented by the stability derivative  $C_{l\beta}$  in the roll equation ( $\dot{p}$  equation).

The derivation of  $C_{l\beta}$  followed a procedure used in [2]. The stability derivative is a function of five parameters: 1) influence of sweepback, 2) influence of fuselage, 3) influence of the tail fin, 4) contribution of the wing planform, and 5) influence of dihedral.

1. Influence of sweepback of the wings.

The X-14's wings are swept forward  $4.6^\circ$  at the quarter-chord line [15]. The interpretation of the effect of sweepforward (or sweepback, depending on the situation) is that a change in lift between the two wings occurs when the aircraft is yawed with respect to the wind. The derivative  $C_{l\beta}$  is then a function of the lift coefficient  $C_L$ .

The difference in lift of two panels between the two wings is

$$\Delta L = C_L \cdot 1/2 \cdot \rho \cdot 1/2 \cdot S \cdot v^2 \cdot \{\cos^2(\beta - \Lambda) - \cos^2(\beta + \Lambda)\} \quad (\text{III-A1-1})$$

where  $\Delta L$  is the change in lift between the two panels,

$C_L$  is the local lift coefficient for the panels,

$\rho$  is the density of the atmosphere at sea level,

$S$  is the wing area,

$v$  is the local relative velocity between the panels and the atmosphere,

$\beta$  is the angle of sideslip, and

$\Lambda$  is the sweepforward at the quarter-chord.

Assuming  $\beta$  a small angle, equation (A1-1) reduces to



$$\Delta L = C_L \cdot 1/2 \cdot \rho \cdot S \cdot V^2 \cdot \beta \cdot \sin(2\Lambda) . \quad (\text{III-A1-2})$$

The rolling moment produced by the panels will be 1/2 the difference  $\Delta L$  multiplied by the distance between the centers of pressure of the two panels

$$L = 1/2 \cdot d \cdot C_L \cdot 1/2 \cdot \rho \cdot S \cdot V^2 \cdot \beta \cdot \sin(2\Lambda) . \quad (\text{III-A1-3})$$

The corresponding rolling moment coefficient is

$$C_L = \frac{1/2 \cdot d \cdot C_L \cdot 1/2 \cdot \rho \cdot S \cdot V^2 \cdot \beta \cdot \sin(2\Lambda)}{1/2 \cdot \rho \cdot V^2 \cdot S \cdot b} , \quad (\text{III-A1-4})$$

which reduces to

$$C_L = \frac{1/2 \cdot d \cdot C_L \cdot \beta \cdot \sin(2\Lambda)}{b} \quad (\text{III-A1-5})$$

where  $d$  is the distance between the centers of pressure of the panels and  $b$  is the wing span.

The stability derivative  $C_{\ell_\beta}$  is

$$\frac{\partial C_L}{\partial \beta} = C_{\ell_\beta} = \frac{1/2 \cdot d \cdot C_L \cdot \sin(2\Lambda)}{b} . \quad (\text{III-A1-6})$$

The total effect would be the integration of the changes in lift over the entire wing span. For purposes of this derivation, it will be assumed that  $C_{\ell_\beta}$  is a representative average of the  $C_{\ell_\beta}$ 's of all the panels. The  $d$  for this average will be assumed to be the distance between the mean aerodynamic chords (approximately 2/5 of the wing span). Therefore

$$\begin{aligned} C_{\ell_\beta} &= \frac{1/2 \cdot 2/5 \cdot b \cdot C_L \cdot \sin(2 \cdot 4.6^\circ)}{b} \\ &= 0.031976 \cdot C_L . \end{aligned} \quad (\text{III-A1-7})$$

## 2. Influence of the fuselage.

The wing-body interference effect on  $C_{\ell_\beta}$  can be calculated from

$$\Delta C_{\ell\beta} = 1.2 \cdot A^{1/2} \cdot \frac{z_w}{b} \cdot \frac{h + w}{b} \quad (\text{III-A1-8})$$

where A is the aspect ratio of the wings,

$z_w$  is the vertical distance the wing-root quarter-chord point is below the fuselage center line,

b is the wing span,

h is the average fuselage height at the wing root, and

w is the average fuselage width at the wing root.

The parameters  $z_w$ , h, and w were estimated from drawings in [15] to have values of 1 foot, 3.36 feet, and 4.38 feet respectively. Therefore

$$\begin{aligned} \Delta C_{\ell\beta} &= 1.2 \cdot (6.2)^{1/2} \cdot \frac{1}{33.83} \cdot \frac{4.38 + 3.36}{33.83} \\ &= 0.0202 \end{aligned} \quad (\text{III-A1-9})$$

### 3. Influence of the tail fin.

When the aerodynamic center of the vertical tail fin is appreciably offset from the roll axis (x-axis of the aircraft), the side force on the vertical surface (side force due to sideslip) may produce a significant contribution to the roll moment. For hover, this contribution was assumed to be negligible.

### 4. Contribution of wing planform.

The contribution of wing planform on  $C_{\ell\beta}$  is found from the lower figure of Figure B.11.2, page 489 of [2]. The lower figure is for taper ratios ( $\lambda$ ) of 0.50. The taper ratio of the X-14 is 0.48. For A equal to 6.2 and  $\Lambda_{1/4}$  (sweepforward of the wings at the quarter-chord) of  $-4.6^\circ$  (negative for sweepforward), the value of  $-(C_{\ell\beta})_w/C_L$  is approximately 0.0275. Therefore

$$C_{\ell\beta} = -0.0275 \cdot C_L \quad (\text{III-A1-10})$$

## 5. Influence of dihedral.

The influence of dihedral on  $C_{l_{\beta}}$  is found from Figure 11.3, page 490 of [2]. The top curve gives  $C_{l_{\beta}}$  for zero sweepback. This can be converted to  $C_{l_{\beta}}$  for the dihedral angle involved by using the formulas

$$C_{l_{\beta}} = C_{l_{\beta\Gamma}} \cdot \left\{ \Gamma - \frac{(C_{l_{\beta\Gamma}})_{\text{partial span } \Gamma}}{(C_{l_{\beta\Gamma}})_{\text{full span } \Gamma}} \cdot \Gamma \right\} \quad (\text{III-A1-11})$$

where  $C_{l_{\beta\Gamma}}$  is given by the equation

$$C_{l_{\beta\Gamma}} = \frac{A + 4 \cdot \cos(\Lambda)}{(A + 4) \cdot \cos(\Lambda)} \cdot (C_{l_{\beta\Gamma}})_{\Lambda=0} \quad (\text{III-A1-12})$$

A is the aspect ratio, and

$\Gamma$  is the dihedral of the partial span.

For the X-14  $\Gamma$  is zero. Therefore, for A equal to 6.2 and a taper ratio of 0.50, the top figure gives a value of  $(C_{l_{\beta\Gamma}})_{\Lambda=0}$  of -0.0162.

Then

$$\begin{aligned} C_{l_{\beta\Gamma}} &= \frac{6.2 + 4 \cdot \cos(-4.6^\circ)}{(6.2 + 4) \cdot \cos(-4.6^\circ)} \cdot (-0.0162) \\ &= -0.0162 \end{aligned} \quad (\text{III-A1-13})$$

and

$$\begin{aligned} C_{l_{\beta}} &= -0.0162 \quad (2 - 0) \\ &= -0.0324 \end{aligned} \quad (\text{III-A1-14})$$

6.  $C_{l_{\beta}}$ .

The total of all contributions on  $C_{l_{\beta}}$  is

$$\begin{aligned} C_{l_{\beta}} &= 0.032 \cdot C_L + 0.0202 - 0.0275 \cdot C_L - 0.0324 \\ *** \quad C_{l_{\beta}} &= 0.0045 \cdot C_L - 0.0122 \end{aligned} \quad (\text{III-A1-15})$$

APPENDIX 2

Calculation of the Diverter Vane Efficiency Factor.

The comparison of results for the hover mode (no disturbances) between the simulated and the actual results showed a discrepancy in the engine speeds. Simulation results gave an engine speed at 90.02 percent of maximum speed whereas actual results gave the engine speed at 98 to 99 percent of the maximum speed. It was then concluded that the efficiency factor for the diverter vane had been omitted from the model.

Reference [1] calculated this factor by simply dividing the theoretical speed by the actual speed. Hence

$$\xi_{\tilde{\sigma}_\Omega} = \frac{90.02}{98.50} = 0.9139 . \quad (\text{III-A2-1})$$

However, the equations of the model calculate the engine speed from the engine thrusts since the thrust was solved for explicitly as one of the control parameters. Therefore, if the efficiency factor was based on the thrusts, the value was

$$\xi_{\tilde{\sigma}_T} = \frac{4194}{5200} = 0.80654 . \quad (\text{III-A2-2})$$

The thrusts 4194 and 5200 were obtained from Figure 29, which shows the total thrust as a function of engine speed. Figure 29 was derived from Figure 30, which shows the thrust curves of each engine.

The model uses this efficiency factor in that it takes the calculated net thrust (obtained from the control vector) and multiplies it by the inverse of  $\xi_{\tilde{\sigma}_T}$  (1.23986). This thrust is then sent to a subroutine which calculates the engine speed from the total gross thrust. The equations are

$$T_{\text{gross}} = 1.23986 \cdot T_{\text{net}} \quad (\text{III-A2-3})$$

for the gross thrust,

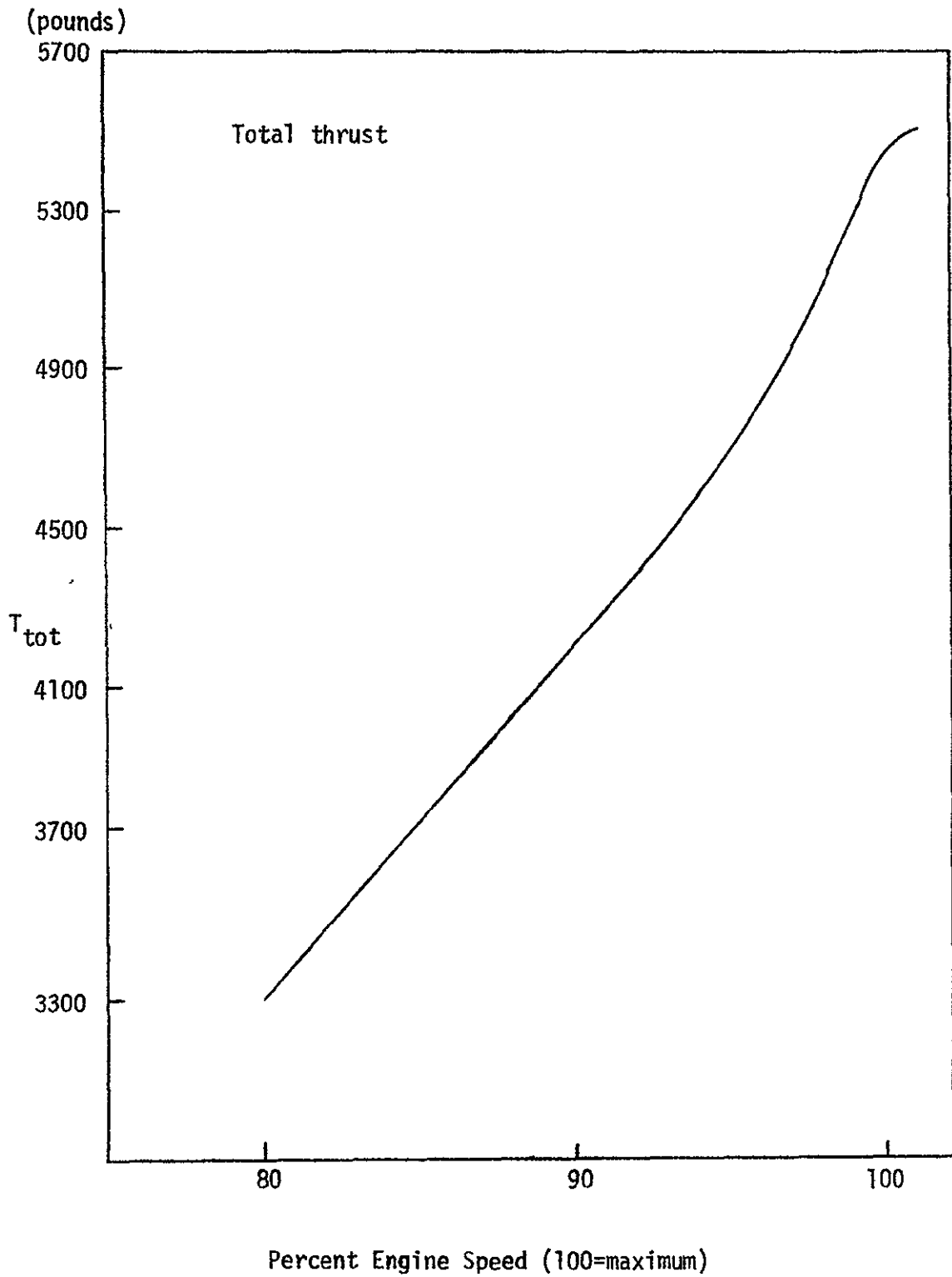


Figure 29. Total Thrust vs. Percent Maximum Engine Speed

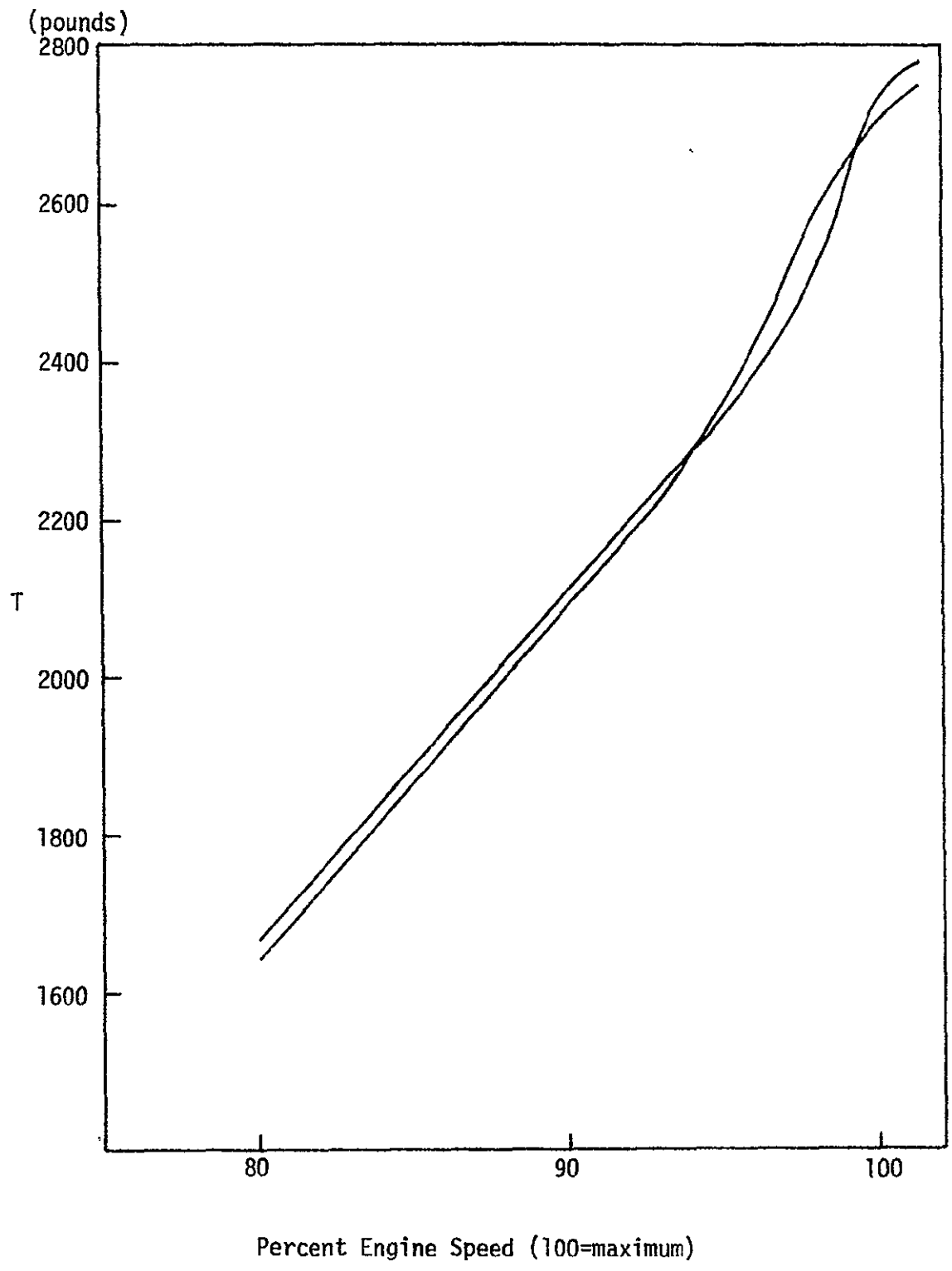


Figure 30. Thrust vs. Engine Speed Curves for Each Engine

$$\Omega = 4.52 \times 10^{-9} \cdot (T-4370)^3 - 9.31 \times 10^{-6} \cdot (T-4370)^2 + 1.25 \times 10^{-2} \cdot (T-4370) + 92 \quad (\text{III-A2-4})$$

for the engine speed of gross thrusts greater than 4370 pounds, and

$$\Omega = (T - 3305)/88.75 + 80 \quad (\text{III-A2-5})$$

for the engine speed of gross thrusts greater than 3305 pounds, but less than 4370 pounds.

The exit velocity,  $V_j$ , of the engine exhausts was 2000 fps. The diverter vane efficiency also reduces this value to  $\xi_{\tilde{\sigma}_T} \cdot V_j$ , or 1613 fps.

This is based on

$$T_{\text{gross}} = \dot{m} \cdot V_j \quad (\text{III-A2-6})$$

at the engine exhausts. The net thrust is  $T_{\text{gross}} \cdot \xi_{\tilde{\sigma}_T}$  so that

$$T_{\text{gross}} \cdot \xi_{\tilde{\sigma}_T} = T_{\text{net}} = (\dot{m} \cdot V_j) \cdot \xi_{\tilde{\sigma}_T} \quad (\text{III-A2-7})$$

The mass flow rate,  $\dot{m}$ , is constant. Therefore

$$T_{\text{net}} = \dot{m} \cdot V_{j_0} \quad (\text{III-A2-8})$$

where  $V_{j_0}$  is 1613 fps.

APPENDIX 3

Modification of  $\Delta C_L$  and  $\Delta C_{M_0}$  of the Aircraft Model.

The aerodynamic coefficients  $\Delta C_L$  and  $\Delta C_{M_0}$  were defined initially by [16] to be functions of  $U_0$ , relative longitudinal velocity, and  $T_c$ , thrust coefficient, which, in turn, was a function of  $T_{net}$ , the net thrust. The equations for  $\Delta C_L$  and  $\Delta C_{M_0}$  were

$$\Delta C_L = T_c \cdot f(U_0) \quad \text{and} \quad \text{(III-A3-1)}$$

$$\Delta C_{M_0} = T_c \cdot f^1(U_0) \quad \text{(III-A3-2)}$$

where 
$$T_c = T_{net} / (1/2 \cdot \rho \cdot U_0^2 \cdot S) \quad \text{(III-A3-3)}$$

Therefore,  $T_{net}$  must be known in order to calculate  $\Delta C_L$  and  $\Delta C_{M_0}$ . However, the net thrust contained, among other things, the term  $\Delta C_L$ . This posed a problem in that  $T_{net}$  could not be calculated without first knowing  $\Delta C_L$ , and also,  $\Delta C_L$  and  $\Delta C_{M_0}$  were to be calculated before  $T_{net}$  was to be calculated. The procedure through the program was:

- i) Define initial conditions;  $\underline{x}(0) = \underline{x}_0$ .
- ii) Calculate the aerodynamic coefficients for  $\underline{x}(0)$ .
- iii) Calculate the control vector for the initial conditions;  $\underline{u}(0) = \underline{u}(\underline{x}(0))$ .
- iv) Introduce the disturbances  $\underline{w}(1)$ .
- v) Calculate the new values for the state variable vector;  $\underline{x}(1) = f(\underline{x}(0), \underline{u}(0), \underline{w}(1))$ .
- vi) And so on.

$T_{net}$  was not calculated until (iii) whereas  $\Delta C_L$  and  $\Delta C_{M_0}$  were calculated at (ii). One way to solve this dilemma was to estimate  $T_{net}$  at (i). This would then require that  $T_{net}$  be estimated for each different set of wind conditions. A second solution was found through algebraic manipulation of the equations involving  $\Delta C_L$  and  $\Delta C_{M_0}$ . These equations were, for  $\Delta C_L$ ,



forward velocity,  $\dot{u} = v \cdot r - w \cdot q - g \cdot \sin(\theta) + (T_{\text{net}}/m) \cdot \{ \sin(\tilde{\sigma}) \cdot \cos(\lambda) - U_{\text{rel}}/V_{\text{jet}} \} + (1/2) \cdot (1/m) \cdot \rho \cdot U_0^2 \cdot S \cdot \{ (C_{Lpo} + \Delta C_L) \cdot \sin(\alpha) - C_D \cdot \cos(\alpha) \}$  , and (III-A3-4)

vertical velocity,  $\dot{w} = u \cdot q - v \cdot p + g \cdot \cos(\theta) \cdot \cos(\phi) - (T_{\text{net}}/m) \cdot \{ \cos(\tilde{\sigma}) \cdot \cos(\lambda) - W_{\text{rel}}/V_{\text{jet}} \} - (1/2) \cdot (1/m) \cdot \rho \cdot U_0^2 \cdot S \cdot \{ (C_{Lpo} + \Delta C_L) \cdot \cos(\alpha) + C_D \cdot \sin(\alpha) \}$  . (III-A3-5)

For  $\Delta C_{M_0}$ ,

pitch rate,  $\dot{q} = \{ (I_z - I_x)/I_y \} \cdot p \cdot r + (I_{xz}/I_y) \cdot (r^2 - p^2) - 2 \cdot (I_e/I_y) \cdot \Omega \cdot r + (T_{\text{net}}/I_y) \cdot \{ (W_{\text{rel}} \cdot x_1 - U_{\text{rel}} \cdot z_1)/V_{\text{jet}} + \cos(\lambda) \cdot (z_2 \cdot \sin(\tilde{\sigma}) + x_2 \cdot \cos(\tilde{\sigma})) \} + (M_q/I_y) \cdot q + (M_{\delta_y}/I_y) \cdot \delta_y + (1/2) \cdot (1/I_y) \cdot \rho \cdot U_0^2 \cdot S \cdot c \cdot (C_{M_0po} + \Delta C_{M_0} + (C_{M_{\alpha po}} + \Delta C_{M_{\alpha}}) \cdot \alpha + (1/2) \cdot (1/U_0) \cdot c \cdot C_{Mq} \cdot q + C_{M_{\delta_e}} \cdot \delta_e)$  . (III-A3-6)

By substituting equation (A3-3) into equations (A3-2) and (A3-1), and then substituting (A3-1) into equations (A3-4) and (A3-5) and then (A3-2) into equation (A3-6), the equations for  $\dot{u}$ ,  $\dot{w}$ , and  $\dot{q}$  were

$$\dot{u} = \dots + (1/2) \cdot (1/m) \cdot \rho \cdot U_0^2 \cdot S \cdot \{ (C_{Lpo} + T_{\text{net}}/(1/2 \cdot \rho \cdot U_0^2 \cdot S) \cdot f(U_0)) \cdot \sin(\alpha) \} \cdot (III-A3-7)$$

$$\dot{w} = \dots - (1/2) \cdot (1/m) \cdot \rho \cdot U_0^2 \cdot S \cdot \{ (C_{Lpo} + T_{\text{net}}/(1/2 \cdot \rho \cdot U_0^2 \cdot S) \cdot f(U_0)) \cdot \cos(\alpha) \} \cdot (III-A3-8)$$

$$\dot{q} = \dots + (1/2) \cdot (1/I_y) \cdot \rho \cdot U_0^2 \cdot S \cdot c \cdot \{ C_{M_0po} + (T_{\text{net}}/(1/2 \cdot \rho \cdot U_0^2 \cdot S) \cdot f^1(U_0)) \} + \dots \cdot (III-A3-9)$$

The quantity  $(1/2) \cdot \rho \cdot U_0^2 \cdot S$  cancelled and the resulting expressions,

$(T_{\text{net}} \cdot \Delta C_L \cdot \sin(\alpha))/m$  and  $(T_{\text{net}} \cdot \Delta C_{M_0} \cdot c)/I_y$ , were incorporated into the net thrust terms of the equations. The resulting equations were

$$\dot{u} = \dots (T_{\text{net}}/m) \cdot \{ \dots + \Delta C_L \cdot \sin(\alpha) \} + (1/2) \cdot (1/m) \cdot \rho \cdot U_0^2 \cdot S \cdot \{ C_{Lpo} \cdot \sin(\alpha) - \dots \} \cdot (III-A3-10)$$

$$\dot{w} = \dots (T_{\text{net}}/m) \cdot \{ \dots + \Delta C_L \cdot \cos(\alpha) \} - (1/2) \cdot (1/m) \cdot \rho \cdot U_0^2 \cdot S \cdot \{ C_{Lpo} \cdot \cos(\alpha) + \dots \} \cdot (III-A3-11)$$

$$\dot{q} = \dots (T_{\text{net}}/I_y) \cdot \{ \dots + \Delta C_{M_0} \cdot c \} + \dots + (1/2) \cdot (1/I_y) \cdot \rho \cdot U_0^2 \cdot S \cdot c \cdot (C_{M_0po} + \dots) \cdot (III-A3-12)$$

where  $\Delta C_L$  and  $\Delta C_{M_0}$  were no longer functions of  $T_c$  and  $U_0$ , but  $U_0$  only,

that is  $\Delta C_L = f(U_0)$  and  $\Delta C_{M0} = f^1(U_0)$ . Therefore, the estimation of  $T_{net}$  was not needed now.

APPENDIX 4Equations of the System and Terms of the Equations.

The equations of the twelfth-order system are presented in this appendix.

$$\dot{u} = v \cdot r - w \cdot q - g \cdot \sin(\theta) + (T_{\text{net}}/m) \cdot \{\sin(\tilde{\sigma}) \cdot \cos(\lambda) - U_{\text{rel}}/V_{\text{jet}} + \Delta C_L \cdot \sin(\alpha)\} + (1/2) \cdot (1/m) \cdot \rho \cdot U_0^2 \cdot S \cdot \{C_{Lpo} \cdot \sin(\alpha) - C_D \cdot \cos(\alpha)\} \quad (\text{III-A4-1})$$

$$\dot{v} = w \cdot p - u \cdot r + g \cdot \sin(\phi) \cdot \cos(\theta) + (T_{\text{net}}/m) \cdot (\sin(\lambda) - V_{\text{rel}}/V_{\text{jet}}) + (1/2) \cdot (1/m) \cdot \rho \cdot \bar{U}_0^2 \cdot S \cdot C_y \quad (\text{III-A4-2})$$

$$\dot{w} = u \cdot q - v \cdot p + g \cdot \cos(\phi) \cdot \cos(\theta) - (T_{\text{net}}/m) \cdot \{\cos(\tilde{\sigma}) \cdot \cos(\lambda) - W_{\text{rel}}/V_{\text{jet}} + \Delta C_L \cdot \cos(\alpha)\} - (1/2) \cdot (1/m) \cdot \rho \cdot U_0^2 \cdot S \cdot \{C_{Lpo} \cdot \cos(\alpha) + C_D \cdot \sin(\alpha)\} \quad (\text{III-A4-3})$$

$$\begin{aligned} \dot{p} = & \{I_x \cdot I_z / (I_x \cdot I_z - I_{xz}^2)\} \cdot \dot{\lambda} \cdot \{((I_y - I_z)/I_x) \cdot q \cdot r + (I_{xz}/I_x) \cdot p \cdot q + (T_{\text{net}}/I_x) \cdot \{(z_1 \cdot V_{\text{rel}})/V_{\text{jet}} - \sin(\lambda) \cdot \{z_2 + l_1 \cdot \cos(\tilde{\sigma})\}\} + (L_p/I_x) \cdot p + \\ & (L_{\delta_x}/I_x) \cdot \delta_x + (1/2) \cdot (1/I_x) \cdot \rho \cdot \bar{U}_0^2 \cdot S \cdot b \cdot (C_{\ell 0} + C_{\ell \delta_a} \cdot \delta_a + C_{\ell \beta} \cdot \beta) + \{I_{xz}/I_x\} \cdot \{((I_x - I_y)/I_z) \cdot p \cdot q - (I_{xz}/I_z) \cdot q \cdot r + 2 \cdot (I_e/I_z) \cdot \Omega \cdot q + \\ & (T_{\text{net}}/I_z) \cdot \{\sin(\lambda) \cdot \{x_2 - l_1 \cdot \sin(\tilde{\sigma})\} - (x_1 \cdot V_{\text{rel}})/V_{\text{jet}}\} + (N_r/I_z) \cdot r + (N_{\delta_z}/I_z) \cdot \delta_z + (1/2) \cdot (1/I_z) \cdot \rho \cdot \bar{U}_0^2 \cdot S \cdot b \cdot (C_{n0} + C_{n\delta_r} \cdot \delta_r + \\ & C_{n\delta_a} \cdot \delta_a)\} \} \quad (\text{III-A4-4}) \end{aligned}$$

$$\begin{aligned} \dot{q} = & \{((I_z - I_y)/I_y) \cdot p \cdot r + (I_{xz}/I_y) \cdot (r^2 - p^2) - 2 \cdot (I_e/I_y) \cdot \Omega \cdot r + (T_{\text{net}}/I_y) \cdot \{(W_{\text{rel}} \cdot x_1 - U_{\text{rel}} \cdot z_1)/V_{\text{jet}} + \cos(\lambda) \cdot \{z_2 \cdot \sin(\tilde{\sigma}) + x_2 \cdot \cos(\tilde{\sigma})\} + \\ & c \cdot \Delta C_{M0}\} + (M_q/I_y) \cdot q + (M_{\delta_y}/I_y) \cdot \delta_y + (1/2) \cdot (1/I_y) \cdot \rho \cdot U_0^2 \cdot S \cdot c \cdot \{C_{M0po} + (C_{M\alpha po} + \Delta C_{M\alpha}) \cdot \alpha + (1/2) \cdot (1/U_0) \cdot c \cdot C_{Mq} \cdot q + C_{M\delta_e} \cdot \delta_e\} \quad (\text{III-A4-5}) \end{aligned}$$

$$\begin{aligned} \dot{r} = & \{I_x \cdot I_z / (I_x \cdot I_z - I_{xz}^2)\} \cdot \dot{\lambda} \cdot \{I_{xz}/I_z \cdot \{((I_y - I_z)/I_x) \cdot q \cdot r + (I_{xz}/I_x) \cdot p \cdot q + (T_{\text{net}}/I_x) \cdot \{(z_1 \cdot V_{\text{rel}})/V_{\text{jet}} - \sin(\lambda) \cdot \{z_2 + l_1 \cdot \cos(\tilde{\sigma})\}\} + \\ & (L_p/I_x) \cdot p + (L_{\delta_x}/I_x) \cdot \delta_x + (1/2) \cdot (1/I_x) \cdot \rho \cdot \bar{U}_0^2 \cdot S \cdot b \cdot (C_{\ell 0} + C_{\ell \delta_a} \cdot \delta_a + C_{\ell \beta} \cdot \beta)\} + \{((I_x - I_y)/I_z) \cdot p \cdot q - (I_{xz}/I_z) \cdot q \cdot r + 2 \cdot (I_e/I_z) \cdot \Omega \cdot q + \end{aligned}$$

$$\left. \left( \frac{T_{net}}{I_z} \right) \cdot \left\{ \sin(\lambda) \cdot \left[ x_2 - x_1 \cdot \sin(\tilde{\sigma}) \right] - \left[ x_1 \cdot V_{rel} / V_{jet} \right] + \left( N_r / I_z \right) \cdot r + \left( N_{\delta_z} / I_z \right) \cdot \delta_z + (1/2) \cdot (1/I_z) \cdot \rho \cdot \bar{U}_0^2 \cdot S \cdot b \cdot \left( C_{no} + C_{n\delta_r} \cdot \delta_r + C_{n\delta_a} \cdot \delta_a \right) \right\} \right\} \quad (III-A4-6)$$

$$\dot{\theta} = q \cdot \cos(\phi) - r \cdot \sin(\phi) \quad (III-A4-7)$$

$$\dot{\phi} = p + q \cdot \sin(\phi) \cdot \tan(\theta) + r \cdot \cos(\phi) \cdot \tan(\theta) \quad (III-A4-8)$$

$$\dot{\psi} = (r \cdot \cos(\phi) + q \cdot \sin(\phi)) / \cos(\theta) \quad (III-A4-9)$$

$$\dot{z} = v \cdot \sin(\phi) \cdot \cos(\theta) + w \cdot \cos(\phi) \cdot \cos(\theta) - u \cdot \sin(\theta) \quad (III-A4-10)$$

$$\dot{x} = u \cdot \cos(\theta) \cdot \cos(\psi) + v \cdot \{ \sin(\phi) \cdot \sin(\theta) \cdot \cos(\psi) - \cos(\phi) \cdot \sin(\psi) \} + w \cdot \{ \cos(\phi) \cdot \sin(\theta) \cdot \cos(\psi) + \sin(\phi) \cdot \sin(\psi) \} \quad (III-A4-11)$$

$$\dot{y} = u \cdot \cos(\theta) \cdot \sin(\psi) + v \cdot \{ \sin(\phi) \cdot \sin(\theta) \cdot \sin(\psi) + \cos(\phi) \cdot \cos(\psi) \} + w \cdot \{ \cos(\phi) \cdot \sin(\theta) \cdot \sin(\psi) - \sin(\phi) \cdot \cos(\psi) \} \quad (III-A4-12)$$

where  $\alpha = \sin^{-1}(W_{rel}/U_0) \quad (III-A4-13)$

$$\beta = \sin^{-1}(V_{rel}/\bar{U}_0) \quad (III-A4-14)$$

$$U_0 = (U_{rel}^2 + W_{rel}^2)^{1/2} \quad (III-A4-15)$$

$$\bar{U}_0 = (U_{rel}^2 + V_{rel}^2 + W_{rel}^2)^{1/2} \quad (III-A4-16)$$

$$U_{rel} = u - UW - UG \quad (III-A4-17)$$

$$V_{rel} = v - VW - VG \quad (III-A4-18)$$

$$W_{rel} = w - WW - WG \quad (III-A4-19)$$

The equations for  $\dot{T}_{net}$ ,  $\tilde{\sigma}$ ,  $\lambda$ ,  $\delta_x$ ,  $\delta_y$ , and  $\delta_z$  are presented in Appendix 5.

APPENDIX 5

Equations for the Control Vector.

The equations for the six control parameters were derived in [1] and will be restated here. The equations were derived by setting the  $\dot{\underline{x}}$  vector equal to the  $\underline{0}$  vector and solving for the control vector,  $\underline{u}$ .

The net thrust equation was

$$T_{\text{net}} = \{-E + (E^2 + DF)^{1/2}\}/D \quad (\text{III-A5-1})$$

where  $E = (A \cdot U_{\text{rel}} + B \cdot V_{\text{rel}} + C \cdot W_{\text{rel}})/V_{\text{jet}} - \Delta C_L \cdot (A \cdot \sin(\alpha) - C \cdot \cos(\alpha))$  ,

$$D = 1 - \bar{U}_0^2/V_{\text{jet}}^2 - \Delta C_L^2 + 2 \cdot \Delta C_L \cdot \{U_{\text{rel}} \cdot \sin(\alpha) - W_{\text{rel}} \cdot \cos(\alpha)\}/V_{\text{jet}} ,$$

$$F = A^2 + B^2 + C^2 ,$$

$$A = m \cdot \{v \cdot r - w \cdot q - g \cdot \sin(\theta)\} + (1/2) \cdot \rho \cdot U_0^2 \cdot S \cdot \{C_{Lpo} \cdot \sin(\alpha) - C_D \cdot \cos(\alpha)\} ,$$

$$B = m \cdot \{w \cdot p - u \cdot r + g \cdot \sin(\phi) \cdot \cos(\theta)\} + (1/2) \cdot \rho \cdot \bar{U}_0^2 \cdot S \cdot C_y , \text{ and}$$

$$C = m \cdot \{u \cdot q - v \cdot p + g \cdot \cos(\phi) \cdot \cos(\theta)\} - (1/2) \cdot \rho \cdot U_0^2 \cdot S \cdot \{C_{Lpo} \cdot \cos(\alpha) + C_D \cdot \sin(\alpha)\} .$$

The diverter vane angles were

$$\lambda = \sin^{-1} \{V_{\text{rel}}/V_{\text{jet}} - B/T_{\text{net}}\} \text{ and} \quad (\text{III-A5-2})$$

$$\tilde{\sigma} = \sin^{-1} \{ \{U_{\text{rel}}/V_{\text{jet}} - A/T_{\text{net}} - \Delta C_L \cdot \sin(\alpha)\} / \cos(\lambda) \} . \quad (\text{III-A5-3})$$

The reaction control angles and the aerodynamic control angles were

$$\delta_x = \delta_a = \{ (I_z - I_y) \cdot q \cdot r - T_{\text{net}} \cdot \{ (V_{\text{rel}} \cdot z_1)/V_{\text{jet}} - \sin(\lambda) \cdot \{ z_2 + x_1 \cdot \cos(\tilde{\sigma}) \} \} - \\ L_p \cdot p - (1/2) \cdot \rho \cdot \bar{U}_0^2 \cdot S \cdot b \cdot (C_{\ell\alpha} + C_{\ell\beta} \cdot \beta) - I_{xz} \cdot p \cdot q \} / \{ L_{\delta_x} + (1/2) \cdot \rho \cdot \\ \bar{U}_0^2 \cdot S \cdot b \cdot C_{\ell\delta_a} \} , \quad (\text{III-A5-4})$$

$$\delta_y = \delta_e = \{ (I_x - I_z) \cdot p \cdot r + I_{xz} \cdot (p^2 - r^2) + 2 \cdot I_e \cdot \Omega \cdot r - T_{\text{net}} \cdot \{ (W_{\text{rel}} \cdot x_1 - U_{\text{rel}} \cdot z_1)/ \\ V_{\text{jet}} + \cos(\lambda) \cdot \{ z_2 \cdot \sin(\tilde{\sigma}) + x_2 \cdot \cos(\tilde{\sigma}) \} + c \cdot \Delta C_{M0} \} - M_q \cdot q - (1/2) \cdot \rho \cdot \\ U_0^2 \cdot S \cdot c \cdot (C_{M\alpha po} + (C_{M\alpha po} + C_{M\alpha}) \cdot \alpha + (1/2) \cdot (1/U_0) \cdot c \cdot C_{Mq} \cdot q) \} / \quad (\text{III-A5-5})$$

$$\{M_{\delta_y} + (1/2) \cdot \rho \cdot U_0^2 \cdot S \cdot c \cdot C_{M\delta_e}\} , \text{ and}$$

$$\delta_z = \delta_r = \frac{\{(I_y - I_x) \cdot p \cdot q + I_{xz} \cdot q \cdot r - 2 \cdot I_e \cdot \Omega \cdot q + T_{net} \cdot \{(V_{rel} \cdot x_1) / V_{jet} - \sin(\lambda) \cdot \{x_2 - x_1 \cdot \sin(\tilde{\sigma})\} - N_r \cdot r - (1/2) \cdot \rho \cdot \bar{U}_0^2 \cdot S \cdot b \cdot (C_{n\delta_a} + C_{n\delta_a} \cdot \delta_a)\} / \{N_{\delta_z} + (1/2) \cdot \rho \cdot \bar{U}_0^2 \cdot S \cdot b \cdot C_{n\delta_r}\}}\}}{(III-A5-6)}$$

The control parameters had certain bounds or saturation points.

They were

$$T_{gross \ max} = 5515 \text{ pounds} ,$$

$$\tilde{\sigma} = 0^\circ \text{ to } 70^\circ ,$$

$$\lambda = -25^\circ \text{ to } +25^\circ \text{ when used, otherwise } 0^\circ ,$$

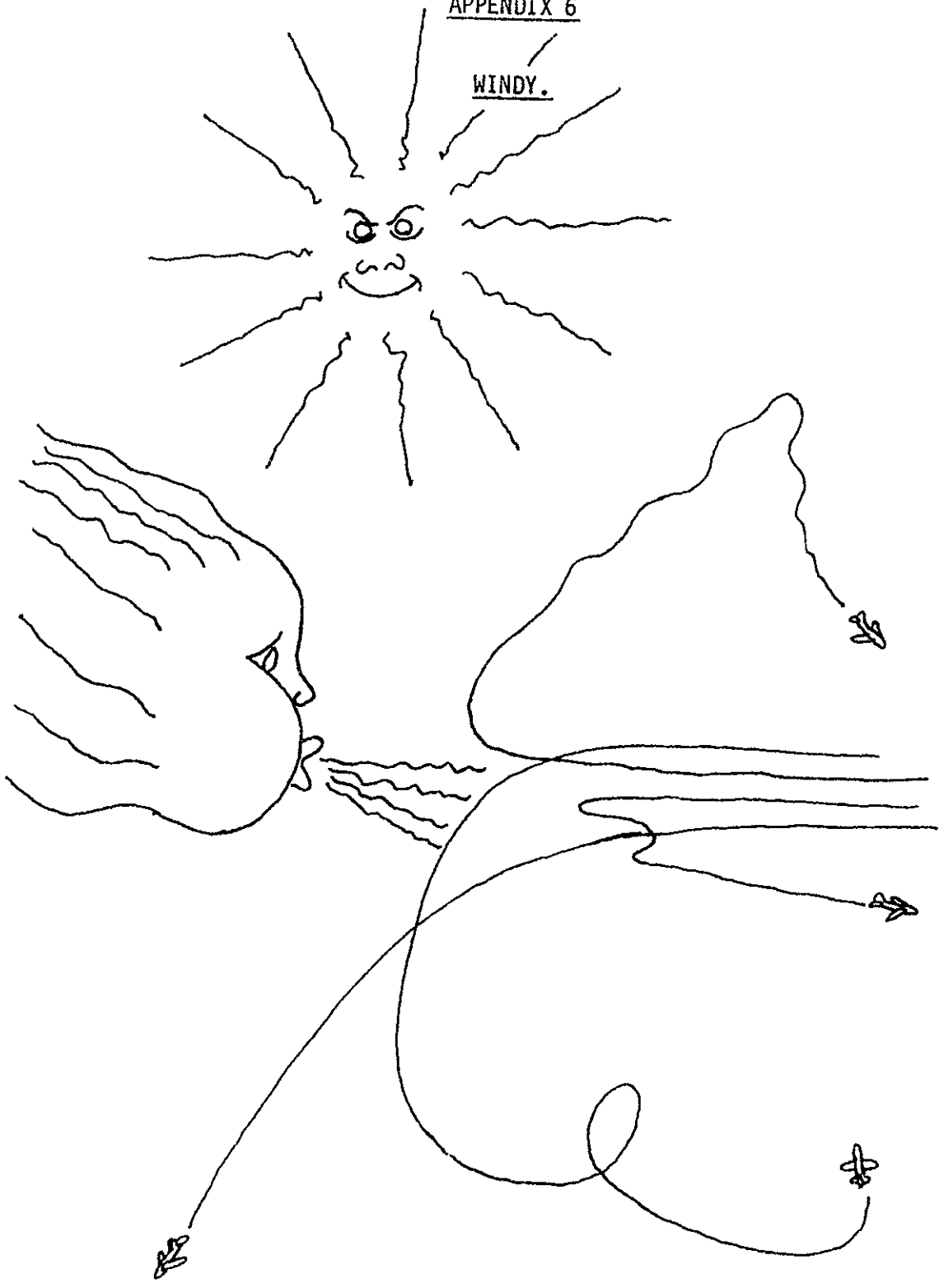
$$\delta_x, \delta_y, \delta_z, \delta_a = -20^\circ \text{ to } +20^\circ ,$$

$$\delta_e = -25^\circ \text{ to } +15^\circ , \text{ and}$$

$$\delta_r = -30^\circ \text{ to } +30^\circ .$$

APPENDIX 6

WINDY.





```

C *****
C
C THIS PROGRAM SIMULATES A VTOL AIRCRAFT (IN HOVER) WHICH IS
C SUBJECTED TO A GUST FIELD. THE PROGRAM READS THE INITIAL
C WIND CONDITIONS--UWI, HEADWIND MAGNITUDE = GSMAG(U, V, OR W),
C THE MAXIMUM MAGNITUDE OF THE COMPONENT GUST = DENOM, THE PERIOD
C OF THE GUST (DFNUM=50--PERIOD=10 SECONDS, DENOM=25--PERIOD=5
C SECONDS, DENOM=15--PERIOD=3 SECONDS) = AND JGUST, AN IDENTIFIER
C TO SPECIFY WHICH COMPONENT GUST IS BEING CONSIDERED (1, LONGI-
C TUDINAL GUST 2, POSITIVE LATERAL GUST 3, NEGATIVE LATERAL GUST
C 4, POSITIVE VERTICAL GUST 5, NEGATIVE VERTICAL GUST). THE
C PROGRAM THEN TAKES THESE PARAMETERS AND ITERATES UNTIL THE
C MAXIMUM MAGNITUDE OF THE GUST THE AIRCRAFT CAN WITHSTAND IS FOUND.
C *****
C
REAL MASS,IX,IY,IZ,IXZ,LONE,IENG,LDXIX,LPIX,MDYIY,MQIY,NDZIZ,NRIZ,
INUNDIM,LAMBDA,YI(10,1),YY(11,101),TIME(101),LSTAR(101),NSTAR(101)
2,PDUR(101),QDOT(101),RDIT(101),YA(6,101),YB(8,101),THRSTG(101)
COMMON/ESUCUM/N,XI,YI(99),X,Y(99),TR,H,KSTP,DY(99)
COMMON/FUNCI/G,THRUST(101),MASS,SIGMA(101),LAMBDA(101),
TUO,WARFA,CLPO,DELCL,ALPHA,CD,VREL,UUBAR,CY,IX,IZ,IXZ,IY,
2ZTWO,LONE,ZONE,LPIX,LUXIX,DELX(101),SPAN,WREL,CLD,CLDELA,
3DELA,CLBETA,IENG,OMEGA,XTWO,XONE,NRIZ,NDZIZ,DELZ(101),CNO,
4CNDELR,DELRCNDELA,MDYIY,DELY(101),MQIY,CHORD,CMUPO,
5DELCHO,CMALPO,DELCHA,CMQ,CMDELE,DELE,BETA,J,UREL,VJET,RHO
6,CDALPH,CLALPH
DATA G,MASS,VJET,RHO,WARFA,SPAN,CHORD,IX,IY,IZ,IXZ,ZONE,IENG,XONE,
1XTWO,ZTWO,LONE,LDXIX,LPIX,MDYIY,MQIY,DELCHA,CMDELE,NDZIZ,NRIZ,CMQ,
2ANGVFL,LA,3DA,CDALPH,CLALPH/32.174,130.3537,1613.,0.002378,182.69
333.83,5.56,2340.,3400.,5400.,180.,0.583,6.0,0.0133,0.916,0.167,
40.0681,0.45,0.0350,0.15,0.576,0.0178,0.0166,0.20,11.4,1728.,
5101*0.0,0.0,0.0/
DATA -VI,WI,PI,QI,RI,THETA,PHI,PSI/8*0.0/
100 READ(5,10,END=9000) UWI,GSMAGU,GSMAGV,GSMAGW,DENOM,JGUST
10 FORMAT(5F10.2,15)
UI=ABS(UWI)/3.0
ITA=0
ITB=0
ITD=0
80 H=0.10
ITC=0
ITF=1
TIME(1)=0.0
TIMEX=TIME(1)
IDENT=0
J=1
K=1
L=2
U=UI
V=VI
W=WI
P=PI
Q=QI
R=RI
THETA=THETA
PHI=PHI
PSI=PSI
UG=0.0
VG=0.0

```

WG=0.0  
GO TO 20

C  
C  
C  
C

INTRODUCTION OF THE GUST VELOCITY FIELD. IF A STEP IS DESIRED,  
REPLACE THE APPROPRIATE EQUATION BY, FOR EXAMPLE, GW=GSMAGW.

30 PIE=3.14159

JIK=J-1

GU=0.5\*GSMAGU\*(1.0-COS(PIE\*JIK/DENOM))

GV=0.5\*GSMAGV\*(1.0-COS(PIE\*JIK/DENOM))

GW=0.5\*GSMAGW\*(1.0-COS(PIE\*JIK/DENOM))

C  
C  
C  
C

ROTATION OF THE GUST VELOCITY FIELD FROM THE ATMOSPHERE-FIXED  
REFERENCE FRAME INTO THE AIRCRAFT REFERENCE FRAME.

UG=GU+COS(PSI)\*COS(THETA)+GV\*SIN(PSI)\*COS(THETA)+GW\*SIN(THETA)  
VG=GV\*(COS(PSI)\*COS(PHI)+SIN(PSI)\*SIN(THETA)\*SIN(PHI))+GU\*(SIN  
1(PSI)\*COS(PHI)-COS(PSI)\*SIN(THETA)\*SIN(PHI))+GW\*COS(THETA)\*SIN  
2(PHI)

WG=GW\*COS(PHI)\*COS(THETA)+GU\*(COS(PSI)\*SIN(THETA)\*COS(PHI)+SIN(PSI  
1)\*SIN(PHI))+GV\*(COS(PSI)\*SIN(PHI)-SIN(PSI)\*SIN(THETA)\*COS(PHI))

1 UW=U+UW-UG

VW=UW\*(COS(PSI)\*SIN(THETA)\*SIN(PHI)-SIN(PSI)\*COS(PHI))

WW=UW\*(SIN(THETA)\*COS(PHI)\*COS(PSI)+SIN(PSI)\*SIN(PHI))

UREL=U-UW-UG

VREL=V-VW-VG

WREL=W-WW-WG

UD=SQRT(UREL\*\*2+WREL\*\*2)

UOHAR=SQRT(UREL\*\*2+VREL\*\*2+WREL\*\*2)

ALPHA=ARCSIN(WREL/UD)

BETA=ARCSIN(VREL/UOHAR)

C  
C  
C

CALCULATION OF THE AERODYNAMIC COEFFICIENTS

IF(UO,LT,51.) CLPO=0.61+0.002763\*UO

IF(UO,GE,51.) CLPO=0.75

DELCL=2.403009E-05\*UO\*\*2-2.248398E-07\*UO\*\*3-1.332149E-03\*UO

CO=0.11+1.7/(7.152195\*UO+12.5)

IF(ABS(BETA),LT,0.189) CY=-1.851\*BETA

IF(ABS(BETA),GE,0.189,AND,ABS(BETA),LT,0.418) CY=(-0.35+0.393\*

1(ABS(BETA)-0.189))\*(ABS(BETA)/BETA)

IF(ABS(BETA),GE,0.418,AND,ABS(BETA),LT,1.22) CY=(-0.26+0.362\*

1(ABS(BETA)-0.418))\*(ABS(BETA)/BETA)

IF(ABS(BETA),GE,1.22) CY=-0.55\*(ABS(BETA)/BETA)

IF(ABS(BETA),LT,0.169) CLU=-0.083\*BETA

IF(ABS(BETA),GE,0.169,AND,ABS(BETA),LT,0.471) CLU=(-0.014+0.0066\*

1(ABS(BETA)-0.169))\*(ABS(BETA)/BETA)

IF(ABS(BETA),GE,0.471,AND,ABS(BETA),LT,1.395) CLU=(-0.012+0.00665\*

1(ABS(BETA)-0.471))\*(ABS(BETA)/BETA)

IF(ABS(BETA),GE,1.395) CLU=-0.02\*(ABS(BETA)/BETA)

CLDELA=0.003\*COS(BETA)\*\*2

CLBETA=0.0045+CLPO-0.012\*

IF(UO,LT,34.) CMOPU=-0.6+0.00237\*UO

IF(UO,GE,34.0,AND,UO,LT,51.) CMOPU=-0.52+0.0148\*(UO-34.)

IF(UO,GE,51.0,AND,UO,LT,101.) CMOPU=-0.27+0.001579\*

1(UO-51.)

IF(UO,GE,101.) CMOPU=-0.19

DELCO=4.90035E-07\*UO\*\*3-3.16462E-05\*UO\*\*2+1.529505E-03\*UO

IF(UO,LT,34.) CMALPO=4.1+0.04145\*UO

IF(UO,GE,34.0,AND,UO,LT,51.) CMALPO=-2.7+0.1007\*(UO-34.)

```

IF(UO,GE,51.) CMALPO=1.0
IF(ABS(BETA),LT,0.1945) CND=0.113*BETA
IF(ABS(BETA),GE,0.1945,AND,ABS(BETA),LT,0.594) CND=0.022*(ABS(BETA)
1/BETA)
IF(ABS(BETA),GE,0.594,AND,ABS(BETA),LT,1.395) CND=(0.022+0.1348*
1*(ABS(BETA)-0.594))*(ABS(BETA)/BETA)
IF(ABS(BETA),GE,1.395) CND=0.13*(ABS(BETA)/BETA)
CNDEIR=0.00118*COS(BETA)**2
CNDEIA*=0.00014*COS(BETA)**2

```

```

C
C INCLUDE THE LIFT AND DRAG COEFFICIENTS WITH RESPECT TO THE
C ANGLE OF ATTACK AT THIS POINT

```

```

C IF(UO,LT,34.0) CDALPH=0.0
C IF(UO,LT,34.0) CLALPH=5.3-0.03235*UO
C IF(UO,GE,34.0) CDALPH=-0.3
C IF(UO,GE,34.0,AND,UO,LT,51.0) CLALPH=4.2-0.0611*(UO-34.0)
C IF(UO,GE,51.0) CLALPH=3.2

```

```

C INCLUDE ALPHA+110DEGREES (OR WHATEVER ANGLE) AT THIS POINT.
C ALPHA=ALPHA+0.192

```

```

C

```

```

IF(TIMEX,EQ,0.0,AND,K,EQ,1) GO TO 40

```

```

IF(IDENT,EQ,1) GO TO 50

```

```

YII(1,1)=UI

```

```

YII(2,1)=VI

```

```

YII(3,1)=WI

```

```

YII(4,1)=PI

```

```

YII(5,1)=QI

```

```

YII(6,1)=RI

```

```

YII(7,1)=THETA1

```

```

YII(8,1)=PHI1

```

```

YII(9,1)=PSI1

```

```

YII(10,1)=-100.0

```

```

DO 60 I=1,10

```

```

IJ=I+1

```

```

YI(I)=YII(I,1)

```

```

YY(IJ,1)=YII(I,1)

```

```

60 CONTINUE

```

```

YI(11)=0.0

```

```

YI(12)=0.0

```

```

YY(1,1)=TIME(1)

```

```

N=12

```

```

XI=0.0

```

```

KSTP=0

```

```

KODE=1

```

```

C
C ESNDFQ CALCULATES THE STATE VECTOR. THE OUTPUT OF ESNDFQ
C ARE THE Y(I)'S.

```

```

C

```

```

- 50 CALL ESNDFQ(KODE,1)

```

```

KODE=3

```

```

J=J+1

```

```

JI=J-1

```

```

JLAST=J

```

```

TIME(J)=TIME(JI)+H

```

```

YY(1,J)=TIME(J)

```

```

TIMEX=TIME(J)

```

```

C

```

```

C STORAGE OF THE STATE VECTOR IN THE ARRAY YY

```

```

C

```

IK=I+1  
 YY(IK,J)=Y(I)

70 CONTINUE

U=Y(1)  
 V=Y(2)  
 W=Y(3)  
 P=Y(4)  
 Q=Y(5)  
 R=Y(6)  
 THETA=Y(7)  
 PHI=Y(8)  
 PSI=Y(9)

ITC=ITC+1  
 NN=L-ITC  
 THRUST(L)=THRUST(NN)  
 SIGMA(L)=SIGMA(NN)  
 DELX(L)=DELX(NN)  
 DELY(L)=DELY(NN)  
 DELZ(L)=DELZ(NN)

C

STORAGE OF THE CONTROL VECTOR IN THE ARRAY YB

C

YB(1,L)=TIME(L)  
 YB(2,L)=THRUST(L)  
 YB(3,L)=THRUST(L)\*1.23986  
 YB(4,L)=SIGMA(L)  
 YB(6,L)=DELX(L)  
 YB(7,L)=DELY(L)  
 YB(8,L)=DELZ(L)

C

CALCULATION OF ANGULAR ACCELERATIONS (EQUIVALENT TO THE CONTROL EFFORTS).

C

LSTAR(L)=(IY-IZ)\*Q\*R/IX+IX7\*P\*Q/IX+THRUST(L)/IX\*(ZONE\*VREL/VJET  
 1-SIN(LAMBDA(L))\*(ZTWO+LONE\* $\cos(\text{SIGMA}(L))$ ))+LPIX\*P+LDXIX\*DELX(L)+  
 20.5/IX\*RHO\*UOBAR\*\*2+WAREA\*SPAN\*(CLO+CLDELA\*DELA+CLBETA\*BETA)  
 NSTAR(L)=(IX-IY)\*P\*Q/IZ-IXZ\*Q\*R/IZ+2.\*IENG\*OMEGA\*Q/IZ  
 1+THRUST(L)/IZ\*( $\sin(\text{LAMBDA}(L))$ )\*(XTWO-LONE\* $\sin(\text{SIGMA}(L))$ )-XONE  
 2\*VREL/VJET)+NRIZ\*R+NDZIZ\*DELZ(L)+0.5/IZ\*RHO\*UOBAR\*\*2+WAREA  
 3\*SPAN\*(CMO+CNDELR\*DELX+CNDFLA\*DELA)  
 PDOT(L)=IX\*IZ/(IY+IZ-IXZ\*\*2)\*(LSTAR(L)+IXZ\*NSTAR(L)/IX)  
 RDOT(L)=IX+IZ/(IX+IZ-IXZ\*\*2)\*(IXZ\*LSTAR(L)/IZ+NSTAR(L))  
 QDOT(L)=(IZ-IX)\*P\*R/IY+IXZ\*(R\*\*2-P\*\*2)/IY+2.\*IENG\*OMEGA\*R/IY  
 1+THRUST(L)/IY\*(VREL\*XONE+UREL\*ZONE)/VJET+ $\cos(\text{LAMBDA}(L))$   
 2\*(ZTWO\* $\sin(\text{SIGMA}(L))$ )+XTWO\* $\cos(\text{SIGMA}(L))$ )+DELCMO\*CHORD)+MDYIY\*  
 3DELY(L)+MQIY\*Q+0.5/IY\*RHO\*UO\*\*2+WAREA\*CHORD\*(CMOPO+(CMALPO+  
 4DELCMA)\*ALPHA+0.5\*CHORD\*CMQ\*Q/UO+CMUELE\*DELE)  
 YA(1,L)=TIME(L)

C

STORAGE OF THE ANGULAR ACCELERATIONS IN THE ARRAY YA, YA(5)  
 AND YA(6) STORE THE LAST TWO STATE VARIABLES, LONGITUDINAL  
 AND LATERAL DISPLACEMENT RESPECTIVELY.

C

YA(2,L)=PDOT(L)  
 YA(3,L)=QDOT(L)  
 YA(4,L)=RDOT(L)  
 YA(5,L)=Y(11)  
 YA(6,L)=Y(12)  
 PDDTA=PDOT(L)

QDOTA=QDOT(L)

243.

RDOTA=RDOT(L)

C  
C  
C

CHECK THE STABILITY CRITERIA.

IF(ABS(THETA).GT.0.43634) ITF=2

IF(ABS(PHI).GT.0.43634) ITF=2

IF(ABS(PDOTA).GT.1.361) ITF=2

IF(ABS(QDOTA).GT.0.698) ITF=2

IF(ABS(RDOTA).GT.0.332) ITF=2

L=L+1

IF(ITF.EQ.2.OR.J.GE.101) GO TO 1000

IDENT=1

K=K+1

C  
C  
C

ITC IS THE COUNTER TO SIMULATE THE TIME DELAY OF THE PILOT.

IF(ITC.LT.3) GO TO 30

K=K-1

C  
C  
C  
C  
C  
C

CALCULATION OF THE CONTROL VECTOR. THE FIRST TIME THROUGH THE PROGRAM, THIS VECTOR IS CALCULATED IMMEDIATELY AFTER THE AERODYNAMIC COEFFICIENTS ARE CALCULATED. AFTER THAT, THIS VECTOR IS CALCULATED WHENEVER ITC=3.

40 A=MASS\*(V\*P-W\*Q+G\*SIN(THETA))+0.5\*RHO\*UO\*\*2\*WAREA\*((CLPO+CLALPH\*  
IALPHA)\*SIN(ALPHA)+(CD+CDALPH\*ALPHA)\*COS(ALPHA))

B=MASS\*(W\*P-U\*R+G\*SIN(PHI)\*COS(THETA))+0.5\*RHO\*UOBAR\*\*2  
1\*WAREA\*CY

C=MASS\*(U\*Q-V\*P+G\*COS(PHI)\*COS(THETA))-0.5\*RHO\*UO\*\*2  
1\*WAREA\*((CLPO+CLALPH\*ALPHA)\*COS(ALPHA)+(CD+CDALPH\*ALPHA)\*SIN  
2(ALPHA))

AA=DELCL

D=1-UOBAR\*\*2/VJET\*\*2-AA\*\*2+2.\*AA\*(SIN(ALPHA)\*UREL-COS  
1(ALPHA)\*WREL)/VJET

E=(A\*UREL+B\*VREL+C\*WREL)/VJET-AA\*(A\*SIN(ALPHA)-C  
1\*COS(ALPHA))

F=A\*\*2+B\*\*2+C\*\*2

THRUST(K)=(-E+SQRT(E\*\*2+D\*F))/D

THRSTG(K)=THRUST(K)\*1.23986

THRST=THRSTG(K)

CALL ENGRPM(THRST,OMEGPC,UMEGA)

C  
C  
C  
C

IF LAMBDA IS TO BE CALCULATED, INSERT

LAMBDA(K)=ARCSIN(VREL/VJET-B/THRUST(K))

SIGMA(K)=ARCSIN((UREL/VJET-A/THRUST(K)-AA\*SIN(ALPHA))

1/COS(LAMBDA(K)))

DELX(K)=((IZ-IY)\*Q\*R-THRUST(K)\*(VREL+ZONE/VJET-SIN(LAMBDA(K))

1\*(ZTWO+LONE\*COS(SIGMA(K))))-LPIX\*P\*IX-0.5\*RHO\*UOBAR\*\*2\*WAREA

2\*SPAN\*(CLD+CLBETA\*BETA)-IXZ\*P\*Q)/(LIXIY+IX+0.5\*RHO\*UOBAR\*\*2\*

3WAREA\*SPAN\*CLDELA)

DELY(K)=((IX-IY)\*P\*R+(P\*\*2-R\*\*2)\*IX/2,+IENG\*OMEGA\*R-THRUST(K)

1\*(C\*WREL-XONE-UREL\*ZONE)/VJET+COS(LAMBDA(K))\*(ZTWO\*SIN(SIGMA(K))

2+XTWO\*COS(SIGMA(K))+CHORD\*DELCMO)-HOIY\*Q\*TY-0.5\*RHO\*UO\*\*2\*WAREA

3\*CHORD\*(CMOPO+(CMALPH+DELCMA)\*ALPHA+0.5\*CHORD\*CMQ\*Q/UO)/

4(MDYTY\*TY+0.5\*RHO\*UO\*\*2\*WAREA\*CHORD\*CMDFLF)

DELZ(K)=((IY-IX)\*P\*Q+IXZ\*Q\*R-2.\*IENG\*OMEGA\*Q-THRUST(K)\*(-VREL\*XONE

1/VJET+SIN(LAMBDA(K))\*(XTWO-LONE\*SIN(SIGMA(K))))-NRIZ\*R\*IZ-0.5\*RHO

2\*UOBAR\*\*2\*WAREA\*SPAN\*(CND+CNDCLA\*DELA))/(ND/IY+IZ+0.5\*RHO

3\*UOBAR\*\*2\*WAREA\*SPAN\*CNDELRL)

YB(1,K)=TIME(K)

YB(2,K)=THRUST(K)

YB(3,K)=THRSTG(K)

YB(4,K)=SIGMA(K)

YB(6,K)=DELX(K)

YB(7,K)=DELY(K)

YB(8,K)=DELZ(K)

C

C

C

CHECK FOR SATURATION OF CONTROL PARAMETERS.

IF(DELX(K).GT.20.0) DELX(K)=20.0

IF(DELX(K).LT.-20.0) DELX(K)=-20.0

IF(DELY(K).GT.20.0) DELY(K)=20.0

IF(DELY(K).LT.-20.0) DELY(K)=-20.0

IF(DELZ(K).GT.20.0) DELZ(K)=20.0

IF(DELZ(K).LT.-20.0) DELZ(K)=-20.0

DELA=DELX(K)

DELE=DELY(K)

DELK=DELZ(K)

IF(DFLE.GT.15.0) DELE=15.0

IF(SIGMA(K).GT.1.22173) SIGMA(K)=1.22173

IF(SIGMA(K).LT.0.0) SIGMA(K)=0.0

IF(THRSTG(K).GT.5515.) THRUST(K)=5515./1.23986

ITC=0

K=K+1

GO TO 30

C

C

C

C

C

C

C

ITERATION PROCEDURE FINDS THE RANGE A TO A+10 FIRST, THEN IT

FINDS THE RANGE A TO A+2, AND FINALLY THE EXACT VALUE,

IT CAN GO TO EITHER GREATER OR LESSER VALUES FROM THE INITIAL

VALUES OF THE GUST MAGNITUDES.

1000 IF(ITF.EQ.1) GO TO 998

IF(ITB.EQ.1) GO TO 996

IF(JGUST.EQ.1) GSMAGU=GSMAGU+10.0

IF(JGUST.EQ.2.OR.JGUST.EQ.3) GSMAGV=GSMAGV+10.0

IF(JGUST.EQ.4.OR.JGUST.EQ.5) GSMAGW=GSMAGW+10.0

ITA=1

GO TO 80

996 IF(JGUST.EQ.1) GSMAGU=GSMAGU+1.0

IF(JGUST.EQ.2.OR.JGUST.EQ.3) GSMAGV=GSMAGV+1.0

IF(JGUST.EQ.4.OR.JGUST.EQ.5) GSMAGW=GSMAGW+1.0

ITD=1

GO TO 80

998 IF(ITA.EQ.1) GO TO 997

IF(JGUST.EQ.1) GSMAGU=GSMAGU-10.0

IF(JGUST.EQ.2.OR.JGUST.EQ.3) GSMAGV=GSMAGV-10.0

IF(JGUST.EQ.4.OR.JGUST.EQ.5) GSMAGW=GSMAGW-10.0

GO TO 80

997 IF(JGUST.EQ.1) GSMAGU=GSMAGU-2.0

IF(JGUST.EQ.2.OR.JGUST.EQ.3) GSMAGV=GSMAGV-2.0

IF(JGUST.EQ.4.OR.JGUST.EQ.5) GSMAGW=GSMAGW-2.0

ITB=1

IF(ITD.EQ.1) GO TO 1001

GO TO 80

1001 WRITE(6,800)((YY(I,J),I=1,11),J=1,JLAST)

800 FORMAT(1P11E11.4)

WRITE(6,801)((YA(I,J),I=1,6),J=1,JLAST)

801 FORMAT(1P6E11.4)

```

WRITE(6,802)((YB(I,J),I=1,8),J=1,JLAST)
802 FORMAT(1P0E11.4)
GO TO 100
9000 STOP
END
FUNCTION F(I,X,Y)
C
C FUNCTION SUBROUTINE FOR ESODEQ.
C
COMMON/ES0/NOB0
REAL Y(99)
COMMON/FUNCI/G,THRUST(101),MASS,SIGMA(101),LAMBDA(101),
1U0,WAREA,CLPD,DELCL,ALPHA,CO,VREL,UOBAR,CY,IX,IZ,IXZ,IY,
2ZTWO,LONE,ZONE,LPIX,LOXIX,DELX(101),SPAN,WREL,CLO,CLDELA,
3DELA,CLBETA,IFNG,OMEGA,XTWO,XONE,NRIZ,NDZIZ,DELZ(101),CNO,
4CNDELR,DELR,CNDELA,MDYIY,DELY(101),MQIY,CHORD,CMQPO,
5DELCMO,CMALPO,DELCMA,CMQ,CMDELE,DELE,BETA,J,UREL,VJET,RHO
6,CDALPH,CLALPH
IF(I.EQ.1) F=Y(2)*Y(6)-Y(3)*Y(5)-G*SIN(Y(7))+THRUST(J)/MASS
1*(SIN(SIGMA(J))*COS(LAMBDA(J))-UREL/VJET+DELCL*SIN(ALPHA))+0.5/
2MASS*RHO*U0**2*WAREA*((CLPD+CLALPH*ALPHA)*SIN(ALPHA)-(CO+CDALPH*
3ALPHA)*COS(ALPHA))
IF(I.EQ.1) RETURN
IF(I.EQ.2) F=Y(3)*Y(4)-Y(1)*Y(6)+G*SIN(Y(8))*COS(Y(7))
1+THRUST(J)/MASS*(SIN(LAMBDA(J))-VREL/VJET)+0.5/MASS*RHO*UOBAR
2**2*WAREA*CY
IF(I.EQ.2) RETURN
IF(I.EQ.3) F=Y(1)*Y(5)-Y(2)*Y(4)+G*COS(Y(8))*COS(Y(7))
1-THRUST(J)/MASS*(COS(SIGMA(J))*COS(LAMBDA(J))+WREL/VJET+DELCL+
2COS(ALPHA))-0.5/MASS*RHO*U0**2*WAREA*((CLPD+CLALPH*ALPHA)*COS
3(ALPHA)+(CO+CDALPH*ALPHA)*SIN(ALPHA))
IF(I.EQ.3) RETURN
IF(I.EQ.4) F=(IX+IZ/(IX+IZ-IXZ**2))*((IY-IZ)*Y(5)*Y(6)/IX
1+IXZ*Y(4)*Y(5)/IX+THRUST(J)/IX*(ZONE+VREL/VJET-SIN(LAMBDA(J))*
2(ZTWO+LONE*COS(SIGMA(J))))+LPIX*Y(4)+LOXIX*DELX(J)+0.5/IX
3*RHO*UOBAR**2*WAREA*SPAN*(CLO+CLDELA*DELA+CLBETA*BETA)
4+IXZ/IX*((IX-IY)*Y(4)*Y(5)/IZ-IXZ*Y(5)*Y(6)/IZ+2.*IENG
5*OMEGA*Y(5)/IZ+THRUST(J)/IZ*(SIN(LAMBDA(J))*(XTWO-LONE*SIN
6(SIGMA(J)))-XONE*VREL/VJET)+NRIZ*Y(6)+NDZIZ*DELZ(J)+0.5/IZ*RHO
7*UOBAR**2*WAREA*SPAN*(CNO+CNDELR*DELR+CNDELA*DELA))
IF(I.EQ.4) RETURN
IF(I.EQ.5) F=(IZ-IX)*Y(4)*Y(6)/IY+IXZ*(Y(6)**2-Y(4)**2)
1/IY-2.*IENG*OMEGA*Y(6)/IY+THRUST(J)/IY*((WREL*XONE-UREL
2*ZONE)/VJET+COS(LAMBDA(J))*(ZTWO+SIN(SIGMA(J))+XTWO+COS
3(SIGMA(J))+CHORD*DELCMO)+MDYIY*DELY(J)+MQIY*Y(5)+0.5/IY*RHO*U0**2
4*WAREA*CHORD*(CMQPO+(CMALPO+DELCMA)*ALPHA+0.5*CHORD*CMQ*Y(5)/U0
5+CMDELE*DELE)
IF(I.EQ.5) RETURN
IF(I.EQ.6) F=(IX*IZ)/(IX+IZ-IXZ**2)*(IXZ/IZ+((IY-IZ)*Y(5)
1*Y(6)/IX+IXZ*Y(4)*Y(5)/IX+THRUST(J)/IX*(ZONE+VREL/VJET-SIN(LAMBDA(
2J))*(ZTWO+LONE*COS(SIGMA(J))))+LPIX*Y(4)+LOXIX*DELX(J)+0.5/IX*
3RHO*UOBAR**2*WAREA*SPAN*(CLO+CLDELA*DELA+CLBETA*BETA))+((IX-IY)*
4Y(4)*Y(5)/IZ-IXZ*Y(5)*Y(6)/IZ+2.*IENG*OMEGA*Y(5)/IZ+THRUST(J)/IZ*
5(SIN(LAMBDA(J))*(XTWO-LONE*SIN(SIGMA(J)))-XONE*VREL/VJET)+NRIZ*
6Y(6)+NDZIZ*DELZ(J)+0.5/IZ*RHO*UOBAR**2*WAREA*SPAN*(CNO+CNDELR*
7DELR+CNDELA*DELA))
IF(I.EQ.6) RETURN
IF(I.EQ.7) F=Y(5)*COS(Y(8))-Y(6)*SIN(Y(8))
IF(I.EQ.7) RETURN
IF(I.EQ.8) F=Y(4)+Y(5)*SIN(Y(8))*TAN(Y(7))+Y(6)*COS(Y(8))

```

1\*TAN(Y(7))

IF(I.EQ.8) RETURN

IF(I.EQ.9) F=(Y(6)\*COS(Y(8))+Y(5)\*SIN(Y(8)))/COS(Y(7))

IF(I.EQ.9) RETURN

IF(I.EQ.10) F=Y(2)\*SIN(Y(8))+COS(Y(7))+Y(3)\*COS(Y(8))\*COS(Y(7))-  
Y(1)\*SIN(Y(7))

IF(I.EQ.10) RETURN

IF(I.EQ.11) F=Y(1)\*COS(Y(7))+COS(Y(9))+Y(2)\*(SIN(Y(8))\*SIN(Y(7))\*  
100S(Y(9))-COS(Y(8))\*SIN(Y(9)))+Y(3)\*(COS(Y(8))\*SIN(Y(7))\*COS(Y(9))  
2+SIN(Y(7))\*SIN(Y(9)))

IF(I.EQ.11) RETURN

IF(I.EQ.12) F=Y(1)\*COS(Y(7))\*SIN(Y(9))+Y(2)\*(SIN(Y(8))\*SIN(Y(7))\*  
1SIN(Y(9))+COS(Y(8))\*COS(Y(9)))+Y(3)\*(COS(Y(8))\*SIN(Y(7))\*SIN(Y(9))  
2-SIN(Y(8))\*COS(Y(9)))

RETURN

END

SUBROUTINE ENGRPM(THRST,OMEGPC,OMEGA)

C  
C SUBROUTINE TO CALCULATE THE ENGINE ANGULAR  
C VELOCITY FROM THE THRUST.

C

ANGVEL=1728.

IF(THRST.LE.4370.) GO TO 300

GO TO 301

300 OMEGPC=(THRST-3305.)/88.75+80.

GO TO 302

301 BA=4.5244623E-09

BB=9.3130978E-06

BC=1.2498497E-02

BD=THRST-4370.

OMEGPC=BA\*BD\*\*3+BB\*BD\*\*2+BC\*BD+92.0

302 OMEGA=OMEGPC\*ANGVEL/100.

RETURN

END

SUBROUTINE ESODEG(KODE,NRO)

COMMON/ESU/NRO

COMMON/ESQCOM/N,XI,YI(99),X,Y(99),TR,H,KSTP,DY(99)

REAL XC,YC(99),DYP(4,99),S(99)

DATA HU/0/,DYP/396\*0/

DATA MSTP,NSTP,INI,IN2,IN3,IN4/0,0,1,2,3,4/

TR=(=1.0)

NOBO=1

IF(N.GT.99) GO TO 7777

GO TO (1000,2000,3000),KODE

1000 DD 1001 I=1,N

Y(I)=-YI(I)

1001 DY(I)=F(I,XI,YI)

X=XI

IN1=1

IN2=-2

IN3=3

IN4=4

1050 MSTP=KSTP

NSTP=0

HU=H

GO TO 4000

2000 GO TO 1050

3000 IF (HU.NE.H) GO TO 1050

GO TO 4000

3001 RETURN



```

4000 DO 4001 I= 1,N
4001 DYP(IN1,I) = DY(I)
      IF (NSTEP.LE.2) GO TO 4500
      DO 4002 I=1,N
4002 YC(I) = Y(I) + H*(55.0*DYP(IN1,I)-59.0*DYP(IN2,I)+37.0*DYP(IN3,I)
      I                                     -9.0*DYP(IN4,I))/24.0
      MSTP = NSTP-1
      IF (MSTEP.LE.0) GO TO 4100
      DO 4003 I=1,N
4003 YC(I) = YC(I)
      X = X + H
      GO TO 4300
4100 X = X + H
      DO 4101 I=1,N
4101 DY(I) = F(I, X, YC)
      DO 4102 I=1,N
4102 Y(I) = Y(I) + H*(9.0*DY(I)+19.0*DYP(IN1,I)-5.0*DYP(IN2,I)
      I                                     +DYP(IN3,I))/24.0
      MSTP = KSTP
      TR = 0.0
      DO 4103 I=1,N
4103 TR = TR + (.930*(Y(I)-YC(I)))**2
      TR = SQRT(TR)
      GO TO 4300
4500 DO 4501 I=1,N
      S(I) = H*DY(I)
4501 YC(I) = Y(I) + S(I)/2.0
      XC = X + H/2.0
      DO 4502 I=1,N
      DY(I) = F(I, XC, YC)
      S(I) = S(I) + 2.0*H*DY(I)
4502 YC(I) = Y(I) + (H*DY(I))/2.0
      DO 4503 I=1,N
      DY(I) = F(I, XC, YC)
      S(I) = S(I) + 2.0*H*DY(I)
4503 YC(I) = Y(I) + H*DY(I)
      XC = X + H
      DO 4504 I=1,N
      DY(I) = F(I, XC, YC)
      S(I) = S(I) + H*DY(I)
4504 Y(I) = Y(I) + S(I)/6.0
      X = XC
      NSTP = NSTP + 1
4800 DO 4801 I=1,N
4801 DY(I) = F(I, X, Y)
      I = IN4
      IN4 = IN3
      IN3 = IN2
      IN2 = IN1
      IN1 = I
      GO TO 3001
7777 WRITE (6, 777)
      CALL EXIT
777 FORMAT(1H1, 9H TOO MUCH)
      END

```

APPENDIX 7Inclusion of  $C_{L\alpha}$  and  $C_{D\alpha}$  in the Aircraft Model.

$C_L$  and  $C_D$  are to be included in equations (A4-1) and (A4-3) in Appendix 4. The altered equations are

$$\dot{u} = \dots + (1/2) \cdot \rho \cdot U_0^2 \cdot S \cdot \{(C_{Lp0} + C_{L\alpha} \cdot \alpha) \cdot \sin(\alpha) - (C_D + C_{D\alpha} \cdot \alpha) \cdot \cos(\alpha)\} \cdot (1/m) \quad (\text{III-A7-1})$$

and

$$\dot{w} = \dots - (1/2) \cdot \rho \cdot U_0^2 \cdot S \cdot \{(C_{Lp0} + C_{L\alpha} \cdot \alpha) \cdot \cos(\alpha) + (C_D + C_{D\alpha} \cdot \alpha) \cdot \sin(\alpha)\} \cdot (1/m) \quad (\text{III-A7-2})$$

These two coefficients are also included in the terms A and C of the thrust equation (A5-1) of Appendix 5. These terms are altered in the same manner as above with the exception that (1/m) does not appear.

$$A = \dots + (1/2) \cdot \rho \cdot U_0^2 \cdot S \cdot \{(C_{Lp0} + C_{L\alpha} \cdot \alpha) \cdot \sin(\alpha) - (C_D + C_{D\alpha} \cdot \alpha) \cdot \cos(\alpha)\} \quad (\text{III-A7-3})$$

$$C = \dots - (1/2) \cdot \rho \cdot U_0^2 \cdot S \cdot \{(C_{Lp0} + C_{L\alpha} \cdot \alpha) \cdot \cos(\alpha) + (C_D + C_{D\alpha} \cdot \alpha) \cdot \sin(\alpha)\} \quad (\text{III-A7-4})$$

APPENDIX 8Determination of Gust RMS Intensity.

The longitudinal gust will be used in this example. The value of  $v_m$  from WINDY was 52 fps. The gust field was moving at a speed equal to the headwind, 10 fps and the gust frequency was 0.10 cps. The displacement of the aircraft was 23.9 feet in the positive x-direction. The displacement was in the opposite direction to the movement of the gust field. Therefore,

$$2d_m = (10) \cdot (1/0.10) + 23.9 = 100 + 23.9 = 123.9 \text{ feet.}$$

Also  $L_u = 854$  feet which implies that

$$d_m/L = (123.9)/(2 \cdot 854) = 0.0724 \text{ .}$$

Using the probabilities of occurrence of 10, 1, and 0.10 percent of exceeding  $v_m$  (52 fps) for a specific  $d_m/L$  (0.0724), the ratios ( $v_m/\sigma$ ) for each probability can be found from Figure 12.

$\frac{P(v_m/\sigma)}$	$\frac{v_m/\sigma}{.}$
0.10 $\rightarrow$ 10%	0.62
0.01 $\rightarrow$ 1%	0.95
0.001 $\rightarrow$ 0.1%	1.25

The corresponding intensities are

$$\sigma_{10} = 52/0.62 = 84.0 \text{ fps rms ,}$$

$$\sigma_1 = 52/0.95 = 54.7 \text{ fps rms , and}$$

$$\sigma_{0.1} = 52/1.25 = 41.6 \text{ fps rms .}$$

REFERENCES

1. Hoffman, M. A., Loscutoff, W. V., and Seevers, J., "Equations of Motion for the X-14 Aircraft," Report, Phase II Study, September 1970-September 1973, NASA Grant NGR-05-004-051, December 1972.
2. Etkin, B., Dynamics of Flight, John Wiley and Sons, Inc., New York, 1959.
3. Feistel, T.W., Gerdes, R.M., and Fry, E.B., "An Investigation of a Direct Side-Force Maneuvering System on a Deflected Jet VTOL Aircraft," NASA TN D5175, April 1969.
4. Grief, R.K., Fry, E.B., Gerdes, R.M., and Gossett, T.D., "VTOL Control Systems Studies on a Six-degree-of-freedom Motion Simulator," Ames Research Center, NASA, Moffett Field, California, Aerospace Proceedings 1966.
5. Etkin, B., Dynamics of Atmospheric Flight, John Wiley and Sons, Inc., New York, 1972.
6. Hacker, T., Flight Stability and Control, American Elsevier Publishing Company, Inc., New York, 1970.
7. Wolkovitch, J., and Walton, R.P., "VTOL and Helicopter Approximate Transfer Functions and Closed-loop Handling Qualities," STI Technical Report No. 128-1, June 1965.
8. Lumley, J.L., and Panofsky, H.A., The Structure of Atmospheric Turbulence, John Wiley and Sons, Inc., New York, 1964.
9. Pao, Y.H., and Goldberg, A., editors, Clear Air Turbulence and Its Detection, Plenum Press, New York, 1969.
10. Sutton, O.G., Micrometeorology, McGraw-Hill Book Company, Inc., New York, 1953.
11. Gault, J.D., and Gunter, D.E., Jr., "Atmospheric Turbulence Considerations for Future Aircraft Designed to Operate at Low Altitudes," Journal of Aircraft, vol. 5 no. 6, November-December 1968.

12. Skelton, G.B., "Investigation of the Effects of Gusts on V/STOL Craft in Transition and Hover," Technical Report AFFDL-TR-68-65, October 1968.
13. Chalk, C.R., Neal, T.P., Harris, T.M., Pritchard, F.E., and Woodcock, R.J., "Background Information and User Guide for MIL-F-8785B(ASG), 'Military Specification-Flying Qualities of Piloted Airplanes'," Technical Report AFFDL-TR-69-72, August 1969.
14. Donnasch, D.O., Aeroplane Dynamics, John Wiley and Sons, Inc., New York, 1962.
15. Anonymous, Report 68-978-002, Bell Aircraft Corporation, September 1958.
16. Sinacori, J.B., partial report of the coupled equations of motion for the X-14, June 1968.
17. Private conversation with Mr. Lloyd Corliss of NASA Ames.